

# Proceedings of the 1993 DOE/NREL Hydrogen Program Review

May 4-6, 1993  
Cocoa Beach, Florida

*Hosted by the National Renewable  
Energy Laboratory*

*Sponsored by the Advanced Utility  
Concepts Division, Office of Energy  
Management, U.S. Department of Energy*



National Renewable Energy Laboratory  
1617 Cole Boulevard  
Golden, Colorado 80401-3393  
Operated by Midwest Research Institute  
for the U.S. Department of Energy  
under Contract No. DE-AC02-83CH10093  
Prepared under task no. HY31.1010

August 1993

MACTER

JB

## Foreword

The U.S. Department of Energy has conducted programs of research and development in hydrogen and related technologies since 1975. The current program is conducted in accordance with the DOE *Hydrogen Program Plan FY 1993 - FY 1997* which was published in June 1992. The plan establishes program priorities and guidance for the allocation of funding. The core program, currently under the Office of Energy Management, supports projects in the areas of hydrogen production, storage and systems research. A program review is held annually to evaluate each research project for technical quality, progress and programmatic benefit. The evaluation is conducted by a panel of technical experts.

This proceedings of the Program Review conducted in May 1993 is a compilation of all research projects supported by the Hydrogen Program during FY 1993. It is produced in the anticipation that will serve as a useful technical reference for those interested in the status of hydrogen technologies.

William Hoagland, Sr. Project Coordinator  
Hydrogen Program  
National Renewable Energy Laboratory  
Golden, Colorado

## TABLE OF CONTENTS

	Page No.
<i>Solar Energy Conversion with Cyanobacteria</i> , E. Bylina, University of Hawaii .....	1
<i>Photobiological Hydrogen Production Using Whole-Cell Or Cell-Free Systems</i> , P. Weaver, P.-C. Maness, A. Frank, M. Lange, J. Blaho, National Renewable Energy Laboratory.....	7
<i>Biological Hydrogen Photoproduction (Task B)</i> , A. Mitsui, University of Miami .....	13
<i>Photoelectrochemical Production of Hydrogen</i> , R. Rocheleau, University of Hawaii .....	35
<i>Photoelectrochemical Based Direct Conversion Systems</i> , S. Kocha, M. Peterson, J. Turner, National Renewable Energy Laboratory .....	49
<i>Nonclassical Polyhydride Metal Complexes as Hydrogen Storage Materials</i> , C. Jensen, University of Hawaii at Honolulu .....	63
<i>Carbon Nanotubes for Hydrogen Storage</i> , M. Heben, National Renewable Energy Laboratory.....	79
<i>Activated Carbon-Based Hydrogen Storage System</i> , J. Schwarz, Syracuse University .....	89
<i>Hydrogen Storage by Chemical Synthesis Techniques</i> , D. Slattery, R. Zidan, Florida Solar Energy Center, M. Hampton, University of Central Florida .....	103
<i>A New System for the Evaluation of Hydrogen Storage Compounds</i> , M. Hampton, J. Slattery, C. Bender, University of Central Florida .....	119

	Page No.
<i>Magnesium Alloys for High Hydrogen Storage Capacity at Low Temperatures,</i> S. Srinivasan, M. Kumar, K. Petrov, A. Visintin, A. Appleby, Texas A&M University .....	137
<i>Modeling of the Solar Hydrogen Energy System,</i> F. Barbir, H. Plass, T. Veziroglu University of Miami .....	151
<i>Assessments of Renewable Hydrogen Energy Systems,</i> J. Ogden, Princeton University .....	163
<i>Gaseous Fuel Transport Line Leakage - Natural Gas Compared to Hydrogen,</i> M. N. Swain, G. J. Schade, M. R. Swain, University of Miami .....	187
<i>A Survey of Industrial Interest in Hydrogen-Related Technologies,</i> R. Mauro, D. Smith, J. Serfass, National Hydrogen Association .....	197

# SOLAR ENERGY CONVERSION WITH CYANOBACTERIA

Edward J. Bylina  
Pacific Biomedical Research Center  
University of Hawaii at Manoa  
Honolulu, HI 96822

## Abstract

Hydrogen production in cyanobacteria is particularly attractive because these organisms are able to generate their own source of organic substrates using light energy and use water as their ultimate source of reductant. Molecular biology approaches are being applied to understanding and increasing hydrogen production in filamentous strains of cyanobacteria. The soluble hydrogenase structural genes of *Anabaena* PCC 7120 were not identified by hybridization experiments. Characterization of an *Anabaena* PCC 7120 DNA fragment identified by hybridization analysis using the soluble hydrogenase gene from *Anabaena cylindrica* as a heterologous probe resulted in the identification of the genes for a putative restriction-modification enzyme system of *Anabaena* PCC 7120. Experiments have continued towards the development of a genetic system for *Spirulina pacifica*. These include (1) the identification of three unique restriction enzymes and (2) PCR amplification of the gene encoding the 16S ribosomal RNA in this strain.

## Introduction

In order to capitalize on the photosynthetic biological production of hydrogen, one must gain a better understanding of the mechanisms and the regulation of the systems involved. Characterization of hydrogen evolution in *Spirulina* is important, since this species is already cultivated on an industrial scale. Although *Spirulina* species do not form heterocysts and do not fix nitrogen (Durand-Chastel, 1982), these organisms are capable of hydrogen evolution (Gu and Wang, 1984). While hydrogen production in a number of cyanobacterial species is predominantly formed by nitrogenase, hydrogen evolution is catalyzed by hydrogenase in *Spirulina*. The hydrogenase from *Spirulina platensis* has been partially purified (Gu and Zhou, 1987). No genetic system has yet been described for these organisms.

In prior years of this program, we reported on our efforts to identify the structural genes of cyanobacterial hydrogenases from *Anabaena* PCC 7120 using hybridization experiments. While our efforts to isolate the uptake hydrogenase genes were unsuccessful using a number of different probes, we identified a 2.6 kb HindIII DNA fragment which hybridized to a probe containing the gene encoding the 42 kDa subunit of the soluble hydrogenase from *Anabaena cylindrica* (Ewart et al., 1990). We also initiated experiments using the commercially important cyanobacterial species *Spirulina pacifica*. In this report, we describe the characterization of the DNA fragment identified by hybridization experiments using the soluble hydrogenase probe. DNA sequence analysis of this fragment indicates that the soluble hydrogenase structural genes are not present on this DNA fragment. Our ongoing experiments with *Spirulina* will also be discussed.

The goals of this on-going subtask of the Hydrogen from Renewable Resources Program are to investigate the molecular basis of hydrogen metabolism and evolution in cyanobacteria and to develop enhancement methodologies for the production of improved strains of hydrogen producers. The use of hydrogen production in cyanobacteria to convert solar energy to useful energy is particularly attractive because these organisms are able to generate their own source of organic substrates using light energy and use water as their ultimate source of reductant. We are currently concentrating our efforts using the commercially important cyanobacterial species *Spirulina pacifica* to elucidate the molecular mechanisms of hydrogen metabolism in these organisms.

## Results and Discussion

Our attempts to isolate the soluble hydrogenase structural genes from *Anabaena* PCC 7120 using hybridization experiments have been concluded. In our last report, we described the identification of three clones from our selected size DNA library which hybridized to the *Anabaena cylindrica* soluble hydrogenase probe. Our attempts to subclone the 2.6 kb HindIII DNA fragment into M13 were complicated by the presence of multiple inserts in our selected size library clones. Using the dideoxy sequencing method (Sanger et al, 1977), our initial sequencing efforts indicated that several different *Anabaena* DNA fragments were introduced into M13 during the subcloning process. Hybridization

experiments (Southern 1975) were used to identify the M13 subclones containing inserts with homology to the *A. cylindrica* hydrogenase probe.

Once the subclones containing the correct fragment of interest were identified by hybridization, restriction analysis of the RF form of these M13 clones was performed to determine the orientation of the DNA insert. This restriction analysis indicated that the 2.6 kb HindIII fragment was inserted into M13 in both orientations. Clones containing opposite orientations of the insert were sequenced with the universal sequencing primer. Approximately 200 bp of sequence was obtained from each end of the insert. This sequence does not show homology with our probe, suggesting that the hydrogenase gene (or another sequence which is similar to the probe) is in the middle of this fragment.

In order to obtain the remainder of the sequence of the 2.6 kb HindIII fragment, we have 'walked' along both orientations of the fragment by synthesizing oligonucleotides based on the sequences we have obtained. Using seven synthesized oligonucleotides, sequence for >90% of the fragment was obtained. Only ~200 bp in the middle of the fragment has remained unsequenced. This sequence should be considered preliminary, since sequence was obtained from only one of the two DNA strands. Computer analysis (Genetics Computer group, 1991) of the obtained sequence identified a 100 bp region which showed ~60% homology with a region of the *A. cylindrica* probe, possibly explaining the hybridization to this fragment. An open reading frame encoding a possible hydrogenase was not found in the 2.6 kb HindIII fragment.

Homology searches with the sequences in GenBank have uncovered >50% homology between our sequence and PstI restriction-modification genes (Walder et al., 1984). The HindIII fragment appears to contain the carboxy-terminal half of the methylase gene and the entire restriction enzyme. While the PstI methylase gene and the PstI restriction enzyme gene are transcribed in opposite directions, our putative methylase and restriction enzyme genes are tandemly arranged on the same DNA strand. This finding is unexpected, since a PstI isoschizomer is not known to exist in *Anabaena* PCC 7120. Homology between restriction enzymes is typically only observed between isoschizomers, therefore it is unlikely that these genes encode a restriction enzyme with a different specificity. A closer examination of the preliminary DNA sequence obtained indicates a number of stop codons/frameshifts found in the putative restriction enzyme sequence. While a PstI isoschizomer is not thought to currently exist in *Anabaena* PCC 7120 (Duyvesteyn et al., 1983), only ~10 PstI sites exist in the entire chromosome (Bancroft et al., 1989). Our results may suggest that *Anabaena* possessed PstI activity at some time in the past, but that the enzyme is currently inactivated.

One of the requirements for the development of a genetic system in *Spirulina pacifica* is the characterization of the DNA restriction-modification system present in this strain. Three restriction enzymes were identified in *Spirulina platensis* subspecies *siamese* (Kawamura et al., 1986). The same enzyme purification protocol was used with cell extracts of *Spirulina pacifica*. Three different restriction enzyme activities in the cell extract from *Spirulina pacifica* have been found and the recognition sites for each of the enzymes have been identified. All three enzymes are isoschizomers of known enzymes. However, only one of the three enzyme activities is found in both *Spirulina* species.

Using chromosomal DNA isolated from *Spirulina*, PCR was used (Weisburg et al., 1991) to amplify the 16S rRNA gene of *Spirulina pacifica*. Eubacterial specific 16S rRNA oligonucleotides were used for the amplification of this *Spirulina* gene. This strain originated from the UTEX strain collection (UTEX 1926), however little work has been published on the strain. Determination of the 16S rRNA sequence will allow us to determine the phylogenetic relationship between *Spirulina pacifica* and other *Spirulina* strains in use in other laboratories. A distinct fragment of expected size (~1500 bp) was observed after PCR amplification.

## Future Work

Continuing the work of the on-going research program, we are pursuing several research goals with respect to our experiments with *Spirulina*. Since *Spirulina* species are probably the most commercially exploited among the cyanobacteria, experimental successes may have some practical applications. The sequence of the 16S rRNA gene of *Spirulina pacifica* will be determined. The isolated PCR product containing the 16S rRNA gene of *Spirulina* will be cloned into a plasmid vector and checked by restriction analysis. Single strand DNA will be isolated from a number of independent clones and used in DNA sequencing experiments.

Growth conditions for maximal hydrogen production in *Spirulina pacifica* will be established. The *Spirulina* hydrogenase will be purified to homogeneity from cultures grown under these conditions. The hydrogenase from *Spirulina platensis* has already been partially purified (Gu and Zhou, 1987). Once this enzyme complex has been isolated, the amino-terminal sequence of the protein subunits shall be determined. A DNA library of *Spirulina* chromosomal DNA will be constructed (DeRossi et al., 1985). Degenerate oligonucleotide probes based on the amino acid sequence of the hydrogenase will be synthesized. These probes will be used in hybridization studies to identify the *Spirulina* DNA fragments which contain the hydrogenase genes.

We will continue our efforts to develop a genetic system for *Spirulina pacifica*. With the identification of the restriction enzymes present in this strain, the genes for the DNA modification enzymes corresponding to these restriction enzymes can be isolated and characterized. These modification enzymes will be used to modify DNA that will be introduced into *Spirulina*. These modifications will make the introduced DNA resistant to cleavage inside the *Spirulina* cell, thereby increasing DNA transformation efficiencies. We will use a variation of the genomic DNA library enrichment strategy (Renbaum et al., 1990) that was used to isolate the CpG methylase gene from *Spiroplasma*. Other requirements of a genetic system include: (1) establishing conditions to reproducibly regenerate *Spirulina* filaments from fragments containing only a few cells; (2) designing a DNA vector which will be stably maintained in *Spirulina* (either in plasmid form or integrated into the chromosome); and (3) developing either physical or biological methods for introducing foreign DNA into *Spirulina* cells. Electroporation and particle gun technologies will be investigated.

The future of genetic engineering approaches to hydrogen production in cyanobacteria looks bright. Rapid advances are taking place in the ability to manipulate cyanobacterial strains. Some species (i.e. *Spirulina*) are already being cultivated on an industrial scale. As we learn more about the molecular basis of hydrogen



metabolism in cyanobacteria, these advances can be used to redirect the metabolic energies of cyanobacteria to the production of hydrogen.

## Acknowledgments

We thank the U.S. Department of Energy via the National Renewable Energy Laboratory (XD-0-10089-1) for financial support. We would like to acknowledge Anil Kapila for his work on *Spirulina* restriction enzymes, Craig Moyer for technical assistance on the PCR amplification of the *Spirulina* 16S rRNA gene, and Kathleen Baker for her participation in the work described here.

## References

- Bancroft, I., C.P. Wolk, and E.V. Oren. 1989. "Physical and genetic maps of the genome of the heterocyst-forming cyanobacterium *Anabaena* sp. strain PCC 7120." *J. Bacteriology*, 171:5940-5948.
- DeRossi, E., G. Riccardi, A.M. Sanangelantoni, and O. Ciferri. 1985. "Construction of a cosmid library of *Spirulina platensis* as an approach to DNA physical mapping." *FEMS Microbiol. Lett.*, 30:239-244.
- Durand-Chastel, H. 1982. "General characteristics of blue-green algae (cyanobacteria): *Spirulina*." In: *C.R.C. Handbook of Biosolar Resources*, Vol.1, part 2, 19-23.
- Duyvesteyn, M.G.C., J. Korsuize, A. de Waard, A. Vonshak, and C.P. Wolk. 1983. "Sequence-specific endonucleases in strains of *Anabaena* and *Nostoc*." *Arch. Microbiol.*, 134: 276-281.
- Ewart, G.D., K.C. Reed, and G.D. Smith. 1990. "Soluble hydrogenase of *Anabaena cylindrica*. Cloning and sequencing of a potential gene encoding the tritium exchange subunit." *Eur. J. Biochem.*, 187:215-223.
- Genetics Computer Group. 1991. Program Manual for the GCG Package, Version 7, April 1991, 575 Science Drive, Madison Wisconsin USA 53711.
- Gu, T. and F. Wang. 1984. "Studies on H<sub>2</sub> evolution by *Spirulina platensis*." *Hydrobiologia*, 116/117:467-470.
- Gu, T. and P. Zhou. 1987 "Isolation and characterization of hydrogenase from *Spirulina platensis*." *Hydrobiologia*, 151/152:557-561.
- Kawamura, M., M. Sakakibara, T. Watanabe, K.Kita, N. Hiraoka, A. Obayashi, M. Takagi, and K. Yano. 1986. "A new restriction endonuclease from *Spirulina platensis*." *Nucleic Acids Res.*,

14:1985-1989.

Renbaum, P., D. Abrahamove, A. Fainsod, G.G. Wilson, S. Rottem, and A. Razin. 1990. "Cloning, characterization, and expression in *Escherichia coli* of the gene coding for the CpG DNA methylase from *Spiroplasma* sp. strain MQ1 (M-SssI)." *Nucleic Acids Res.*, 18:1145-1152.

Sanger, F., S. Nicklen, and A.R. Coulson. 1977. "DNA sequencing with chain terminating inhibitors." *Proc. Natl. Acad. Sci. USA*, 74:5463-5467.

Southern, E. 1975. "Detection of specific sequences among DNA fragments separated by gel electrophoresis." *J. Mol. Biol.*, 98:503-517.

Walder, R.Y., J.A. Walder, and J.E. Donelson. 1984. "The organization and complete nucleotide sequence of the PstI restriction-modification system." *J. Biol. Chem.*, 259:8015-8026.

Weisburg, W.G., S.M. Barns, D.A. Pelletier, and D.J. Lane. 1991. "16S ribosomal DNA amplification for phylogenetic study." *J. Bacteriology*, 173:697-703.

# PHOTOBIOLOGICAL HYDROGEN PRODUCTION USING WHOLE-CELL OR CELL-FREE SYSTEMS

P. Weaver, P.C. Maness, A. Frank, M. Lange, and J. Blaho  
National Renewable Energy Laboratory  
Golden, CO 80401

## Abstract

Many microbes, especially photosynthetic microbes, evolve and consume hydrogen as a normal part of their metabolic activities. Several distinct metabolic mechanisms have been examined for their potential for large-scale production of hydrogen. Ideally, the biological process should meet the following criteria: (1) hydrogen derived from water; (2) solar driven; (3) highly efficient; (4) durable; (5) insensitive to hydrogen pressure; and (6) inexpensive to construct and operate. Both whole-cell and cell-free systems have been identified that meet, or have the potential to meet, most of these criteria. Of the whole-cell systems, only the nitrogenase- or hydrogenase-mediated metabolisms of photosynthetic bacteria are currently capable of producing hydrogen at high rates over prolonged periods (months). Most promising are pure strains of photosynthetic bacteria that are able to produce hydrogen at ambient temperature and pressure from carbon monoxide (generated by thermal gasification of biomass into a synthesis gas) at rates up to 1520  $\mu\text{mol}/\text{min}\cdot\text{g}$  cdw and for durations of more than 3 months. The CO-linked hydrogenase is distinct from other hydrogenases within the cell. Recent bacterial isolates, selected under semi-aerobic conditions, have a greatly enhanced tolerance to  $\text{O}_2$ , as does their evolving hydrogenase enzyme. The  $\text{O}_2$ -tolerant hydrogenase may have potential for genetic transfer to cyanobacteria or algae and for use in cell-free production of  $\text{H}_2$  from  $\text{H}_2\text{O}$ .

Cell-free work concentrated on reversibly binding and electrically linking hydrogenase and water-splitting enzyme complexes (PS II) to electrodes. In this hybrid biological/electrochemical system, sunlight should drive water oxidation that is coupled exclusively to hydrogen production without competition from other electron sinks. Graphite and tin oxide electrodes have been surface derivatized with benzoquinone (an electron acceptor for PS II) and other electrochemically active functional groups. When oxidized, a positive charge on the electrode surface electrostatically binds negatively charged biological materials. When the functional groups on the electrode are electrochemically reduced, thereby generating a neutral or negative surface charge on the electrode, the biological materials should be released. This cycle will permit the facile replacement of spent enzymes. As a test system, 100% of intact bacterial cells in flowing streams were bound to oxidized electrode surfaces where they remained metabolically active in monolayer films. Release of the adsorbed microbes upon reduction of the electrode is not yet optimal.

## Introduction

An economic process for producing hydrogen, whether biologically or chemically based, would ideally be: (1) H<sub>2</sub>O derived; (2) solar driven; (3) highly efficient; (4) durable; (5) insensitive to hydrogen partial pressure; and (6) inexpensive to build and operate. A complete system fulfilling all of these goals is not currently available. Of the biological options, systems employing intact cells of photosynthetic bacteria are the most advanced. Unlike cyanobacteria or algae, however, photosynthetic bacteria do not oxidize water. They instead require a reduced form of carbon, which may be biomass and therefore indirectly derived from water, as their source of electrons and protons for H<sub>2</sub> production. They are capable of producing H<sub>2</sub> at high rates over long periods of time, however.

The desired criterion of sustained hydrogen production based on water oxidation is the most difficult to achieve. Oxygen production is inherent in the oxidation of water, and the hydrogen evolving enzymes of cyanobacteria and algae are usually rapidly inactivated by oxygen. Some oxygenic microbes have partially solved this incompatibility by temporally or spatially (e.g., nitrogenase found in relatively O<sub>2</sub>-impermeable heterocysts) separating O<sub>2</sub> production from H<sub>2</sub> metabolism. A second difficulty with application of intact cell systems is that much of the reductant that they generate goes to other metabolic functions, such as CO<sub>2</sub> reduction, rather than H<sub>2</sub> production, and therefore, solar efficiencies are low. To bypass these intrinsic problems, we are attempting to immobilize only the water oxidizing enzyme complex on one side of an electrode and electrically link it with an immobilized hydrogenase enzyme on the opposite side. Oxygen and hydrogen production sites are spatially separated, and electrons from water oxidation are funneled exclusively into H<sub>2</sub> production. Since enzymes have finite lifetimes and must be replaced, we are incorporating a method to reversibly bind and release the biological materials to the electrode surfaces. The electrodes themselves are therefore reusable.

## Results and Discussion

### ***Whole-Cell Systems for Hydrogen Production***

Of the intact cell metabolisms of phototrophs that evolve hydrogen, the nitrogenase-mediated reactions have been the most studied. Nearly all isolates of photosynthetic bacteria have a nitrogenase enzyme complex (Weaver et al. 1975), which, in the absence of ammonium ion or dinitrogen gas and in the presence of oxidizable organic materials, functions to reduce protons and evolve hydrogen. Hydrogen evolution is largely light dependent (Schultz et al. 1985) and strongly exergonic. The hydrolysis of about 4 ATP (largely synthesized in light) is required to generate each H<sub>2</sub> and can drive the gas production to equilibrium pressures in excess of 100 atmospheres. Radiant energy conversion efficiencies (ignoring the chemical energy of the organic substrate) are about 5.3% for the most active strains of photosynthetic bacteria. The best outdoor, solar-driven efficiency is 3.4%. Previous cultures grown on glutamate as the nitrogen source produced H<sub>2</sub> at linear rates for only 7-10 days before *nif*<sup>-</sup> strains began to dominate the cultures. Experiments with weekly feedings of N<sub>2</sub> maintained the *nif*<sup>+</sup> wild-type genotype dominant and active H<sub>2</sub> production could be observed for more than 30 days.

Many strains of photosynthetic bacteria also produce hydrogen from organic substrates by way of a fermentative hydrogenase enzyme when grown in darkness, or intermittent or low continuous light (Schultz and Weaver 1982). High, continuous light represses synthesis of the enzyme. The enzyme does not

require ATP. It can mediate hydrogen production at rates more than 3-fold those of nitrogenase. However, it equilibrates at low partial pressures of about 0.1 atmospheres of  $H_2$ . The active rates of hydrogen production can thus only be maintained by sparging with inert gas, by vacuuming, or by scavenging with a hydrogen-consuming process (e.g., methanogenesis, which has been demonstrated).  $H_2$  production from cyanobacterial or algal hydrogenases also may be subject to this limitation.

Uptake hydrogenase enzymes are also present in nearly all photosynthetic bacteria and normally function in the unidirectional reaction of hydrogen oxidation, probably due to the relatively high redox potential of the associated cofactors. The isolated enzymes exhibit reversible activity and may be of value in cell-free systems. We have isolated several strains of photosynthetic bacteria that exhibit enhanced  $O_2$  tolerance when growing on  $H_2$ . Presumably, their uptake hydrogenase is relatively resistant to  $O_2$  inactivation.

A unique type of hydrogen producing activity was found in a photosynthetic bacterium by Uffen (1976) that functioned only in darkness to shift CO (and  $H_2O$ ) into  $H_2$  (and  $CO_2$ ). We have isolated more than 350 strains of photosynthetic bacteria that perform this reaction in darkness but additionally in light as well. High rates of activity could be observed in many strains for periods of more than a year with CO as the sole source of carbon.  $H_2$  production was stoichiometric with CO consumption in darkness in many strains. Starting with 200,000 ppm of CO, final CO concentration was less than 18 ppm. Equilibrium pressures were in excess of two atmospheres (perhaps considerably higher) and specific rates of 1520  $\mu\text{mol } H_2/\text{min-gram cell dry weight}$  were obtained. Twenty per cent CO in untreated synthesis gas generated by thermal gasification of biomass could also be shifted to  $H_2$  at similar rates. Mass transfer of gaseous CO into the aqueous environment of the bacteria was rate limiting. Increased pressure strongly enhanced the CO shift into  $H_2$ , but was deemed impractical. We are derivatizing 0.5 mm graphite particles with electroactive groups (described below), which should allow us to reversibly adsorb the bacteria in high-density monolayer films on the particle surfaces, free of a bulk aqueous phase. Passage of a humid gas phase containing CO through the column of adsorbed bacteria should enhance bacterial access to the gas and increase  $H_2$  production rates.

Several CO-utilizing strains of photosynthetic bacteria were isolated from soil and water samples under semi-aerobic conditions (2%  $O_2$ ) in the light with CO as the sole carbon source. Although the number of isolates was drastically reduced from anaerobic enrichment cultures, several of the new isolates exhibit a strongly enhanced  $O_2$ -tolerance in their metabolisms, including those for  $H_2$  evolution. Isolated hydrogenase from these strains also exhibits enhanced  $O_2$ -resistance.

For comparison, representative rates for the more direct production of  $H_2$  from  $H_2O$  in cyanobacteria and algae are about 30  $\mu\text{mol } H_2/\text{min-gram cell dry weight}$ . Both the nitrogenase-based, heterocystous cyanobacterial system (Benemann and Weissman 1977) and the hydrogenase-based, green algal system (Weaver et al. 1980) had to be continuously sparged with inert gas in order to prevent  $O_2$  inactivation. Equilibrium pressures were not determined.

If the  $O_2$ -tolerant hydrogenase enzymes from bacteria could be genetically transferred into cyanobacteria or algae, expressed, integrated into their membranes, and linked to photoreduced ferredoxin, then a whole-cell system for the photoproduction of  $H_2$  from  $H_2O$  becomes feasible. We are pursuing this course.

## **Cell-Free Systems for Hydrogen Production**

The theoretical maximum efficiency of biological H<sub>2</sub> production from water is about 10-12% (Bolton 1977) assuming that hydrogenase is the mediating enzyme. With a nitrogenase-based mechanism, the maximum efficiency should be decreased by about one-half if the aforementioned ATP requirements observed for photosynthetic bacteria are similar for cyanobacteria. Since the current intact-cell efficiencies of H<sub>2</sub> production from water oxidation are in the 0.1-0.3% range, there is considerable room for improvement if the twin problems of O<sub>2</sub> inactivation and competition for reductant can be overcome.

A hybrid biological/electrochemical method is being developed that should confront these problems. In this scheme the water-oxidizing enzyme complex (PSII) is adsorbed to a conducting surface derivatized with benzoquinone, an electron acceptor for PSII. Light shining on PSII oxidizes water and liberates O<sub>2</sub> on the anodic side with electrons entering the electrode through quinone. Other photons absorbed either by a biomimetic chlorophyll or by a semiconductor photoelectrode elevate the electron energy sufficiently to reduce a redox mediator, a viologen dye covalently linked to the cathodic surface. Reduced viologen dyes readily couple with hydrogenase enzymes which then reduce protons to produce H<sub>2</sub> as the exclusive product. Our first choice for the hydrogenase enzyme to be used is the O<sub>2</sub>-resistant, CO-linked hydrogenase of identified strains of photosynthetic bacteria. The isolated enzyme produces H<sub>2</sub> at rates in excess of 1 mol per hr per mg.

Negatively charged biological materials will electrostatically bind to positively charged surfaces. By being adsorbed, thermal stability increases. In one case, O<sub>2</sub>-inactivation of hydrogenase was decreased more than a thousand-fold when it was bound to an ion-exchange surface (Klibanov et al. 1978). We have also adsorbed O<sub>2</sub>-sensitive, purified carbon monoxide dehydrogenase to ion-exchange resins and shown greatly enhanced resistance to O<sub>2</sub> inactivation. Nevertheless, enzymes have finite lifetimes and must be replaced on the electrode surface if the whole apparatus is not to be discarded. To accomplish this, we are adding electroactive groups on the electrode surface that confer a positive surface charge when oxidized, which promotes binding, and a neutral or negative surface charge when electrochemically reduced, which promotes release. Spent enzymes should therefore be readily replaced without replacement of the derivatized electrode.

Singly and in combinations, we have derivatized ITO and graphite electrodes with quaternary amines, ferrocenes, quinones, pyridinium, nickel and ruthenium complexes, and other functional groups to determine their ability to reversibly bind biological materials. As a test system, intact bacterial cells were bound to the oxidized electrode surfaces where they remained metabolically active in monolayer films. Upon reduction of the electrode, the adsorbed cells were released into an effluent stream in a viable state. Multiple cycles of binding and release could be observed with several of the derivatized electrode surfaces.

On planar, transparent electrodes, monolayer bacterial coverage of the surface could be estimated by microscopic observation or by spectral quantitation of bacteriochlorophyll content from adsorbed photosynthetic bacteria. Microbial binding over the surfaces of the electrodes was found to be somewhat variable. Release of the adsorbed microbes was as high as 98%.

Derivatized graphite particles, stacked in columns, served as high surface area electrodes since the particles were in physical and, therefore, electrical contact with each other. Bacterial adsorption and desorption was monitored by viable cell counts of influent and effluent streams on either side of a 2 cm column of derivatized 0.5 mm graphite particles. Particles co-derivatized with ferrocene and tetracyanoquinone in the oxidized state were able to bind up to 100% of the bacteria in an aqueous stream. Upon reduction

of the electroactive groups, up to 93% of the adsorbed bacteria were released into the effluent. At least ten cycles of bacterial binding and release were observed.

A light addressable polymer was obtained from Itamar Willner that generates a stable carbonium ion when exposed to light of 300-400 nm. Columns containing particles of the polymer were completely competent in binding microbes in suspension from a flowing aqueous stream when the polymer was exposed to actinic light. In darkness, the charge was 80% reversible. However, sufficient surface charge remained to prevent release of the microbes.

## **Future Work**

Additional strains of photosynthetic bacteria capable of using CO, especially those tolerant of O<sub>2</sub>, will be screened for their rates and yields of H<sub>2</sub> production, their durability, and their O<sub>2</sub> resistance. Evolving hydrogenases from the more promising strains will be extracted, purified, and examined again for rates, durability, and O<sub>2</sub> resistance.

Planar and particulate electrodes need to exhibit a more controlled release of the microbes and enzymes from their surfaces. Derivatization of the electrodes with functional groups or combinations of groups that can alternate between net positive and net negative surface charge will be the major focus. Viologen-derivatized surfaces will be examined for hydrogenase binding, orientation, stability, and electron mediation.

## References

- Benemann, J.R., and J.C. Weissman. 1977. *Microbial Energy Conversion*. Pergamon Press: Oxford, pp. 413-426.
- Bolton, J.R. 1977. *Proc. of the 4th International Congress on Photosynthesis*, pp. 621-634.
- Klibanov, A.M., N.O. Kaplan, and M.D. Kamen. 1978. *Proc. Nat. Acad. Sci.*, 75:3640-3643.
- Schultz, J.E., and P.F. Weaver. 1982. *J. Bacteriol.*, 149:181-190.
- Schultz, J.E., J.W. Gotto, P.F. Weaver, and D.C. Yoch. 1985. *J. Bacteriol.*, 162:1322-1324.
- Uffen, R.L. 1976. *Proc. Nat. Acad. Sci.*, 73:3298-3302.
- Weaver, P.F., J.D. Wall, and H. Gest. 1975. *Arch. Microbiol.*, 105:207-216.
- Weaver, P.F., S. Lien, and M. Seibert. 1980. *Solar Energy*, 24:3-45.



# **BIOLOGICAL HYDROGEN PHOTOPRODUCTION (TASK B)**

**Akira Mitsui**

Professor, Division of Marine Biology and Fisheries  
Director, International Research Center  
for Biological Hydrogen Photoproduction  
Rosenstiel School of Marine and Atmospheric Science  
University of Miami  
4600 Rickenbacker Causeway, Miami, Florida 33140

## **Abstract**

In order to achieve long-term and high rates of hydrogen photoproduction in the unicellular, aerobic, nitrogen-fixing cyanobacteria, *Synechococcus* sp. strain Miami BG043511, cyanobacterial cells were immobilized in agar. Synchronously grown high density cells were obtained by immobilizing the cells in an agar matrix, by examining various culture conditions, and by changing dark and light periods. Continuously high rates of hydrogen photoproduction were obtained for three weeks by inserting photosynthetic periods during incubation. The data indicates that biological hydrogen photoproduction research has progressed one step further toward practical applications.

## **Introduction**

The marine nitrogen fixing unicellular cyanobacterium, *Synechococcus* sp. Miami BG 043511 produces the highest amount of hydrogen among green algae and cyanobacteria (Mitsui et al., 1983, 1985; Mitsui 1992). This *Synechococcus* sp. has unique characteristics. It is amenable to synchronous growth under nitrogen fixing conditions (Mitsui et al. 1986, 1987) and produces hydrogen under extremely high concentrations of oxygen (Mitsui 1992, also see last year's progress report). Using this cyanobacterial strain, significant progress was made toward the enhancement of hydrogen photoproduction in the past

several years. In the 4th year's project, our efforts were concentrated on hydrogen photoproduction using immobilized cells of this strain. The technique of immobilizing cells has been used to obtain higher and longer-term production in many kinds of cells and enzymes. Generally immobilized cells remain alive for a longer time than free cells and sometimes they have resistance characteristics for stressful conditions during hydrogen production. The filamentous nitrogen-fixing cyanobacterium, *Oscillatoria* sp. Miami BG 7 produced higher amounts of hydrogen and for longer periods of time in immobilized cells than in free cells (Phlips and Mitsui 1986). These immobilized cells produced hydrogen for more than 1 month in outdoor systems.

Experiments using immobilized cells of *Synechococcus* sp. Miami BG 043511 were carried out to observe long-term and stable hydrogen production. As reported previously, an innovative synchronous culture technique (Mitsui et al. 1986, Mitsui et al. 1987) resulted in high hydrogen production by *Synechococcus* sp. Miami BG 043511 (Suda et al. 1992). The synchronously grown cells of this strain were used for immobilization.

This report consists of two parts; the first part is about the hydrogen production by immobilized synchronously grown cells. The second is about the optimization of immobilized synchronous culture for prolonged and high rates hydrogen photoproduction.

## **Results and Discussion**

### **I. Hydrogen Production by Immobilized Synchronously Grown Cells**

#### ***I-1. The Hydrogen Production By Immobilized Synchronously Grown Cells In Agar and Alginate***

*Synechococcus* sp. Miami BG 043511 was precultured in 3 liter culture cylinders at 150 $\mu$ E/m<sup>2</sup>/s light intensity and 30°C in A-N medium (Kumazawa and Mitsui 1981) in which nitrogen compounds have been eliminated and 4% CO<sub>2</sub> enriched air was bubbled from the bottom of the cylinder (Mitsui and Cao 1988). The culture was pretreated with 16 hr. dark and 16 hr. light and 16 hr. dark periods. Then the synchronous culture was subjected to continuous illumination for 10 hr.

The synchronous cells were harvested, washed and resuspended in the medium (modified A-N medium). Dissolved agar (Difco) solution (3% in the medium) was mixed with the cell suspension at the same volume as the cell suspension, after the temperature of the agar solution dropped to below 40°C. The mixture was then cut into rectangular pieces (approximately 2-3 mm per side). The cyanobacterial agar immobilized cubes were washed once with medium and transferred into vessels.

Alternatively, sodium alginate was mixed to a final concentration of 4% with the phosphate free A-N medium. The cell suspension was prepared in the same way using the phosphate free A-N medium, and the alginate solution was mixed with the same volume of cell suspension. The mixture was dropped into 0.5M calcium chloride solution through a needle while stirring and kept for 30 min. The beads were collected and washed with medium and transferred into the reaction vessels.

The reaction vessels (25ml Fernback flasks) containing 5g (gel) of immobilized cells (beads or

cubes) and 5 ml of A-N medium without sodium bicarbonate were plugged with rubber stoppers and the inside gas was replaced with argon. Vessels were then incubated under continuous light at 30°C. The produced hydrogen and oxygen were sampled in certain intervals during incubation and quantified by gas chromatography (Kumazawa and Mitsui 1981).

Fig. 1 shows hydrogen production by agar immobilized cells, calcium alginate immobilized cells and free cells at 150  $\mu\text{E}/\text{m}^2/\text{s}$  light intensity under shaking conditions. As mentioned above, the 10 hr. cells which were grown synchronously, were subjected to immobilization. As compared with the free cells, the agar immobilized cells produced significantly higher amounts of hydrogen for longer periods. In both the free cells and the calcium alginate immobilized cells, hydrogen production stopped around 30-40 hr.

Fig. 2 shows that hydrogen production by agar immobilized cells lasted 200 hr. without additional treatment. The production of hydrogen and oxygen were temporally separated and each gas was produced stepwise. This tendency was also observed in immobilized cells which have a chlorophyll concentration that is 10 times lower (Fig. 3) even though the total hydrogen production was lower. However if the hydrogen production is compared with chlorophyll base at 200 hr. incubation, 200 ml hydrogen/mg chl was produced at a low chl. concentration, whereas 72 ml hydrogen/mg chl. was produced at a high chl. concentration.

### ***I-2. Effect of the Cell Density (Chlorophyll Concentration) on Hydrogen Production by Agar Immobilized Cells***

In the free cells, the optimum chlorophyll concentration for hydrogen production was 0.8-1.0 mg chl./ml cell suspension at 1000  $\mu\text{E}/\text{m}^2/\text{s}$  of light intensity (Mitsui 1992, also see last year's annual report). The effect of chlorophyll concentration in the cells on hydrogen production was examined at up to 0.8 mg chl./ml immobilized cells. Fig. 4 shows hydrogen production by the different chlorophyll concentrations of the immobilized cells after 75 hr incubation at 1000  $\mu\text{E}/\text{m}^2/\text{s}$  under shaking condition. The immobilized cells of 0.8 mg/ml concentration produced the highest amount of hydrogen.

### ***I-3. Comparison of Hydrogen Production by Immobilized Cells and Free Cells Under Shaking or Non-Shaking Conditions***

Shaking the cell suspensions remarkably affected the hydrogen production in free cell suspensions (Table 1). The amount of produced hydrogen while shaking was approximately 6 times higher than that without shaking. On the other hand, in the immobilized cells only 1.3 fold difference was observed between shaking and non-shaking (Table 1). Without shaking, free cells easily sunk to the bottom. On the other hand, the cells immobilized in agar are able to keep the same conditions with or without shaking. This characteristic makes it advantageous to use immobilized cells, especially considering the large scale application of hydrogen production in the outdoors.

**Table 1. Hydrogen Production by Immobilized Cells and Free Cells With or Without Shaking**

	Hydrogen Production (ml/5g agar gel)	
	Shaking	non-shaking
Immobilized cells (agar)	26	20
Free Cells	29	5

Hydrogen was measured at 45 hrs. incubation  
3mg immobilized cells and 3ml free cells were in vessels individually.

## II. High Cell Density Synchronous Growth in Agar Matrix and Hydrogen Photoproduction

Although the advantage of using immobilized cells was shown in Part I, the system needs high free cell biomass for immobilization for the production of high amounts of hydrogen. But if the cells can grow synchronously in an agar matrix at high concentrations, there will be significant advantages for the application of hydrogen photoproduction.

### II-1. Preparation of Immobilized Cell Synchronous Culture

To optimize the conditions of growth of immobilized cells in agar, several factors were examined. At first, the agar concentration and salinity were investigated.

It was found that the cells immobilized in 0.9% and 1.8% agar grew well. In combinations of salinity and agar concentration, the cells immobilized in 0.9% NaCl and 1.5% agar concentration grew more rapidly than those at other salinity-agar concentration combinations.

Secondly, the effect of light intensity on growth of the immobilized cells was studied at 70-400  $\mu\text{E}/\text{m}^2/\text{s}$  of light intensity. The cells grew rapidly at the light intensity of 200-150  $\mu\text{E}/\text{m}^2/\text{s}$ . Under the higher light intensities, changes in cell color and damage to the cells was observed. Fig. 5 showed a microphotograph of section of the immobilized cells in agar matrix after 3 days of cultivation (A) and 7 days of cultivation (B). The cells began to grow and formed colonies. After one week many colonies were observed near the surface area of the agar matrix.

To obtain well synchronized immobilized cells in agar, the effects of pretreatments with various time combinations of light and dark periods were examined. At 2 hour intervals, nitrogenase activity was measured as an indicator of synchronous growth. The method of nitrogenase activity assay was described previously (Mitsui and Kumazawa 1988). Fig. 6 shows the pattern of nitrogenase activities with various

light-dark cycle pretreatments. The three different pretreatment cycles, 18 hr D/6 hr L, 12 hr D/12 hr L and 6 hr D/18 hr L, basically resulted in a similar tendency of the nitrogenase activity appearance after onset of continuous illumination. One major peak appeared in a 24 hr period. In some cases, one peak broke down into two peaks. It seemed that there were two different groups of synchronously grown cells in these cases. As compared with these three different culture cycles, the 12 hr D/12 hr L treated culture was better synchronized and had higher nitrogenase activity. These results were confirmed in repeated experiments.

Previous studies of synchronous cultures using free cell suspensions indicated that the cells were well synchronized when 16 hr D/16 hr L cycle was introduced (Mitsui et al. 1987). 16 hr D/16 hr L cycles were also introduced to the immobilized cell cultures. Fig. 7 shows the variation of nitrogenase activity with time. Two groups of synchronously grown cells appeared in 24 hr intervals. Therefore 12 hr D/12 hr L cycles was a better conditioning for the synchronization of immobilized cells.

### ***II-2. Effect of CO<sub>2</sub> and Bicarbonate on the Immobilized Cell Growth in Agar and Immobilized Synchronous Growth***

To obtain higher hydrogen production (higher nitrogenase activity), synchronously grown higher cell biomass in agar was needed. Therefore, the effect of CO<sub>2</sub> and bicarbonate on higher yields of immobilized cell biomass was tested in several different experimental conditions as follow:

- 1) sodium bicarbonate (2.5g/l) was included in growth medium.
- 2) sodium bicarbonate (2.5g/l) was included in agar matrix.
- 3) aeration gas, 4% carbon dioxide in air was bubbled during culture.

Fig. 8 shows the chlorophyll concentration in agar (immobilized cell biomass) under various conditions after 9 days culture. The best conditions for obtaining higher chlorophyll concentrations (cell biomass) was using sodium bicarbonate in the medium and aeration of 4% CO<sub>2</sub> enriched air. Compared with the control (without sodium bicarbonate in the medium and without CO<sub>2</sub> bubbling), a 2.5 times higher biomass (chl.) was obtained. The pH seemed to be an important factor for growth. The pH was kept at about 7-8 in the medium including sodium bicarbonate with 4% CO<sub>2</sub> enriched air, and the cells grew continuously. But in the case of sodium bicarbonate with air bubbling, the pH reached about 10-11 and growth stopped.

Synchronous cultures were then induced by 12 hr D/12 hr L cycles in the medium including sodium bicarbonate with 4% CO<sub>2</sub> enriched air.

### ***II-3. Hydrogen Photoproduction by Immobilized Cells Grown Synchronously in Bicarbonate Enriched Medium and CO<sub>2</sub> Bubbling***

The immobilized cells were grown under light that gradually increased in intensity by increments of 500  $\mu\text{E}/\text{m}^2/\text{s}$  to avoid damage from switching to high light intensity. A 12 hr D/12 hr L cycle was then introduced and hydrogen production was carried out at 500  $\mu\text{E}/\text{m}^2/\text{s}$  using these immobilized cells. Fig. 9 shows hydrogen production by synchronously grown immobilized cells, which had low and high nitrogenase activity. The immobilized cells having high nitrogenase activity exhibited higher hydrogen production.

### ***II-4. Long-Term Hydrogen Production by Immobilized Cells***

It was previously shown in free cell experiments (Suda et al. 1992, also see last year's report) that hydrogen production stopped when cellular carbohydrate was consumed. Although measurement of

carbohydrate content in agar immobilized cells is not measured because of the technical difficulties, the results in free cells can be applied to the immobilized cells. It was assumed that the insertion of photosynthetic periods at the time of cellular carbohydrate consumption may produce hydrogen again. This assumption proved to be true as shown in Fig. 10. The immobilized cells were prepared as described in the previous section and hydrogen production was carried out at  $500 \mu\text{E}/\text{m}^2/\text{s}$ . When hydrogen production stopped, the photosynthetic periods were introduced by bubbling with 4%  $\text{CO}_2$  enriched air in freshly prepared culture medium. As compared with the control which lacked a photosynthetic period, the immobilized cells with introduced photosynthetic periods (6 or 48 hr.) produced significantly higher amounts of hydrogen (Fig. 10). Both of them produced hydrogen for more than two weeks after the introduction of two photosynthetic processes. This data also indicates that the length of the inserted photosynthetic period seems to be sufficient at 6 hr.

After the immobilized cells produced hydrogen for more than 2 weeks, one additional period of photosynthesis was inserted and the hydrogen and oxygen was measured. As shown in Fig. 11, the immobilized cells maintained the ability of hydrogen and oxygen photoproduction for several additional days. On the other hand, without the insertion of a photosynthetic period, gas flushing (exchange to argon) or medium exchange (gas phase also exchanged) after the cessation of hydrogen production were not effective for additional hydrogen photoproduction (Fig. 12). These results indicate that no element was exhausted in medium and produced oxygen did not inhibit production of hydrogen. This strain has an especially high resistance to oxygen during hydrogen production (Mitsui 1992, also see last year's report).

These results clearly indicate that the insertion of a short term photosynthetic process into the hydrogen photoproduction process extended the period of hydrogen production over long time periods.

### **Proposed Future Work**

Biological hydrogen photoproduction systems have unique characteristics among other hydrogen production systems.

1) Hydrogen can be produced by solar energy, seawater (water), and photosynthetic microorganisms under ambient temperature and atmospheric pressure.

2) In contrast to non-living hydrogen production systems, biological hydrogen production does not need new materials, the living cells multiply themselves, and are a renewable source of hydrogen.

3) Hydrogen is produced directly from water, so that the loss of conversion efficiency that usually occurs in other indirect hydrogen photoproduction can be avoided.

These living organisms, however, have very complex systems physiologically, biochemically, and genetically, and controlling the complex metabolism involved in enhancing hydrogen photoproduction is difficult. Therefore, projects dealing with living organisms need more time, and more laborious efforts than those of non-living systems.

This marine aerobic nitrogen fixing unicellular cyanobacterium *Synechococcus* sp. Miami BG 043511 has remarkable characteristics regarding hydrogen photoproduction as was mentioned previously.

Laborious study in this laboratory for several years on the enhancement of hydrogen photoproduction resulted in this cyanobacterial strain, which produces hydrogen several orders of magnitude higher than green algae and cyanobacterial strains which were studied in other laboratories. Hydrogen photoproduction in closed vessels terminated within a few seconds in green algae, and a few hours in cyanobacteria as was shown in other laboratories and this laboratory.

Our cyanobacterial strain, *Synechococcus* sp. produced large quantities of hydrogen for more than 2 weeks. Thus, this cyanobacterial strain has a high potential for the development of biological hydrogen photoproduction.

Future studies will include: 1) the further improvement of longer term and higher hydrogen photoproduction will be made under the conditions equivalent to sunlight's high radiation using both free cells and immobilized cells of this strain.

2) The results of this laboratory's studies will be applied under sun light conditions, and hydrogen production per unit of light received per area, and per unit of cell volume will be measured. The economic feasibility of this system will be evaluated.

Another important issue is the solar energy conversion efficiency for hydrogen production. A 10% solar energy conversion efficiency in any hydrogen producing strain of green algae and cyanobacteria was easily obtainable, but only for very short time periods. For practical use, however, obtaining a high solar energy conversion efficiency for long periods of time is needed, such as days or weeks.

For this purpose: 1) A facility for the measurement of solar energy conversion efficiency using high light intensities equivalent to sunlight will be constructed.

2) The solar energy conversion efficiency will be measured under various environmental conditions such as light intensity, temperature and salinity.

3) The optimum conditions for high solar energy conversion efficiency obtained in the laboratory will be applied to outdoor experiments and the solar energy conversion efficiency will be measured on a daily and weekly basis.

4) The solar energy conversion efficiency obtained in this strain in the above studies will be compared with those of other non-biological hydrogen production systems. The advantages and disadvantages of this biological hydrogen production system will be evaluated.

5) Further enhancement of solar energy conversion efficiency will be made by environmental optimization and genetic engineering. Enzymes involved in hydrogen photoproduction will be replaced by more efficient molecules.

6) The economical feasibility of this biological hydrogen photoproduction system will be evaluated.

7) If this biological system is economically feasible, an experimental pilot plant will be designed and further experiments will be carried out.

## Concluding Remarks and Acknowledgments

The aerobic nitrogen-fixing unicellular cyanobacterium Miami BG043511 is the greatest hydrogen photoproducer among green algae and cyanobacteria. As was described above, one further step toward the practical application of biological hydrogen photoproduction was achieved during the fourth year's study, by immobilizing and synchronizing the cells of this strain, and inserting photosynthetic processes during incubation. Although the fourth year's study of this project was previously approved by DOE/NREL, internal University of Miami budget distribution problems caused severe budget reduction in this project, which made impossible to achieve the highly experimentally oriented goals of the fourth year. (First year's budget - \$107,000, Fourth year's budget - \$68,000). Fortunately, International Research Organizations supplied the major funding of this project. Without these funds, this fourth year's project could not have succeeded at all. The Director of biological hydrogen photoproduction would like to express his sincere gratitude to Dr. Haruko Takeyama, Post-doctoral Fellow, and to Ms. Catherine Campbell, Graduate Student, for their very difficult experimental research, including many overnight experiments, and Ms. C. Campbell, Ms. L. Varela, and Dr. Y. Luo for the preparation of this report and figures.

## References Cited

- Kumazawa, S. and A. Mitsui (1981). Characterization and optimization of hydrogen photoproduction by a saltwater blue-green alga, Oscillatoria sp. Miami BG 7. I. Enhancement through limiting the supply of nitrogen nutrients. *Int. J. Hydrogen Energy* 6: 339-349.
- Kumazawa, S. and A. Mitsui (1992) Photosynthetic activities of a synchronously grown aerobic N<sub>2</sub>-fixing unicellular cyanobacterium, Synechococcus sp. Miami BG 043511. *J. Gen. Microbiol.* 138: 467-472.
- Mitsui, A. (1992). Hydrogen Photoproduction by Marine Cyanobacteria for alternating the carbon energy sources. In: *Short Communication of the 1991 International Marine Biotechnology Conference*. J.C. Hunter Cevera (Ed). Wm. C. Brown Publishers Dubuque, Iowa, Vol. II p 710-723.
- Mitsui, A. and S. Cao (1988). Isolation and culture of marine nitrogen fixing unicellular cyanobacterium Synechococcus. *Methods in Enzymology* 167: 105-113.
- Mitsui, A., E.J. Philips, S. Kumazawa, K.J. Reddy, S. Ramachandran, T. Matsunaga, L. Haynes and H. Ikemoto (1983). Progress in research toward outdoor biological hydrogen production using solar energy, sea water, and marine photosynthetic microorganisms. *Ann. NY Acad. Sci.* 413: 514-530.
- Mitsui, A., S. Cao, A. Takahashi and T. Arai (1987). Growth synchrony and cellular parameters of the unicellular nitrogen-fixing marine cyanobacterium, Synechococcus sp. strain Miami BG 043511 under continuous illumination. *Physiol. Plant.* 69: 1-8.
- Mitsui, A., S. Kumazawa, A. Takahashi, H. Ikemoto, S. Cao and T. Arai (1986). Strategy by which nitrogen-fixing unicellular cyanobacteria grow photoautotrophically. *Nature* 323: 720-722.
- Mitsui, A., S. Kumazawa, E.J. Philips, K.J. Reddy, K. Gill, T. Matsunaga, B.R. Renuka, T. Kusumi, G.



Reyes-Vasques, K. Miyazawa, L. Haynes, H. Ikemoto, E. Duerr, C.L. Leon, D. Rosner, R. SESCO and E. Nioffat (1985). Mass cultivation of algae and photosynthesis bacteria. In *Biotechnology and Bioprocess Engineering* (ed. T.K. Ghose) United India Press, New Delhi, pp. 119-155.

Philips, E.J. and A. Mitsui (1986). Characterization and optimization of hydrogen production by a salt water blue-green alga Oscillatoria sp. Miami BG7. II. Use of immobilization for enhancement of hydrogen production. *Int. J. Hydrogen Energy* 11: 83-139.

Suda, S., S. Kumazawa and A. Mitsui (1992). Change in the H<sub>2</sub> photoproduction capability in a synchronously grown aerobic nitrogen-fixing cyanobacterium, Synechococcus sp. Miami BG 043511. *Arch. Microbiol.* 158: 1-4.

- Fig. 1 Hydrogen production by immobilized and free cells at  $150 \mu\text{E}/\text{m}^2/\text{s}$  of light intensity and  $30^\circ\text{C}$  with shaking. The synchronously grown cells were used for immobilization and free cells.  
 □: Agar immobilized cell.  
 ×: Calcium alginate immobilized cell. ◇: Free cells  
 Each vessel included 5g immobilized cells gel or 5ml of free cells. Chlorophyll concentration was  $825 \mu\text{g chl./vessel}$ .
- Fig. 2 Hydrogen and oxygen production by agar immobilized cells at  $150 \mu\text{E}/\text{m}^2/\text{s}$  of light intensity and  $30^\circ\text{C}$  with shaking. The synchronously grown cells were used for immobilization.  
 □: Hydrogen. +: Oxygen  
 Chlorophyll concentration was  $825 \mu\text{g chl./5g agar gel}$ .
- Fig. 3 Hydrogen and oxygen production by agar immobilized cells at  $150 \mu\text{E}/\text{m}^2/\text{s}$  of light intensity and  $30^\circ\text{C}$  with shaking. The synchronously grown cells were used for immobilization.  
 □: Hydrogen. +: Oxygen  
 Chlorophyll concentration was  $70 \mu\text{g chl./5g agar gel}$ .
- Fig. 4 Hydrogen production by immobilized cells at different chlorophyll concentration at  $1000 \mu\text{E}/\text{m}^2/\text{s}$  of light intensity and  $30^\circ\text{C}$ . with shaking. The synchronously grown cells were used for immobilization. Each vessel included 3g of immobilized cells  
 Chl. concentration was measured after 70hr incubation.
- Fig. 5 Microphotograph of section of immobilized cells  
 (A) The immobilized cells after 3 days cultivation  
 (B) The immobilized cells after 7 days cultivation
- Fig. 6 Change of nitrogenase activity under the various Dark/Light cycles during synchronous growth of immobilized cells at  $150 \mu\text{E}/\text{m}^2/\text{s}$  of light intensity.
- Fig. 7 Change of nitrogenase activity under continuous light after 16Dark/16Light cycles during synchronous growth of immobilized cells at  $150 \mu\text{E}/\text{m}^2/\text{s}$  of light intensity

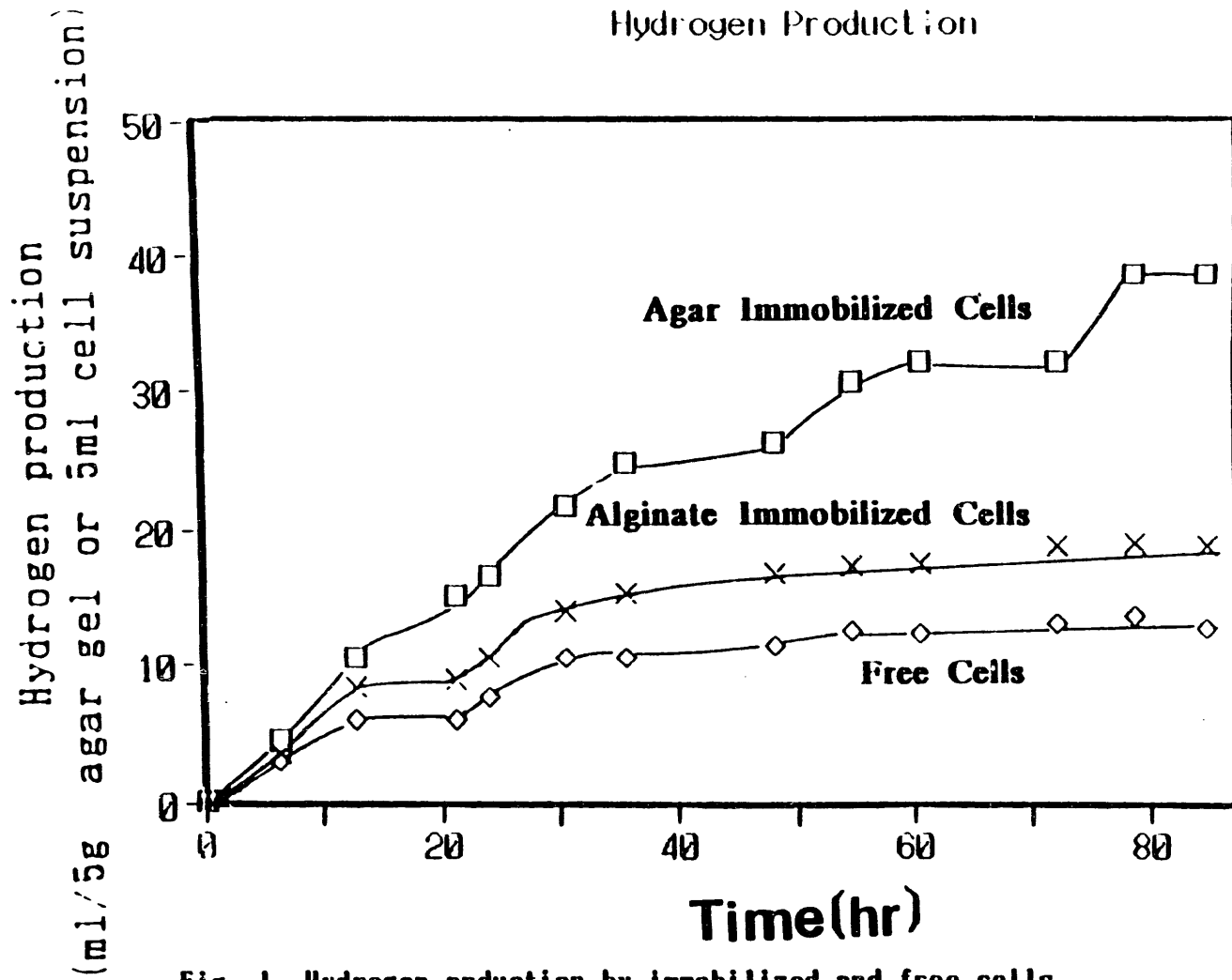


**Fig. 1** Hydrogen production by immobilized and free cells at  $150 \mu\text{E}/\text{m}^2/\text{s}$  of light intensity and  $30^\circ\text{C}$  with shaking. The synchronously grown cells were used for immobilization and free cells.

□: Agar immobilized cell, X: Calcium alginate immobilized cell, ◇: Free cells  
 Each vessel included 5g immobilized cells gel or 5ml of free cells. Chlorophyll concentration was  $825 \mu\text{g chl./vessel}$ .

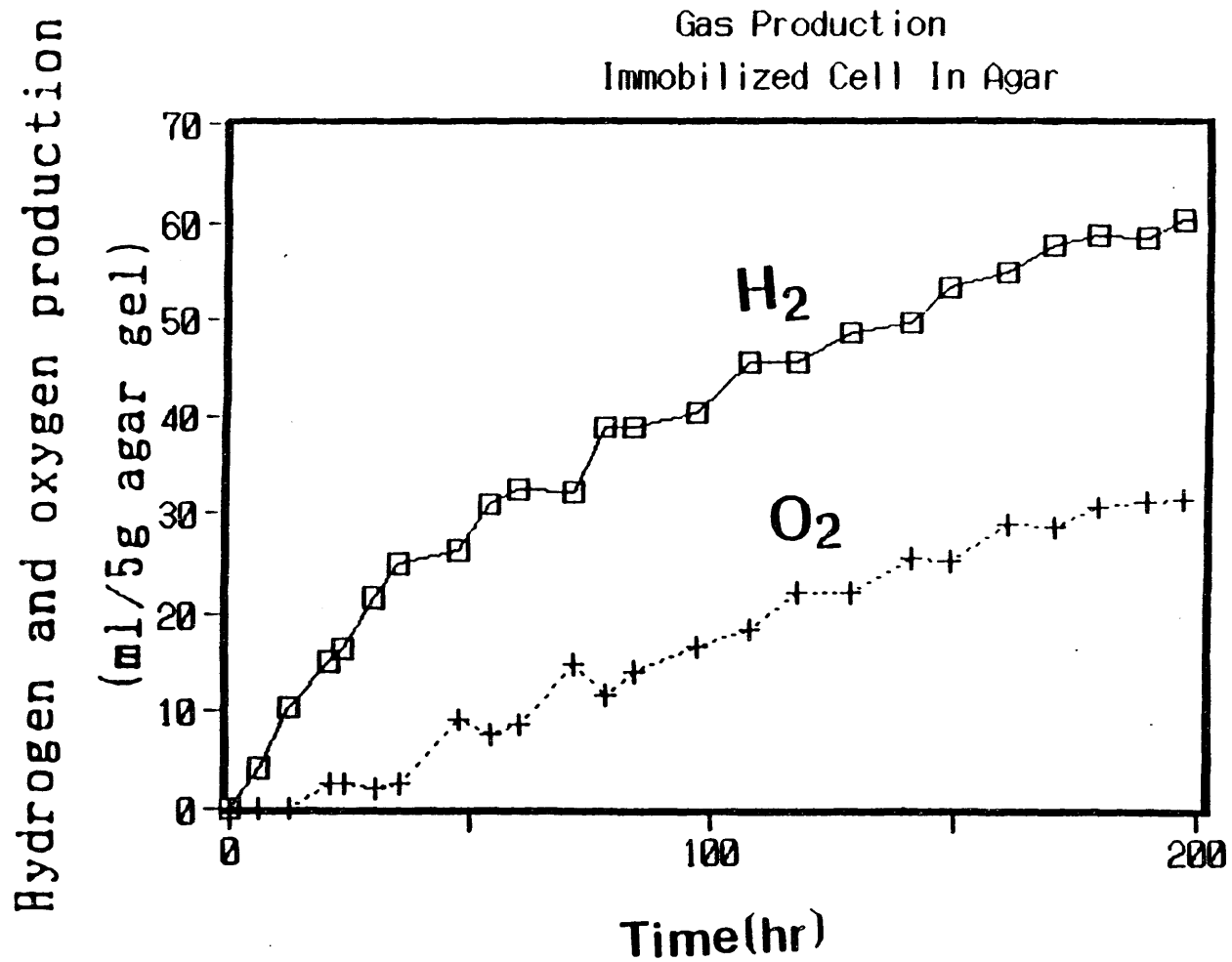


Fig. 2 Hydrogen and oxygen production by agar immobilized cells at  $150 \mu\text{E}/\text{m}^2/\text{s}$  of light intensity and  $30^\circ\text{C}$  with shaking. The synchronously grown cells were used for immobilization.  $\square$ ; Hydrogen,  $+$ ; Oxygen  
Chlorophyll concentration was  $825 \mu\text{g chl.}/5\text{g agar gel}$ .

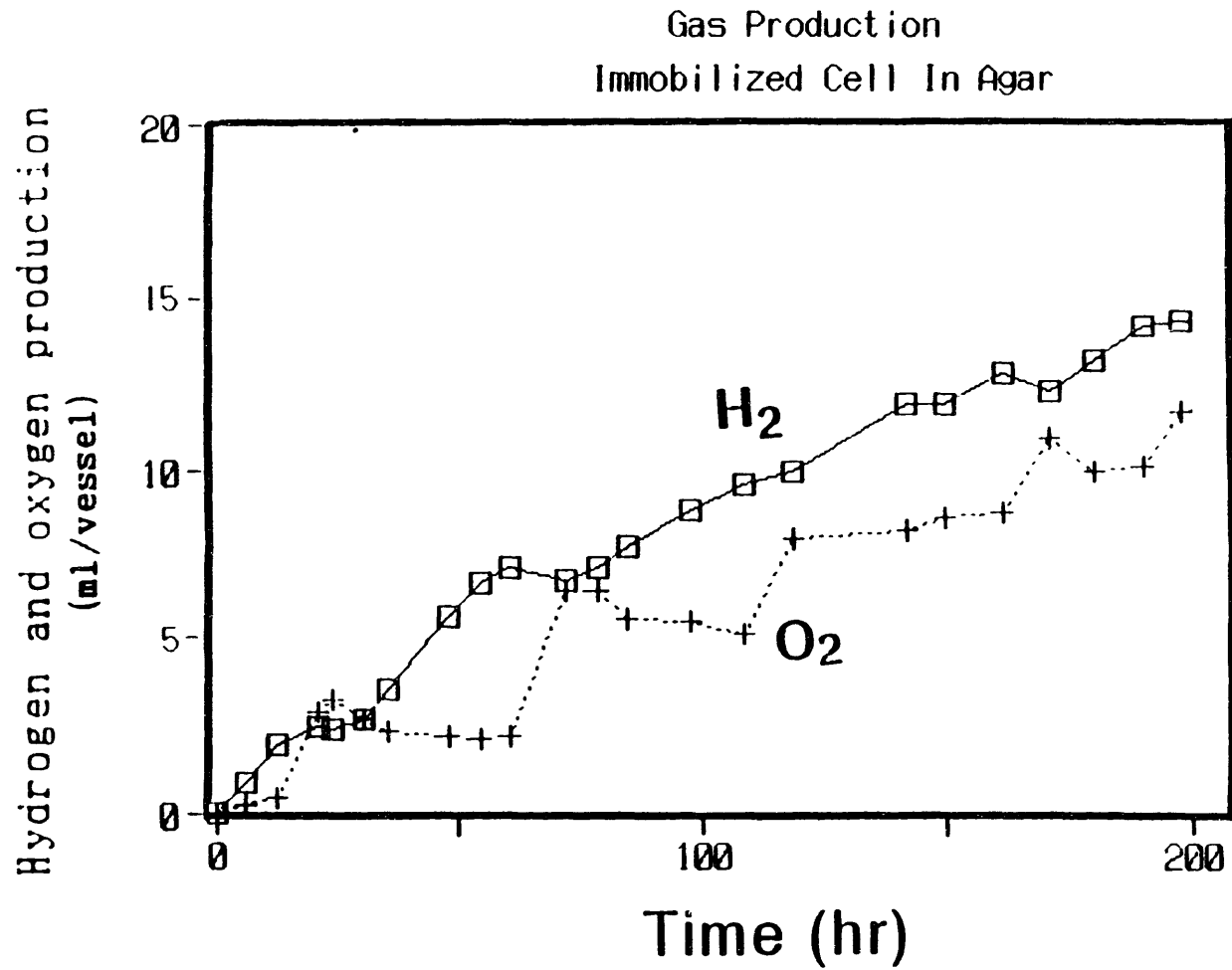
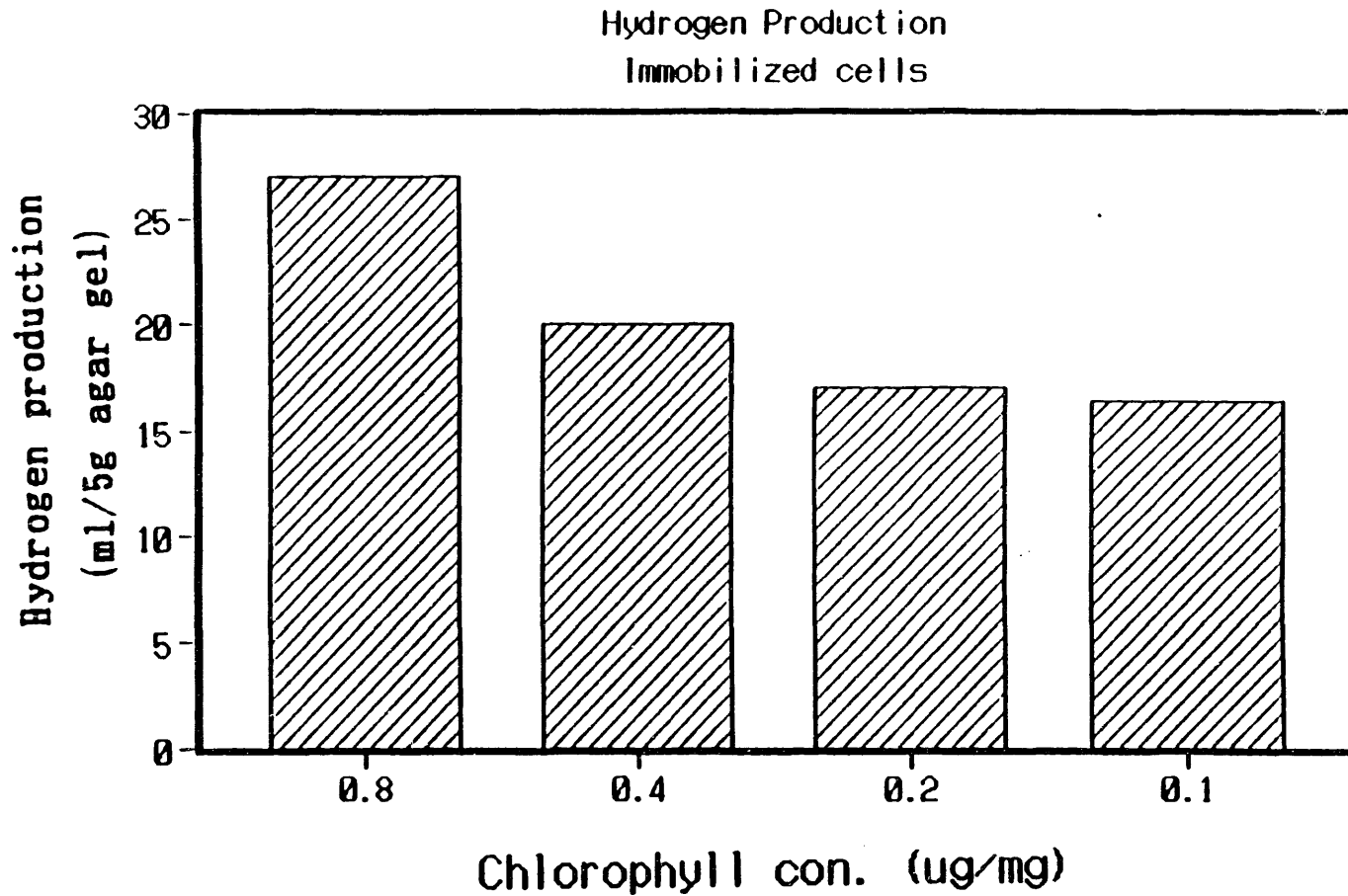


Fig. 3 Hydrogen and oxygen production by agar immobilized cells at  $150 \mu\text{E}/\text{m}^2/\text{s}$  of light intensity and  $30^\circ\text{C}$  with shaking. The synchronously grown cells were used for immobilization.  $\square$ : Hydrogen.  $+$ : Oxygen  
Chlorophyll concentration was  $70 \mu\text{g chl.}/5\text{g agar gel}$ .



**Fig. 4** Hydrogen production by immobilized cells at different chlorophyll concentration at  $1000 \mu\text{E}/\text{m}^2/\text{s}$  of light intensity and  $30^\circ\text{C}$ . with shaking. The synchronously grown cells were used for immobilization. Each vessel included 3g of immobilized cells. Chl. concentration was measured after 70hr incubation.

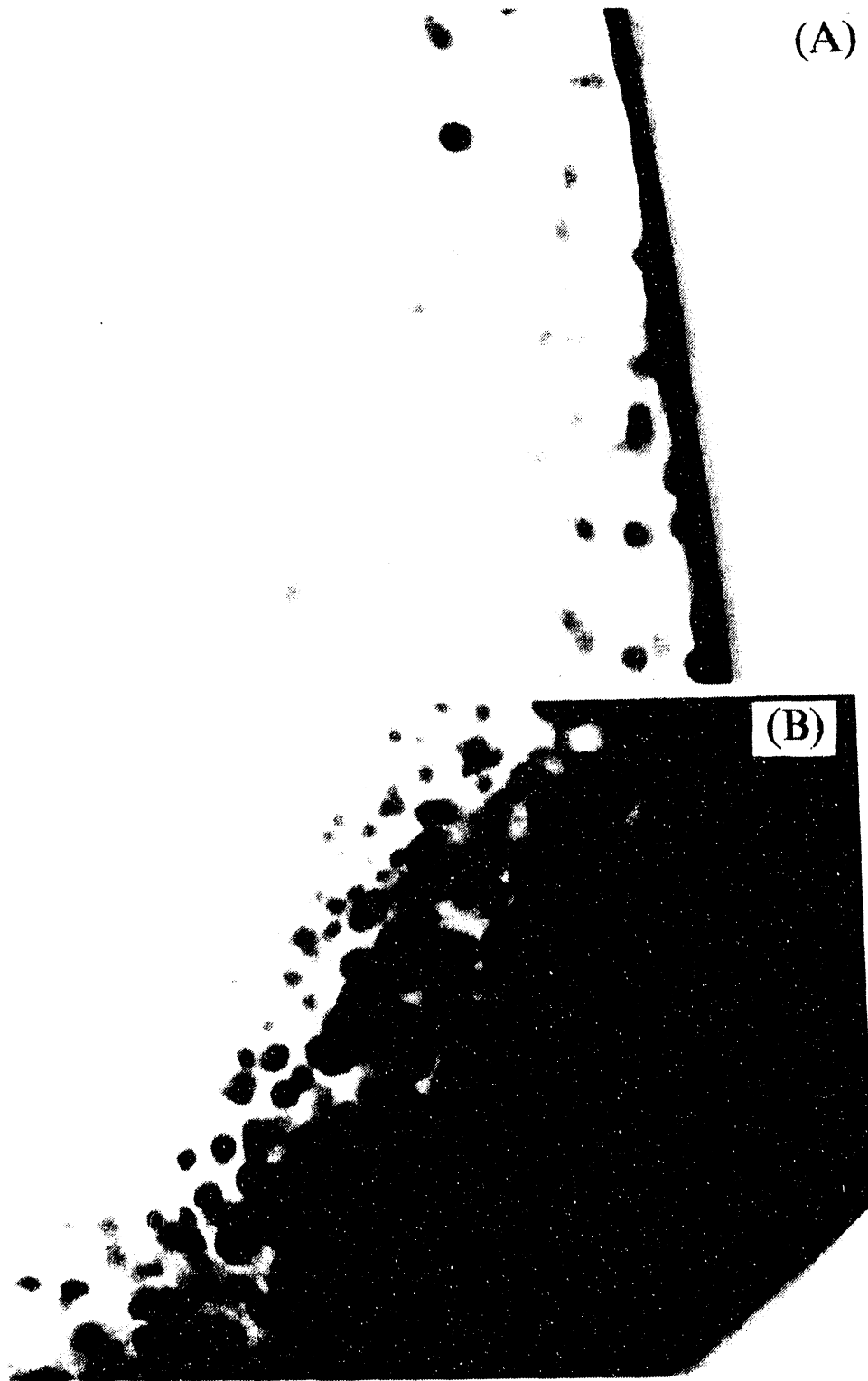


Fig. 5 Microphotograph of section of immobilized cells  
(A) The immobilized cells after 3 days cultivation  
(B) The immobilized cells after 7 days cultivation

Nitrogenase activity  
(nmoles  $C_2H_2$  reduced/g agar gel/hr)

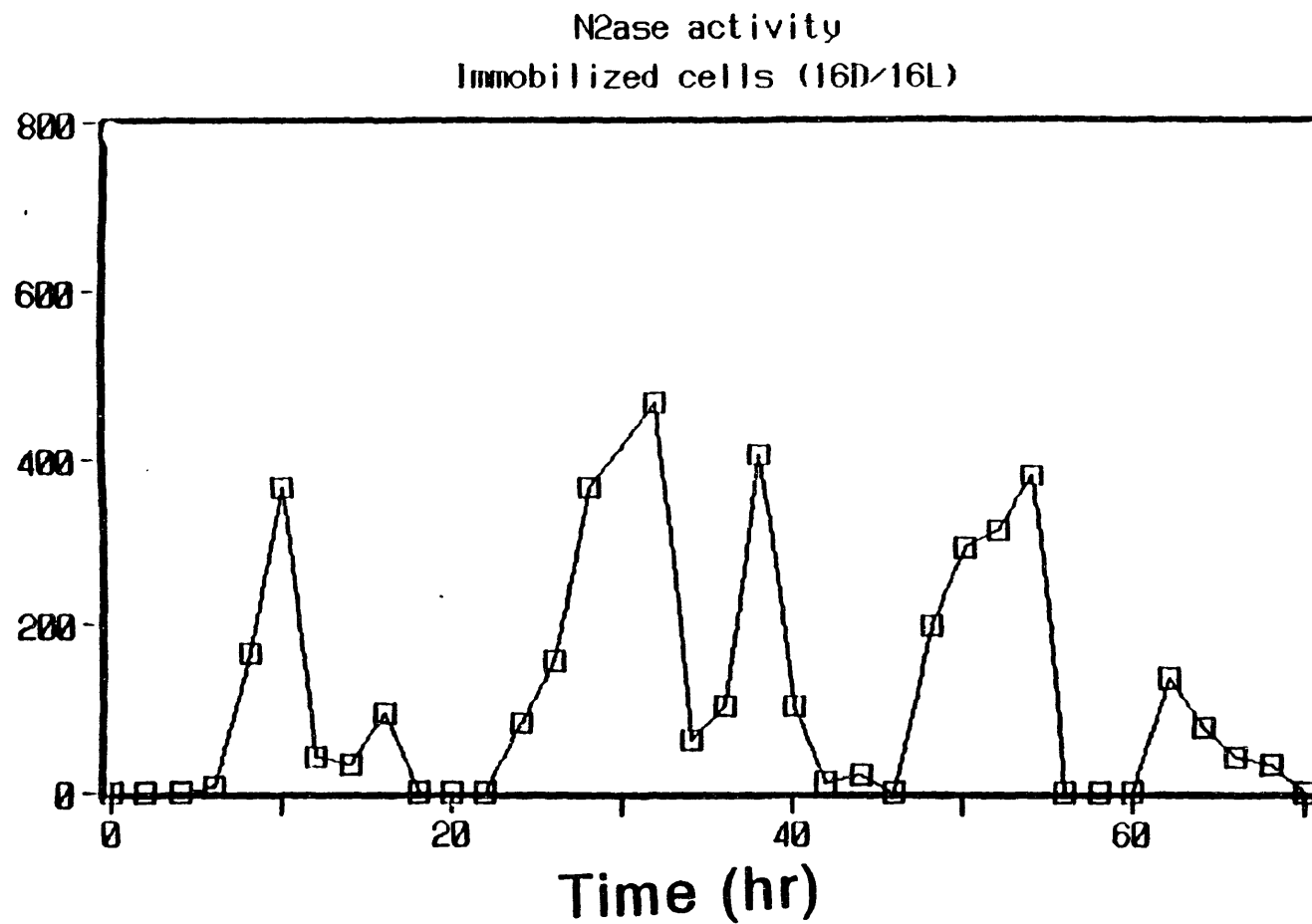


Fig. 7 Change of nitrogenase activity under continuous light after 16Dark/16Light cycles during synchronous growth of immobilized cells at  $150 \mu E/m^2/s$  of light intensity



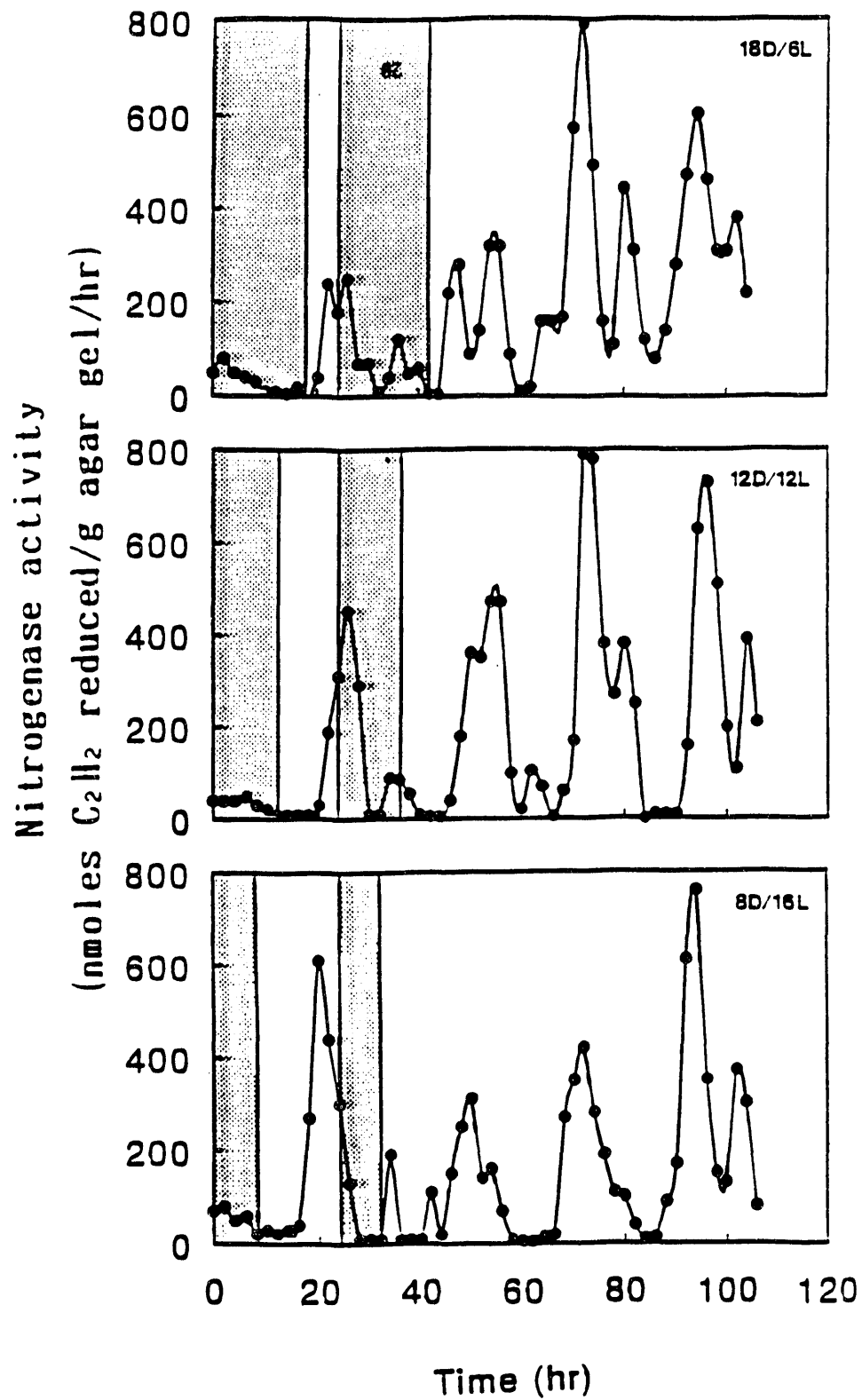


Fig. 6 Change of nitrogenase activity under the various Dark/Light cycles during synchronous growth of immobilized cells at  $150 \mu\text{E}/\text{m}^2/\text{s}$  of light intensity.

Chlorophyll a concentration of immobilized cells  
( $\mu\text{g/g}$  agar gel)

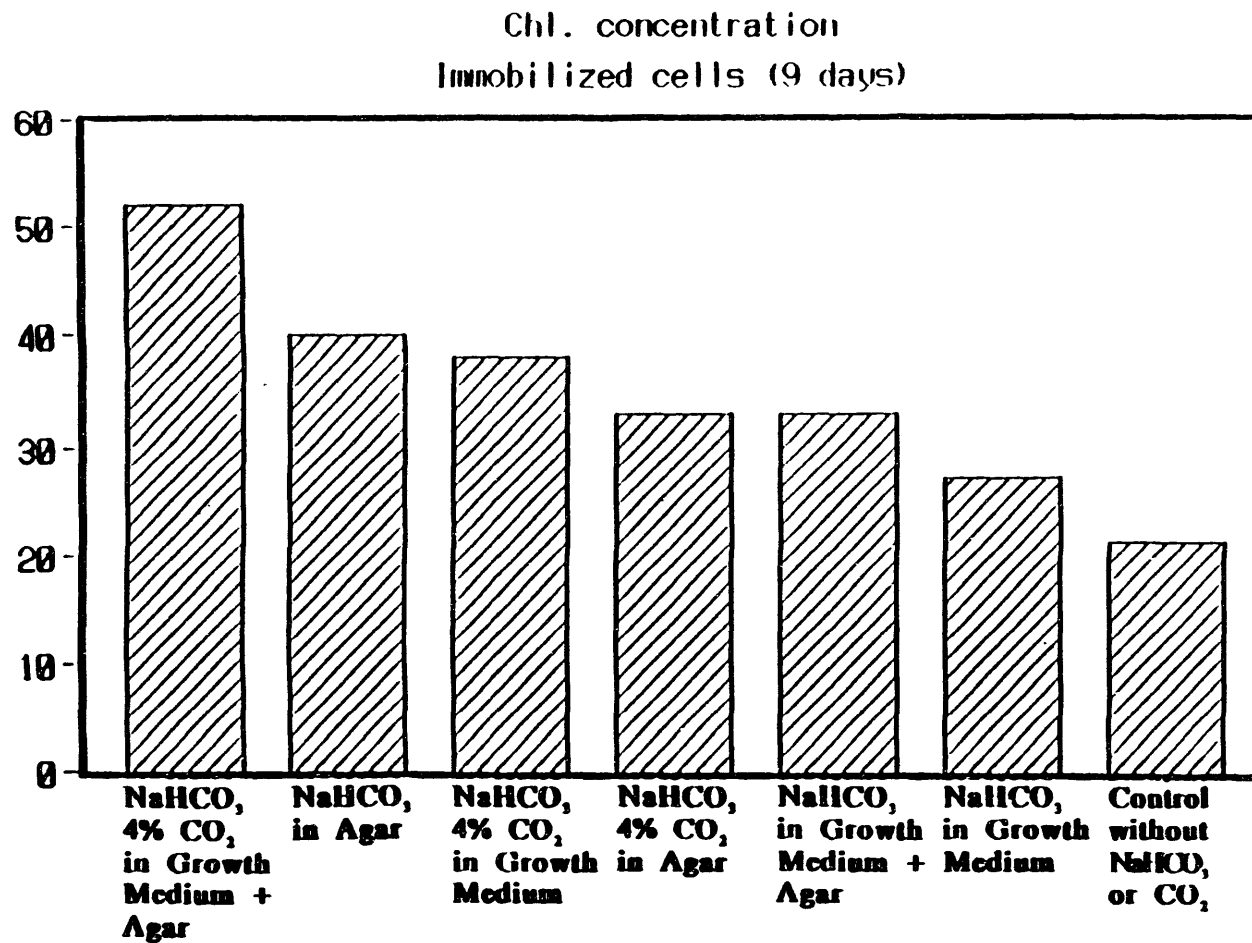


Fig. 8 The growth (chl. concentration) of immobilized cells under various condition at  $150 \mu\text{E}/\text{m}^2/\text{s}$  of light intensity after 9 days culture.

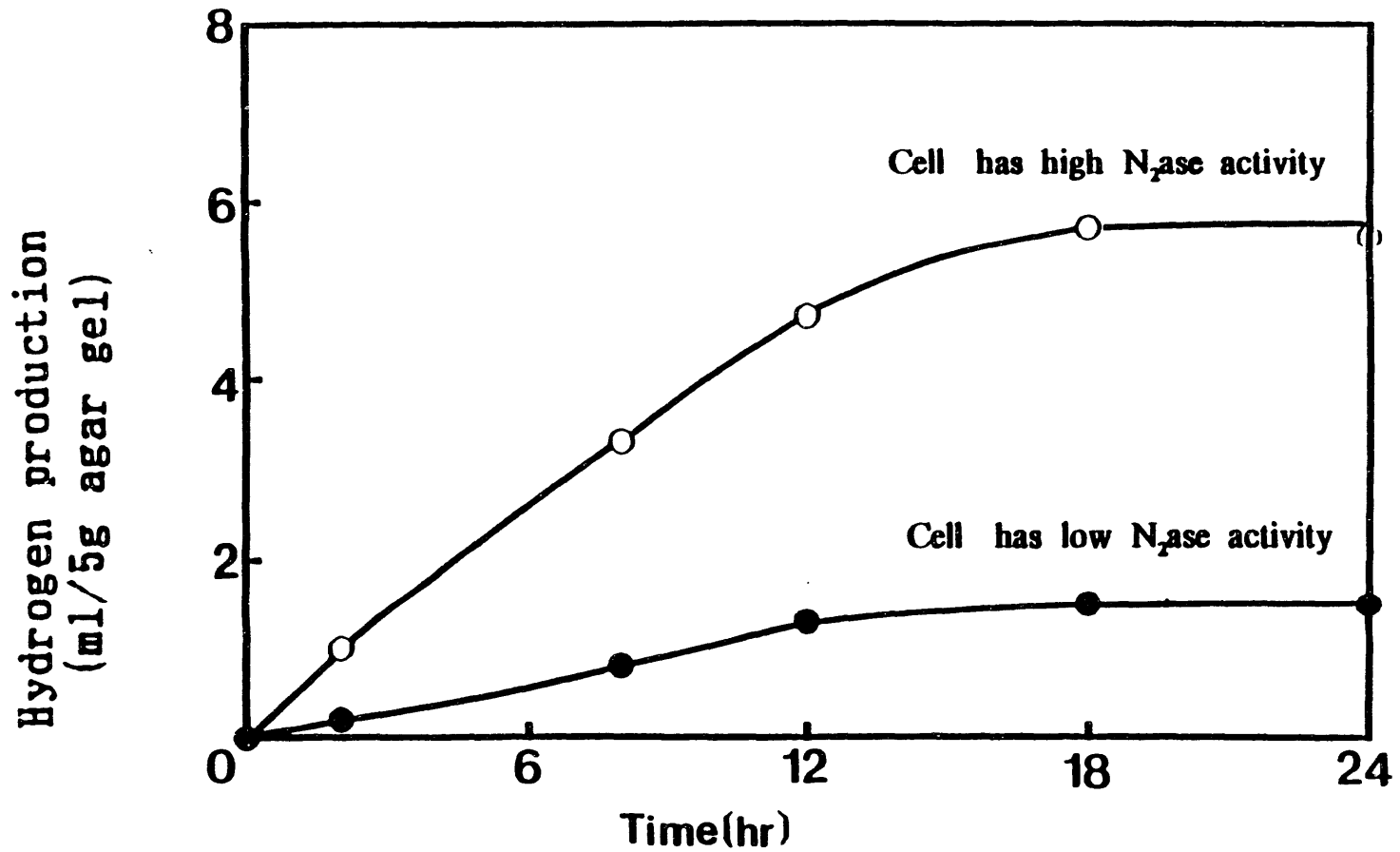


Fig. 9 Hydrogen photoproduction by synchronously grown immobilized cells having different nitrogenase activity at  $500 \mu E/m^2/s$  of light intensity.

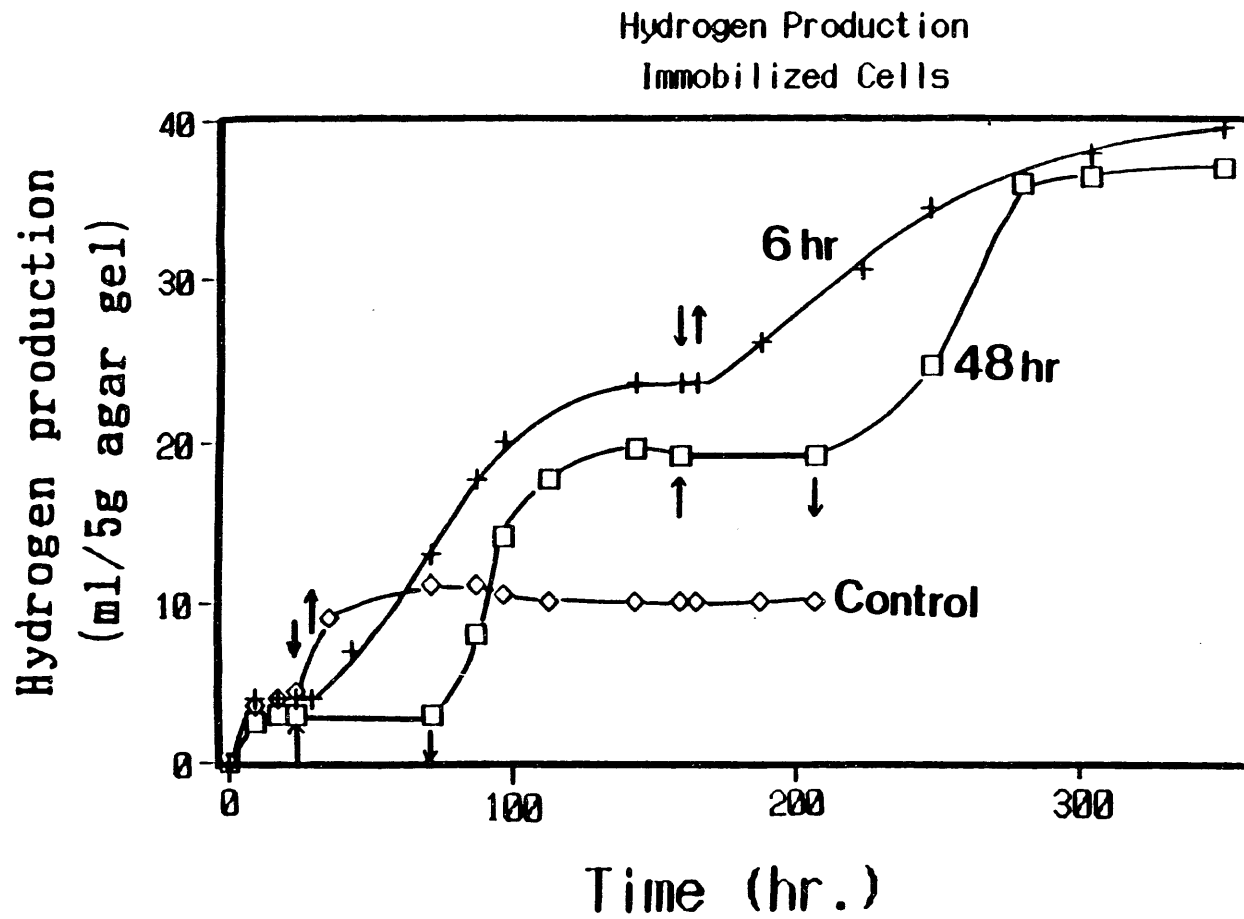


Fig. 10 Hydrogen production by synchronously grown immobilized cells. Arrows show the photosynthesis period (6 or 48 hr.) which was inserted when hydrogen production was stopped.

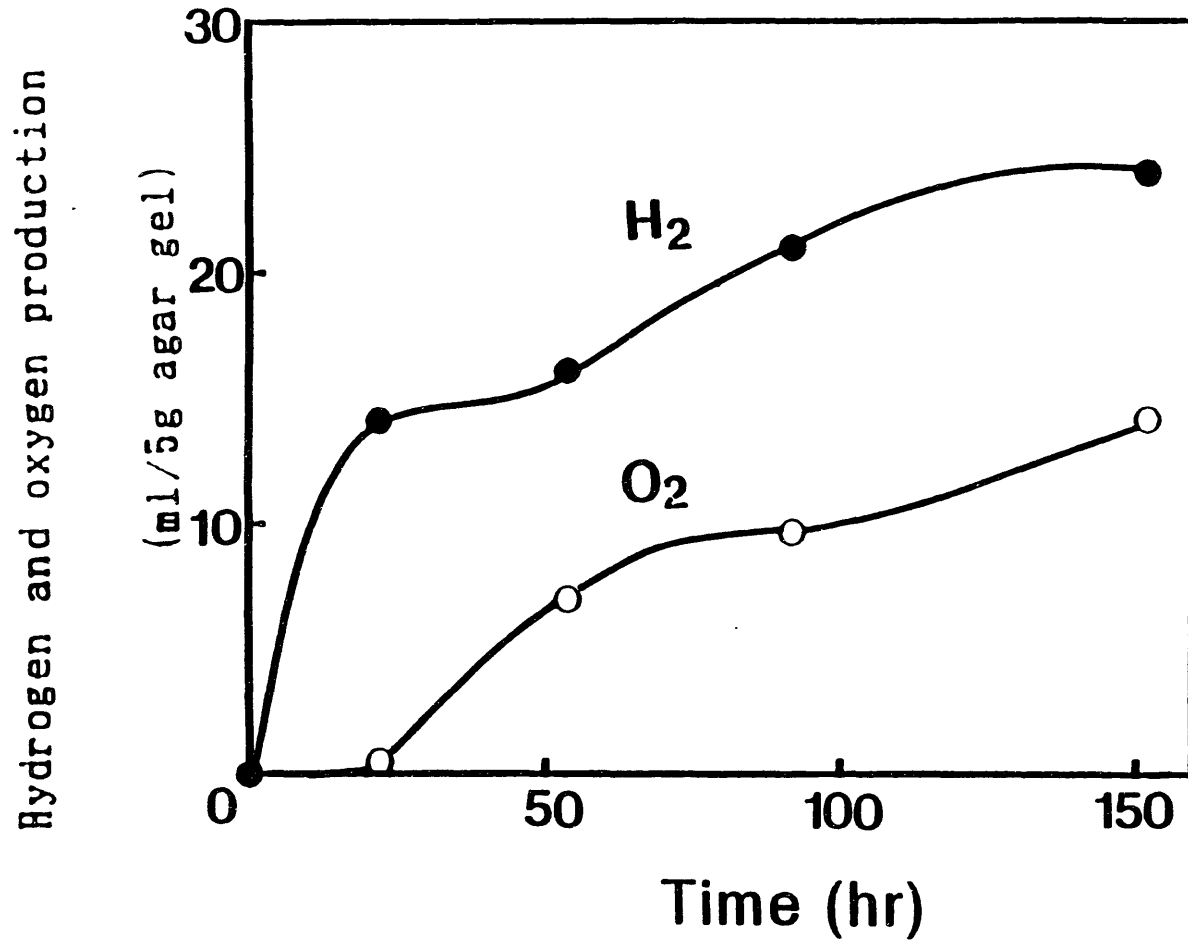


Fig. 11 Hydrogen production by immobilized cells after the insertion of a 3rd photosynthetic period.

Hydrogen Production  
Immobilized Cells

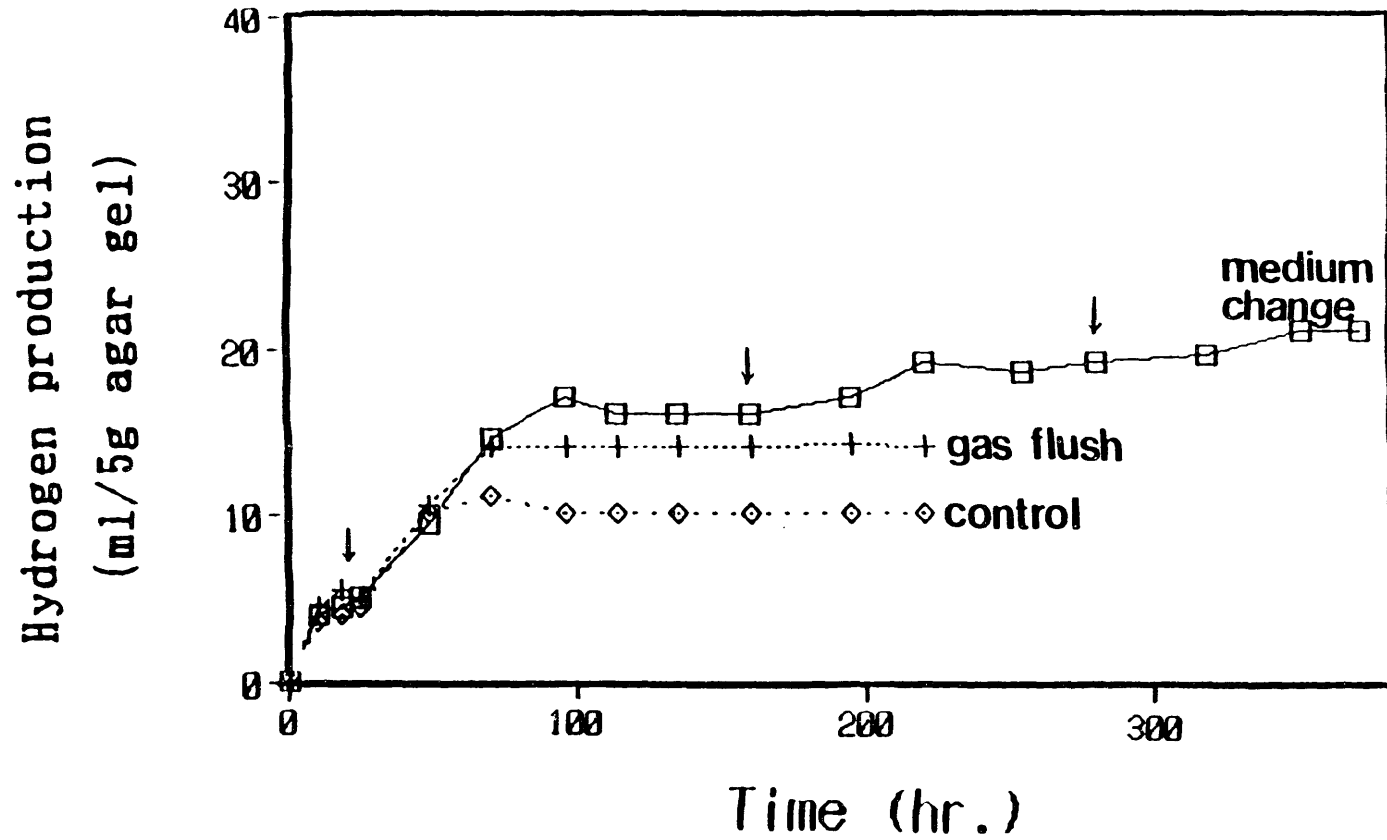


Fig. 12 Hydrogen production by synchronously grown immobilized cells. Arrows show the time of flushing out or medium change.

# PHOTOELECTROCHEMICAL PRODUCTION OF HYDROGEN

Richard E. Rocheleau  
Hawaii Natural Energy Institute  
University of Hawaii  
Honolulu, Hawaii 96822

## Abstract

Semiconductor-based photoelectrochemical cells remain a promising option for the direct production of hydrogen from water using sunlight as the energy source. In this report, we describe an integrated program involving electrode fabrication, characterization, and engineering modeling with the objective to develop high efficiency, amorphous silicon based photoelectrodes. The integrated reactor model developed during the past year quantifies efficiency losses resulting from optical losses, system resistance terms, photodiode behavior, and catalyst properties. Simulations indicate that moderate concentration may be advantageous to the cost effective operation of the photoelectrochemical reactors. Compared to solid state devices, additional efficiency losses arise from the overpotential and mass transfer limitations. Reduction of these losses through optimal catalyst design and reactor operating conditions is both critical and possible.

Photoelectrodes have been fabricated from commercially available triple junction amorphous silicon solar cells. The photoelectrode structure is catalyst/pin/pin/pin/stainless steel. Tests have been conducted with various coatings including indium tin oxide and titanium oxide as well as nickel, titanium, and platinum. Open circuit voltages have been limited to approximately 1.5 volts by a shunt in the electrode which we believe results from cutting the large a-Si sheets as part of our fabrication process. Current densities under anodic bias are in agreement with our model and comparable to those of the solid stated devices.

## INTRODUCTION

### Background

Semiconductor-based photoelectrochemical (PEC) cells remain a promising option for the production of hydrogen from water using sunlight as the primary energy source. In the decades following the report by Fujishima and Honda (1972), that an illuminated n-TiO<sub>2</sub> photoelectrode contributed a significant fraction of the electrical energy needed for the electrolysis of water, there have been numerous activities directed toward the development of photoelectrochemical systems for water electrolysis. The requirements of high voltage, effective surface catalysis, and tendency toward corrosion in aqueous solution places numerous constraints on the choice of materials and electrode configurations (Gerischer 1979, Getoff 1990).

The energetics and voltage requirements associated with the photoelectrolysis processes have been thoroughly summarized by numerous authors (for example Nozik 1978). The minimum voltage required to drive the electrolysis reaction is the free energy for water dissociation (1.23 volts), plus the intrinsic over-potentials associated with the energy levels of the semiconductor and electrolyte acceptor states. The actual operating voltage is even higher due to iR losses from current flow through the semiconductor, electrolyte, and interfaces. For water electrolysis, operating voltages in excess of 1.6 volts are typical. For efficient operation, the semiconductor photoelectrodes must also effectively transfer charge (electrons and/or holes) to the electrolyte at the interface. In practice this involves deposition of a catalyst, usually a group VIII metal or metal-oxide, which effectively reduces electron-hole recombination at the interfaces. Heller (1982 and 1984) has provided two excellent reviews of the chemical processes involved in these systems and has addressed the requirements for high efficiency devices. Even with high quality diode behavior, attaining this voltage at near maximum current requires open circuit voltages greater than 2 volts, a significant impediment on the choice of materials and electrode designs.

In addition to the fundamental limitations imposed by the high voltage requirement, the practical difficulties associated with optimizing system performance where the electrolyte/electrode interface must serve the multiple purposes of barrier formation, semiconductor protection, catalyst, and anti-reflection coating are all too evident in the literature. Given these considerable constraints, more feasible systems are those which utilize classic solid state homo- or hetero-junctions. Solid state barrier formation provides greater flexibility in the photoelectrode design and wider choice of materials to meet the multiple constraints for the catalytic coating. Direct water splitting has been successfully demonstrated in a number of systems utilizing photoelectrodes fabricated from multijunction solar cells (Matsumura 1986, Murphy and Bockris 1984, and Turner 1992) including those based on amorphous silicon (Matsumura 1986 and Lin et. al 1989). While these demonstrations provide irrefutable evidence of the potential for these processes, the stable efficiencies of these systems remain far from optimized. Quantitative analysis of efficiency losses combined with materials and photoelectrode development will significantly advance the performance of this technology and provide additional insights into the fundamental parameters controlling efficiency and stability.

### Objectives

The goal of this on-going subtask of the Hydrogen from Renewable Resources Program is to develop high efficiency, stable, potentially low cost electrodes for the direct photoelectrolysis of water. Specific objectives to meet these goals include: (1) characterization of the electrode/electrolyte interface, (2) identification of efficiency limitations imposed by the reactor and photoelectrode design, and (3)



development of high efficiency photoelectrodes.

### Scope

In order to fulfill these objectives, this task comprises three integrated subtasks: electrode fabrication, photoelectrode characterization, and reactor modeling. In past years, we established significant capability to deposit and characterize viable catalytic materials. Under the current program, these materials are being deposited onto commercially available multijunction amorphous silicon devices to fabricate photoelectrodes for characterization and optimization. Physical and chemical properties of the catalyst including optical properties and stability in various electrolytes are evaluated in our laboratory. Capacitance and potentiodynamic measurements are used to characterize the energy band characteristics near the interface and the intrinsic catalyst activity. Surface analysis techniques can be utilized as appropriate to examine chemical bonding and changes in the materials.

The complex interaction of physical, optical, and electronic effects within a PEC cell requires an operational model and appropriate supportive testing to identify causal relationships in the performance. The development and use of such a quantitative model has been an important part of our effort during the past year. In this report, we describe the development of this model with specific application to the amorphous silicon based system, and progress in the development of high efficiency amorphous silicon photoelectrodes.

## TECHNICAL APPROACH

Our fundamental approach to this effort is to use quantitative loss analysis to guide the fabrication of high efficiency photoelectrodes. The loss analysis developed to date combines and integrated reactor model with detailed equivalent circuit modeling of the photoelectrode to separate and quantify the various optical, electrical, and electrochemical losses. Due to its many promising attributes; flexible design, high voltage, potentially low cost, and commercial availability; multijunction amorphous silicon has been selected for electrode fabrication. Figure 1 shows a simple schematic of a PEC reactor with such a photoelectrode. In contrast to the solid state device connected to an external load, the load of the PEC reactor is integrally linked with the structure of the photoelectrode; being dependent of such characteristics as the intrinsic kinetics (exchange current) of the catalyst and mass transfer in the vicinity of the interface. Potentiodynamic characterization of the photoelectrodes and measurement of hydrogen production rates are analyzed with the models to identify materials and structural limitations. New designs, materials and processes are then developed to eliminate or reduce these losses.

## RESULTS

### Model Development

Figure 2 is a simplified representation of the reactor model developed during the past year. The model is currently operational and is being used to evaluate promising reactor configurations and operating conditions. The optical model uses conventional optics equations with measured or reported materials properties to characterize reflection and absorption losses in the cover, electrolyte, and catalyst. Experiments have been completed to determine the reduction in light transmission caused by gas bubbles in the electrolyte. This loss has been characterized as a function of electrode morphology, hydrogen evolution rate and current density over a wide range of light intensities. An empirical correlation relating the loss to an equivalent gas layer thickness, similar to the void volume used in the literature to

characterize resistive losses (Sides 1986), was developed. With light incident on the anodic side of the photoelectrode, the relatively low current density of the multijunction a-Si devices allows significant concentration (10x) without serious optical losses from the gas.

While the behavior of multijunction amorphous silicon devices can be reasonably fit using a conventional diode equation with a light generation term, such simplification can lead to erroneous characterization of the series resistance losses and is insufficient to determine the effect of changes in the spectral content of the incident light. Accurate characterization of the series resistance is an essential element of our analysis, allowing independent determination of the intrinsic catalyst properties and physical limitation such as mass transfer resistance under real operating conditions. We have addressed this concern by extending our equivalent circuit model to three diodes in series using optical and film properties provided by both Energy Conversion Devices Inc. and Solarex Thin Film Division. The model accurately describes the behavior of single junction devices and is currently being tested for the multijunction application.

The electrochemical components of the model relies on a combination of literature reported values and experimental results. Effects of bulk electrolyte resistivity and geometry are estimated from electrolyte properties and published analysis (Ito et. al. 1990). Our diode analysis (HNEI 1992) has been extended to allow independent determination of the exchange current and physical limitations under real operating conditions. The results from such an analysis are summarized in Figures 3 and 4 for a silicon MIS photocathode. Figure 3 shows the J-V curve of a single crystal silicon MIS diode measured in the solid state at several light intensities and as a photoelectrode. At comparable values of light generated current, the solid state cell and photoelectrode (shifted for theoretical onset potential) exhibit identical open circuit voltages indicating no change in the junction characteristics. However, the series resistance as a photoelectrode is significantly higher leading to low fill factor, and lower efficiency. Although not shown, independent measurements showed this series loss to be approximately 4 times that of a bulk Pt cathode as well. Figure 4 shows the low current behavior photoelectrode in a conventional Tafel plot along with data from the bulk platinum electrode. This figure shows that the exchange current  $i_0$  and Tafel slope are quite comparable for the two forms of the catalyst. The limiting behavior appears to be a mass transfer limitation at the higher current regime which we attribute to deactivation of a portion of the thin film catalyst. Our laboratory apparatus and analysis has been modified to carry out similar analysis on the a-Si based photoelectrodes when measured relative to a reference electrode. We anticipate initial results shortly for these systems.

### **Amorphous silicon photoelectrodes**

Photoelectrodes have been fabricated from high efficiency triple junction amorphous silicon solar cells on stainless steel provided by ECD Inc. Samples both with and without a transparent indium tin oxide (ITO) antireflection and top contact layer were processed for comparison. The performance characteristics of the as received samples with ITO were :  $V_{oc} = 2.38$  volts,  $J_{sc} = 6.65$  mA/cm<sup>2</sup>, and  $FF = 0.64$  for a net electrical efficiency of slightly over 10% under AM1 conditions. The as received samples were approximately 10cm by 20cm. Photoelectrodes ranging in size from 1cm x 1cm to 5cm x 5 cm were fabricated by cutting coupons from these samples. Based on the ease of deposition and previous experience, Ni, Ti and Pt films were selected for evaluation in these initial tests. Thin films of these catalytic metals were tested in both H<sub>2</sub>SO<sub>4</sub> and NaOH electrolyte for their oxygen evolution characteristics. Based on overpotential and stability, Ni and Ti in NaOH were selected for testing as catalytic films on the a-Si. Photoelectrodes were fabricated by vacuum depositing approximately 200\_ of catalyst metal onto the amorphous silicon. The electrodes were completed by fixing copper wire leads to the stainless steel

with conductive epoxy, and potting the entire electrode except for the active surface in an insulating epoxy.

The fabricated devices were characterized both as solid-state solar cells, and as photoelectrodes in a 1N solution of NaOH. The photoelectrode was characterized using a standard three terminal configuration with a saturated calomel reference electrode. The three terminal configuration was used to allow anodic and cathodic half cell performance to be measured. The polarization curves were measured using the apparatus previously described (HNEI 1991 and 1992). This set-up includes a Keithley Model 236 source-measurement unit interfaced to a Macintosh LC computer running labview software. Data were acquired every 20 to 50 mV at a rate of 2 seconds per step.

Although the specifications for the large area triple junction material include an open circuit voltage over 2 volts, voltage in our fabricated photoelectrodes even in the solid-state was limited to 1.5V. Subsequent discussions with ECD and testing of different size samples indicate that this shunt is being caused by damage incurred at device edges during cutting of the sheets. Alternative procedures for device construction are currently being developed to eliminate this problem.

Figure 5 shows the polarization behavior of a Ni anode and two triple junction amorphous silicon photoelectrodes tested under slightly greater than three suns concentration; one with only ITO as a catalyst and one with a Ni/ITO bilayer. The maximum voltage relative to the Ni anode was again approximately 1.5V indicating that the junction characteristics are comparable in both the solid state and as a photoelectrode. The photocurrent at 3 suns for the nickel-coated device is approximately 11mA/cm<sup>2</sup>, only about half that of the ITO catalyzed electrode. This value is consistent with the appearance of the Ni/ITO film which appears metallic and reflective. The current density for the ITO/pin/pin/pin/SS electrode is comparable to that for the solid state cell at the same light intensity. More accurate calibration of the light source at these intensities are currently being made to allow better quantification.

The achievement of open circuit voltages and photocurrents nearly comparable to those of solid state device used for the fabrication is a very promising result. Voltage increases of 0.6 to 0.8 volts are expected once the shunting problem is solved. Several promising approaches to eliminate this shunt have been identified and are currently under evaluation. The high current densities with the oxide catalyst show that optical losses will be manageable. The critical task, as expected, is optimization of the catalyst performance in thin film form and improvement of the stability. Certain of the samples deposited with Ti resulted in an optically transparent TiO<sub>2</sub> layer which we attribute to reaction with the ITO. Unfortunately, the shunt characteristics of the starting coupons were poor, severely limiting performance. Other oxide catalysts and processes for deposition compatible with the amorphous silicon are currently being explored. We anticipate significant improvements shortly.

## **SUMMARY AND PLANS**

Demonstration of multijunction amorphous silicon photoelectrodes with open circuit voltages and current densities comparable to those obtained in the same devices in the solid state is a very positive result. Clearly, our immediate objective is to develop a fabrication process for our test devices which eliminates the serious shunt evident in the present devices. We believe this is a simple edge effect caused by our physical cutting of the samples. It is also possible that a partial contributor is shunting through pinholes when the highly conductive catalyst is deposited over the a-Si surface. While the edge shunt is likely to be reduced or eliminated by a simple change in procedures, the latter effect will be reduced by the use of less conductive metal-oxide catalyst. Fortunately, the use of such a metal oxide will concurrently

reduce optical losses (per reported experiments and model) and will likely result in greater stability of the anode surface to which it is applied. Development and testing of metal oxide catalyst compatible with the a-Si is a top priority. Based on the preliminary measurement, net unbiased hydrogen production efficiencies in excess of 6% should be easily achievable with elimination of the shunt. It is our intent to demonstrate such performance.

As a means of optimizing and understanding the critical electrolyte/catalyst/a-Si interface, we will prepare test structures of p-type amorphous SiC with metal-oxide catalysts such as pure or doped NiO, RuO, SnO and TiO. Potentiostatic and potentiodynamic polarization studies will be conducted in our existing facilities to characterize intrinsic catalytic properties and stability. Capacitance measurements will be utilized for flat band potential. We have recently deposited a-SiC in our laboratory and are currently fabricating the test structures. As pinholes are a significant factor in any effort to provide corrosion protection, we will also explore the behavior of the catalyst/a-Si interface in a wider range of aqueous electrolytes. Preliminary testing of SiC samples deposited in our laboratory show significant differences in anodic corrosion rates with different electrolytes.

While our modeling efforts will continue to be the primary tool for analysis of our experimental results and will provide guidance in future system design, the emphasis in the foreseeable future will be on the development of the necessary catalyst/electrolyte combinations required to demonstrate stable high efficiency performance with the multijunction a-Si photoelectrodes.

### **Acknowledgements**

I wish to thank the National Renewable Energy Laboratory for support of this project under subcontract No. XD-0-10089-1. I also wish to thank Dr. Rosa Young of Energy Conversion Devices and Subhendu Guha of United Solar Systems for the amorphous silicon samples used in this work, and Dr. Scott Wiedeman for useful discussions and data being provided in support of the diode model development.

## References

- Delahoy, A. E., S. C. Gau, O. J. Murphy, M. Kapur, and J. O'M. Bockris. 1985. *Int. J. Hydrogen Energy* 10:113
- Fujishima, A., and K. Honda. 1972. *Nature*, 238:37.
- Gerischer, H. 1979. "Solar Photoelectrolysis with Semiconductor Electrodes" in Topics in Applied Physics, Ed. B. O. Seraphin. Vol 31:115
- Getoff, N. 1990. *Int. J. Hydrogen Energy*, 15(6):407
- Hawaii Natural Energy Institute. 1991. "Hydrogen from Renewable Resources Research" annual report to the Solar Energy Research Institute.
- Hawaii Natural Energy Institute. 1992 "Hydrogen from Renewable Resources Research" annual report to the Solar Energy Research Institute.
- Heller, A. 1982. *Solar Energy*, 29(2):153.
- Ito, R., Y. Inouye, and M. Hayamizu. 1990. *Kagaku Kogaku Ronbunshu*. 16(4):812
- Lin, G. H., M. Kapur, R. C. Kainthla, and J. O'M. Bockris. 1989. *Appl. Phys. Lett.* 55(4):386
- Matsumura, M., Y. Sakai, S. Sugahara, Y. Nakato, and H. Tsubomura. 1986. *Solar Energy Materials*, 12:57.
- Murphy, A.J., and J. O'M. Bockris. 1984. *Int. J. Hydrogen Energy*, 9(7):557.
- Nozik, A.J. 1978. *Ann. Rev. Phys. Chem.*, 29:189.
- Sides, P. 1986. "Phenomena and Effects of Electrolytic Gas Evolution" in Modern Concepts of Electrochemistry. Vol 18:303
- Turner, J. May 1992. Presentation at SERI Hydrogen Subcontractors Review Meeting. Honolulu HI.

## Figures

Fig 1: Schematic of triple junction amorphous silicon photoelectrochemical cell.

Fig 2: Flow diagram of photoelectrochemical reactor model.

Fig 3: Comparison of current-voltage behavior of silicon MIS photodiode and photoelectrode.

Fig 4: Comparison of exchange current of bul kPt electrode and Si photoelectrode with thin PT catalyst.

Fig 5: Polarization behavior of triple junction a-Si photoelectrode with ITO and Ni/ITO catalyst.

Figure 1. Schematic of Triple Junction Amorphous Silicon Photoelectrochemical Cell

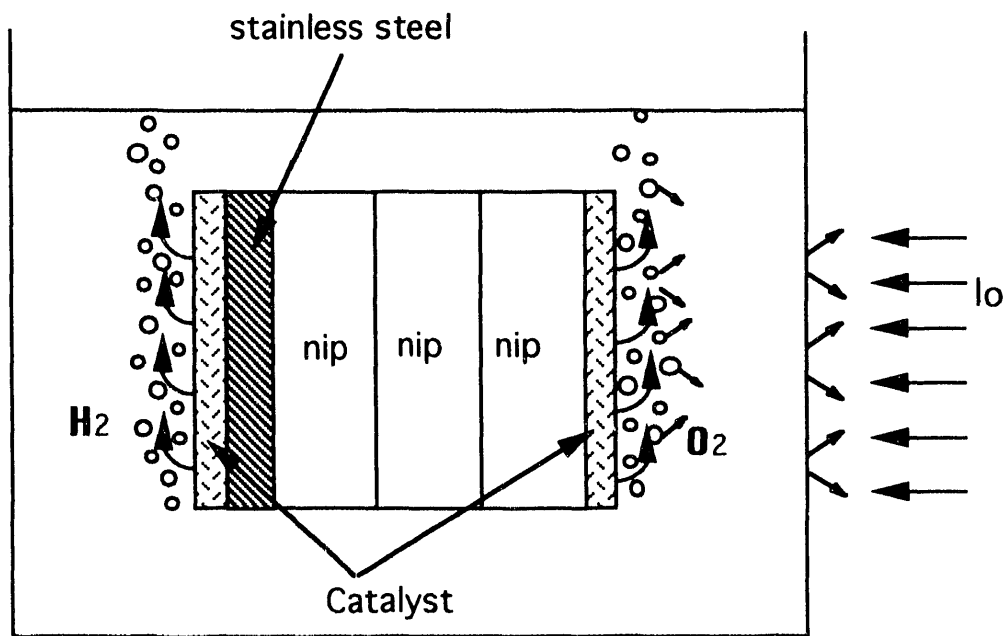


Figure 2. Flow Diagram of Photoelectrochemical Reactor Model

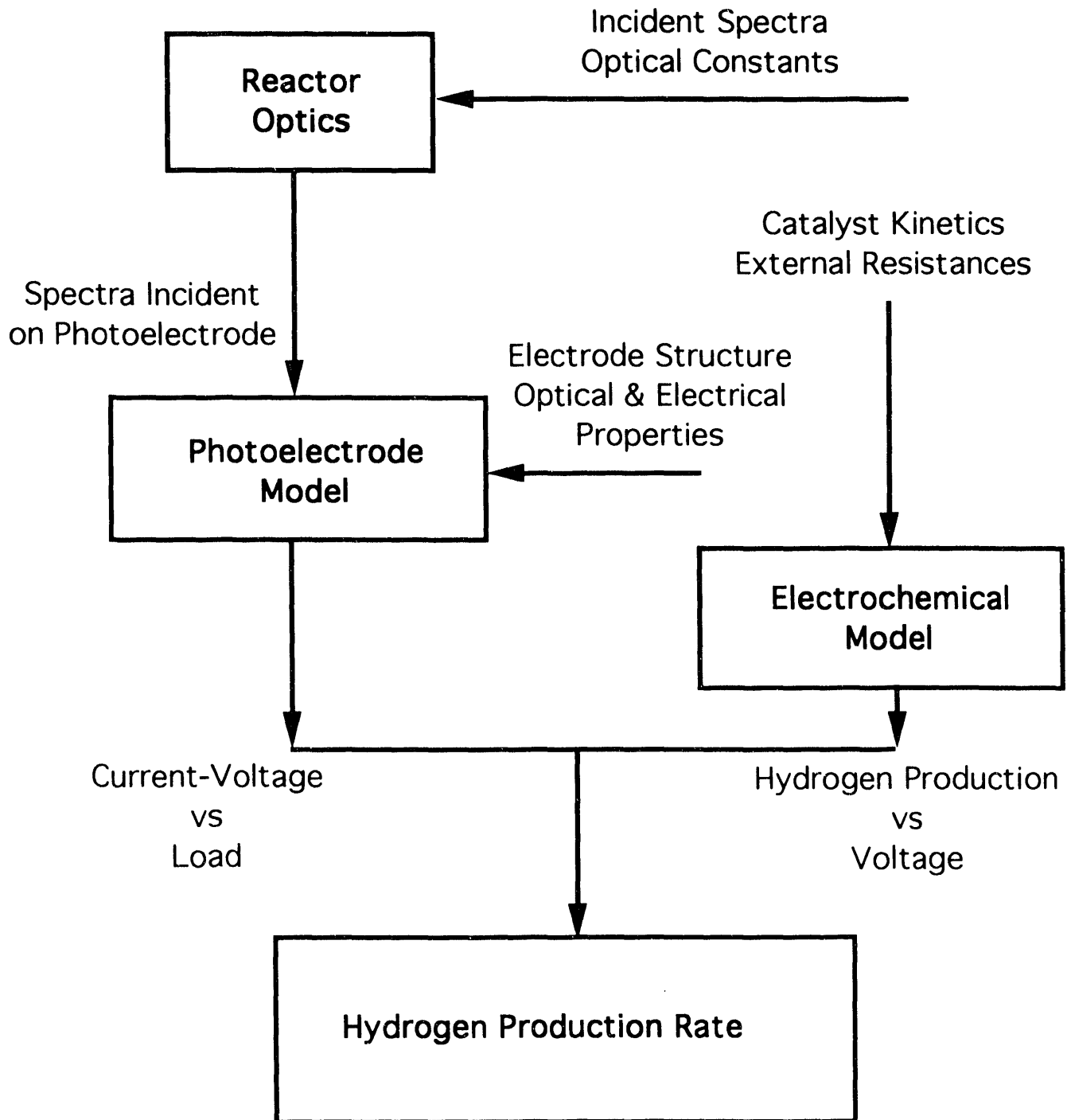




Figure 3. Comparison of Current-Voltage Behavior of Silicon MIS Photodiode and Photoelectrode

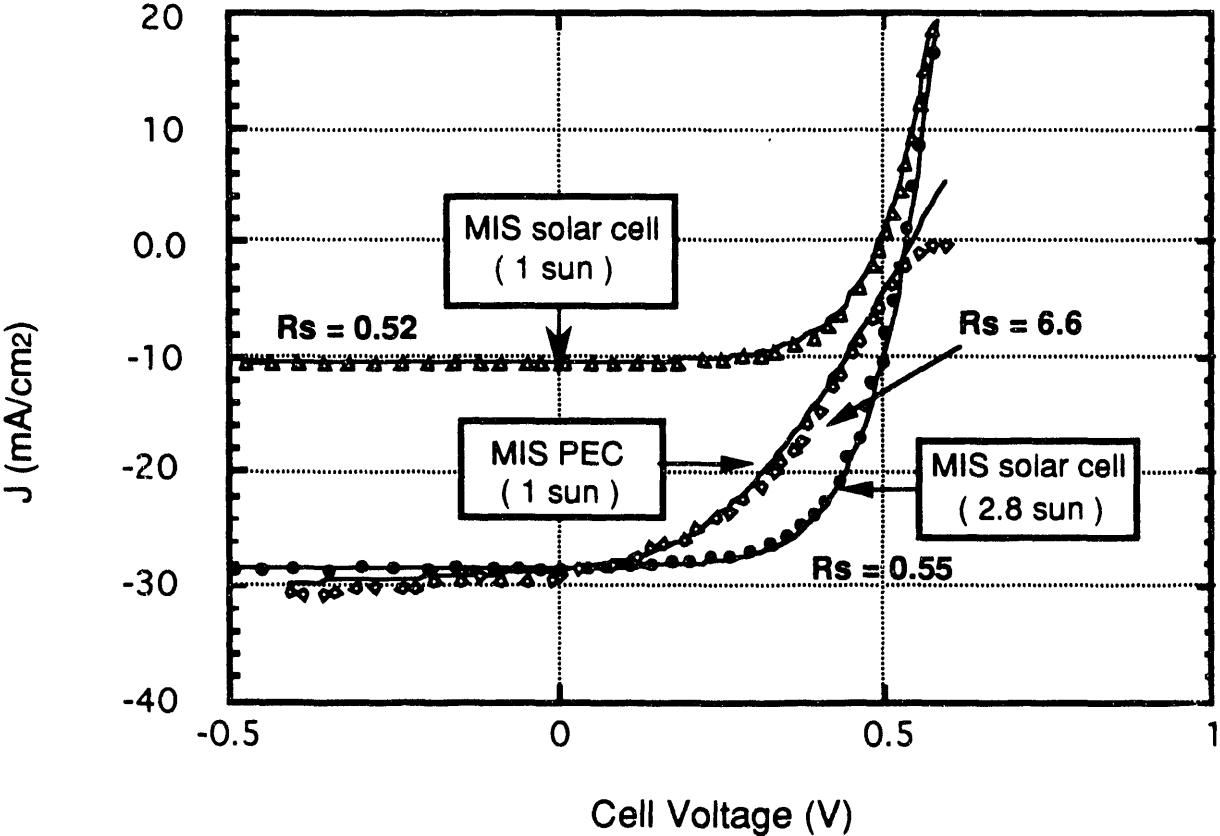


Figure 4. Comparison of Exchange Current of bul kPt Electrode and SI Photoelectrode with Thin PT Catalyst

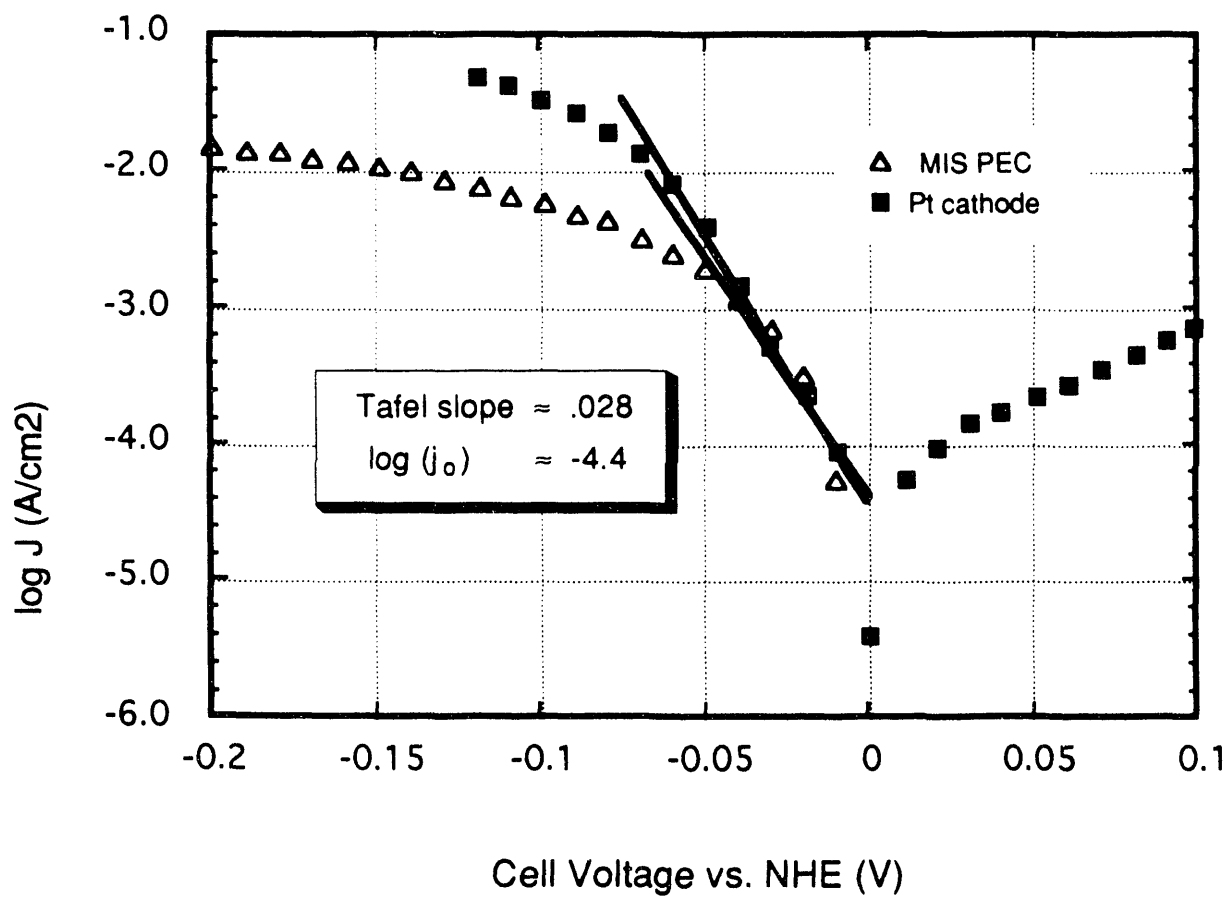
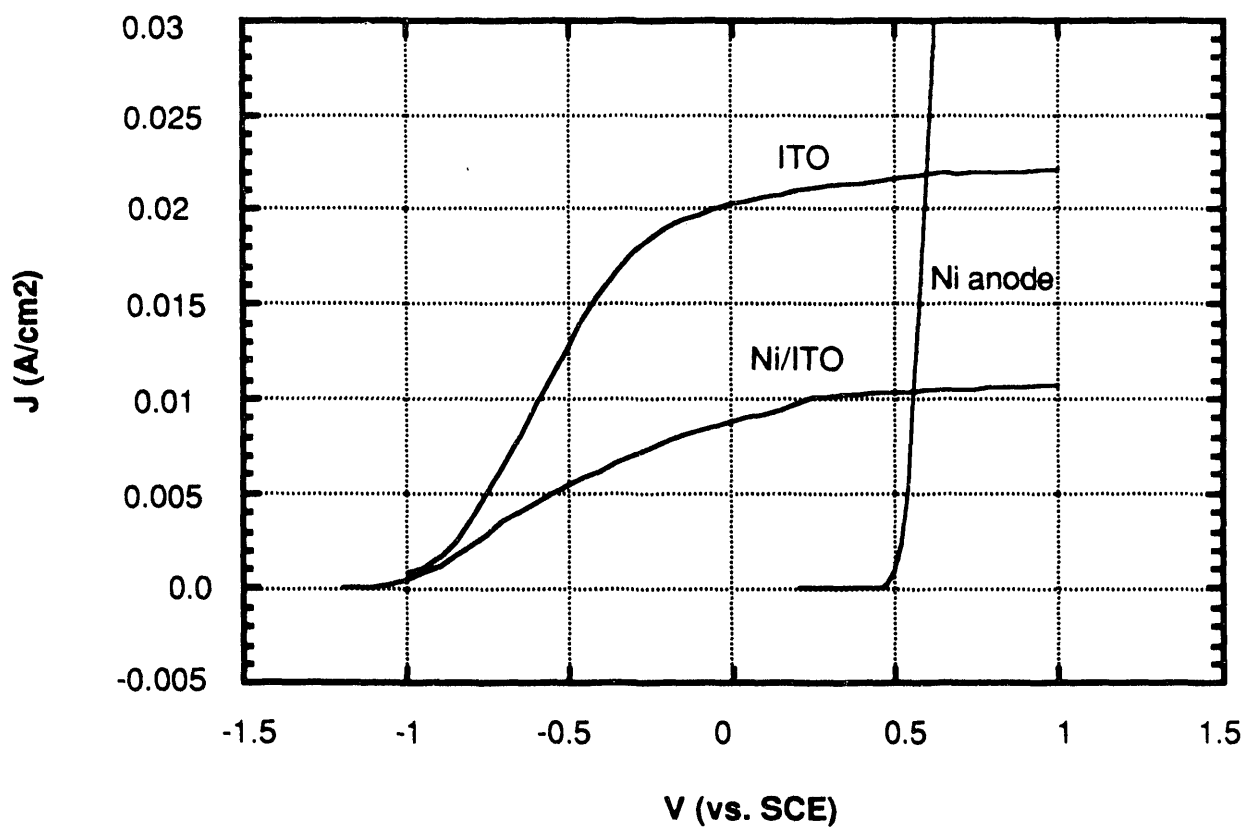


Figure 5. Polarization Behavior of Triple Junction a-Si Photoelectrode with ITO and Ni/ITO Catalyst





# PHOTOELECTROCHEMICAL BASED DIRECT CONVERSION SYSTEMS

Shyam Kocha, Mark Peterson, and John A. Turner  
National Renewable Energy Laboratory  
Golden, CO 80401-3393

## Abstract

Photon driven direct conversion systems consist of a light absorber and a water splitting catalyst as a monolithic system; water is split directly upon illumination. This one-step process eliminates the need to generate electricity externally and subsequently feed it to an electrolyzer. These configurations require only the piping necessary for transport of hydrogen to an external storage system or gas pipeline. We have focused our work on the GaInP<sub>2</sub> semiconductor based system. Our studies include surface passivation, catalysts and energetics.

## Introduction

An ideal renewable direct hydrogen production system would consist of an efficient light harvesting system and a highly catalytic water electrolysis system as a monolithic device. For a one-step process to be viable, the light harvesting system must generate sufficient voltage to effect the decomposition of water, and the system also must be stable in an aqueous environment. Splitting water into hydrogen and oxygen requires a thermodynamic potential of 1.23 eV at 25 °C. Typical values of the overvoltage for the cathode and anode reactions are 100 mV and 250 mV respectively. A potential then, of at least 1.6 eV is required for a water splitting system.

For a single gap semiconductor based direct conversion water splitting system, the fundamental requirement of at least 1.6 eV implies a minimum bandgap of 1.6 electron volts. Surface catalysts would also be required in order to bring the overvoltage for the oxygen and hydrogen evolution reactions down to an acceptable level. An additional requirement is that the semiconductor band edges span both redox potentials of the hydrogen and oxygen evolution reactions.

The goal of this research is to develop a stable semiconductor based system that will split water directly. We are focusing our study of these systems in three basic areas: materials research, surface stability and catalysts. NREL's Photovoltaic and Basic Sciences Divisions provide a state of the art resource for new solid state materials that could be used in a direct conversion system. From a study of their materials, we have focused on gallium indium phosphide, GaInP<sub>2</sub>, as a very promising material for a semiconductor based system.

Our past work on single crystal GaInP<sub>2</sub> has shown that while its bandgap is sufficient, its band edges are from 100 to 400 mV more negative than would be ideal. For this material, our approach has been to study the feasibility of inducing changes in the surface to obtain a more energetically favorable situation. Additional studies include passivating and stabilizing the semiconductor surface, and colloidal platinum catalysts.

The type of catalyst needed depends on whether oxygen or hydrogen is being generated at the illuminated surface of the electrode. The nature and coverage of the catalyst are critical for an optimized direct water-splitting system. Catalyst coverage must be sufficient to both protect the semiconductor from undesirable side reactions (corrosion) and provide sufficient catalytic activity to handle the current flux. Transparency of the catalyst is also needed so as to minimize light losses. The best catalyst for oxygen evolution is ruthenium dioxide, for hydrogen evolution it is platinum. These are expensive materials that will add to the cost of any direct conversion system.

### Technical Approach

The most stable materials in aqueous solutions are oxides (e.g., TiO<sub>2</sub>). These materials typically have such large bandgaps, that they have very low efficiencies under solar irradiation. However, with proper choice of semiconductor material the stabilizing properties of these wide bandgap oxides can be used. Indium phosphide is stable even in concentrated acid solution due to the formation of an indium oxide surface layer. While indium phosphide's bandgap is only 1.35 eV and would not ordinarily be stable, the formation of the wide bandgap (>3.0eV) insoluble indium oxide semiconductor passivates the surface, stabilizing the material. Another example is the sulfide and selenide treatment of GaAs (1). This surface treatment, used for solid state applications, apparently removes the surface states involved in surface

recombination losses, thereby increasing the efficiency of devices based on GaAs. It is interesting to note that gallium sulfide and gallium selenide are also very insoluble compounds. This leads to a concept that may have general use in the area of semiconductor surface modification, the formation of insoluble surface species. If one can place a uniformly thin coat of a very insoluble compound on the surface, it may have a stabilizing effect. Forming it using one of the semiconductor constituents would provide a more direct path for the reaction.

Our measurements of the position of the band edges of the 'as-grown' p-type samples suggests a surface sensitivity to impurities. This suggests that it may be possible to permanently modify the surface of the GaInP<sub>2</sub>, shifting the band edges to a more energetically favorable position. The analytical chemistry literature describes many compounds that are used to precipitate cations for analytical analysis, including both inorganic and organic precipitating agents. We propose to try several of these agents in an attempt to increase the stabilization and improve the energetics of the band edges of GaInP<sub>2</sub>. An anodic shift of the band edges of p-GaInP<sub>2</sub> by 200 to 500 mV would provide the correct driving force for a water splitting system. Interestingly enough, a positive shift in the band-edges would be beneficial for the n-type also, as it would give an increase in the overvoltage for the oxygen evolution reaction. Modification of the surfaces may be as easy as soaking the semiconductor sample solution of the precipitating agent. An alternative technique would be to apply an anodic voltage pulse to the sample in solution, dissolving a thin layer of the surface and forming a precipitate.

A number of possible surface treatments to meet these requirements are discussed below and include etching, fluoride treatments and oxinate treatments.

### **Inorganic Fluoride Treatments**

Due to its small size and high electronegativity, most metal fluorides are highly insoluble. In addition, the closeness of F<sup>-</sup> and O<sup>2-</sup> relates oxides and fluorides and allows easy substitution. Oxygen fluorine substitution has been noted to have a strong influence on metal-non metal transitions in oxides by increasing electron localization (Na<sub>x</sub>WO<sub>3-y</sub>F<sub>y</sub>) [2] or lowering the conduction band (VO<sub>2-x</sub>F<sub>x</sub>) [3]. The oxidation rates of niobium, tantalum, and tungsten have been found to be highly retarded by a fluoride treatment. Metals in powder or sheet form treated with KHF<sub>2</sub> solutions were found to have decreased reactivity to O<sub>2</sub> on heating. It was concluded by Bhat et al. (4,5) that the fluorine was substituted for oxygen in the oxide layer and enhanced the oxidation resistance. Chong et al. (6) have also reported shifting of flat-band potentials on titanium dioxide and variation in band gap with fluoride treatment.

### **Oxinate Treatments**

A study of the literature concerning the solubility of precipitates revealed a number of organic compounds that could be applied towards the formation of insoluble compounds with III-V elements (7). 8-Hydroxyquinoline or Oxine (HOx) is a reagent that gives precipitates with most metals except alkali metals and are often used in gravimetric separations. For example, the oxinates of gallium, aluminum, indium and iron have solubility constants as shown below (8,9):

**Table 1. Solubility Product constants for some oxinates.**

Compound	Ksp ( $[M^{3+}][Ox^-]^3$ )
AlOx <sub>3</sub>	10 <sup>-32.3</sup>
GaOx <sub>3</sub>	10 <sup>-40.8</sup>
InOx <sub>3</sub>	10 <sup>-33.9</sup>
FeOx <sub>3</sub>	10 <sup>-43.5</sup>

The oxinate (Ox<sup>-</sup>) ion concentration and hence the solubility of the metal oxinate are strongly controlled by the pH of the solution. The oxinates or quinolates can be precipitated by immersion of the original compounds in 8-quinolinol dissolved in an acetic acid-acetate buffer. The solids formed are usually of the type MOx<sub>n</sub>, in which the H of the OH group is replaced by the metal. Due to its organic nature, the uncharged complex is also soluble in some organic solvents. The pH ranges for precipitation of In and Ga are approximately 4.11 and 2.511.5 respectively. In the oxinates of trivalent metals all six coordination positions are occupied by oxinate groups and no water is coordinated. Anhydrous oxinates (such as Al, Ga, Fe(III)) can be heated to 150-200°C without decomposition (7).

## Results and Discussions

### Etching Studies

Etching the semiconductor surface not only polishes it, but also can produce a more stable and reproducible surface. Three etchants were used: A) 1:20:1 HCl:CH<sub>3</sub>COOH:H<sub>2</sub>O<sub>2</sub> and B) 1:20:1 HCl:H<sub>3</sub>PO<sub>4</sub>:H<sub>2</sub>O<sub>2</sub> and C) 1:20:1 HCl:CH<sub>3</sub>COOH:H<sub>2</sub>O<sub>2</sub>:8-Quinolinol in pH 4.8 buffer. The acetic acid buffer (etchant A) has been used before and etch rates have been determined by Flemish et al. (10). The etchant B was studied based on the fact that the phosphates of gallium and indium are insoluble which could result in a more stable surface. The last etchant C incorporated a small amount of Quinolinol solution and was expected to speed up the formation of oxinates on the surface and an alternative to simple immersion and drying. Etchants A, B, and C all were found to produce smooth surfaces and linear Mott-Schottky plots when the time of etching was limited to 1530 seconds. The Mott-Schottky plots did not display appreciable change in the flat-band potential, but exhibited slightly higher apparent doping densities (slopes). This effect could be explained on the basis of a change in actual area of the surface as a result of etching and not taken into account in calculations. PL spectra showed an increase in peak height after etching, indicating the removal of surface recombination centers. Capacitance studies showed that etching reduced the variation of the calculated doping density and flat-band potential in different electrolytes.

### Fluoride Treatments

Fluoride substitution into the surface native oxide was attempted by immersion of samples in a 1M KF solution or by anodically biasing (positive of the open circuit voltage), permitting some charge flow to occur. Direct immersions in KF yielded no change on the sample surface and Mott-Schottky studies. Anodically biasing n-GaInP<sub>2</sub> initially resulted in Mott-Schottky plots that exhibited hysteresis and non-linearity. Repeating the process with increasing anodic bias reversed the effect and Mott-Schottky plots reverted to linear behavior with diminished hysteresis. It was possible to bias the sample over a range of 3 volts with this procedure (see Figure 1). It is speculated that fluoride is incorporated into



the oxide film rendering it more stable. Further studies will include photocurrent, current-voltage, XPS, PL and PR. One study was carried out on a p-type AlGaAs sample; studies are difficult on this material since anodic biasing or pulsing can easily result in severe oxidation of the sample. On carrying out an anodic scan, the Mott-Schottky plot showed a sudden change to linear behavior and very high apparent doping densities (see Figure 2). Unfortunately, on the next anodic sweep, the sample was destroyed.

## **Oxine treatments**

GaInP<sub>2</sub>, AlGaAs and GaAs single crystal epi-layers grown in MOCVD reactors were studied before and after treatments with 8-Quinolinol. It was found after several experiments with 8-Quinolinol dissolved in aqueous solutions of various pHs, as well as alcohol and alcohol/aqueous solution mixtures, that a saturated solution of 8-Quinolinol in an acetate buffer of pH ~5 was best suited for formation of oxinates on the semiconductor surfaces. Immersion time for the samples was varied from 60 seconds to 18 hours. Samples were dried in air for 412 hours or in an oven at 100°C for 12 hours. It was found that drying time was quite critical and sufficient drying time had to be ensured for effective treatment. It was observed (see Figure 3) that after treatment, the flat-band potential of the samples shifted positive for GaInP<sub>2</sub> by as much as 300 mV. Figure 4 shows the band positions at pH 7 with respect to the water splitting reaction. A shift in the flat-band potential was also noted for some samples treated with etchant C though to a lesser extent. We speculate that gallium or indium oxinates formed on the surface produce these shifts. Flat band potential shifts were observed only in near neutral electrolytes (phosphate buffers), lesser shifts in slightly acidic or basic electrolytes and no shifts at pH 0 and 14. Aluminum hydroxyquinolate is also insoluble and probably stabilizes the surface, however, the flat-band potential shifted negative after quinolinol treatments of AlGaAs (see Figure 5). On adding a small quantity of In<sub>2</sub>O<sub>3</sub> to the quinolinol solution and then immersing the AlGaAs samples, a positive shift was observed. This is speculated to be due to some deposition of indium oxinates on the surface. The Mott-Schottky plots for gallium arsenide were non-linear and though some shifts were noticeable, it could not be conclusively determined whether the flat-band had shifted positive or negative.

Further studies have to be carried out to determine the composition of the surface using XPS. Preliminary PL and PR studies indicate that the PL does not change appreciably and in one case the PR was lowered.

## **Platinum Colloids**

We have continued our efforts to understand the nature of the interaction of the platinum colloids with the semiconductor surface. Photoluminescence experiments were carried out on treated and untreated GaInP<sub>2</sub> electrodes. The photoluminescence of the platinum colloid treated electrode was much higher than the untreated electrode (see Figure 6). This was unexpected as one would anticipate that a metal center on the surface would act as a recombination center and decrease the PL not increase it. The Pt apparently reduces the number of surface recombination centers, improving the quality of the surface.

## Conclusions

One of the goals for this research was to investigate the possibility of changing the surface energetics and stability of GaInP<sub>2</sub> by using precipitating agents. These studies demonstrate that it is possible through appropriate surface modifications to passivate the surface and modify flat-band potentials, rendering the material more propitious for water splitting.

## Future Work

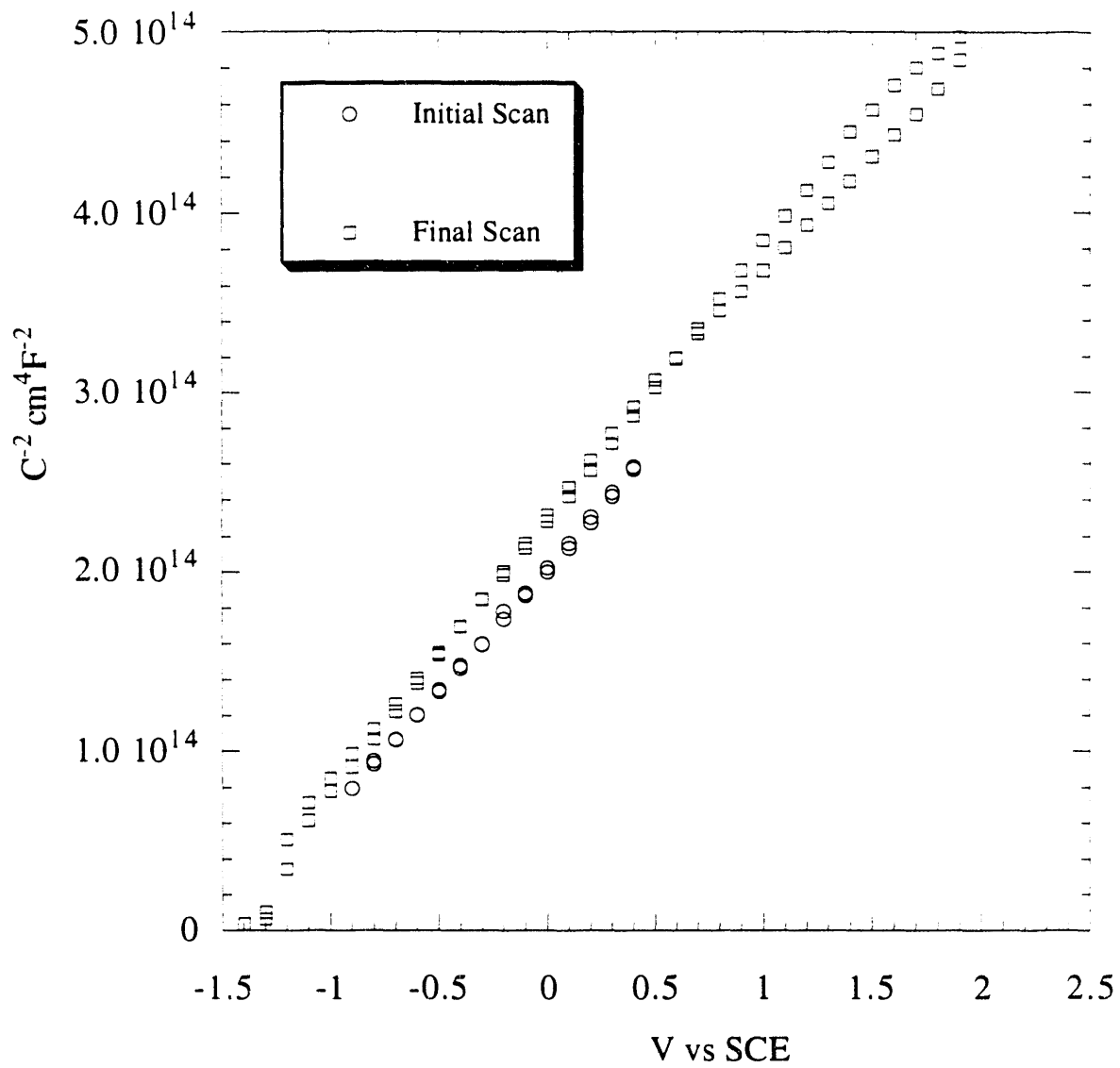
We will continue to work on modifying the surface of GaInP<sub>2</sub> to stabilize the surface and to obtain more favorable energetics for water splitting. We have initiated a collaboration with Dr. Art Frank of NREL to address the stability of n-GaInP<sub>2</sub> and the application of specialized catalysts for water oxidation. Dr. Frank has considerable expertise in this area (11-14). We will continue to study tandem cells of various structures and materials. Dr. Simon Tsou will be collaborating with us to provide us with a-silicon based tandem cells. Further characterization of the platinum colloids will be done to determine their size distribution and catalytic activity.

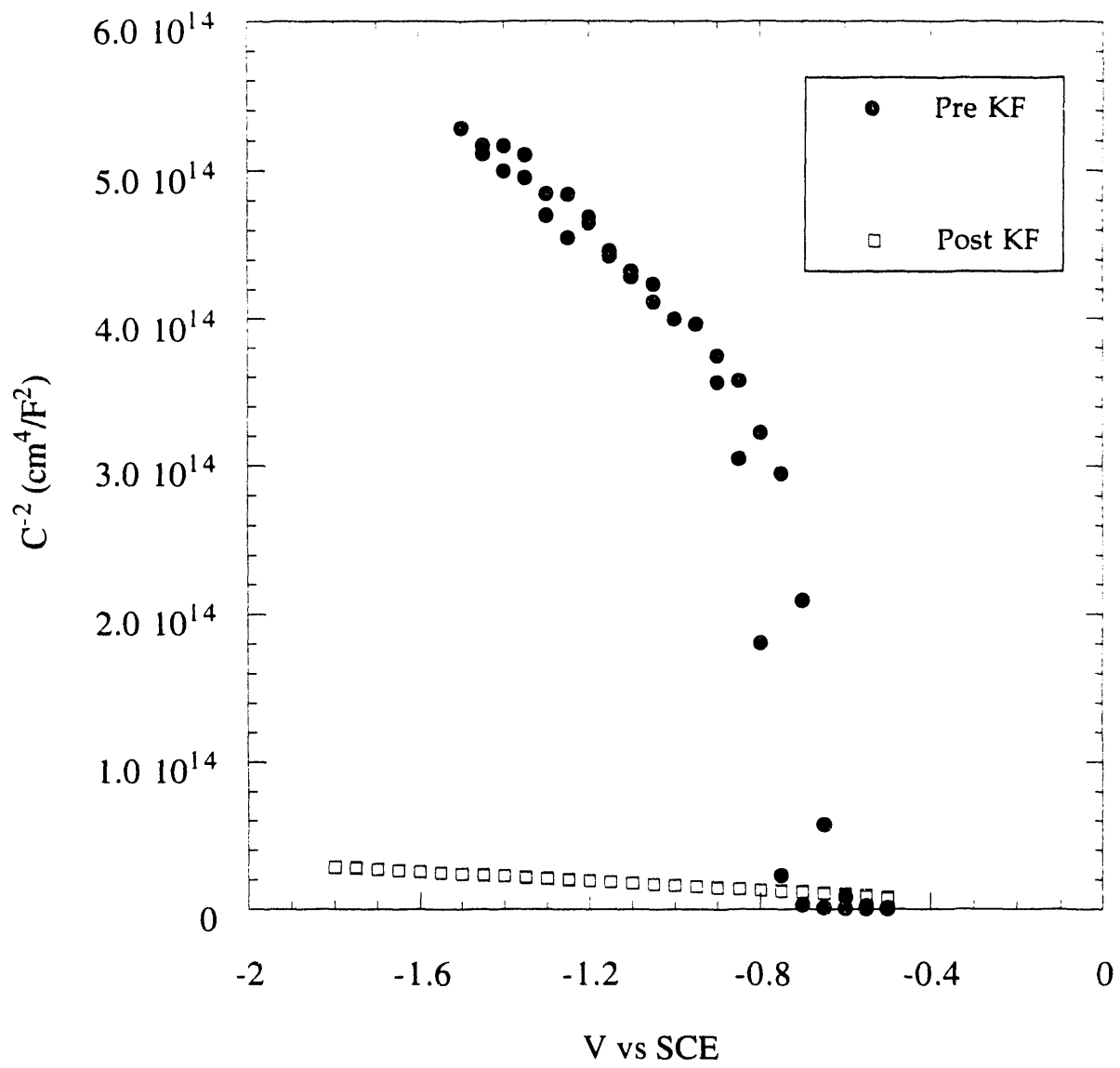
## References

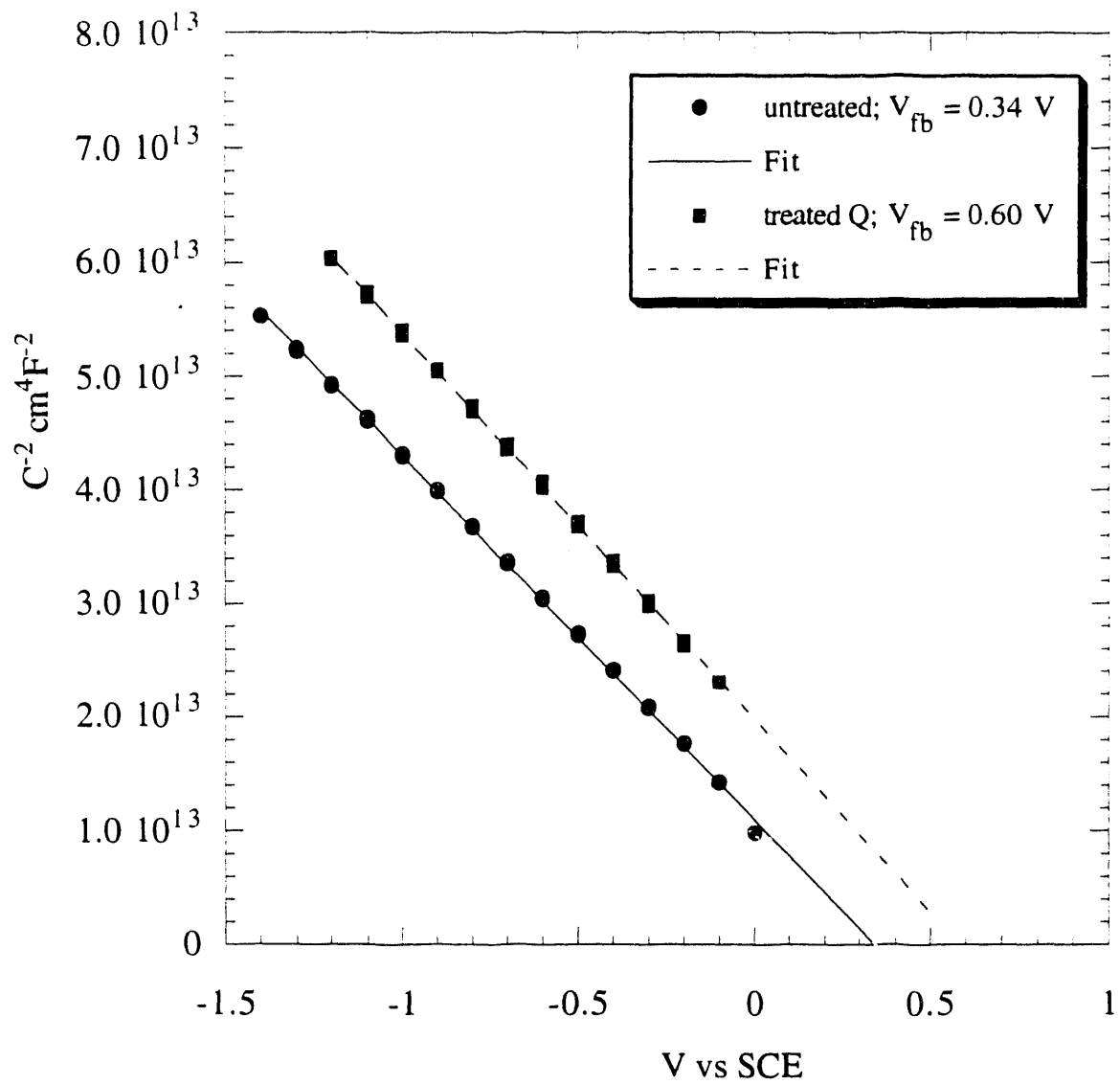
1. C. J. Sandroff, R. N. Nottenburg, J.-C. Bischoff and R. Bhat, *Appl. Phys. Lett.*, **51**, 33 (1987).
2. Doumerc, J.P. (Universite de Bordeaux I.,1974).
3. Bayard, M., Pouchard, M., Hagenmuller, P. & Wold, A. J. *Solid State Chem.* **12**, 41 (1975).
4. Bhat, T.R. & Khan, I.A. *J. Less-Common Met.* **9**, 388 (1965).
5. Bhat, T.R. & Khan, I.A. *J. Less-Common Met.* **11**, 290 (1966).
6. Chong, M.W. & Thomas, E.M. *J. Phys. Chem.* **94**, 4276 (1990).
7. Kolthoff, I.M., Sandell, E.B., Meehan, E.J. & Bruckenstein, S. *Quantitative Chemical Analysis* (The Macmillan Company, London, 1969).
8. Lacroix, S. *Anal. Chim. Acta* **1**, 260 (1947).
9. Turnquist, T. (University of Minnesota, 1965).
10. Flemish, J.R. & Jones, K.A. *J. Electrochem. Soc.* **140**, 844 (1993)
11. R. Noufi, A. J. Frank, and A. J. Nozik, *J. Amer. Chem. Soc.*, **103**, 1849 (1981).
12. A. J. Frank and K. Honda, *J. Phys. Chem.*, **86**, 1933 (1982).
13. K. Honda and A. J. Frank, *J. Phys. Chem.*, **88**, 5577 (1984).
14. A. J. Frank, S. Genlis, and A. J. Nelson, *J. Phys. Chem.*, **93**, 3818 (1989).

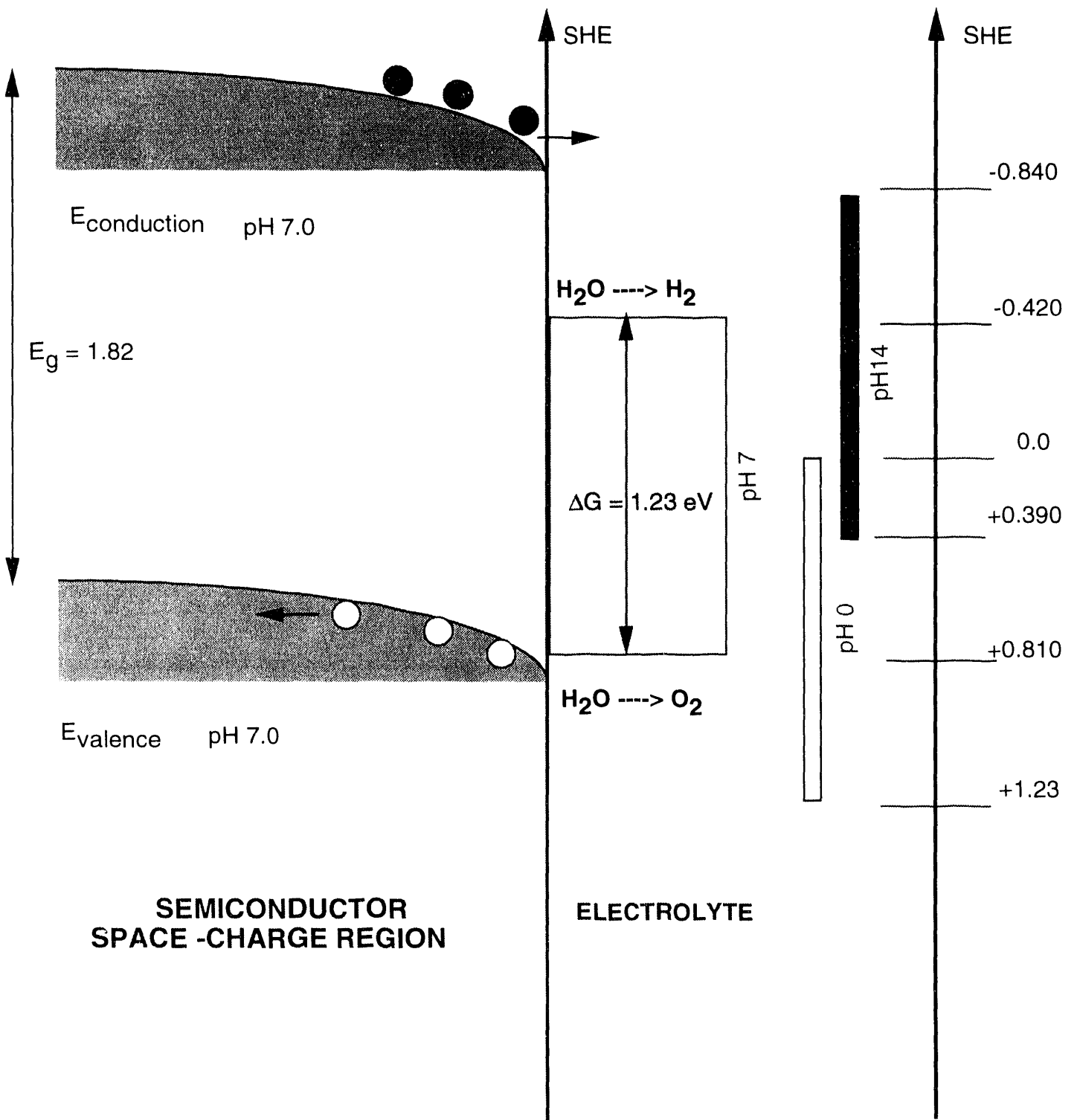
## Figures

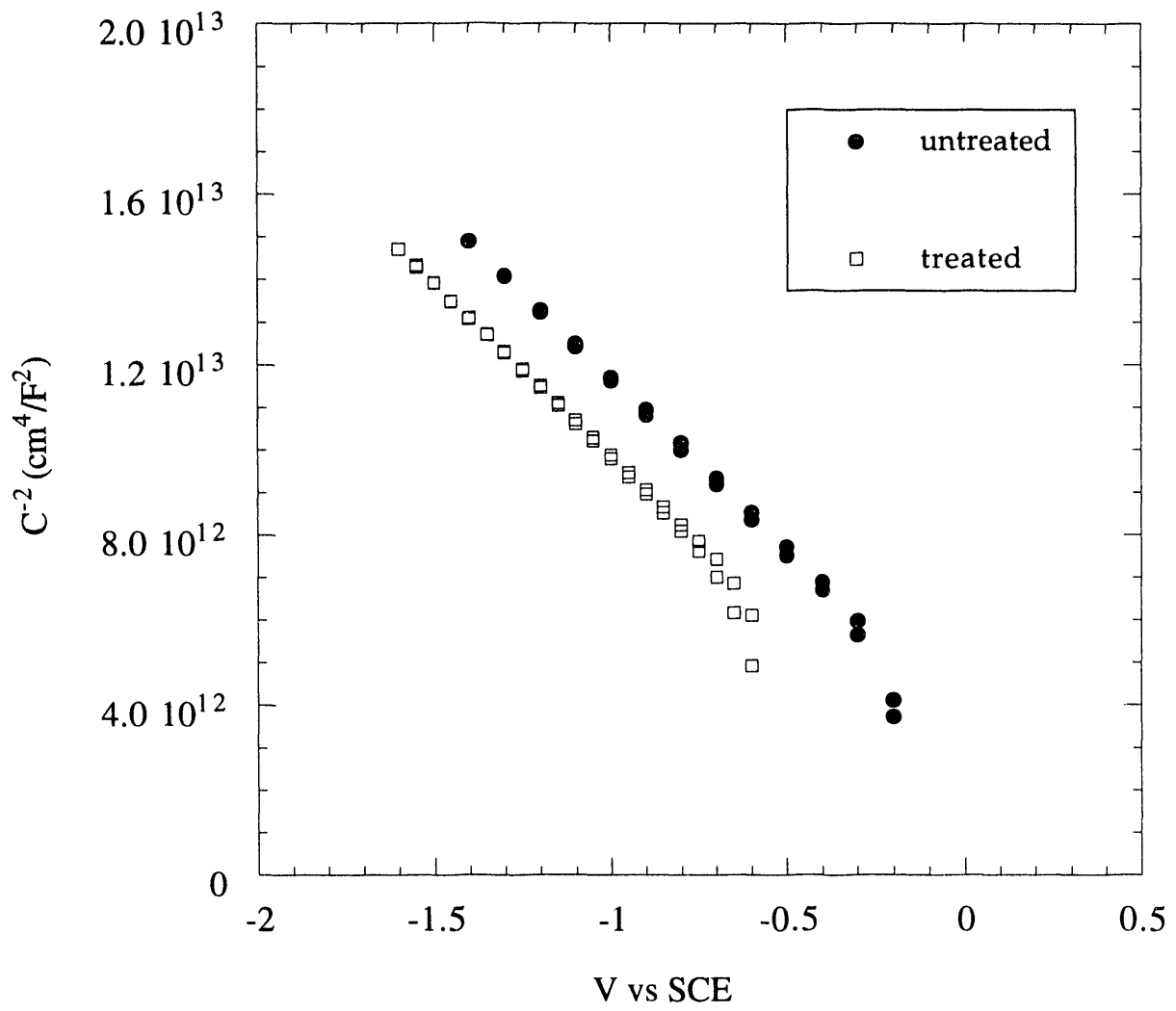
- Figure 1 Mott-Schottky plots of n-GaInP<sub>2</sub> in 1M KF at 10 kHz.
- Figure 2 Mott-Schottky plots of p-AlGaAs before and after anodic scans in 1M KF.
- Figure 3 Mott-Schottky plots of p-GaInP<sub>2</sub> at pH 7 before and after treatment with 8-quinolinol.
- Figure 4 Band positions of p-GaInP<sub>2</sub> after quinolinol treatment.
- Figure 5 Mott-Schottky plots of p-AlGaAs showing effects of quinolinol treatment.
- Figure 6 Photoluminescence of colloidal platinum treated electrodes.



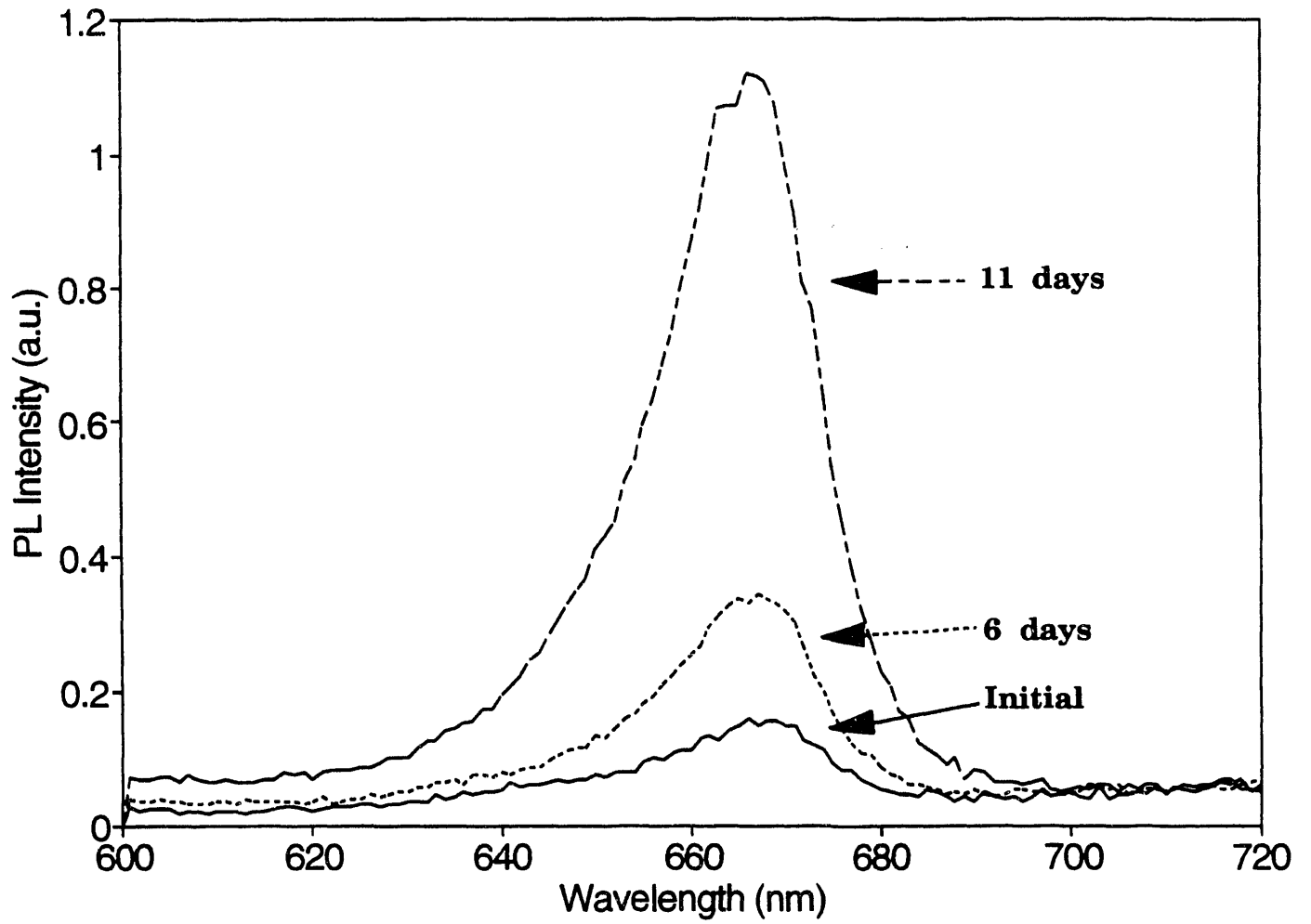














# NONCLASSICAL POLYHYDRIDE METAL COMPLEXES AS HYDROGEN STORAGE MATERIALS

Craig Jensen  
Department of Chemistry  
University of Hawaii Honolulu, HI 96822

## Abstract

An alternate class of metal hydrides, nonclassical polyhydride metal complexes, are being developed as hydrogen storage materials. Novel cobalt group nonclassical polyhydride complexes of the formula:  $\text{IrH}_a\text{X}_b(\text{H}_2)(\text{PR}_3)_3$  ( $\text{X} = \text{Cl}, \text{Br}, \text{I}; \text{R} = \text{C}_6\text{H}_{11}, \text{C}(\text{CH}_3)_3, \text{CH}(\text{CH}_3)_2$ ;  $a = 1-2, b = 1-2$ ) and have been synthesized and characterized through multinuclear NMR spectroscopy and single crystal X-ray diffraction. The complexes undergo a rapid and highly reversible loss of  $\text{H}_2$  in solution and the solid state. This process has been studied by variable temperature  $^1\text{H}$  and  $^{31}\text{P}$  NMR as well as FTIR spectroscopy. The energetics of the reversible loss of  $\text{H}_2$  can be fine-tuned by small changes in the ligand environment such as the steric bulk of the phosphine ligands or variation of the halide. The observed trends in the kinetic and thermodynamic stabilities of the halide complexes can be explained by the  $\text{I}_- > \text{Br}_- > \text{Cl}_-$  trend in the donor strengths of the halide ligands and establishes the influence of this parameter on the stability of dihydrogen complexes. Novel ruthenium and cobalt hydride complexes which are stabilized by cyclopentadienyl ligands have also been synthesized and are being characterized. These complexes may possess significant weight percent available hydrogen contents.

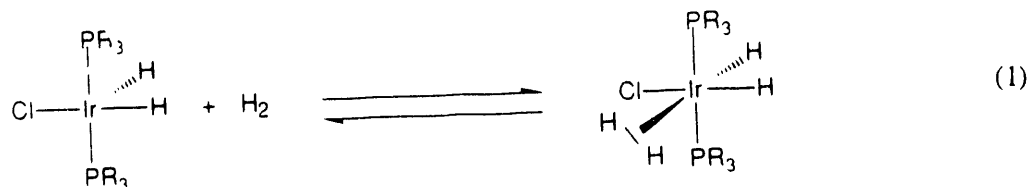
## Introduction

A major concern in the development of hydrogen as a fuel is the problem of hydrogen storage. Hydrogen has traditionally been stored as a compressed gas or cryogenic liquid. The disadvantages of cylinder

storage are the extreme pressure, weight, and volume requirements. Storage of hydrogen as a cryogenic liquid is unattractive due to the requirements of extremely low temperatures and high consumption of primary energy. Additionally, both of these traditional storage methods entail considerable safety risks. Solid hydrogen storage systems based on metal hydrides are safer and require far less volume than either high pressure or cryogenic storage systems. Unfortunately, the metals and alloys which reversibly bind hydrogen at adequate rates, generally form hydrides which contain less than 1.0 weight per cent hydrogen. As a result, the weight of hydrogen storage systems based on traditional metal hydrides severely restricts their practical application [1]. Although alloys such as iron-titanium have shown acceptable kinetic behavior and can attain up to 2.0 weight percent hydrogen, their utilization for hydrogen storage is extremely limited due to other problems such as high sensitivity to impurities [2]. Metals and alloys may eventually find limited commercial hydrogen storage applications, but it would appear that a new class of materials must be developed to allow utilization of hydrogen as an energy carrier.

We are developing an alternate class of metal hydrides, nonclassical polyhydride metal complexes, as hydrogen storage materials. Polyhydride metal complexes with relatively high hydride weight percentages have been known for many years. However, classical polyhydride complexes generally undergo irreversible dihydrogen elimination. Recently, a new class of metal hydride complexes in which hydrogen bonds to the metal center while retaining a significant amount of H-H bonding have been recognized [3]. In most cases, these nonclassical hydride or molecular hydrogen complexes have been found to undergo complete and reversible loss of H<sub>2</sub> under mild conditions.

In our laboratory we have synthesized and characterized novel cobalt group nonclassical polyhydride complexes of the formula: IrH<sub>a</sub>X<sub>b</sub>(H<sub>2</sub>)(PR<sub>3</sub>)<sub>3</sub> (X = Cl, Br, I; R = C<sub>6</sub>H<sub>11</sub>, C(CH<sub>3</sub>)<sub>3</sub>, CH(CH<sub>3</sub>)<sub>2</sub>; a = 1-2, b = 1-2). When these complexes were initially isolated, they displayed very unusual spectroscopic properties. We have established that the properties were due to the rapid equilibrium seen in equation 1. We have studied this reversible loss of H<sub>2</sub> from these complexes



both in solution by variable temperature <sup>1</sup>H and <sup>31</sup>P NMR spectroscopy as well as in the solid state by infrared spectroscopy [4,5]. The rapid kinetics of the reversible loss of H<sub>2</sub> from these complexes is exceptional among metal hydrides in general. The ability of these complexes to undergo complete loss of H<sub>2</sub> without application of a high vacuum system is quite remarkable and demonstrates the high potential of metal complexes of this type as hydrogen storage materials. We have also demonstrated that the kinetics and thermodynamics of the reversible loss of H<sub>2</sub> by these complexes are very sensitive to small changes in the ligand environment at the metal center such as the steric constraints introduced by the phosphine alkyl groups[5]. Thus materials of this type could be tailored to maximize their utility to a variety of energy carrier applications. During the past year we have examined the effect of another ligand field parameter, the influence of the halide ligands, on the reversible elimination of H<sub>2</sub>.

The nature of the metal-dihydrogen bond in the nonclassical hydride complexes has been a point of considerable interest and controversy [3,6,7]. Elucidation of these interactions has increased the

fundamental understanding of the formation of metal hydrides as these compounds represent the early transition state along the reaction coordinate corresponding to the formation of a hydride complex. Unlike many other reported nonclassical polyhydride complexes, our complexes can be isolated and have therefore attracted the attention of research groups around the world. In the past year, we have continued our collaborative research projects involving: inelastic neutron scattering with Dr. Juergen Eckert of Los Alamos National Laboratory; extended Huckel calculations with Dr. Odile Eisenstein at the Universite de Paris-Sud, France; and solid state NMR spectroscopy with Prof. Kurt Zilm of Yale University. These collaborations have significantly advanced the fundamental understanding of the metal hydrogen interactions [8,9] and provided independent verification of the low kinetic barrier to H<sub>2</sub> elimination.

Attempts to prepare analogous nonclassical hydride complexes stabilized by relatively low molecular weight phosphines lead instead to the isolation of complexes which contain one or more additional phosphine ligands and no available coordination site(s) for H<sub>2</sub> ligands. Thus while our phosphine containing complexes serve as excellent models on which to test the effects of ligand environment on hydrogen binding, we believe this class can be eliminated as potential hydrogen storage materials as hydrogen binding occurs only in complexes of low percentage available hydrogen content. In the past year we have continued our efforts to prepare and characterize a new class of nonclassical polyhydride complexes. The targeted iron and cobalt complexes are stabilized by an  $\eta^5$ -cyclopentadienyl ligands. The low cost and relatively low molecular weight of these metals as well as the cyclopentadienyl ligand make these complexes especially attractive candidates as hydrogen storage materials. These should have the same desirable kinetic properties as the cobalt group phosphine complexes while containing greater weight per cent available hydrogen content.

## Results

### Iridium Nonclassical Polyhydride Complexes.

During the past year, we have studied the dynamics of reversible H<sub>2</sub> binding in the complexes, IrXH<sub>2</sub>(H<sub>2</sub>)(PPr<sub>3</sub>)<sub>2</sub> (X = Cl, 1a; Br, 2a; I, 3a). Our goal was to determine the effects of varying the halide ligand electronic donor strength on the energetics of binding of H<sub>2</sub>. We investigated this phenomenon by variable temperature solution <sup>1</sup>H NMR spectroscopy.

A procedure similar to Werner's method [10] of preparing IrClH<sub>2</sub>(PPr<sub>3</sub>)<sub>2</sub>, 1b, was used to synthesize IrBrH<sub>2</sub>(PPr<sub>3</sub>)<sub>2</sub>, 2b. A solution of [IrBr(C<sub>8</sub>H<sub>14</sub>)<sub>2</sub>]<sub>2</sub> [11] in pentane was treated with PPr<sub>3</sub>. After stirring for 5 min, hydrogen was bubbled through the solutions for 5 min. Removal of solvent by vacuum followed by recrystallized in pentane gave purified, yellow-orange 2b in 74% yield. Reaction of a solution of [IrCl(C<sub>8</sub>H<sub>14</sub>)<sub>2</sub>]<sub>2</sub> [12] and NaI in methylene chloride with PPr<sub>3</sub> followed by the same synthetic procedure gave purified, orange IrH<sub>2</sub>(PPr<sub>3</sub>)<sub>2</sub>, 3b in 71% yield. We have definitively characterized complex 3b through a single crystal structure determination, the results of which are depicted Figure 1.

Variable temperature <sup>1</sup>H and <sup>31</sup>P NMR spectroscopic studies have demonstrated [5] that in the presence of H<sub>2</sub>, the chloro complex, 1b establishes an equilibrium with the dihydrogen complex 1a. Variable temperature <sup>1</sup>H NMR spectra at 500 MHz of the hydride region of equimolar samples of 2b and 3b dissolved in toluene and placed under 0.5 atm of hydrogen are seen in Figures 2 and 3. These spectra are

similar to those obtained in our study of **1b** and indicate that **2b** and **3b** establish rapid equilibria with the dihydrogen complexes,  $\text{IrBrH}_2(\text{H}_2)(\text{PPr}^3)_2$ , **2a** and  $\text{IrIH}_2(\text{H}_2)(\text{PPr}^3)_2$ , **3a**. As seen in Figure 2, separate resonances are observed at low temperature for the hydride ligands of **2b** at -33.1 ppm and the metal bound hydrogens of **2a** at -10.9 ppm which coalesce at 15\_C. Separate resonances are also observed at low temperature for the metal bound hydrogens of **3b** and **3a** at -33.3 and -10.7 ppm respectively which coalesce at a higher, 40\_C temperature as seen in Figure 2. The minimum  $T_1$  values found for the resonances of **2a** (54 ms, -60\_C) and **3a** (43 ms, -60\_C) at 500 MHz are consistent [13,14,15] with the presence of rapidly exchanging hydride and dihydrogen ligands in these complexes. The minimum  $T_1$  values of 353 and 386 msec observed for the hydride resonance of **2b** and **3b** respectively establishes that a classical hydride ligand in a similar coordination environment does not have a similarly short value of  $T_1$  due to heteroatom-hydrogen dipole-dipole interactions [16]. A 5\_C coalescence temperature is observed at 500 MHz for the resonances of the equilibrating metal bound hydrogens of **1b** and **1a** in an equimolar sample of **1b** dissolved in toluene and placed under 0.5 atm of hydrogen. From the observed coalescence temperatures ( $T_c$ ), activation energies of 10.5, 10.9, and 11.9 kcal/mol can be estimated [17] for the interconversion of the dihydrogen and unsaturated chloro, bromo, and iodo complexes respectively from the equation 2 where  $\Delta\nu$  is the

$$\Delta G^\ddagger = 2.3RT_c(10.32 + \log[\Delta\nu/(\pi \Delta\nu_c + 2)]) \quad (2)$$

distance in Hertz between the two resonances at slow exchange. A notable shift in the equilibrium position between the dihydrogen and unsaturated complexes can also be seen by comparison of the spectra obtained at -80\_C. Considering **2a** and **3a** contain twice the number of metal bound hydrogens as **2b** and **3b**, the ratios of the integrated intensities of the equilibrating complexes at -80\_C show the equilibria to consist of the unsaturated and dihydrogen complexes in 1.10:1, and 0.64:1 ratios for bromo, and iodo complexes respectively. This difference in equilibrium position reflects a greater thermodynamic stabilization of the dihydrogen ligand in the case of the iodo complex. The dihydrogen ligand in both complexes is highly stabilized in comparison to the chloro analog for which the ratio of **1b** to **1a** was found to be 1.74 at 0.5 atm of hydrogen.

The thermodynamic stability of our dihydrogen complexes follows the  $\text{I} > \text{Br} > \text{Cl}$  trend in  $\sigma$ -donor strengths [18]. Increasing halide  $\sigma$ -donation results in increased electron density at the metal center and thus enhancement of the  $d-\sigma^*$  metal-dihydrogen interaction. This explanation is consistent with the lack of dihydrogen character found for the metal bound hydrogen in  $\text{IrH}_2(\text{PPr}^3)_2$  [19] where a strong  $\sigma$ -donating hydride replaces the halide ligand in our complexes. The observation of a lower activation energy for the interconversion of the chloro complexes than for bromo complexes is also accounted for by the weaker  $\sigma$ -donor strength of Cl\_ versus Br\_ since lower electron density at the iridium center results in a lower barrier to the initial approach of dihydrogen. Unfortunately, the dihydrogen complex predominates the **3b/3a** equilibrium rather than the unsaturated complex as is the case for the **2b/2a** and **1b/1a** equilibria. Therefore, the activation energy observed for the interconversion of the iodo complexes reflects the barrier to elimination of dihydrogen from **3a** and thus cannot be compared to the activation energies found for the uptake of dihydrogen by **1b** and **2b**. We conclude that in addition to the established influences of  $\pi$ -acceptor abilities and steric constraints, the  $\sigma$ -donor abilities of ancillary ligands contribute to the kinetic and thermodynamic stabilities of dihydrogen complexes.

In a collaborative research projects with Prof. Kurt Zilm of Yale University we are studying the dynamic behavior the H<sub>2</sub> ligand of **1a** through single crystal, variable temperature solid state <sup>1</sup>H and <sup>2</sup>H NMR spectroscopy. These studies have indicated that the dihydrogen and hydride ligands intraconvert through a bis(dihydrogen) intermediate. As seen in Scheme 1, the metal-bound hydrogen remain paired in this process [8]. The connection of these studies to the process of reversible hydrogen binding by these complexes has emerged from collaborative research with Dr. Juergen Eckert of Los Alamos National Laboratory. Dr. Eckert has developed expertise in estimating the strength of metal-dihydrogen and hydrogen-hydrogen interactions in dihydrogen complexes through inelastic neutron scattering experiments [20]. Our studies [9] have revealed an extremely low barrier to rotation of the dihydrogen ligand of **1a**, reflecting a remarkable preservation of hydrogen-hydrogen bonding. In addition to the direct interaction between the metal center and the dihydrogen ligand a strong interaction between the dihydrogen and hydride ligands has been demonstrated [21]. The extremely rapid intramolecular dihydrogen-hydride interconversion observed for **1a** appears to be responsible for the extremely low degree of disruption of the H-H bonding interaction in the dihydrogen ligand of these complexes.

### Nonclassical Polyhydride Iron Complexes Containing $\pi$ -Ancillary Ligands.

We have continued our efforts to prepare complexes stabilized by  $\eta^5$ -cyclopentadienyl ligands. We have sought to generate such a nonclassical polyhydride complex through protonation of the diruthenium complex  $\{(\eta^5\text{-C}_5(\text{CH}_3)_5)\text{Ru}(\mu\text{-H})_2\}_2$ , **4**, [22] with HOSO<sub>2</sub>CF<sub>3</sub> followed by neutralization with a hydride source, LiBH(C<sub>2</sub>H<sub>5</sub>)<sub>3</sub> under an atmosphere of hydrogen. In arene solvents this reaction sequence leads to formation of  $\eta^6$ -arene complexes as seen in Scheme 2. Reaction in methylene chloride solution, led to the formation of new polyhydride complexes. However, characterization of the products through multinuclear NMR and far infrared spectroscopy has revealed that the products are the  $\mu$ -chloro substituted dimeric products:  $\{\eta^5\text{-C}_5(\text{CH}_3)_5\}\text{Ru}(\mu\text{-H})_3(\mu\text{-Cl})\text{Ru}\{\eta^5\text{-C}_5(\text{CH}_3)_5\}$ ,  $\{\eta^5\text{-C}_5(\text{CH}_3)_5\}\text{Ru}(\mu\text{-H})_2(\mu\text{-Cl})_2\text{Ru}\{\eta^5\text{-C}_5(\text{CH}_3)_5\}$ , and  $\{\eta^5\text{-C}_5(\text{CH}_3)_5\}\text{Ru}(\mu\text{-H})_3(\mu\text{-Cl})\text{Ru}\{\eta^5\text{-C}_5(\text{CH}_3)_5\}$  seen in Scheme 1 rather than the desired product,  $\{\eta^5\text{-C}_5(\text{CH}_3)_5\}\text{RuH}_5$ . We have subsequently found that the H/Cl substitution reaction occurs slowly in solution of **4** in chlorinated solvents and that HOSO<sub>2</sub>CF<sub>3</sub> acts to catalyze the substitution reaction. We have recently obtained new polyhydrides from the protonation of **4** in tetrahydrofuran solution. <sup>1</sup>H NMR spectroscopic studies have confirmed the presence of metal-bound hydrogens in the complex. However, determination of the number metal-bound hydrogens as well as the determination of their hydride versus dihydrogen character awaits further studies.

This past year, a dimeric cobalt complex which was initially reported [23] as  $\{(\eta^5\text{-C}_5(\text{CH}_3)_5)\text{Co}\}_2$ , was found [24] to actually be the polyhydride complex,  $(\eta^5\text{-C}_5(\text{CH}_3)_5)\text{Co}(\mu\text{-H})_3\text{Co}(\eta^5\text{-C}_5(\text{CH}_3)_5)$ , **5**. The misidentification of the complex was due to complex's paramagnetic nature which resulted in failure to detect the hydride ligands by NMR spectroscopy. Bridging hydride complexes of this type had not previously been reported for any of the first transition series metals. Thus when the true identity of complex **5** was reported we

quickly sought to apply the reaction sequence we had developed for the target ruthenium complex to the synthesis of an analogous cobalt complex. As seen in Scheme 3, the reaction of **5** with  $\text{HOSO}_2\text{CF}_3$  in pentane under an atmosphere of hydrogen gives rise to a mixture of diamagnetic hydrides which we have tentatively identified on the basis of  $^1\text{H}$  NMR as  $\{\eta^5\text{-C}_5(\text{CH}_3)_5\}\text{CoH}_2(\text{H}_2)$  and  $[\{\eta^5\text{-C}_5(\text{CH}_3)_5\}\text{CoH}(\text{H}_2)]^{1+}$ .

## Future Directions

The iridium nonclassical polyhydride complexes have proven to be excellent models for the study the influences of ancillary ligands on the energetics of reversible hydrogen binding. We plan to extend our study the electronic effects of other ancillary fluoride and alkoxide ligands. The insights gained in the study of these model complexes should be directly applicable to cyclopentadienyl nonclassical polyhydride complexes once they are developed.

We are cautiously optimistic that our synthetic efforts may have yielded the target cyclopentadienyl nonclassical polyhydride cobalt and ruthenium complexes. We are currently characterizing these complexes by multinuclear NMR and infrared spectroscopy. We also hope to carry out single crystal X-ray structure determinations of the product complexes.

Finally, we plan to explore synthesis of the indenyl complexes,  $\{\eta^5\text{-indenyl}\}\text{FeH}(\text{H}_2)_2$  and  $\{\eta^5\text{-indenyl}\}\text{CoH}_2(\text{H}_2)$ . The indenyl ligand is known to hydrogenate under mild conditions [25]. Also the coordinated  $\eta^5$ -cyclopentadienyl ring of the indenyl ligand is known [26] to undergo "ring slippage" from an  $\eta^5$  to an  $\eta^3$  coordination mode thus providing an additional coordination site at the metal center. As seen in Scheme 4, occurrence of ring slippage in conjunction with hydrogenation of the indenyl ligand would allow uptake several additional equivalents of hydrogen than the corresponding cyclopentadienyl complex. The indenyl complex seen in Scheme 3 would liberate 6.5 weight percent hydrogen if proposed hydrogenation process proves reversible. The  $\eta^5$ -indenyl polyhydride complex,  $\text{ReH}_2(\eta^5\text{-C}_9\text{H}_7)(\text{PPh}_3)_2$ , was recently prepared [27] through the reaction of the polyhydride complex,  $\text{ReH}_7(\text{PPh}_3)_2$  with indene. Guided by this precedent, we will explore the reaction of the complex anions  $[\text{FeH}_6]^{4-}$  and  $[\text{CoH}_5]^{4-}$  [28] with indene in the presence of oxidants such as  $\text{CuCl}_2$  in hopes of preparing  $\{\eta^5\text{-indenyl}\}\text{FeH}(\text{H}_2)_2$  and  $\{\eta^5\text{-indenyl}\}\text{CoH}_2(\text{H}_2)$ .



## References

- Selvan P., B. Viswanathan, and C.S. Srinivassan. 1986. *Int.J. Hydrogen Energy* 11:169 and references therein.
  - Suda S. 1987. *Int. J. Hydrogen Energy* 12:2323.
- Wallace W.E., R.S. Craig, O.V.S. Rao. 1980. *Adv. Chem.Ser.* 186:207.
  - Pick M.A., and M. Wenzel. 1977. *Int. J. Hydrogen Energy* 1:413.
- Kubas G.L. 1988. *Acc. Chem Res.* 21:120 and references therein.
- Mediati, M., G.N. Tachibana, and C.M. Jensen. 1990. *Inorg. Chem.* 29:3.
- Mediati, M., G.N. Tachibana, and C.M. Jensen. 1992. *Inorg. Chem.* 31:1827.
- Hay, P.J. 1987. *J. Am. Chem. Soc.* 109:705.
  - Saillard, J.Y. and R. Hoffmann. 1984. *J. Am. Chem. Soc.* 106:2006.
  - Jean, Y., O. Eisenstein, F. Volatron, B. Maouche, and F. Sefta. 1986. *J. Am. Chem. Soc.* 108:6587.
  - Burdett, J.K., J.R. Phillips, M.R. Pourian, M. Poliakoff, J.J. Turner, and R. Upmacis. 1987. *Inorg. Chem.* 26:3054.
- Cotton, F.A. and R.L. Luck. 1989. *J. Am. Chem. Soc.* 111:5757.
  - Howard, J.A.K., S.A. Mason, O. Johnson, I.C. Diamond, C. Crennell, P.A. Kellar, and J.L. Spencer. 1988. *J. Chem. Soc., Chem. Commun.* 1502.
  - Heinekey, D.M., N.G. Payne, and G.K. Schulte. 1988. *J. Am. Chem. Soc.* 110:2303. (d) Zilm, K.W., Heinekey, J.M. Millar, N.G. Payne, and P. Demou. 1989. *J. Am. Chem. Soc.* 111:3088.
- Wisniewski, L.L., M. Mediati, C.M. Jensen, and K.W. Zilm. 1993. *J. Am. Chem. Soc.* in press.
- Eckert, J., C.M. Jensen, M. Mediati, G.R. Iseminger, and O. Eisenstein. submitted to *J. Am. Chem. Soc.*
- Werner, H., J. Wolf, A. Hohn. 1985. *J. Organomet. Chem.* 287:395.
- Onderdelinden, A.L., A. van der Ent. 1971. *Inorg. Chim. Acta.* 6:420.
- van der Ent, A., A.L. Onderdelinden. 1973. *Inorg. Synth.* 14:92.
- Crabtree, R.H. 1990. *Acc. Chem. Res.* 23:95 and references therein.
- Crabtree, R.H., D.G. Hamilton. 1988. *Adv. Organomet. Chem.* 28:299.
- Luo, X.; R. H. Crabtree. 1990. *Inorg. Chem.* 29:2788.

16. (a) Cotton, F.A., R.L. Luck, D.R. Root, R.A. Walton. 1990. *Inorg. Chem.* 29:43.  
(b) Desrosiers, P.J.; L. Cai, Z. Lin, R. Richards, J. Halpern. 1991. *J. Am. Chem. Soc.* 113:4173.
17. Lambert, J.B., H. F. Shurvell, L. Verbit, R.G. Cooks, G.H. Stout. 1976. *Organic Structural Analysis*. New York: Macmillan. p116-117.
18. (a) Atwood, J.D. 1985. *Inorganic and Organometallic Reaction Mechanisms*. Monterey: Brooks/Cole. p 54.  
(b) Cotton, F.A., G. Wilkinson, *Advanced Inorganic Chemistry*, 5th ed. 1988. New York: John Wiley & Sons. p. 1300.
19. Garlaschelli, L., S.I. Khan, R. Bau, G. Longoni, T.F. Koetzle, 1985. *J. Am. Chem. Soc.* 107:7212.
20. Eckert, J., G.J. Kubas, P.J. Hay, J.H. Hall, C.M. Boyle. 1990. *J. Am. Chem. Soc.* 112:2324.
21. Van Der Sluys, L.S., J. Eckert, O. Einsenstein, J.H. Hall, J.C. Huffman, S.A. Jackson, T.F. Koetzle, G.J. Kubas, P.J. Vergamini, and K.G. Caulton. 1990. *J. Am. Chem.* 112:4831.
22. Suzuki, H., H. Omori, D.H. Lee, Y. Yoshida, Y. Moro-oka. 1988. *Organometallics*. 7:2243.
23. Schneider, J.J., R. Goddard, S. Werner, C. Kruger. 1991. *Angew. Chem. Int. Ed. Engl.* 30:1124.
24. Kersten J.L., A.L. Rheingold, K.H. Theopold, C.P. Casey, R.A. Widenhoefer, C.E.C.A. Hop. 1992. *Angew. Chem. Int. Ed. Engl.* 31:1341.
25. Osiechi, J.H., C.J. Hoffman, and D.P. Hollis. 1965. *J. Organomet. Chem.* 3:107.
26. Casey, C.P. and J.M. O'Connor. 1985. *Organometallics* 4:384.
27. Rosini, G.P., and W.D. Jones. 1993. *J. Am. Chem. Soc.* 115:965.
28. (a) Didisheim, J.J., P. Zolliker, K. Yvon, P. Fischer, J. Schefer, M. Gubelmann, and A.F. Williams. 1984. *Inorg. Chem.* 23:1953.  
(b) Zolliker, P., K. Yvon, P. Fischer, and J. Schefer. 1985. *Inorg. Chem.* 24:4177.

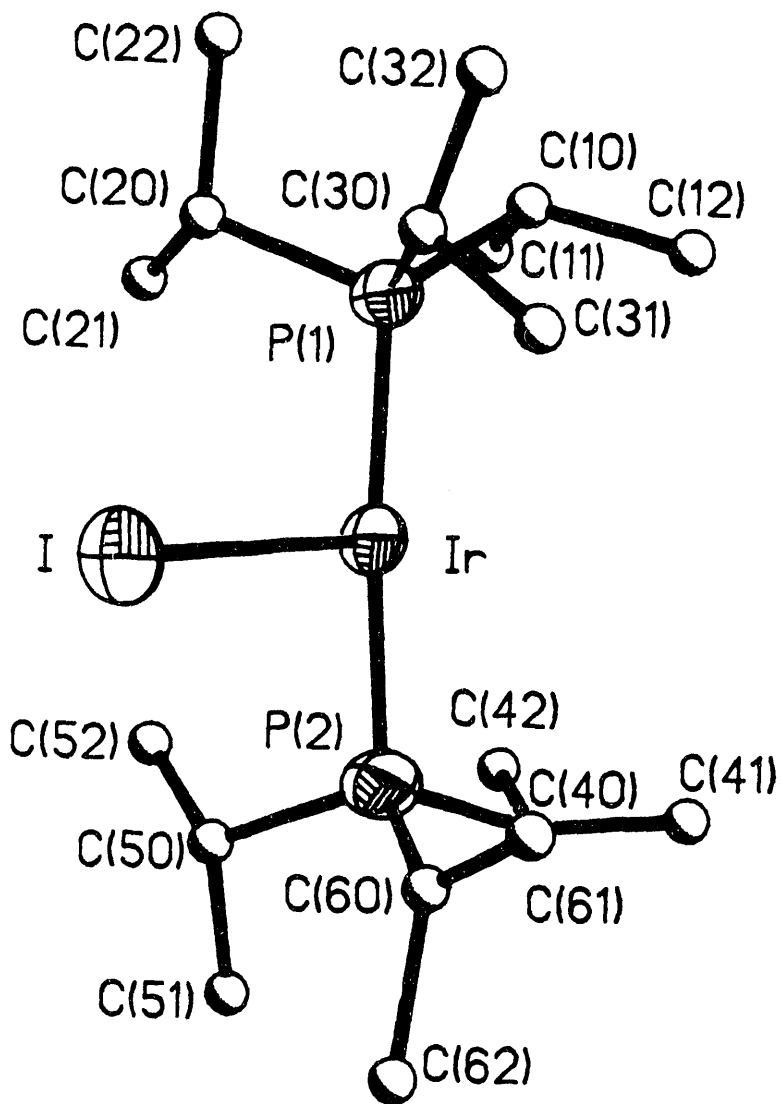


Figure 1. ORTEP Project of IrH<sub>2</sub>(H<sub>2</sub>)(PPr<sup>i</sup><sub>3</sub>)<sub>2</sub>

Figure 2. Variable-temperature  $^1\text{H}$  NMR Spectra (500 MHz) of the Hydride Region of  $\text{IrBrH}_2(\text{PPr}^i_3)_2$ , Dissolved in Toluene- $d_8$  Under 0.5 atm of  $\text{H}_2$  (total pressure)

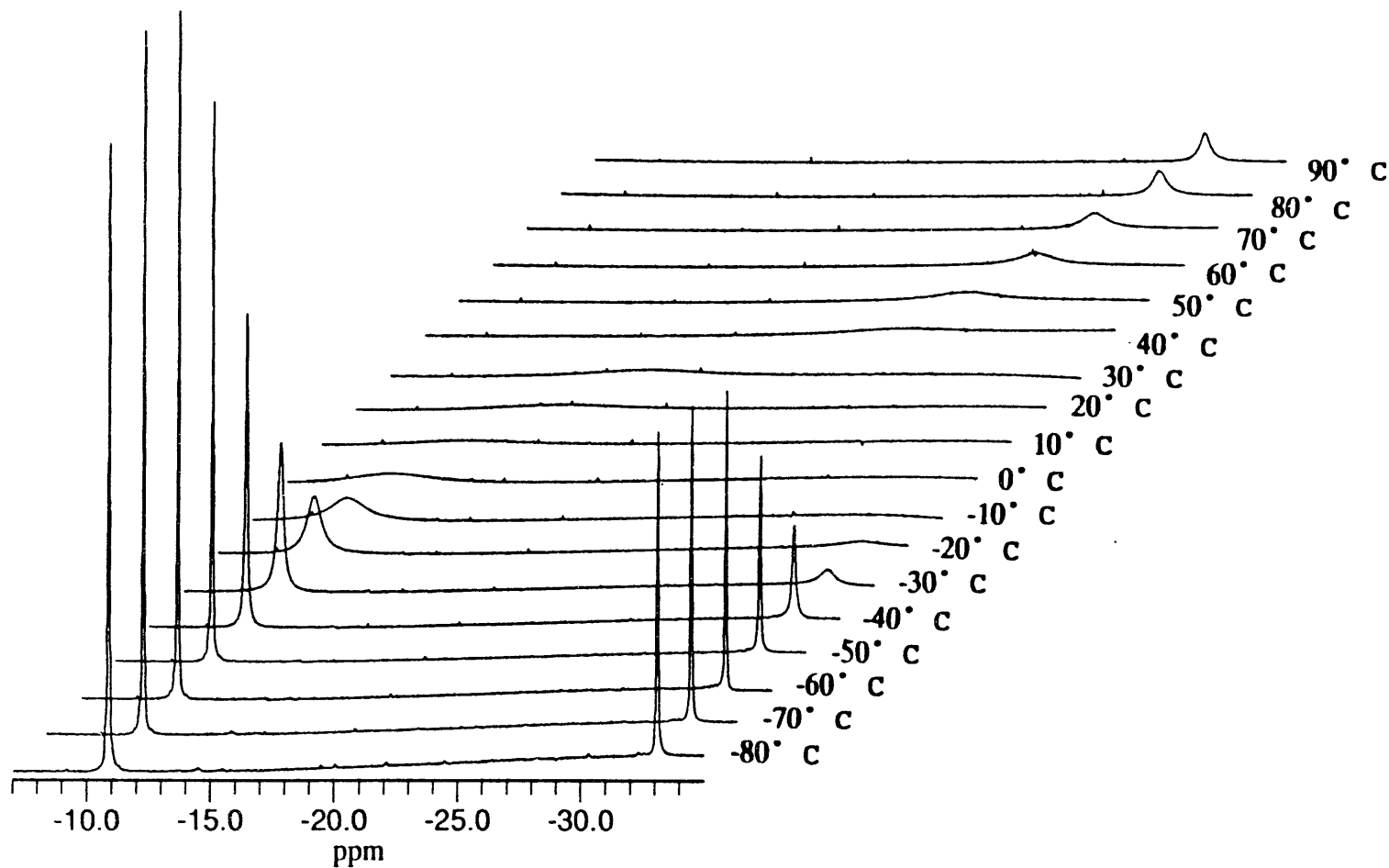
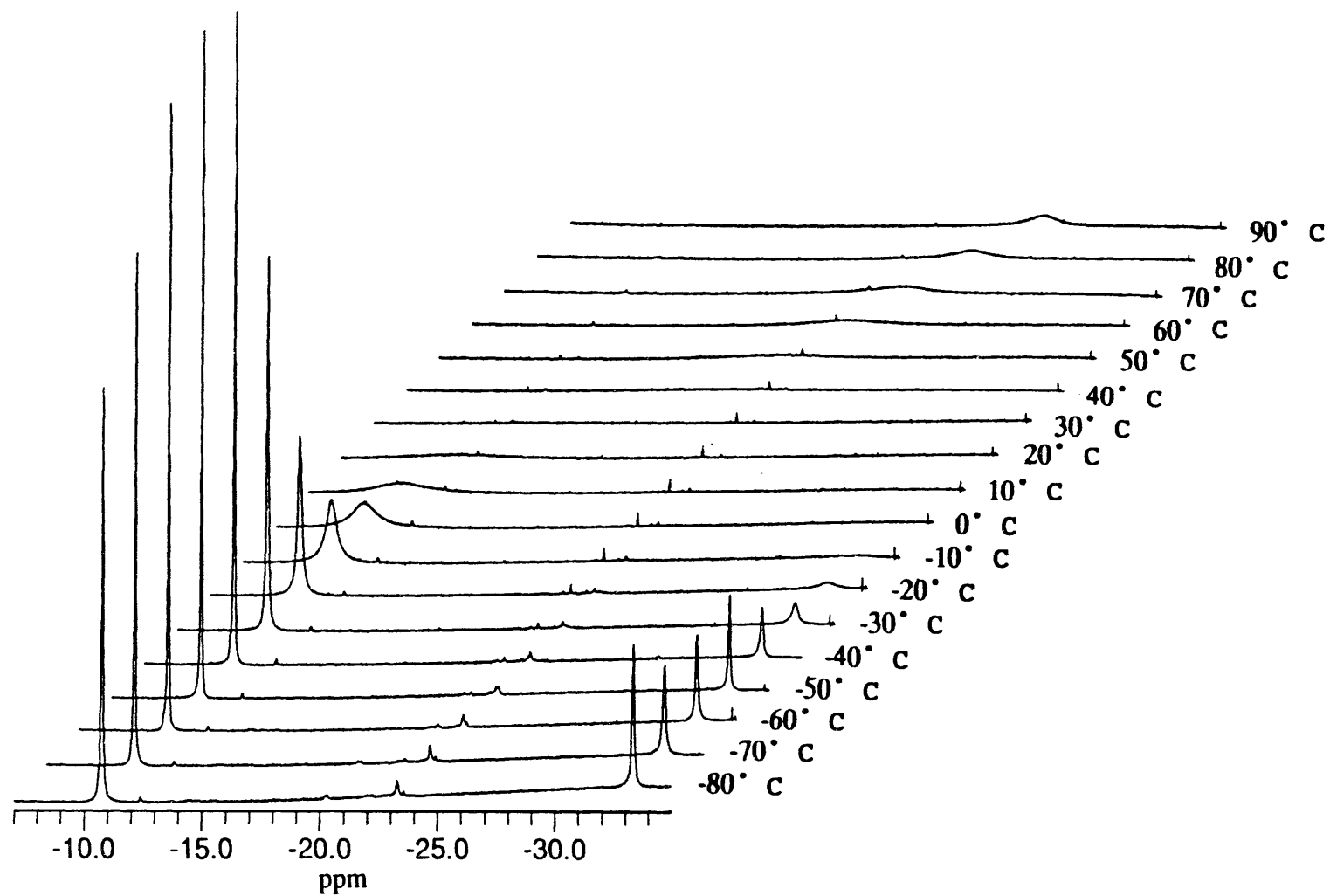
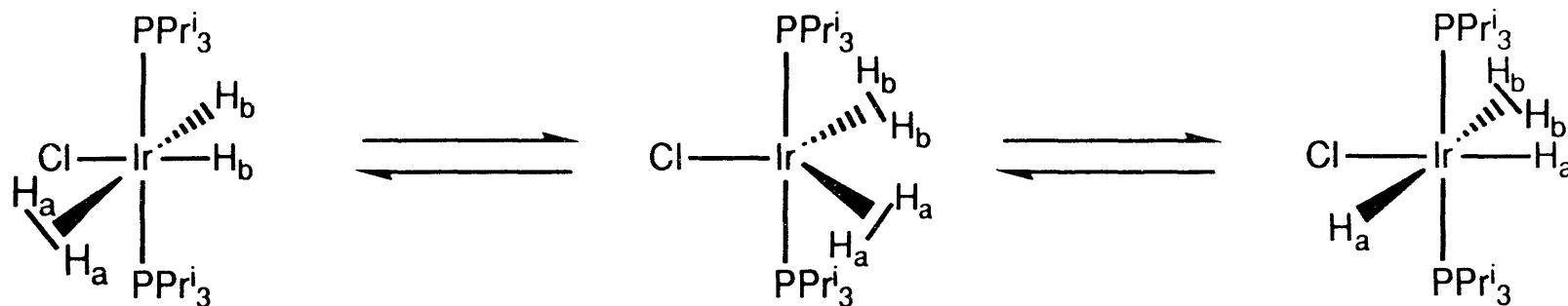


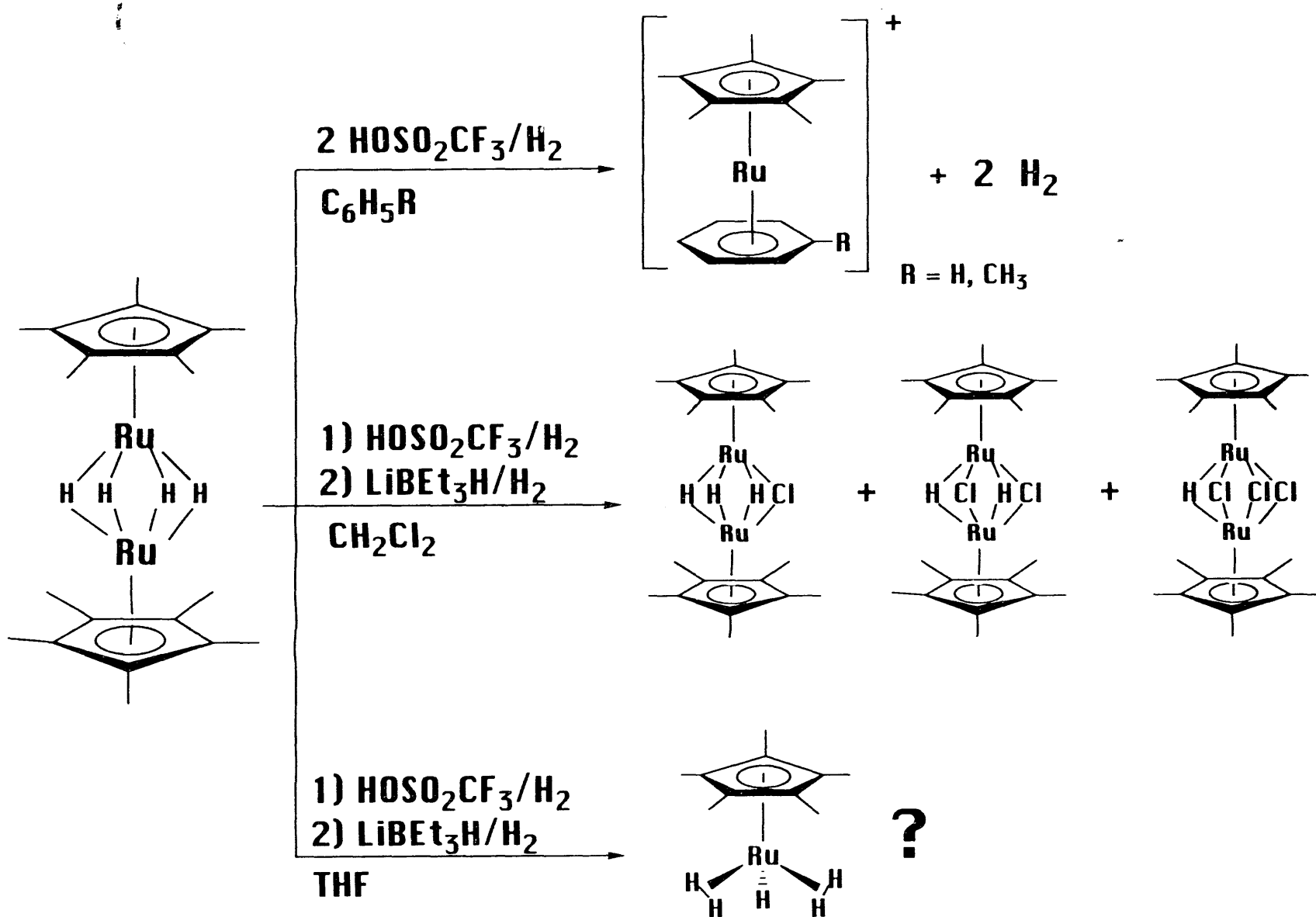
Figure 3. Variable-temperature  $^1\text{H}$  NMR Spectra (500 MHz) of the Hydride Region of  $\text{IrH}_2(\text{PPr}^i_3)_2$  Dissolved in Toluene- $d_8$  Under 0.5 atm of  $\text{H}_2$  (total pressure)



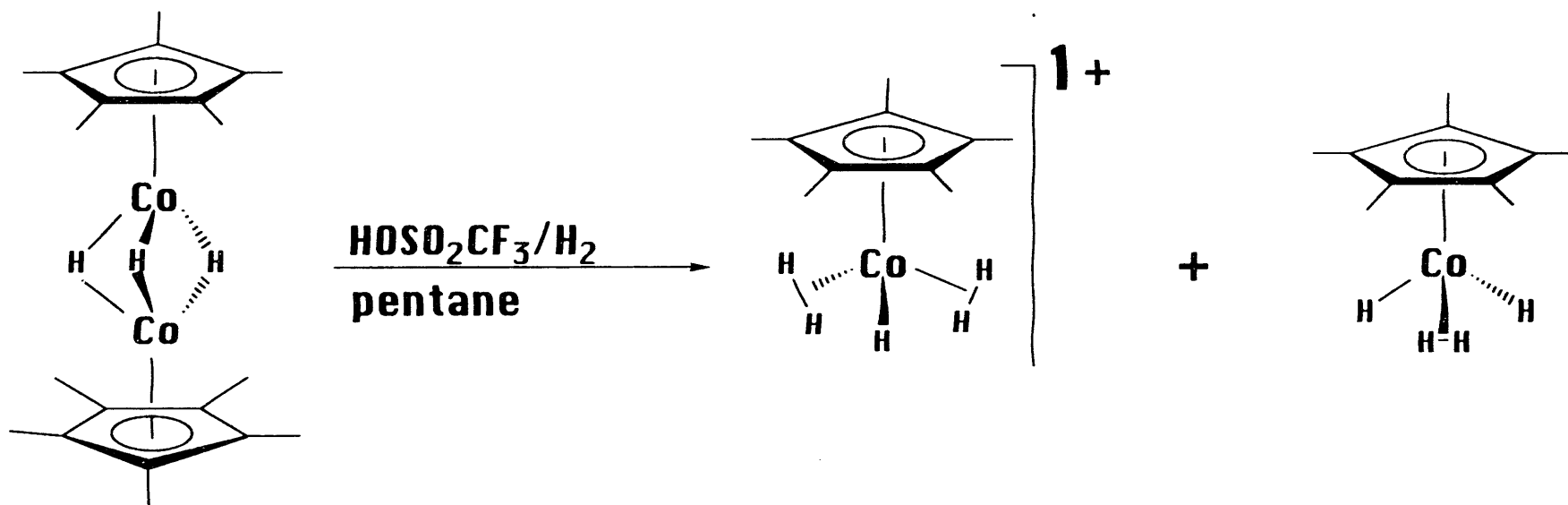
# Scheme 1.



# Scheme 2.

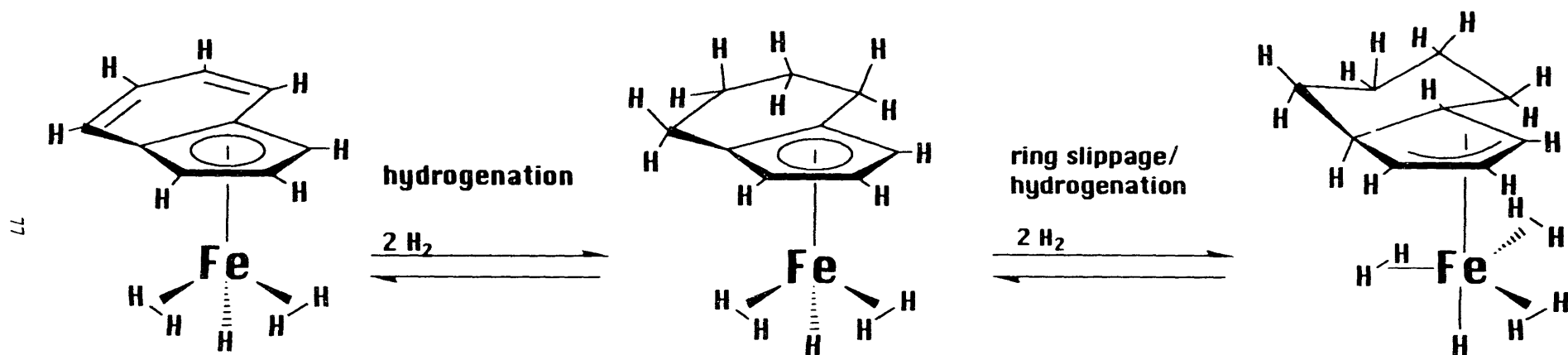


# Scheme 3.





# Scheme 4.





# CARBON NANOTUBULES FOR HYDROGEN STORAGE

Michael J. Heben  
National Renewable Energy Laboratory  
Golden, CO 80401-3393

## Abstract

The lack of convenient and cost-effective hydrogen storage options is a major impediment to wide scale use of hydrogen in the U.S. energy economy. Improvements in both the volumetric and gravimetric energy densities of hydrogen storage systems are required before viable hydrogen energy use pathways can be established. The need for compact and light-weight hydrogen storage systems is particularly evident when the requirements for personal transportation vehicles are examined. Activated carbon materials have been projected to meet and exceed the U.S. Department of Energy hydrogen storage energy density targets for transportation if concurrent increases in hydrogen storage capacity and carbon density can be achieved. These two goals are in conflict for conventional porous materials such as activated carbons. However, the desired results may be obtained if the void spaces in high surface area materials can be organized into an optimal configuration. Recent demonstrations of the synthesis of carbon nanotubes by the process of spark-gap evaporation indicate that such organization is possible. In addition to surface adsorption storage, pores within assemblies of carbon nanotubes might be of the proper size to allow nanocapillary filling mechanisms to become operative. This paper describes the progress we have made during the first six months of our research program to investigate the hydrogen storage properties of carbon nanotubes.

## Introduction

The hydrogen storage properties of high-surface-area "activated" carbons have been extensively studied before (Carpetis and Peshka, 1980; Schwarz, 1; Agarwal et al., 1987, Amankwah, 1992). These carbons are normally prepared from a variety of biological or mineralogical carbonaceous materials by processing that might include: i) chemical activation to produce dehydration or decomposition of organic constituents during subsequent heat treatments, ii) low-temperature carbonization (400-500 °C) to remove volatile organics, and iii) high-temperature oxidation (800-1000 °C) to develop porosity and surface area (Kirk et al., 1978). These methods produce microcrystalline, non-graphitic carbon materials with specific surface areas of 300-2500 m<sup>2</sup>/gm. The best currently available activated carbon adsorbs ~9 wt% H<sub>2</sub> at a temperature of 113 K and a pressure of 54.1 atm. Under these same conditions a carbon fiber-wrapped pressure vessel containing this best activated carbon would store H<sub>2</sub> at 7.2 wt% and 39 kg/m<sup>3</sup> (Amankwah, 1992). In this system, a portion of the hydrogen is stored as a compressed gas in the macro-voids of the activated carbon. The quoted energy densities of this system, though larger than expected for an actual system that would include insulation and instrumentation required to maintain a temperature of 113 K, meets the DOE Hydrogen Program Plan (FY 1993 - FY 1997) storage goal for gravimetric energy density (6.5 wt %) but does not satisfy the volumetric energy density requirement (62 kg H<sub>2</sub>/m<sup>3</sup>).

Based on consideration of a compressed gas/adsorption storage system, analysts at Arthur D. Little have concluded (Hynek, 1992) that both Hydrogen Program Plan storage goals could be met if the gravimetric energy density of hydrogen on carbon could be maintained at 8 wt% while carbon density was increased from ~0.4 to 0.8 gm/cc. This is a technically challenging task since the surface area and density of porous materials are generally inversely related. This result could be accomplished if macro-void space within the activated carbons could be organized into an optimal configuration. If the strength and type of H<sub>2</sub>/carbon interaction were to remain constant with changes in porosity and density then the storage capability would be maximized when both the surface area and the nanopore volume fraction were maximized. This situation is obtained at the limit before a high surface area material becomes a densely-packed crystalline form. We believe that this type of structural arrangement can be realized with the use of engineered carbon nanotubules.

Carbon nanotubules have recently been produced by the method of spark-gap evaporation (Iijima, 1991). These tubes can be synthesized in high yield (>75%) with inner diameters as small as 20 Å (Ebbesen and Ajayan, 1992). The synthesis involves flowing electrical current between two closely-spaced (c.a. 1 mm) coaxial graphite rods in ~500 torr of He. A plasma arc is established between the two rods and carbon atoms are evaporated from one rod and transferred to the other via a gas phase reaction. A deposit consisting of an outer shell of soots and carbon fullerenes (C<sub>60</sub>, C<sub>70</sub>, C<sub>80</sub>, etc.), and an inner core of carbon tubules is developed on the second rod. The mechanism of tubule formation is not presently understood though it is believed that the electric field plays an important role. Neither the packing of tubules in the as-deposited core, nor the size distribution of tubules within the core have been elucidated. It is reasonable to assume, however, that a close-packed arrangement of uniformly sized nanotubules could be produced with sufficient control of the synthesis. Control of the deposition process could lead to the production

of an ideal arrangement of carbon atoms where both surface area and nanopore volume would be maximized as discussed above. An idealized nanotubule assembly is shown in Figure 1. A simple calculation indicates that the close-packed assembly of 20Å diameter tubules depicted in the Figure would have a surface area close to the theoretical maximum for graphite (5000 m<sup>2</sup>/gm), and a density of ~1 gm/cc. These values are more than sufficient to reach the storage density goals established in the DOE Hydrogen Program Plan if the interaction between hydrogen and these graphitic structures remains at least as strong as is found for non-graphitic activated carbon materials. Indeed, because all of the open space in an assembly of this type is nanoporous volume (i.e. critical dimensions are only several times larger than the diameter of a hydrogen molecule), capillary filling effects (to be discussed later) could provide an additional storage mechanism that would make nanotubule assemblies particularly attractive for hydrogen storage applications.

### Technical Approach

The characteristics of a material that would exhibit a maximum capacity for hydrogen storage via adsorption have not been elucidated because a link between nanoscopic geometry, surface chemistry and H<sub>2</sub> uptake has not been established. In order to establish this link we are currently constructing and testing instrumentation that will enable carbon nanotubules to be controllably synthesized and evaluated with respect to hydrogen storage capabilities.

### Nanotubule Synthesis

Following the lead of Iijima (Iijima, 1991), we are constructing a spark-gap evaporation system for the synthesis of carbon nanotubules. The instrument is being constructed by modifying a Veeco 400 thermal evaporator and its main features are depicted in Figure 2. Two graphite electrodes, one of ~ 6 mm diameter and the other of ~9 mm diameter, are mounted onto the baseplate of the evaporator by electrically isolated positioners. Electrical feedthroughs (not shown in the figure) connect the graphite rods to a current source capable of supplying more than 100 AC amps. One positioner (P1) allows the two graphite rods to be located co-axially before the bell jar is placed to enclose the system. The second positioner (P2) enables one of the graphite rods to be translated along the axis of the rods. A rotational feedthrough imparts linear motion to this second positioner via the mating between a pinion gear and a rack gear. A pumping system consisting of a liquid nitrogen cold-trap, a diffusion pump and a roughing pump is used to evacuate the bell jar to less than 10<sup>-6</sup> torr. While the system is being pumped the two graphite rods can be brought into contact and resistively heated to remove any adsorbed gases. Once cooled and separated the rods are brought to within c.a. 1 mm of each other and the chamber is back-filled with 500 torr of helium. With an applied potential of c.a. 20 V a plasma will be established between the graphite rods. Carbon atoms are evaporated from the smaller rod and deposited on the larger one such that carbon nanotubules will be formed in a c.a. 2 mm diameter core as previously discussed. Attempts to control the geometry of the deposit will involve choices in electrode spacing, starting materials, deposition conditions (i.e. pulsed or AC currents), and ambient gas composition (e.g. other inert gases, or perhaps a carbon containing gas to provide a carbon source (CH<sub>4</sub>)). Wedge-shaped electrodes will also be employed to investigate

if tubules can be formed from a plasma which is elongated in the X or Y directions (Figure 2). These experiments will comment on the feasibility of synthesizing tubule arrays over larger areas.

### **Characterization of Nanotubules**

The structural characteristics of the carbon nanotubules will be examined by a variety of methods. The nanotubule core may be readily separated from the surrounding fullerene/soot shell by physical means (i.e. cutting) or by washing with an appropriate solvent (e.g. hexanes). Brunauer-Emmett-Teller (B.E.T) adsorption isotherms will be used to determine the surface area of the tubule assemblies. Small angle X-ray scattering (SAXS) measurements will be used to elucidate the pore-size distributions within the assemblies. Atomic force microscopy will be employed to comment on the packing density of the nanotubules. These investigations will be used to establish a relationship between the synthesis conditions and the resultant carbon structures.

The hydrogen storage properties of the nanotubule assemblies will be investigated with the use of a modified Perkin-Elmer Thermogravimetric Analysis System (TGS2). The TGS2 has been customized for our hydrogen storage studies by encasing the sample tube of the microbalance in a glass jacket that can accommodate liquid nitrogen. A temperature controlled furnace that surrounds the sample pan can then be used to achieve sample temperatures from 77K to greater than 750K. With the instrument, the hydrogen storage capacity of samples can be readily determined. The modified TGS2 will also allow the time dependence of hydrogen adsorption and desorption to be measured. This data can be used to determine activation energies for adsorption and desorption, and heats of adsorption (Czanderna, 1980).

Additional characterizations will be performed with the above mentioned techniques after the nanotubules have been released from the deposit by ultrasonication and solvent-based extraction methods. Populations of tubules with narrow size distributions will be obtained by chromatographic separation and ultracentrifugation techniques. The various fullerenes (i.e.  $C_{60}$ ,  $C_{70}$ ,  $C_{80}$ , etc.) that will be produced in the outer shell that surrounds the nanotubule core will also be investigated. Studies on these select populations will allow the hydrogen adsorption mechanisms and properties to be assessed on a well-defined structural basis.

### **Discussion: Hydrogen Adsorption on Nanotubules**

The nature of hydrogen adsorption is expected to be considerably different for graphitic nanotubule assemblies as compared to non-graphitic activated carbons. In particular, the heat of adsorption of hydrogen on Graphon (an exfoliated graphitic carbon material) was shown to be constant at  $\sim 3.8$  kJ/mol until a complete monolayer coverage was reached (Pace and Siebert, 1959), while similar measurements on activated carbons show a higher initial heat of adsorption ( $\sim 6.5$  kJ/mol in one case: Schwarz, 1992) that can be reduced by more than a factor of 5 across the adsorption isotherm (Schwarz, 1). In the former case, the hydrogen adsorption is driven by purely dispersion (van der Waals) forces at structurally similar sites while, in the latter case, a variety of structural and chemical environments are evidently active (Agarwal, 1987). The large initial heats of adsorption observed for activated carbons could be due to the overlap of the adsorption field in pores that possess dimensions comparable to the size of the hydrogen molecule, or to strong specific interactions (Gregg and Sing, 1982). If the former explanation is valid then higher heats of adsorption would be expected for nanotubule assemblies like the one depicted in Figure 1. In particular, the presence of interstitial pores between adjacent tubules might provide sites where

molecular hydrogen species would be affected by the summation of van der Waals attractions by three nearby graphitic layers. Considerations of this type have been used to predict that the heat of adsorption for methane between two graphitic planes would be enhanced by more than a factor of two when the spacing between planes was approximately twice the diameter of the methane molecule (Cracknell et al., 1993). Similar calculations have predicted strong localization of HF molecules within carbon nanotubes (Pedersen and Broughten, 1993). The same type of "molecular straw" phenomena is expected to occur, but to a lesser extent, for non-polar species (like H<sub>2</sub>) interacting with nanotubule walls (J.Q. Broughten, personal communication). The recent demonstration that Pb is sucked into carbon nanotubes by capillary forces (Ajayan and Iijima, 1993) is in agreement with this concept. An increased heat of adsorption for hydrogen on nanotubule assemblies could allow the operating pressures and temperatures of a hydrogen storage system to be decreased and increased, respectively, in comparison to the values required for activated carbon storage materials. These potential enhancements in the heat of hydrogen adsorption indicate that nanotubule assemblies might exhibit storage benefits in addition to those expected from the concurrent increases in surface area and density.

### **Future Work**

Our results so far are conceptual in nature and indicate that carbon nanotubule assemblies may be quite useful in hydrogen storage applications. Our investigations of the hydrogen storage properties of carbon nanotubes will continue during the remaining six months of the fiscal year. In addition, we will acquire and investigate commercially available nanotubule materials. Carbon tubules of micron-sized inner diameters, produced by methane decomposition in the presence of iron particles (Tibbetts, 1984), will also be investigated as a case of hydrogen adsorption on graphitic carbon where capillary forces are expected to be absent.

### **Acknowledgments**

The assistance of David Staebler and Dick Burrows in formulating this research program is greatly appreciated.

## References

- Agarwal, R.K., J.S. Noh, J.A. Schwarz, and P. Davini. 1987. "Effect of Surface Acidity of Activated Carbon on Hydrogen Storage." *Carbon*, 25:219-226.
- Ajayan, P.M., and S. Iijima. 1993. "Capillarity-induced Filling of Carbon Nanotubes." *Nature*, 361:333-334.
- Amankwah, K., 1992. "Hydrogen Storage Technology.", presentation at the Workshop on Hydrogen Storage Technologies, November 11, Golden, CO.
- Carpetis, C., and W. Peshka. 1980. "A Study on Hydrogen Storage by Use of Cryoadsorbents." *Int. J. Hydrogen Energy*, 5:539-554.
- Cracknell, R.F., P. Gordon, and K.E. Gubbins. 1993. "Influence of Pore Geometry on the Design of Microporous Materials for Methane Storage." *J. Phys. Chem.* 97:494-499.
- Czanderna, A.W., 1980. "Chemisorption Studies with the Vacuum Microbalance." in *Microweighing in Vacuum and Controlled Environments*, 175-232. A.W. Czanderna and S.P. Wolsky, Eds., New York, Elsevier Scientific Publishing CO.
- Ebbesen, T.W., and P.M. Ajayan. 1992. "Large-Scale Synthesis of Carbon Nanotubes." *Nature*, 358:220-222.
- Gregg, S.J., and K.S.W. Sing. 1982. *Adsorption, Surface Area and Porosity*, New York: Academic Press.
- Hynek, S., J. Bentley, B. Barnett, E. Shanley, and G. Melhem. 1992. Hydrogen Storage Technologies: Present and Future.", presentation to the Hydrogen Energy Council, December 9, Montreal, Quebec.
- Iijima, S. 1991. "Helical Microtubes of Graphitic Carbon." *Nature*, 354: 56-58.
- Kirk, R.E., D.F. Othmer, M. Grayson, and D. Eckroth. 1978. *Kirk-Othmer Encyclopedia of Chemical Technology*. New York: John Wiley & Sons.
- Pace, E.L., and A.R. Siebert. 1959. "Heat of Adsorption of Parahydrogen and Orthodeuterium on Graphon." *J. Chem. Phys.* 53:1398-1400.
- Pedersen, M.R., and J.Q. Broughten. 1992. "Nanocapillarity in Fullerene Tubules." *Phys. Rev. Lett.* 69:2689-2692.
- Schwarz, J.A., I. "Modification Assisted Cold Storage (MACS).", contract report to Brookhaven National Laboratories, contract # 186193-S.
- Schwarz, J.A., 1992. "Activated Carbon Based Storage System." in *Proceedings of the 1992 DOE/NREL Hydrogen Program Review*, 271-278. Honolulu, HI.



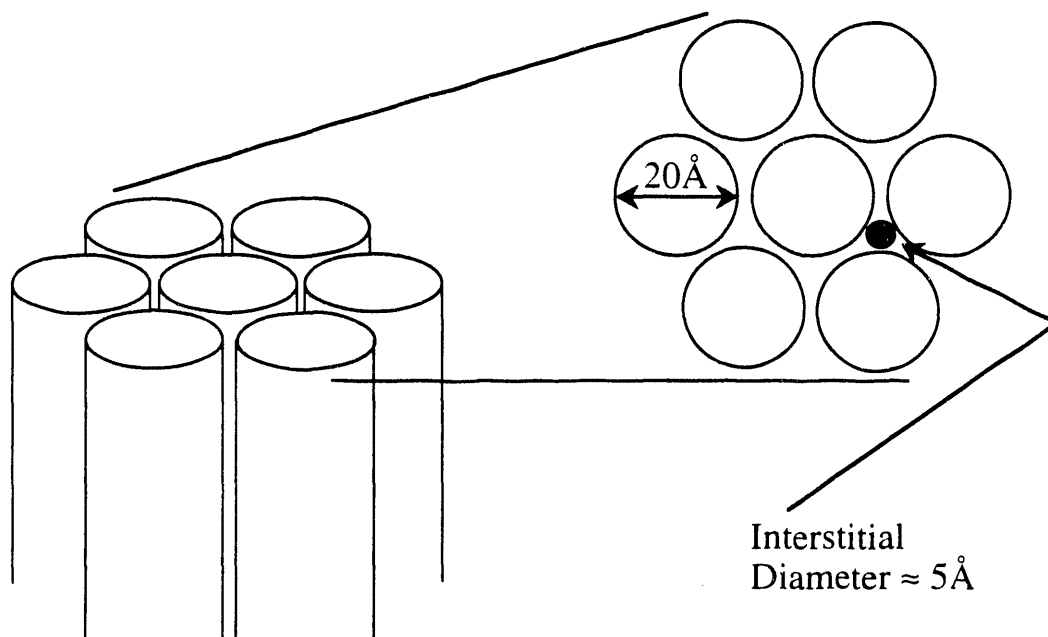
Tibbetts, G.G., 1984. "Why are Carbon Filaments Tubular?" *J. Cryst. Growth*. 66:632-638.

### Figure Captions

Figure 1: Idealized carbon nanotubule assembly.

Figure 2: Schematic diagram of spark-gap evaporation system for the synthesis of carbon nanotubules.

## Assemblies of Carbon Nanotubes



### Synthetic Control:

Pressure and Composition of Background Gas

Electrode and Plasma Geometry

Starting Materials

### Expected Properties:

Density:  $\approx 1 \text{ gm/cc}$

Surface Area:  $\approx 5000 \text{ m}^2/\text{gm}$

Heat of  $\text{H}_2$  Adsorption:  $> 4 \text{ kJ/mole}$

Figure 1

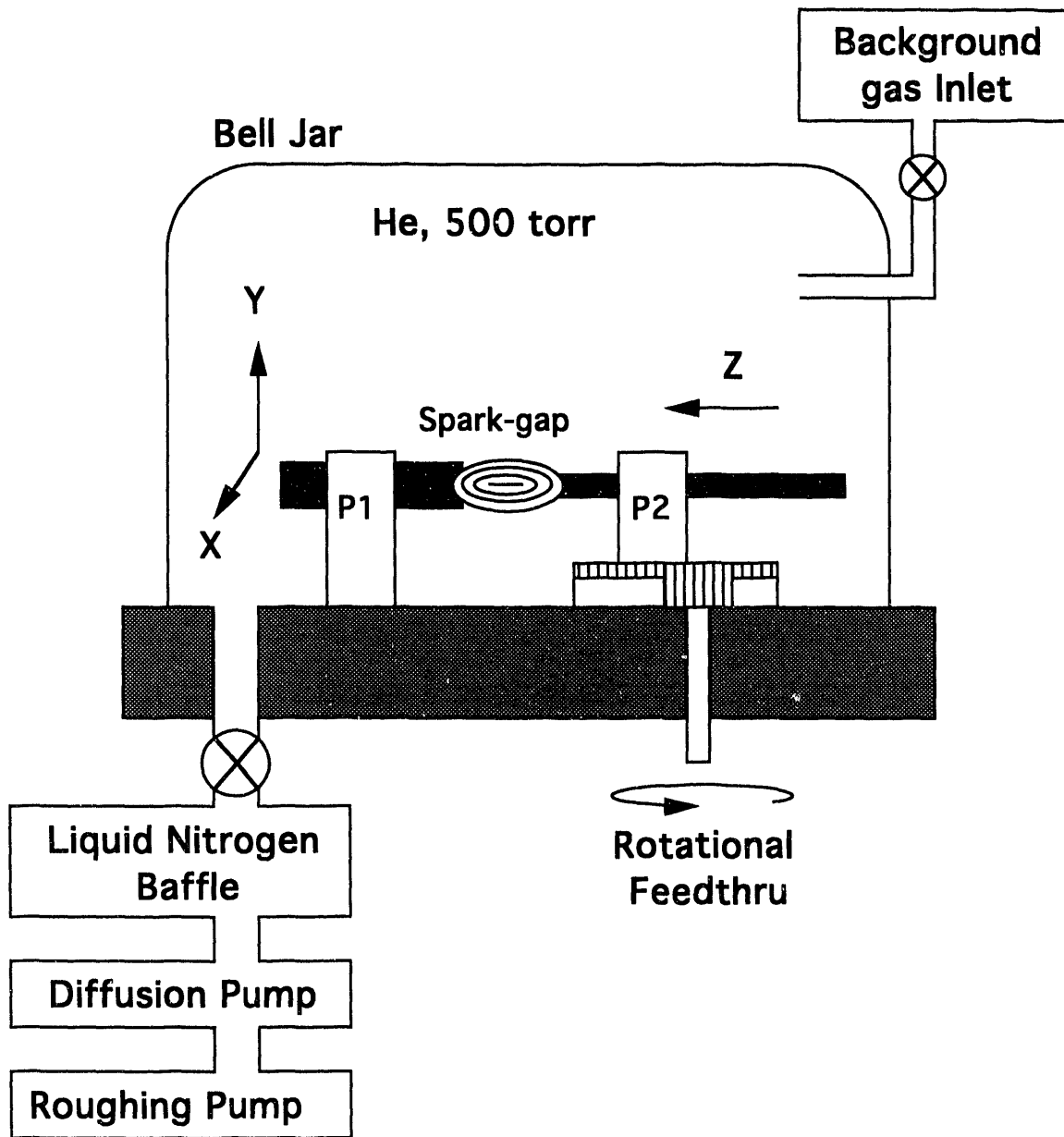


Figure 2



# Activated Carbon-Based Hydrogen Storage System

J.A. Schwarz  
Department of Chemical Engineering and Materials Science  
and  
Laboratory for Advanced Storage Systems for Hydrogen

## Abstract

Experimental results on hydrogen storage demonstrate the feasibility of on-board vehicle storage using high surface area activated carbon. ESC-3, activated carbon with 2230 m<sup>2</sup>/g area, can store up to 9.1% hydrogen by weight of carbon, 4.8% by adsorption, 4.3% by compression in voids at 87 K and 6.0 MPa (59 atm) in the pressure vessel.

## Introduction

### Background

An energy economy begins with energy resources. A sustainable energy economy requires nondepletable resources. Two categories of energy sources meeting this requirement are nuclear-based systems and renewable energy systems. Practically, however, energy use requires a form of energy that is convenient, flexible, adaptable, and controllable. Energy from the source should be deliverable virtually everywhere. Of the options available, hydrogen emerges as a prime candidate to become a significant energy carrier.

The main benefits derived from utilizing hydrogen are associated with hydrogen's versatility after it has been produced and delivered to a user. The benefits include clean combustion in numerous devices and/or efficient conversion to electricity in fuel cells. The major challenges to its use are associated with efficient, cost-effective means for converting primary energy sources to hydrogen while still maintaining an environmentally benign impact and the lack of compact, efficient means of storing hydrogen for mobile and/or stationary applications.

## Scope

Recent attention given to environmental pollution makes hydrogen appear to be an attractive alternative fuel for vehicular application, because it generates no carbon by-product pollutant. In the case of Proton Exchange Membrane (PEM) Fuel Cell powered electric vehicles utilizing hydrogen fuel, water is the sole by-product emitted.

Hydrogen storage is being seriously considered for vehicular applications. In addition to carbon adsorption, three other hydrogen storage methods were analyzed as on-board storage alternatives: compression, liquid, and metal hydride. The large volume required for compressed hydrogen gas at high pressures makes this option unattractive for vehicular applications. The handling of any cryogenic liquid makes this liquid choice difficult for vehicular applications when compared to the other methods. The metal hydride system operates under reasonable temperature and pressure conditions but is susceptible to alloy poisoning and has a weight drawback.

The high surface area activated carbon storage method utilizes physical adsorption, therefore, energy exchange is minimal. For effective hydrogen adsorption on activated carbon, a cold environment is required. Experiments described in this report were performed at temperatures between 78 K and 90 K. These temperatures were chosen primarily because of the convenience and commercial practicality of liquid nitrogen cooling.

The experiments were performed at the Laboratory for Advanced Storage Systems for Hydrogen at Syracuse University, Syracuse, NY, USA. The ESC-3 carbon used was provided by Kansai Coke and Chemicals Co., Ltd., Japan.

## Objective

This report has a two-fold objective. First, the physical adsorption performance on ESC-3 and the charging and discharging performance of a pressure vessel filled with ESC-3 were determined. Secondly, we consider its application for vehicular hydrogen storage.

## Technical

ESC-3 is an activated carbon with an average surface area of 2230 m<sup>2</sup>/g and bulk density of 0.32 kg/l in pellet form. The hydrogen gas used in the experiments has a purity of 99.999%.

Two experimental setups are used to evaluate the performance of the carbon: (1) the gravimetric approach in which a micro-balance is utilized, and (2) the volumetric approach in which a down-scaled version of a "real world" storage system is used.

Briefly, the micro-balance method (Agarwal, 1987) consists of a gravimetric test apparatus using pressurized liquid nitrogen to vary the temperatures. The buoyancy of carbon, sample pan, and the adsorbed phase are used in the calculations in order to produce the adsorption isotherms. Figure 1 depicts the schematic of this hardware configuration.

The pressure vessel method uses a 1.0 x 10<sup>-3</sup> m<sup>3</sup> (1 liter) aluminum-lined container with epoxy/S-glass composite fiber reinforcement, capable of operating at 17 MPa (168 atm) at room temperature. The

pressure vessel is placed in a liquid nitrogen bath in order to maintain a constant temperature within the vessel. Figure 2 depicts the schematic of this hardware configuration.

The first series of experiments using the pressure vessel were conducted in order to determine the total stored amount of hydrogen. The second series of experiments included the charge/discharge rate characteristics with respect to temperature and pressure changes.

To rid the carbon of moisture and pre-adsorbed gases for both the micro-balance and the pressure vessel experimental setups, the carbon is flushed with warm (323 K to 343 K) helium gas, followed by vacuum degassing down to 50  $\mu\text{m}$  overnight. Hydrogen cooled by a liquid nitrogen heat exchanger is then introduced into the pressure vessel to cool the carbon.

In the pressure vessel, the total stored amount of hydrogen consists of the adsorbed and void components. The void component is always calculated based on a given pressure, temperature and the known void volume of the carbon.

## Results

### Micro-Balance Data

Gravimetric data in Figure 3 show the adsorption isotherms of ESC-3 at three temperatures (i.e., 90 K, 85 K and 78 K). The adsorbed amount ranged from 4% to 7% hydrogen by weight of carbon with pressure corresponding to 2.0 MPa to 5.7 MPa (20 atm - 56 atm).

Figure 4 depicts the variation of stored components with pressure at 78 K. It should be noted that the total amount is the sum of the adsorbed and void components which is referred to as "Total" in the figure. The total stored amount of hydrogen observed at 5.7 MPa (56 atm) and 78 K is 11.8%. The difference between the adsorbed and void components is referred to as "Difference" in the figure. The total stored amount increases monotonically with pressure but not necessarily in the case of the difference. In particular, it is observed that its value reaches a maximum around 1.5 MPa (15 atm). This maximum corresponds to the greatest enhancement in adsorption caused by the presence of the carbon.

### Pressure Vessel Data

Volumetric data were obtained by charging the pressure vessel to 6.0 MPa (59 atm) at 87 K. The total stored amount of hydrogen is 2.91 g, which is 9.1% hydrogen by weight of carbon as measured by a mass flow controller and a calibrated totalizer which is shown in Figure 1. The adsorbed component, 4.8% hydrogen by weight of carbon was determined by subtracting the void component from the measured total stored amount. The adsorbed amount of 4.8% appears to be reasonable in light of the adsorption isotherm at 85 K in Figure 3.

There are two basic charge rate profiles investigated in this study. The first one is a high pressure/short time (8.2 MPa(81 atm)/30 sec) charge profile. The equilibrium pressure of 4.2 MPa (42 atm) is attained in less than 10 min. The second one is at a lower and constant pressure of 6.2 MPa (61 atm) held for 10 min, which resulted in higher equilibrium pressure of 4.9 MPa (48 atm) in less than 10 min. The total elapsed time is less than 20 min. Figure 5 shows the characteristics described. These data show that the charge rate profile with relatively lower pressure and longer time held obtained a certain stored amount

of hydrogen with relatively small change of pressure. Because the goal for vehicular refueling is a reasonably short charge time, the charge rate profile is important in determining the total stored amount.

Three discharge rate experiments were conducted at 10 slpm, 25 slpm and 50 slpm, and Figures 6 and 7 show the resultant plots. Desorption is endothermic, but the heat involved is insignificant. The data show that hydrogen storage using the activated carbon can release hydrogen at high rates without additional heating. Therefore, this storage method will be able to satisfy the demands of PEM fuel cells or internal combustion engines for vehicles.

## Discussion of Results

Based on the data from the down-scaled "real world" experiments, the following system design can be extrapolated. Using a  $1.0 \times 10^{-1} \text{ m}^3$  (100 liter) composite pressure vessel (Private Communication), 32.3 kg of carbon will be required to fill the pressure vessel. The pressure vessel is constructed from an aluminum liner reinforced with graphite/epoxy composite fiber overwrap. The designed operational pressure is 8.2 MPa (81 atm), with a safety factor of 2.25. This vessel will be able to store 2.91 kg of hydrogen at 6.0 MPa (59 atm) and 87 K. The weight of the pressure vessel with an additional vacuum jacket and insulation is 32.5 kg, with the total system weight being 67.9 kg including carbon and stored hydrogen. Consequently, the gravimetric energy density will be 5.22 MJ/kg, and the volumetric energy density will be 2390.4 MJ/m<sup>3</sup>.

Hydrogen capacity of 2.91 kg will suffice for vehicular applications, since approximately 3.3 kg of hydrogen is needed for a 200 km driving range for compact hydrogen internal combustion engine powered car (Nikkei, 1991), and a greater driving range is expected in the case of a PEM fuel cell powered vehicle.

The operational pressure of 6.0 MPa (59 atm) is the pressure level where both the adsorbed and void components are approximately equal in value. The void component will become dominant at pressures higher than 6.0 MPa (59 atm), which may not be desirable if the weight of the carbon storage vessel is critical (Amankwah, 1989). Additional comparison data are in Table 1 (Amankwah, 1989).



**Table 1 - Comparison of Hydrogen Storage Systems**

Storage System	Gravimetric Ratio (H <sub>2</sub> /System)	Energy Density (Gravimetric)	Energy Density (Volumetric)
Activated Carbon System (6.0 Mpa, 87 K)	4.2%	5.22 MJ/kg	2390.4 MJ/m <sup>3</sup>
Metal Hydride (1.0 MPa)	1.1%	1.43 MJ/kg	2970.0 MJ/m <sup>3</sup>
Compressed Gas (20.3 MPa) (Kevlar)	3.1%	3.74 MJ/kg	1346.4 MJ/m <sup>3</sup>
Liquid H <sub>2</sub> System (20 K) (Musashi)	6.9%	15.16 MJ/kg	3495.6 MJ/m <sup>3</sup>

### Future Work

Proposed work in this area of study for the future is outlined as follows:

- The use of well-insulated vessels shall lead to detailed studies of warm-up and cooling characteristics of the carbon bed.
- With the use of a pressure vessel in a volumetric approach, saturation points at various temperatures can be determined in the medium pressure range, i.e., 6.1 - 9.1 MPa (60 - 90 atm).
- Investigation on the effect of various distribution ports in the pressure vessel on the charging times of the system.
- Determination of optimum charging procedure.
- Choice of suitable adsorbents for hydrogen storage based on adsorption amount, charging and discharging characteristics.

## Acknowledgements \*

Grateful acknowledgement is expressed to Structural Composites Industries, Inc. of Pomona, CA, for providing design parameters for the composites vessel used in this work. Financial support from the National Renewable Energy Laboratory under Contract Number XC-2-11081-1 is also gratefully acknowledged.

## References

Agarwal, R.K., J.S. Noh, J.A. Schwarz, and P. Davini. 1987. "Effect of Surface Acidity of Activated Carbon on Hydrogen Storage." *Carbon*, 25: 219-226.

Private Communication. Structural Composites Industries, Inc., Pomona, CA.

Amankwah, K.A.G., J.S. Noh, and J.A. Schwarz. 1989. "Hydrogen Storage on Super-Activated at Refrigeration Temperatures." *Int. J. Hydrogen Energy*, 14: 437-444.

1991. *Nikkei Mechanical*, 363: 69-71.

Furuhama, S., and T. Fukuma. 1986. "High Output Power Hydrogen Engine with High Pressure Fuel Injection, Hot Surface Ignition and Turbocharging." *Int. J. Hydrogen Energy*, 11: 399-407.

## Figures

- Figure 1: Schematic of Gravimetric Apparatus
- Figure 2: Schematic of Hardware for Pressure Vessel Tests
- Figure 3: Adsorption Isotherms of ESC-3 Activated Carbon
- Figure 4: Variation of Stored Components with Pressure at 78 K
- Figure 5: Characteristics of Charging Rate Profile
- Figure 6: Pressure Profile of Carbon Bed during Discharge Mode
- Figure 7: Temperature Profile of Carbon Bed during Discharge Mode

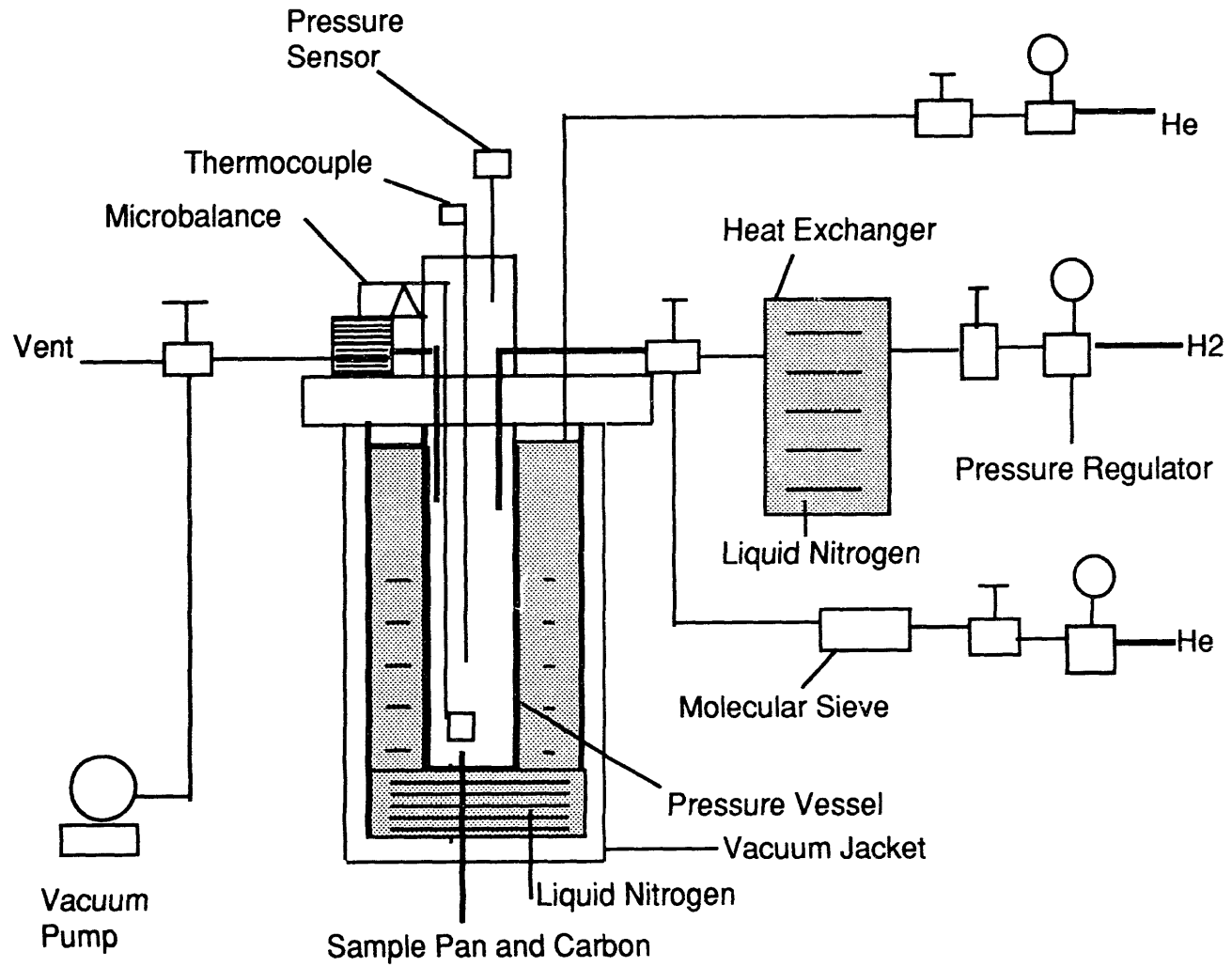


Figure 1.

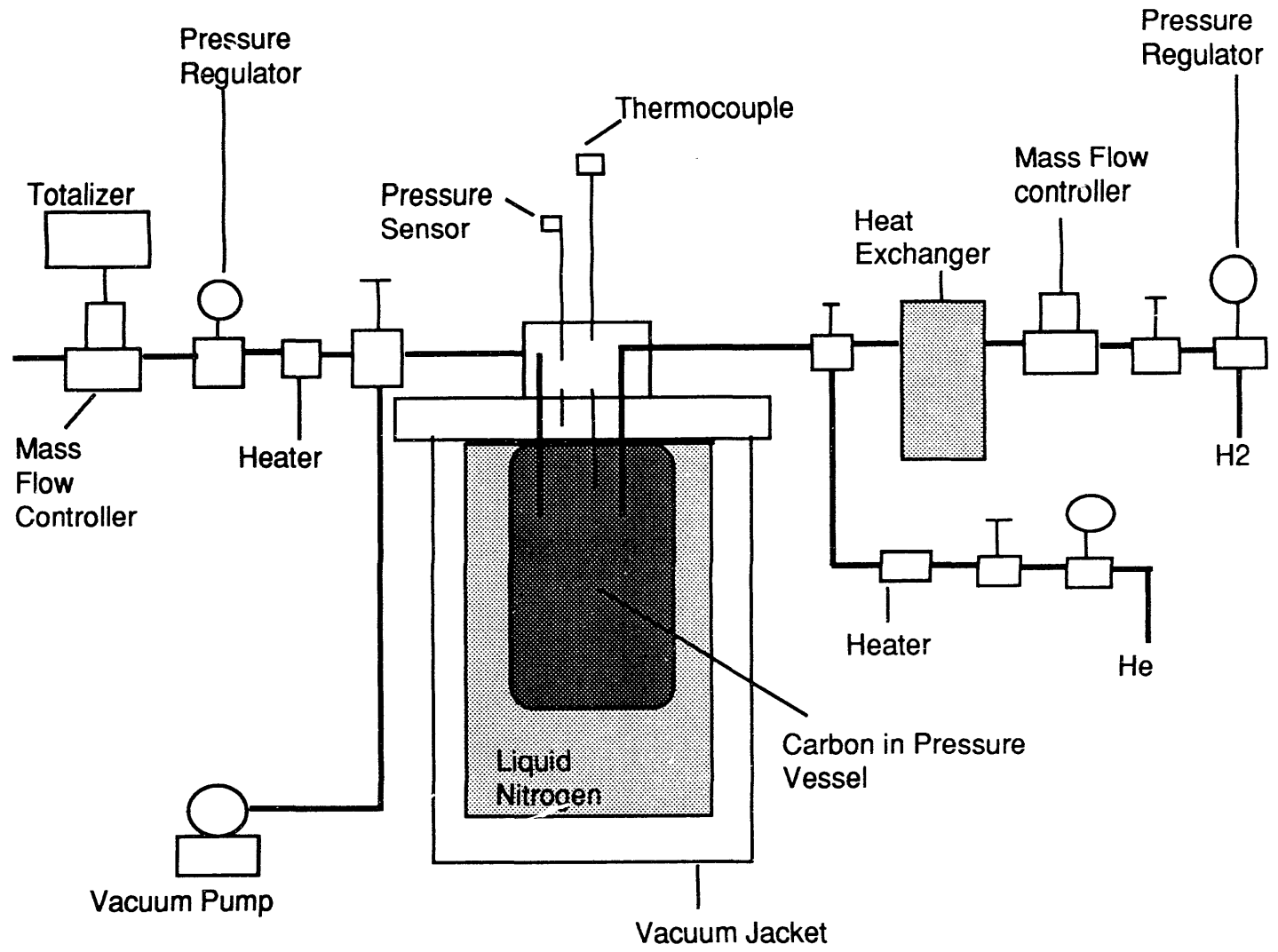


Figure 2.

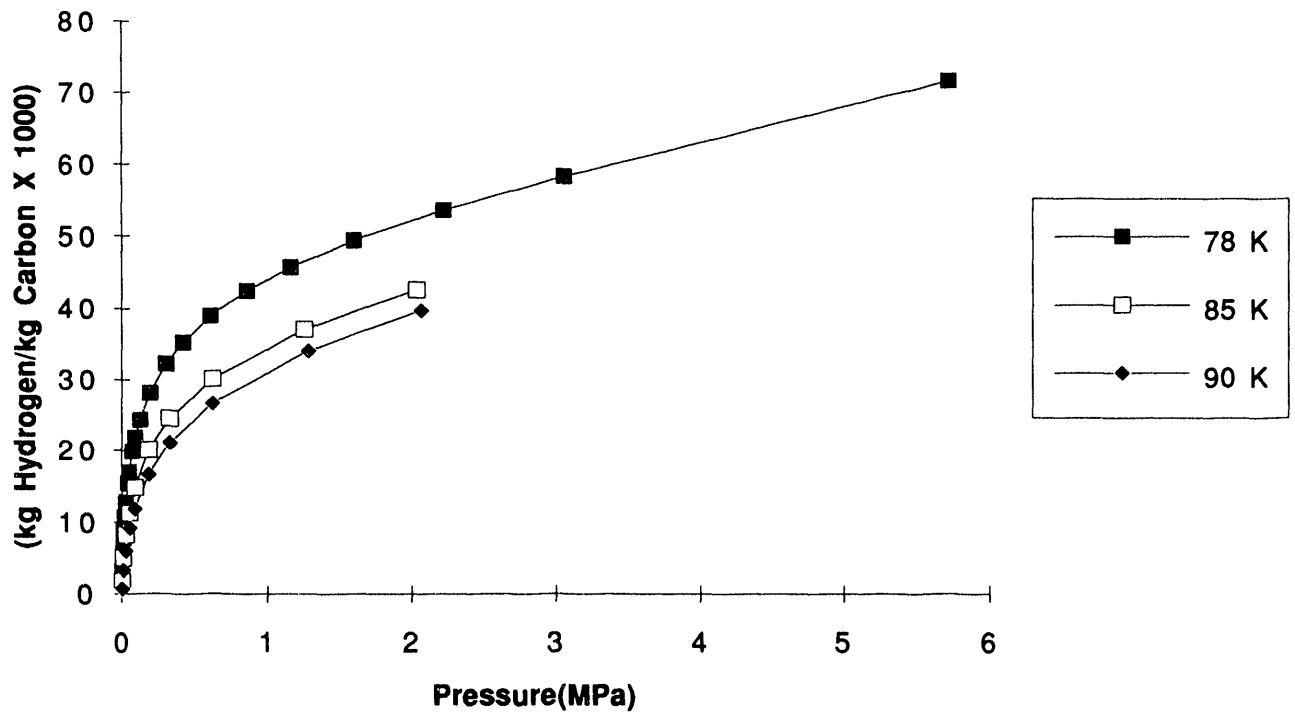


Figure 3.

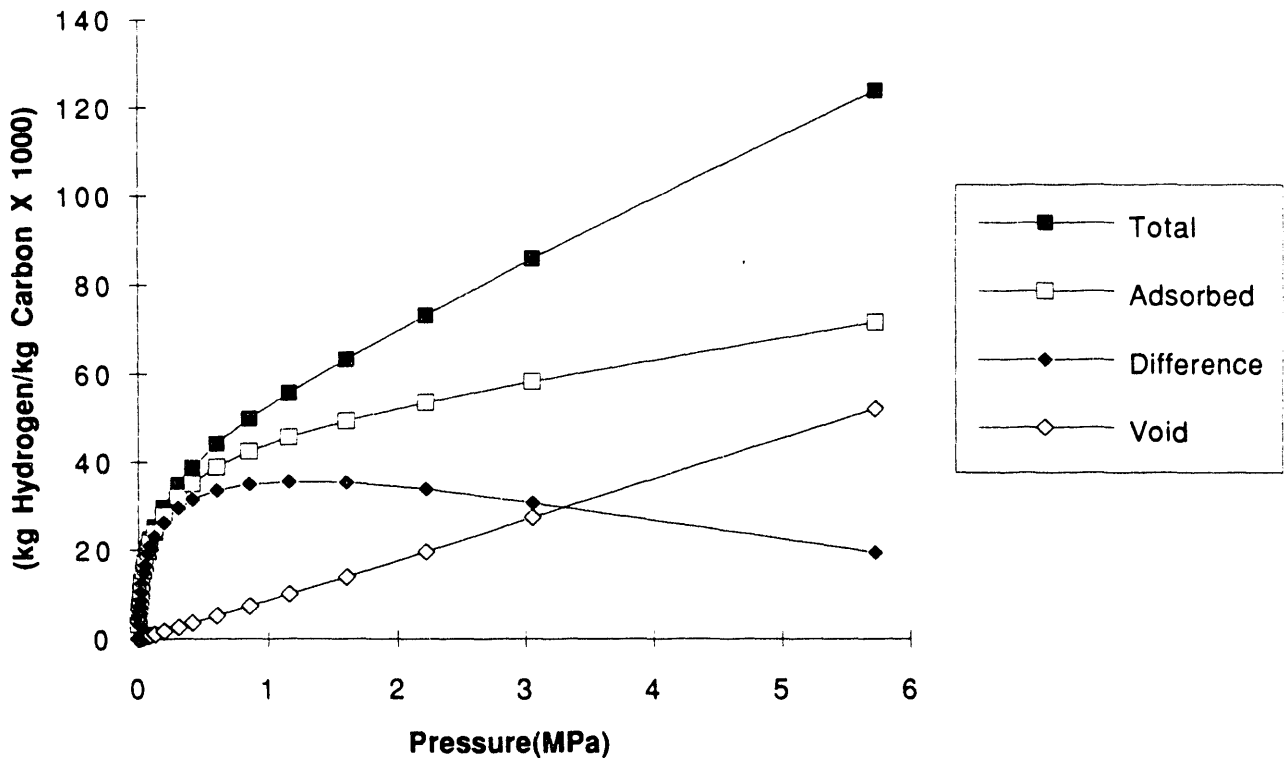


Figure 4.

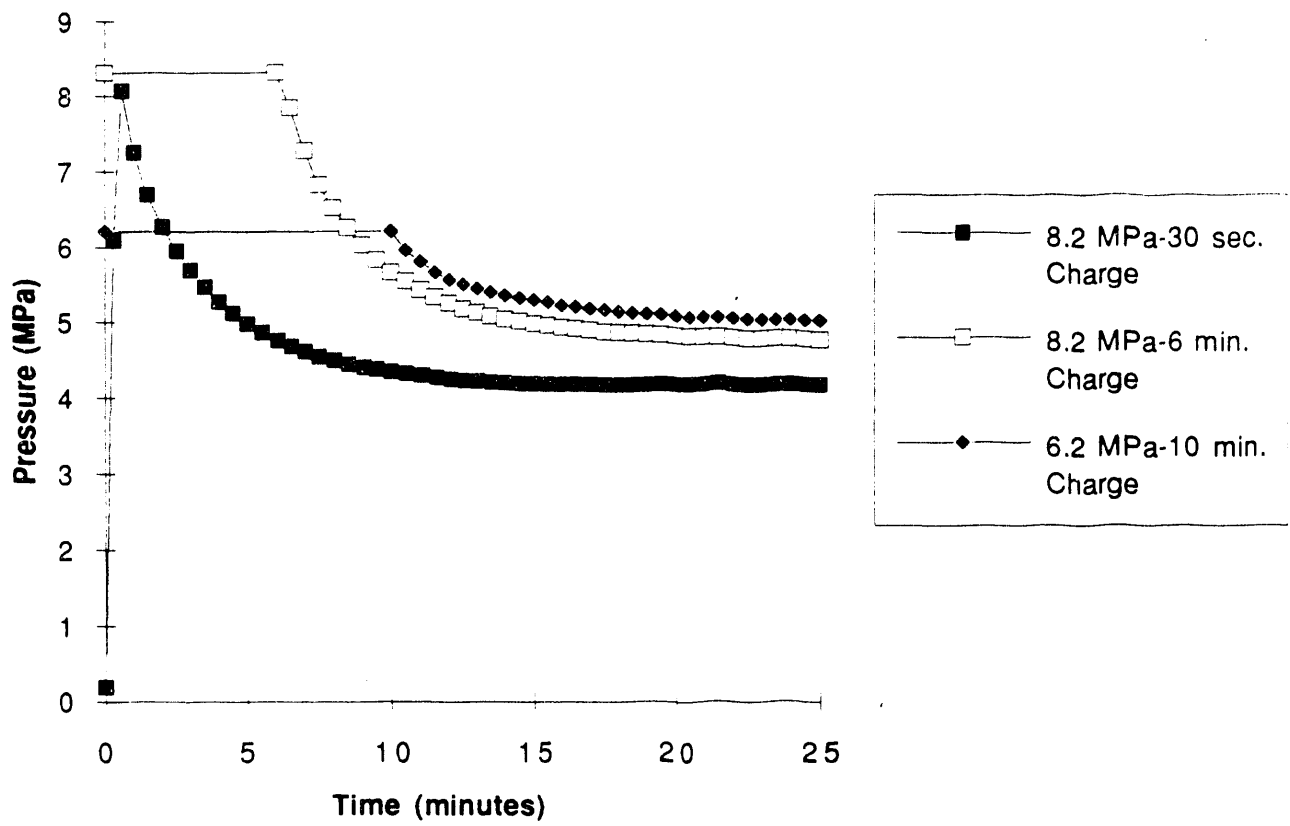


Figure 5.



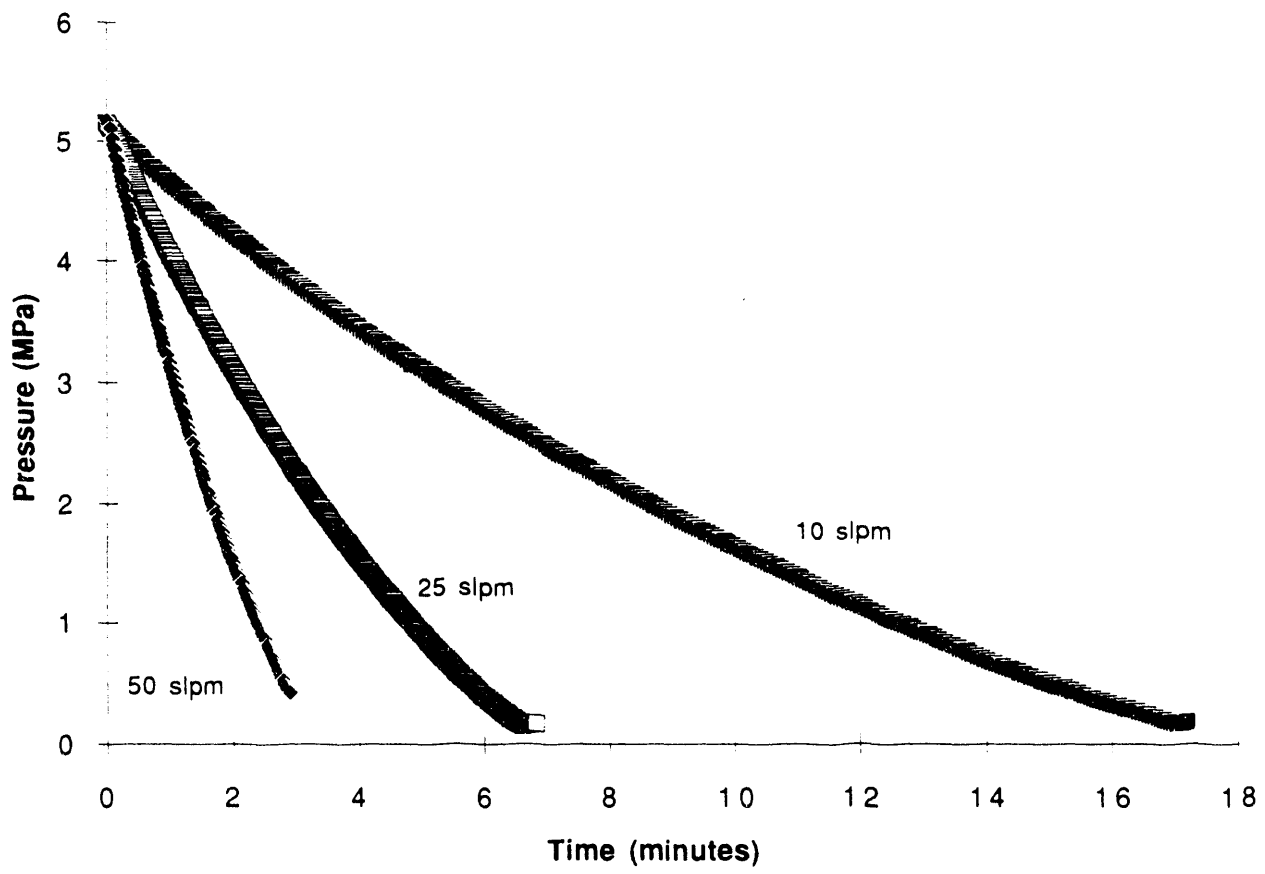


Figure 6.

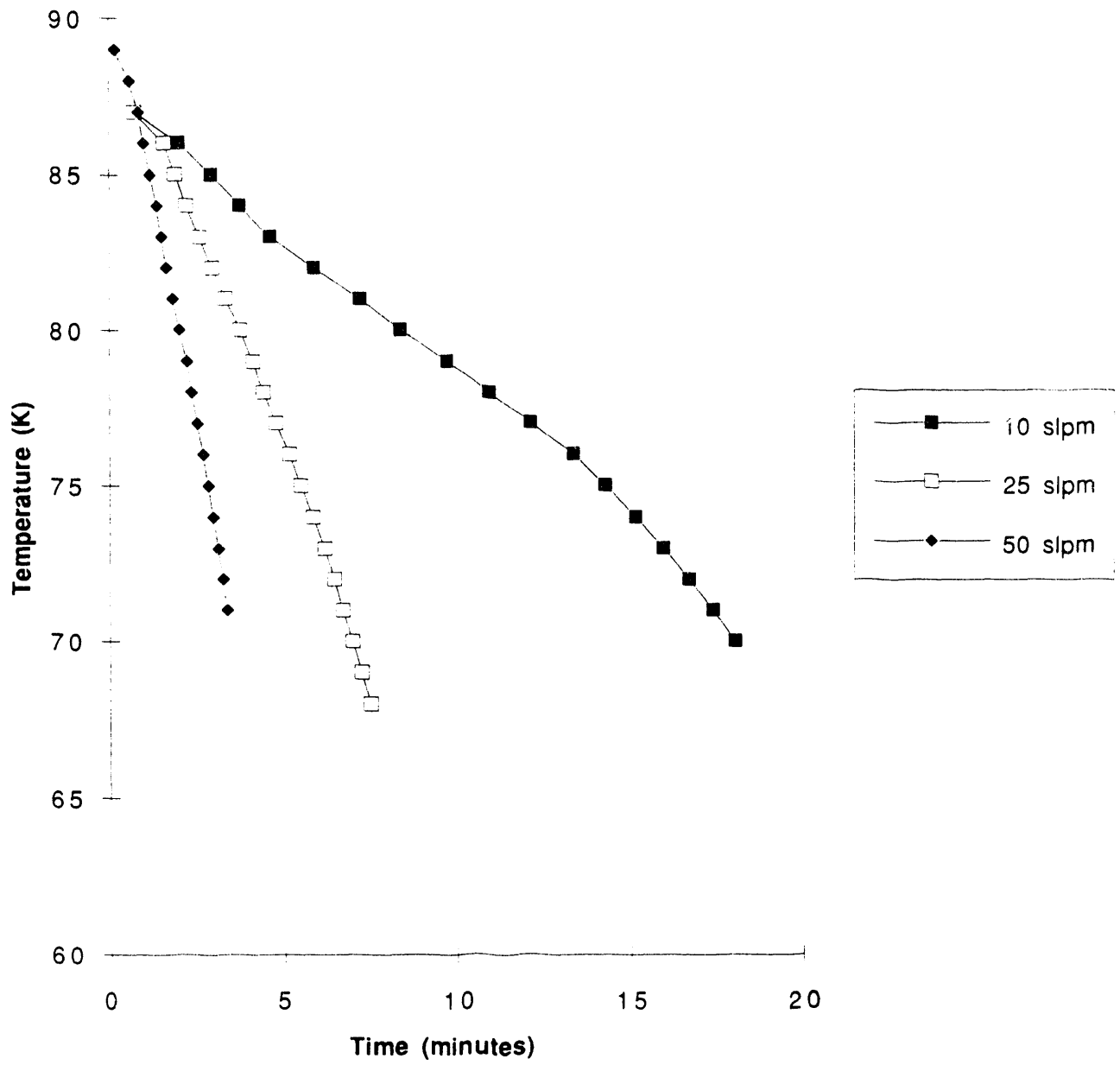


Figure 7.

# HYDROGEN STORAGE BY CHEMICAL SYNTHESIS TECHNIQUES

Darlene K. Slattery  
Ragaiy Zidan  
Florida Solar Energy Center  
300 State Rd. 401  
Cape Canaveral, FL 32927  
Michael D. Hampton  
University of Central Florida  
P.O. Box 25000  
Orlando, FL 32816

## Abstract

A magnesium-nickel-copper hydride was prepared by chemical synthesis techniques. The hydride has been found to be stable in air and is capable of being rehydrided. The sample has been characterized by thermovolumetric analysis, differential scanning calorimetry, and gas chromatography. The material, intended as proof of the ability to chemically form alloys, has been found to have a decomposition temperature that is higher than that of  $MgH_2$ . Additional analyses are in progress.

## Introduction

Last year in Hawaii, we reported on the development of a new method for the simultaneous formation and doping of magnesium hydrides. It was our hypothesis that the dopant, added in this manner, becomes entrained in the bulk of the hydride, resulting in a chemically formed alloy. In order to prove this hypothesis, we set a goal of synthesizing an alloy with known characteristics.

The formation of an alloy by a chemical method is well documented in the literature. There were several

papers presented at the International Symposium on Hydrogen Systems in Beijing in 1985 that involved chemically synthesized alloys. Shen et al. (1985) prepared  $Mg_2Ni - X Mg$  by heating magnesium and nickel(II) chloride in dry DMF. The resulting alloy was identified by differential thermal analysis and x-ray diffraction. In a separate paper, the same research group reported on the chemical synthesis of a TiFe alloy. This synthesis began with ilmenite ore and yielded an easily activated alloy for hydrogen storage. Another research group (Musser 1979) synthesized an iron based alloy that they reported to have characteristics quite different from those of alloys made by metallurgical methods. The method used involved the reduction of metal ions with borohydride in aqueous solution. A patent was applied for by Bushey (1984) for a process for forming a solid solution from two or more metals by way of an ionic reaction with simultaneous precipitation from the reaction medium. Bronger (1991) studied the structure of a large number of complex (i.e., containing more than one metal) transition metal hydrides, all of which were prepared chemically.

All of these researchers list reasons for deciding to prepare alloys via chemical methods instead of metallurgical methods. These reasons range from ease of scale up to industrial quantities to superior or unusual characteristics of the resulting materials.

Although our goal was to synthesize a magnesium-based alloy hydride of documented ratios, it was never our intention that this material would represent a viable storage system. Once we had established that the method of synthesis was resulting in an alloy, we intended to optimize the system to contain the greatest possible hydrogen content while maintaining the lowest possible dehydrating temperature.

## Results and Discussion

Our first attempt was carried out with the targeted alloy being  $Mg_2Ni_{0.75}Fe_{0.25}$ . This alloy was chosen because of its attractive dehydrogenation temperature of 253°C. The synthesis went as expected with the right color changes occurring during the intermediate steps. The uptake upon hydrogenation appeared to be less than is usually expected, however, that was attributed to the smaller amount of magnesium being used. The filtration was unusually easy and the product was a much darker color than for the plain magnesium hydride.

Although the synthesis proceeded as anticipated, characterization indicated that no hydride had formed. Careful review of the procedure indicated no obvious oversights. However, our previous attempts at forming materials containing iron had always given anomalous results. It was decided to repeat the procedure, changing the targeted alloy from  $Mg_2Ni_{0.75}Fe_{0.25}$  to  $Mg_2Ni_{0.75}Cu_{0.25}$ , which has a dehydrating temperature ( $T_d$ ) of 227°C.

It was also decided to add excess magnesium so that even if the amount of hydrogen in the alloy were low, there would still be enough of the  $MgH_2$  present to verify that the reaction had not been poisoned. The problem is, of course, that with excess magnesium, obtaining the exact alloy desired would be impossible. However, it appeared that this would be a necessary trade off in order to be certain that our approach was valid.

The procedure was again carried out with the same indications previously noted. Subsequent

characterization in our thermovolumetric analyzer (TVA), however, gave very different results. The initial hydrogen release appeared to begin at about 230°C (fig. 1) but this pressure increase was assumed to be a result of residual solvent vaporization. Additional cycles indicated that there was a limited release of hydrogen beginning at 230°C but the maximum release was still in the 300°C region. Although it was too early to be sure, we were optimistic that we had chemically prepared an alloy. This alloy appeared to have several phases, based upon the hydrogen release data.

The initial hydrogen release, although slow, occurred at approximately 50°C lower than for the previously prepared hydrides. To confirm this data, a sample was run in a differential scanning calorimeter (DSC), courtesy of our colleagues at the University of Central Florida (UCF). Their data appeared to concur with ours: an endothermic event (fig. 2) occurs at approximately 50°C lower than the main release of hydrogen (fig. 3). This first event was much smaller than that which occurred at the higher temperature. At the time that this analysis was done, Hampton's group had not yet interfaced a gas chromatograph (GC) to the DSC and, unfortunately, our group did not have access to such an instrument. Therefore, it was not possible to analyze the released gases for hydrogen.

Subsequent cycling in the DSC indicated that the compound was fully reversible (fig. 4) although the lower temperature thermal event was now even smaller. There was one discrepancy between UCF's data and ours and that involved the temperature. While we agreed that there was a 50°C difference between the two thermal events, we did not agree on the value of those two temperatures. Our value for the main hydrogen release was <300°C, while they were reporting a value >385°C. Initially, we believed that their calibration was off. However, the standards they were using for calibration were melting at the reported literature values. While the discrepancy was strange, we assumed it was a result of differences in experimental procedure. Additionally, they did not yet have a pressure transducer, so it was possible that there was hydrogen being released or at least desorbed even though a thermal event was not occurring. Any released gas would then create pressure over the sample and, therefore, cause a shift in the temperature required for decomposition.

We did feel that the results of the tests were exciting and that we had proven that our chemical method was allowing us to form alloys. We felt that additional syntheses needed be conducted to prove that the results were repeatable.

The synthesis of the alloy,  $\text{Mg}_2\text{Ni}_{0.75}\text{Cu}_{0.25}$  was then repeated to ascertain that the procedure was reproducible. Special care was taken to insure that the nickel and copper compounds did not mix with the activated magnesium until hydrogen had been added to the reactor. This was done so that reduction of these metals would not occur until the magnesium was being hydrided. It appeared that we were more successful this time. The hydride was stable in air and the calculated hydrogen weight content was around 2% (based upon the pressure increase during heating). Most importantly, however, was the temperature required for pressure increase. Characterization using our thermovolumetric analyzer indicated a slow but steady increase in pressure beginning at around 200°C.

The sample was again transported to UCF to our colleague, Dr. Mike Hampton, for further characterization in the DSC. They had now installed a pressure transducer and their pressure data was found to agree with ours (fig. 5).

A gas chromatograph (GC) had also been interfaced to the DSC, allowing for analysis of the gases as they were evolved from the sample. As can be seen in figure 6, the magnesium-nickel-copper hydride sample had a definite release of hydrogen with a maximum amount being released at 385°C. This is in good

agreement with the temperature at which the second thermal event occurs. Unfortunately, the lower temperature range showed no evidence of hydrogen in the DSC effluent (fig. 7). Earlier, Hampton's group had run a sample of our standard magnesium hydride and had determined that its thermal event occurred at 345°C (fig. 8) and GC analysis of the evolved gases gave a maximum release at 335°C (fig. 9). These values for the standard material were in close agreement with those that we had obtained repeatedly in the TVA. Therefore, it would appear that whatever caused the low temperature pressure increase during the heating of the Mg-Ni-Cu hydride was not hydrogen.

Because the primary gas of interest is hydrogen, the GC is set up with argon as the carrier gas. Therefore, it was not possible to look for organics eluting because their thermal conductivities are too close to that of argon. It was decided to change the carrier gas to helium but in the process a problem developed with the GC, which has not yet been solved. Consequently, we have been unable to determine the nature of the evolved gases.

## Conclusions

The original goal for this year, was to prove that our chemical process resulted in the formation of an alloy hydride. While we cannot yet prove that our material is an alloy, we have proven that we can alter the temperature required for the dehydrogenation. While it was our intent that temperature be lower than is required for pure  $MgH_2$ , the important point is that we did cause a change. If it is possible to cause an increase in temperature, it should also be possible to cause a decrease in temperature.

Our next step will be to determine the nature of the evolved gases. One attempt has been made to run a sample using the solids probe of the mass spectrometer at UCF. The instrument is in need of cleaning, making it necessary to repeat the analysis. Additionally, we hope to have an x-ray analysis done on the material that has the higher dehydrogenation temperature.

While the analysis of the current material continues, we will synthesize an alloy that contains only magnesium and one additional component to see if the results are the same. We may be able to determine which of the materials has caused the elevated  $T_d$ . Also, since the presence of organics in hydrides is known to change certain characteristics, we will do a synthesis that adds the additional metal in the form of a salt rather than an organometallic.

## Acknowledgments

The authors wish to thank DOE and NREL for continued support of this project under subcontract no. XD-010090-1 and James R. Slattery for running the DSC and GC analyses.

## References

Bronger, Welf, 1991. "Complex Transition Metal Hydrides" *Angew Chem. Int. Ed. Engl.*, 30: 759-768.

Bushey, William, U.S. Patent Appl. 645,425,29, Aug. 1984. "Forming Metal Solid Solutions."

Musser, D., C.L. Chien, and H.S. Chen, 1979, *J. Appl. Phys.* **50** 7659.

Shen, P., G. Wang, D. Zhang, F. Wang, S. Shi, X. Wang, and J. Zhang. 1985. "The Chemical Synthesis of Intermetallic Compounds and Their Hydrogen Storage Properties" in *Proceeding of the International Symposium on Hydrogen Systems*, 355-361. Beijing, China.

Shen, P., Y. Zhang, Y. Zhou, H. Yuan, S. Chen, and S. Chen. 1985. "Mg-Based Hydrogen Storage Materials: Replacement-Diffusion Method for Mg<sub>2</sub>Ni-X Mg and Related Hydrogenation" in *Proceeding of the International Symposium on Hydrogen Systems*, 505-512. Beijing, China.



## Figure Titles

Figure 1.: Pressure-temperature data obtained during heating of Mg-Ni-Cu hydride in TVA.

Figure 2.: Thermogram of Mg-Ni-Cu hydride: first thermal event.

Figure 3.: Thermogram of Mg-Ni-Cu hydride: second thermal event.

Figure 4.: Thermogram of Mg-Ni-Cu hydride: cycle 2.

Figure 5.: Pressure-temperature data during heating of Mg-Ni-Cu hydride in DSC.

Figure 6.: Gas chromatogram of Mg-Ni-Cu hydride - gases emitted above 320°C.

Figure 7.: Gas chromatogram of Mg-Ni-Cu hydride - gases emitted below 300°C.

Figure 8.: Thermogram of MgH<sub>2</sub>.

Figure 9.: Gas chromatogram of MgH<sub>2</sub>.

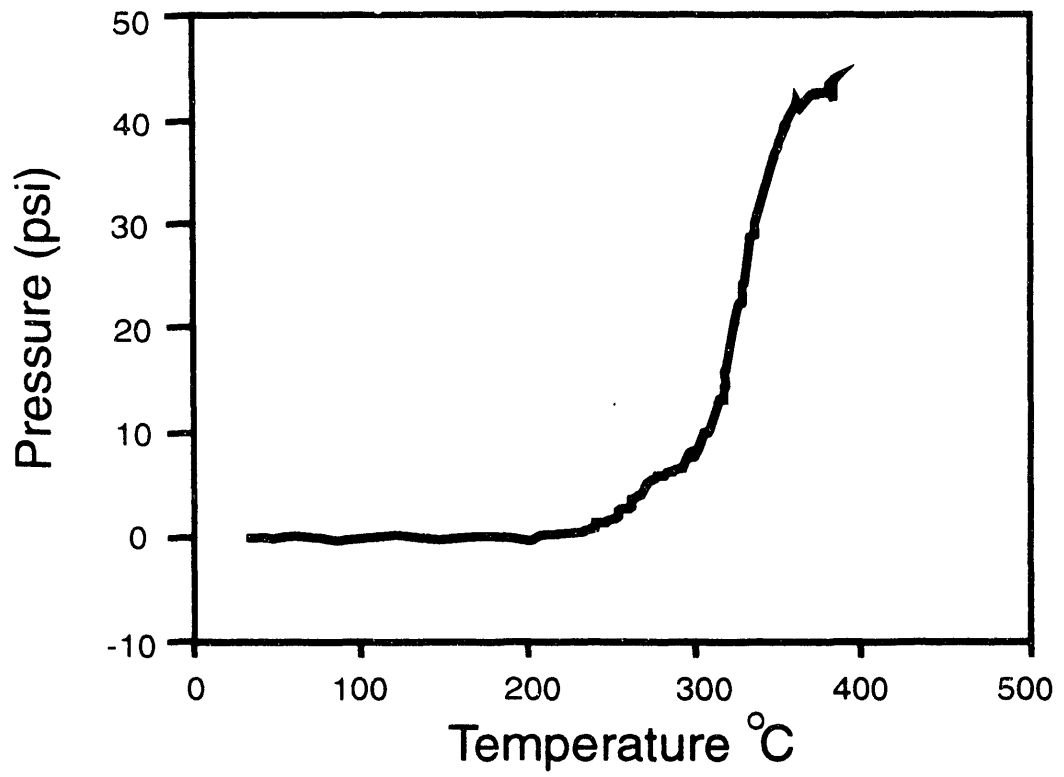


Figure 1

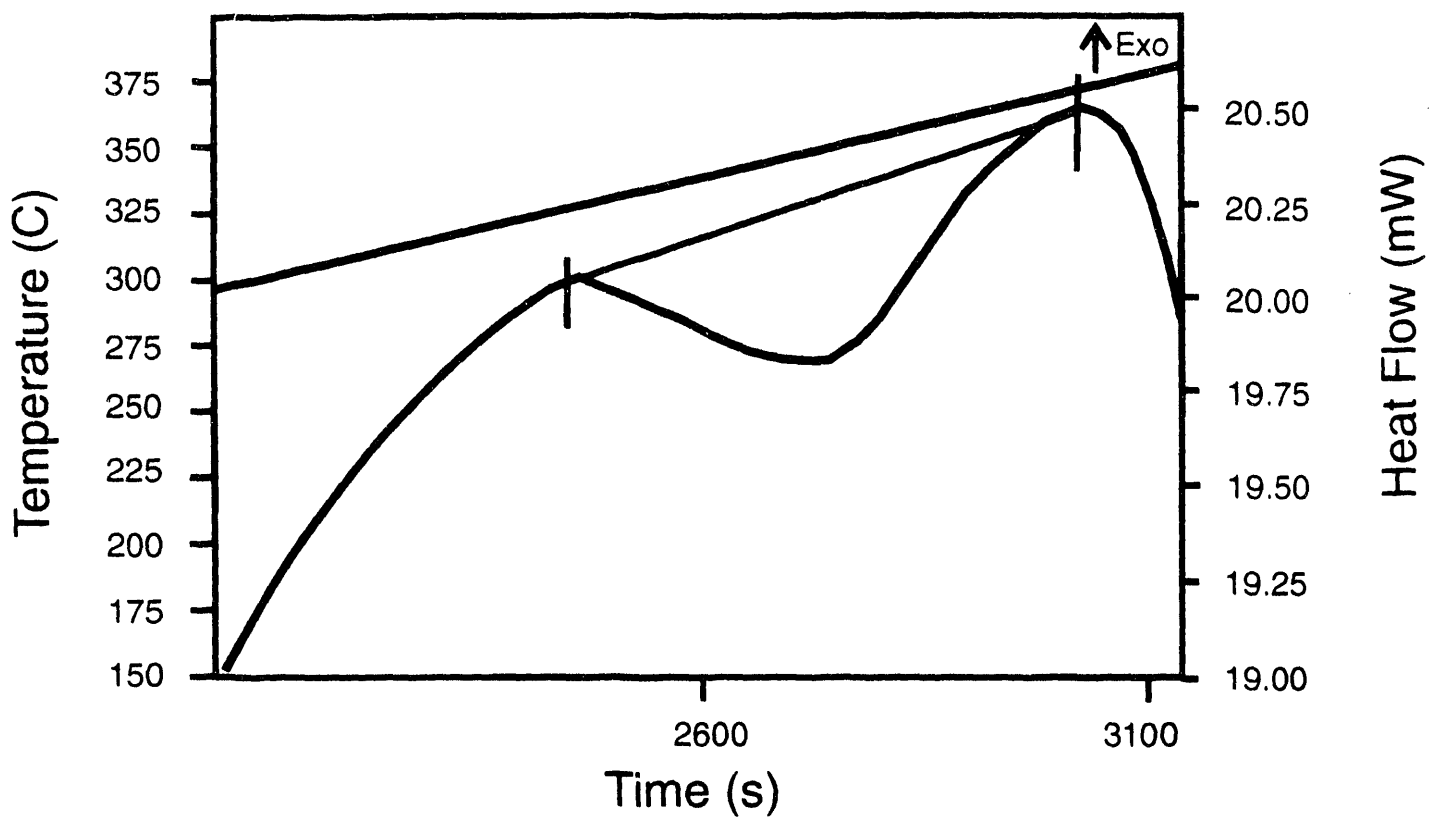


Figure 2

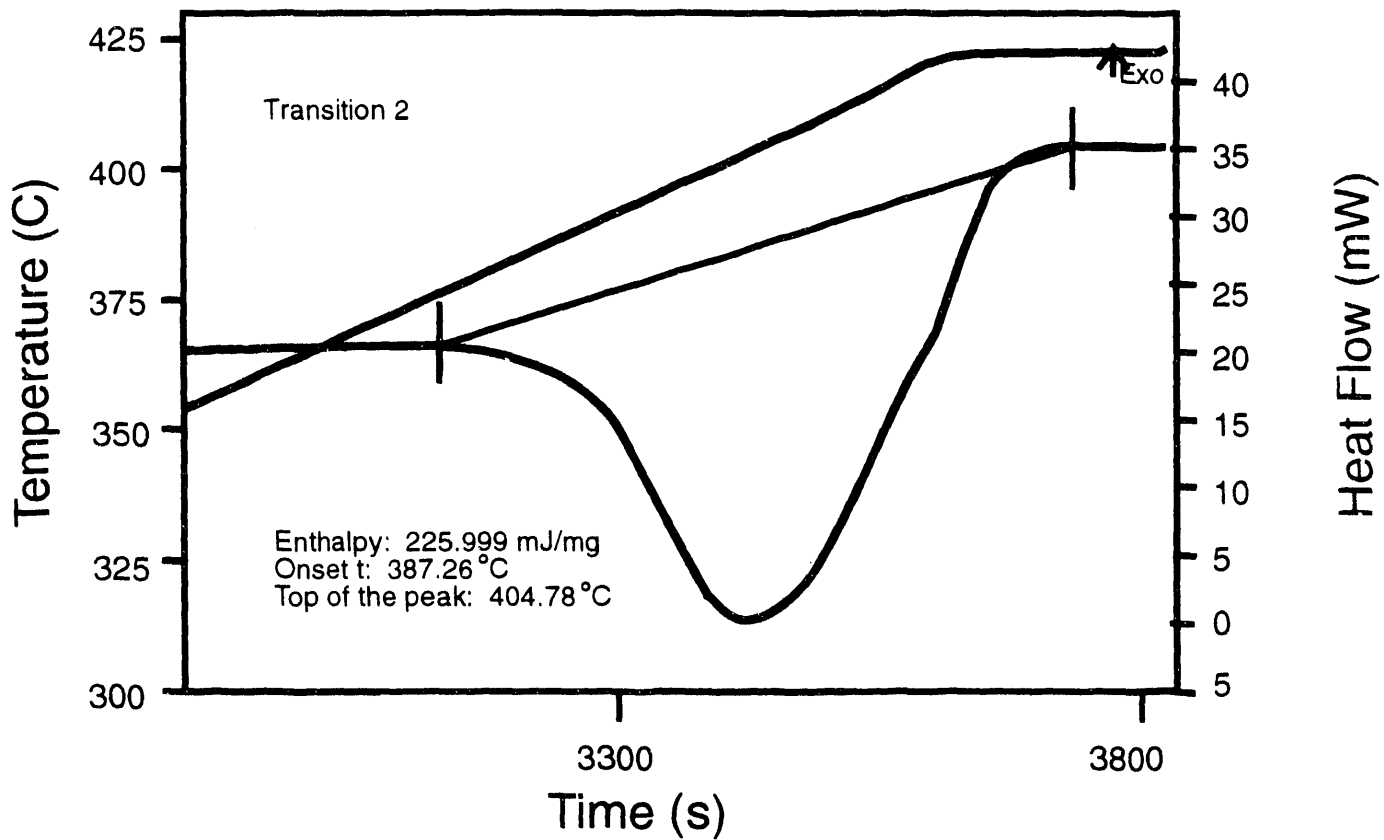


Figure 3

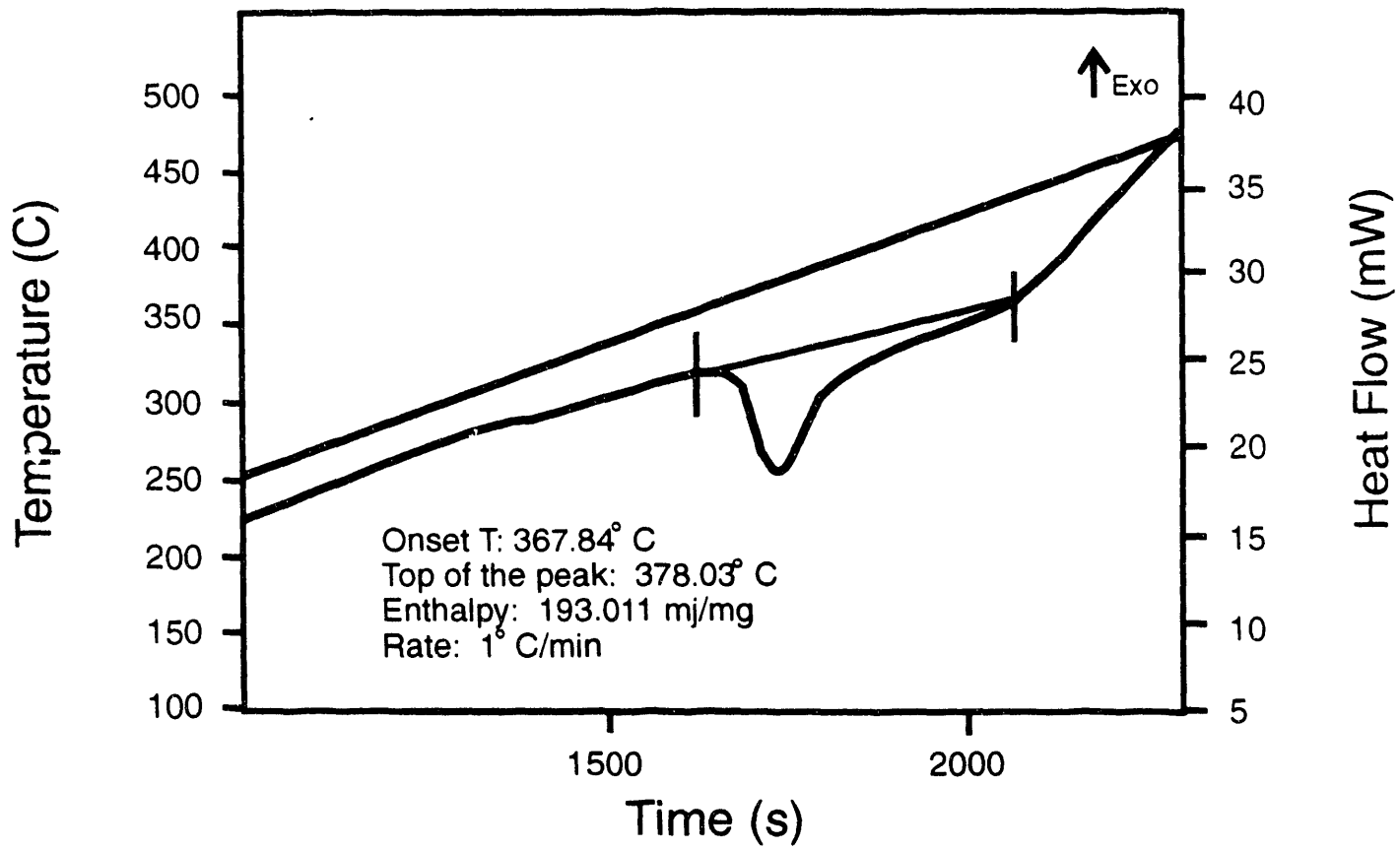


Figure 4

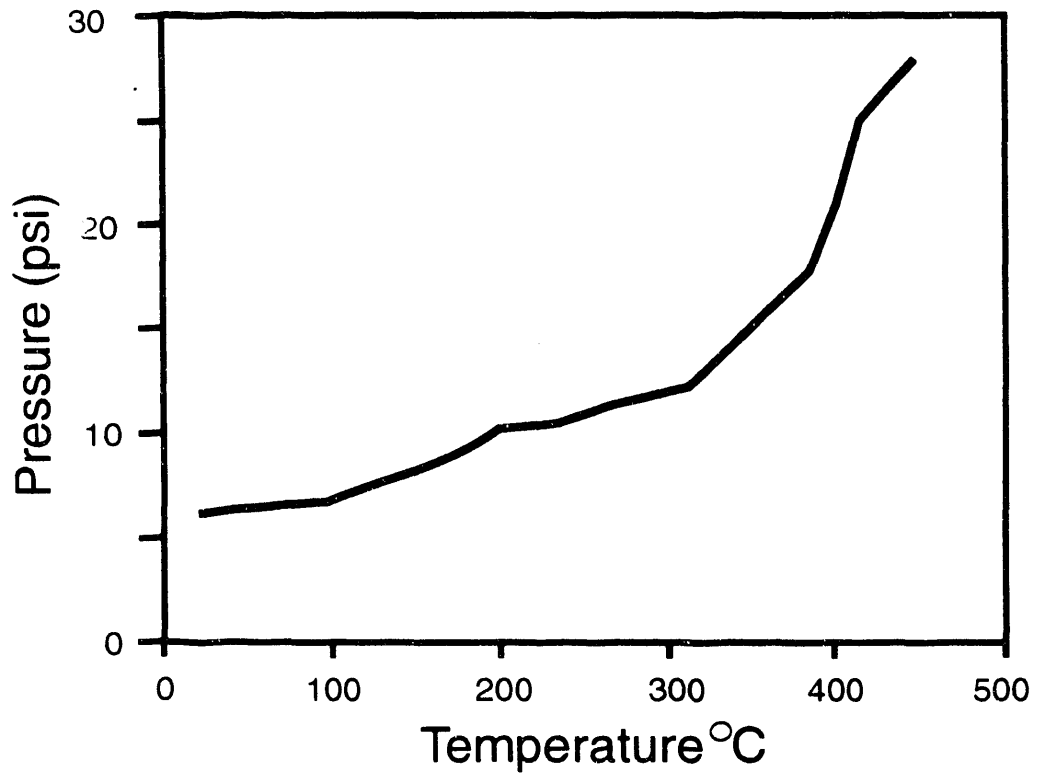


Figure 5

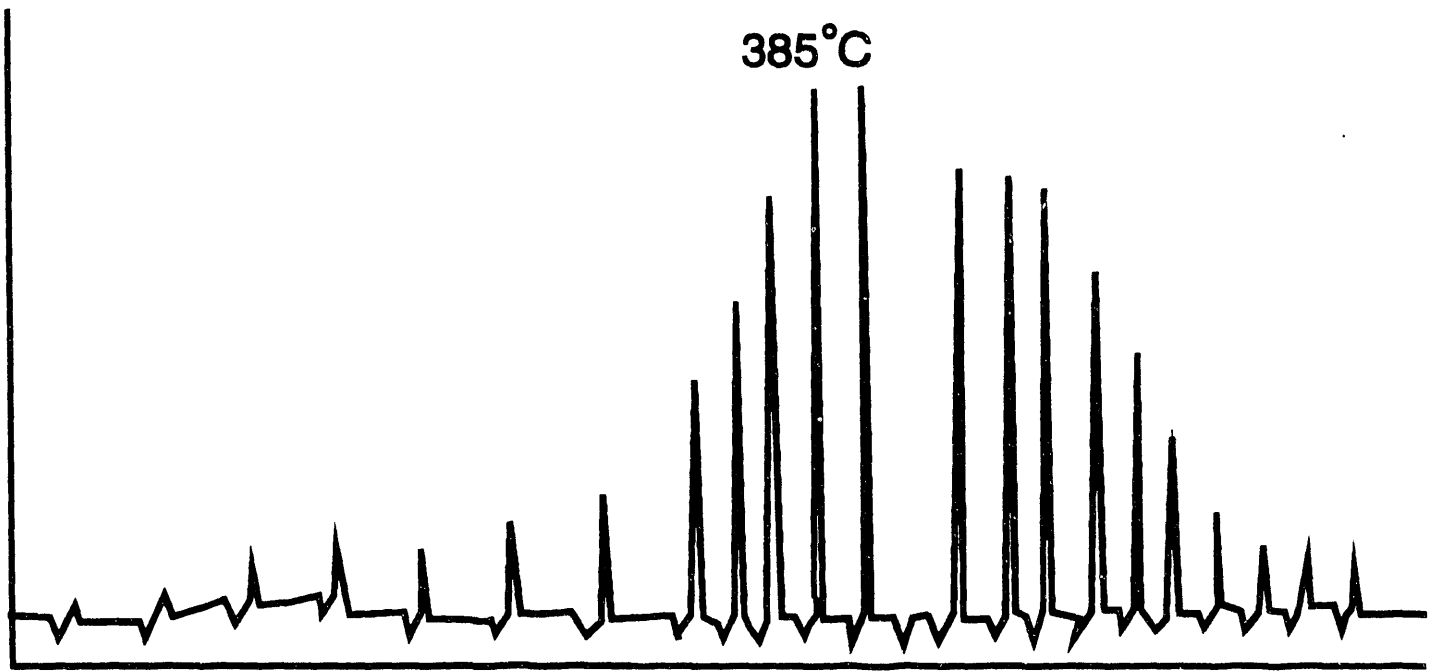


Figure 6

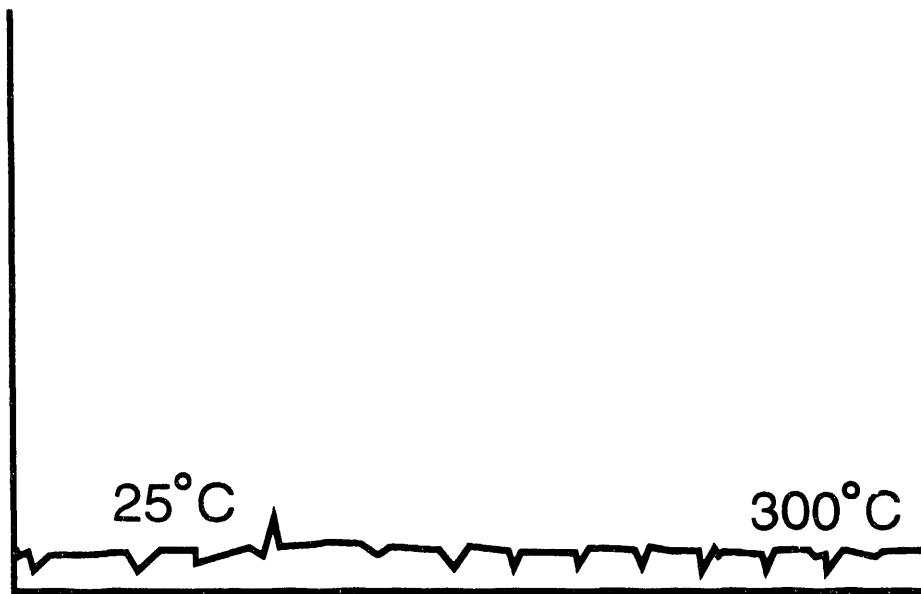


Figure 7



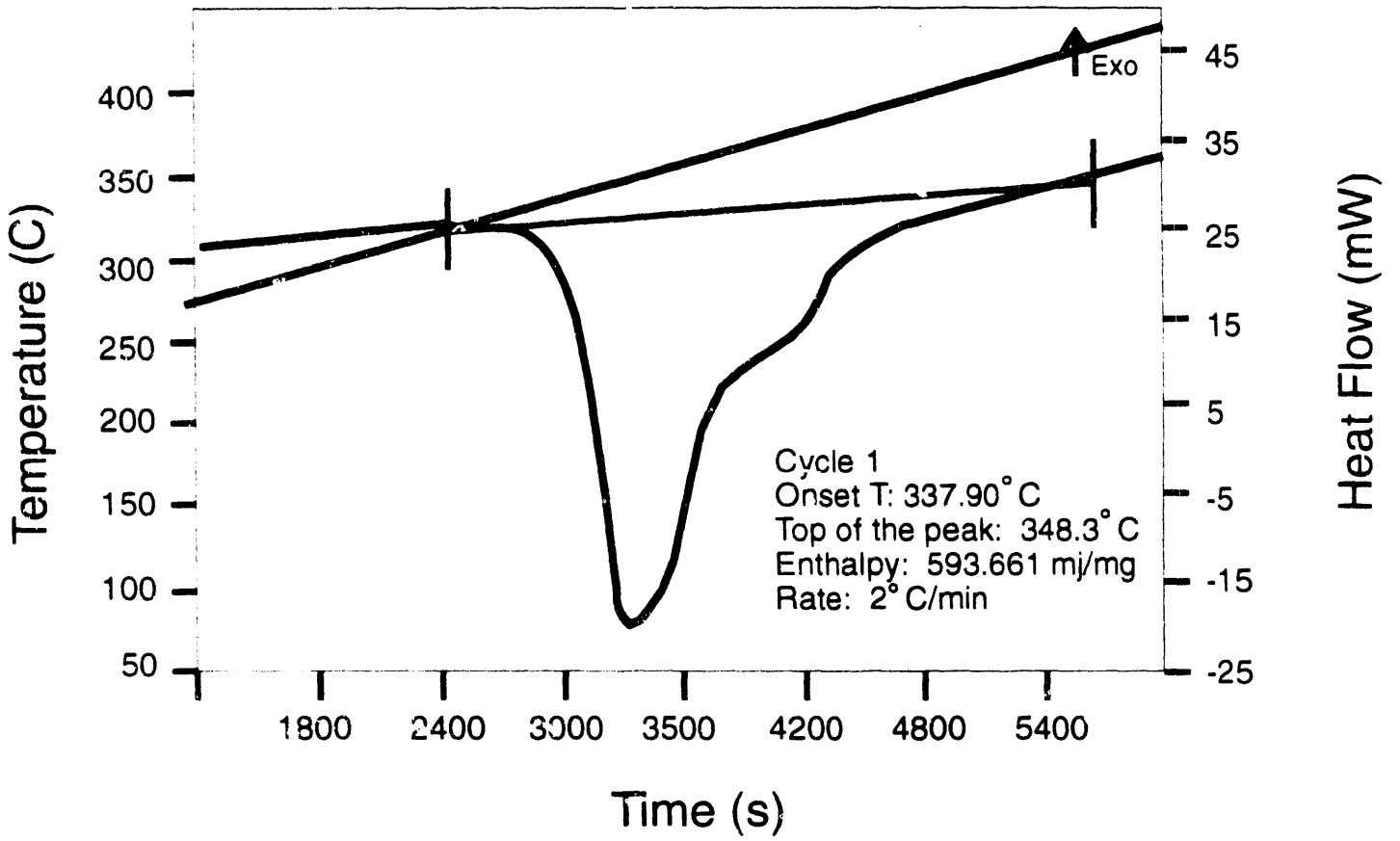


Figure 8

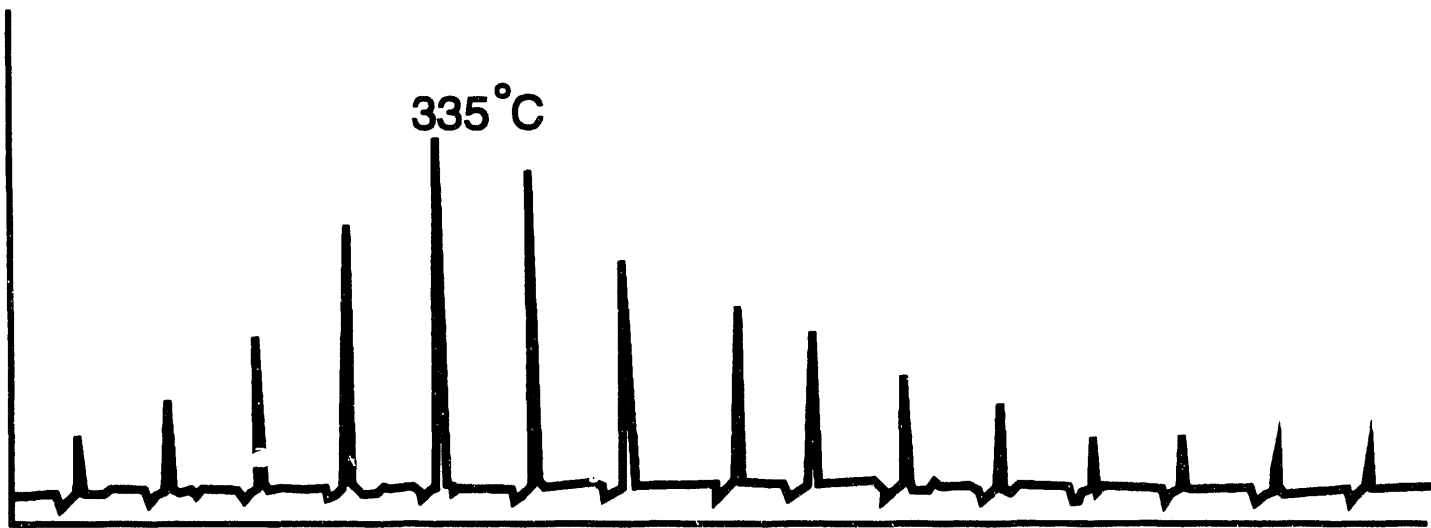


Figure 9

# A NEW SYSTEM FOR THE EVALUATION OF HYDROGEN STORAGE COMPOUNDS

Michael Hampton, James Slattery, and Christopher Bender  
Department of Chemistry  
University of Central Florida  
Orlando, FL 32816

## Abstract

A new system was developed for the evaluation of the characteristics of potential hydrogen storage compounds. This new system utilizes small samples, on the order of 50 mg, and only small amounts of hydrogen and argon. It allows direct measurement of onset temperatures and enthalpies of hydrogen release and uptake, pressure-temperature relationships, and the kinetics of hydrogen release and uptake. Additionally, the identities of evolved gases can be determined to identify the chemistry occurring during heat flow and pressure changes. The system also provides information on phase transitions of samples. The new system provides for rapid analyses and, because of its small volume and small sample requirements, is safer and more efficient to use than current TVA systems.

Future work will involve refinement of the new system to provide more data more rapidly and in better form. The system will also be used to study new candidate hydrogen storage compounds.

## Introduction

In order to design systems to utilize hydrogen stored in the form of hydrides, the thermodynamic, thermal, kinetic, and chemical properties of the hydrides must be known. Thermovolumetric analysis (TVA) instrumentation is commonly used for this characterization. TVA is a method that gives a pressure-temperature relationship for the uptake and release of hydrogen by compounds. The actual composition of any gas evolved or absorbed by the compound under study cannot be directly determined with TVA. Therefore the other methods of analysis must also be used on the compound to determine the composition of these gases. This additional analysis requires the use of more sample

because sampling the gas during a TVA run would invalidate the data of that run. The TVA apparatus is large making it susceptible to leaks. The low sensitivity of the instrument and the heat transfer characteristics of the large apparatus require large sample sizes. This in turn causes a slow response time for analysis and decreases throughput.

In this study, a novel system was developed for the characterization of hydrogen storage compounds through the combination of differential scanning calorimetry, gas chromatography and thermobarometric analysis. The system developed in this project greatly improves upon the current technique. The DSC employed utilized a thermopile to allow accurate monitoring and control of the furnace temperature and heat flow into and out of sample and reference. The pressure change occurring during the release or uptake of gas was monitored with pressure transducers built into the analysis cells. A gas chromatograph was interfaced with the DSC to allow direct analysis of any gas that is being released by a sample. The DSC, GC, and pressure transducers were sensitive enough to allow the use of small samples, on the milligram level.

## **Technical Approach**

### **Apparatus**

A SETARAM DSC 111 was used. The thermal data were recorded and saved on an IBM 286 personal computer. The gas chromatograms were obtained using a GOW-MAC series 580 gas chromatograph (GC) equipped with a porapak Q, 80-100 mesh, 7'x1/8" column, and a Perkin Elmer 8500 GC equipped with an FID detector and an RTX-35, 15 m, 0.54 mm wide bore capillary column. Data from the GOW-MAC GC were recorded on a strip chart recorder. Data from the Perkin Elmer were recorded on a Spectra-Physics Chromjet Integrator. For confirmation of GC data, a Finnigan Mat mass spectrometer equipped with a solids sampling probe was used. The pressure was monitored by an Omega model px602, 5-200 psig pressure transducer and the data were measured using a voltmeter.

The pressure cells were constructed of 1/4" seamless Hastelloy C22 tubing. The sample outlet was connected to the GC with another length of Hastelloy tubing. Details of the assembled cells are shown in Figure 1. All fittings were made of 316 stainless steel. The sample and reference cells both contained inlet and outlet valves and pressure transducers. The inlet sides of the cells were connected to a single T-fitting that was connected to the hydrogen and argon gas cylinders.

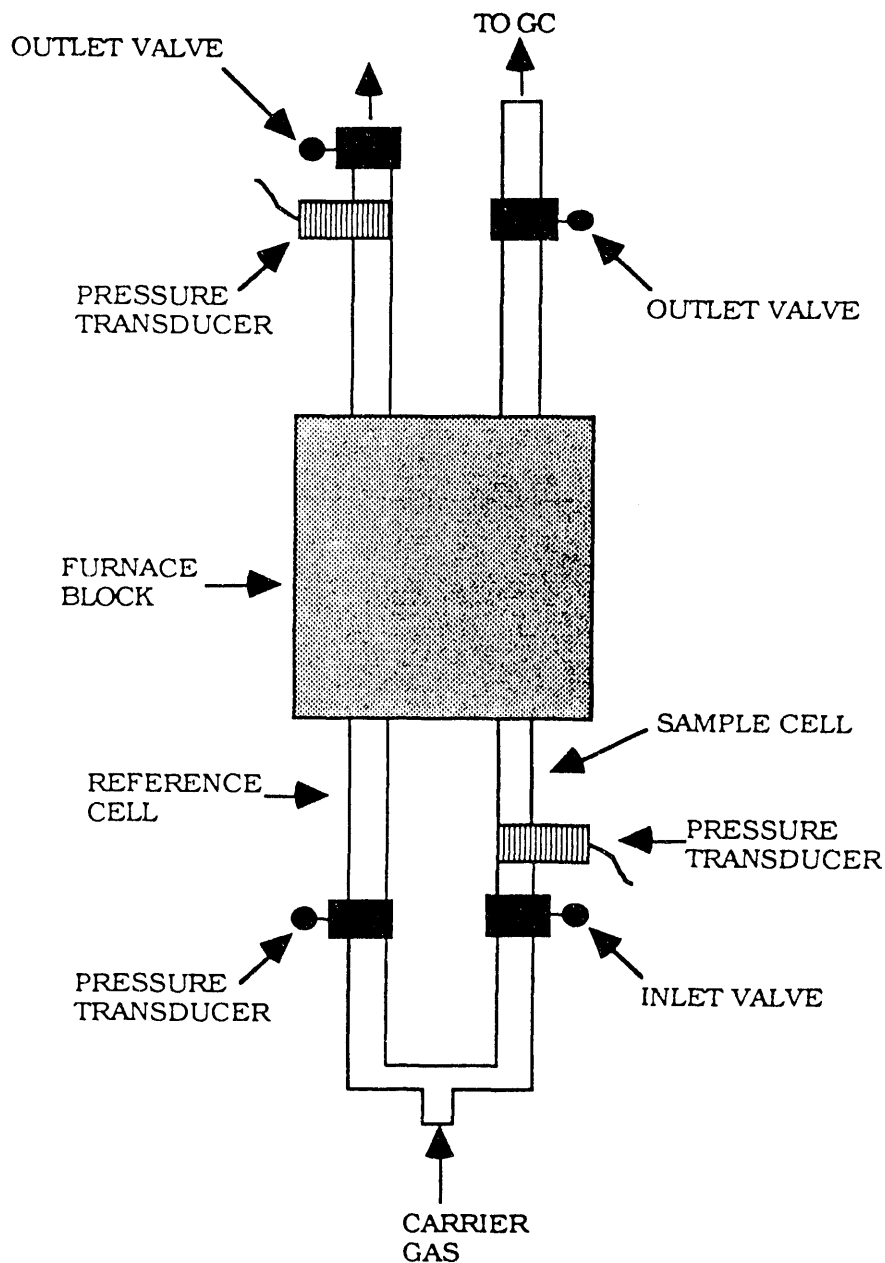


**Figure 1. Diagram of pressure cells for the DSC.**

**Materials**

All standards used in the calibration verifications were purchased from and certified by the National Institute of Standards and Testing (NIST). Magnesium hydride was prepared and furnished by the Florida Solar Energy Center (FSEC). The hydrogen, helium, and argon used to purge the pressure cells and for GC analysis were ultra high purity (UHP) and all hydrides were stored under UHP argon. Samples were run in stainless steel boats that were fabricated and shaped to fit the pressure cells.

## **DSC Evaluation**

The melting transition of a tin (NIST) standard was observed at three different heating rates, 1, 2 and 5°C/min to determine the best heating rate for accurate determination of onset temperatures for thermal events. This comparison was done for the DSC with and without the high pressure cells in place to determine the accuracy of the melting point onset temperature as well as the enthalpy value.

## **Procedure for Testing Hydrides**

The testing of hydrides occurred in two steps. The first step involved purging the system with the carrier gas (argon) for 15 minutes at a flow of 100 mL/min. The gas flow was slowed to approximately 70 mL/min. The stainless steel sample boat into which the hydride was weighed to the nearest 0.01 mg, was then carefully placed in the sample cell and the cell was connected to the inlet port of the GC. The empty reference boat was inserted into the reference cell and the system was allowed to come to equilibrium. The purge gas from the cells was analyzed to determine the baseline. At frequent intervals, 5-10 °C, during the entire experiment, gas chromatographic analyses were performed on the purge gas.

The second step involved running a new sample under a static atmosphere and monitoring the pressure change during the experiment. While holding the temperature at the peak of the thermal program, i.e. 450 °C, the cells were purged with argon to remove any gases that were released during any thermal events. The cells were then cooled to room temperature and purged slowly with hydrogen and then pressurized. The pressure was monitored as the temperature was again increased at 2 °C/min. After the uptake of hydrogen, the system was allowed to cool and the cells were purged with argon to remove any hydrogen gas evolved. This entire second step was repeated several times for a comparison of absorption and desorption characteristics upon recycling.

## **Results to Date and Discussion of Results**

### **DSC Evaluation**

A differential scanning calorimeter was an ideal choice as the basis for our system because the instrument included a furnace with excellent temperature control, small cavity size, separate sample and reference cavities, low thermal mass, and sensitive heat flow measurement. The furnace of the Setaram DSC 111 has tubular openings for the sample and reference cells. These tubular openings were found to be very well suited to accommodate high pressure cells. The Setaram unit utilized thermopiles that allow for very high heat flow sensitivity.

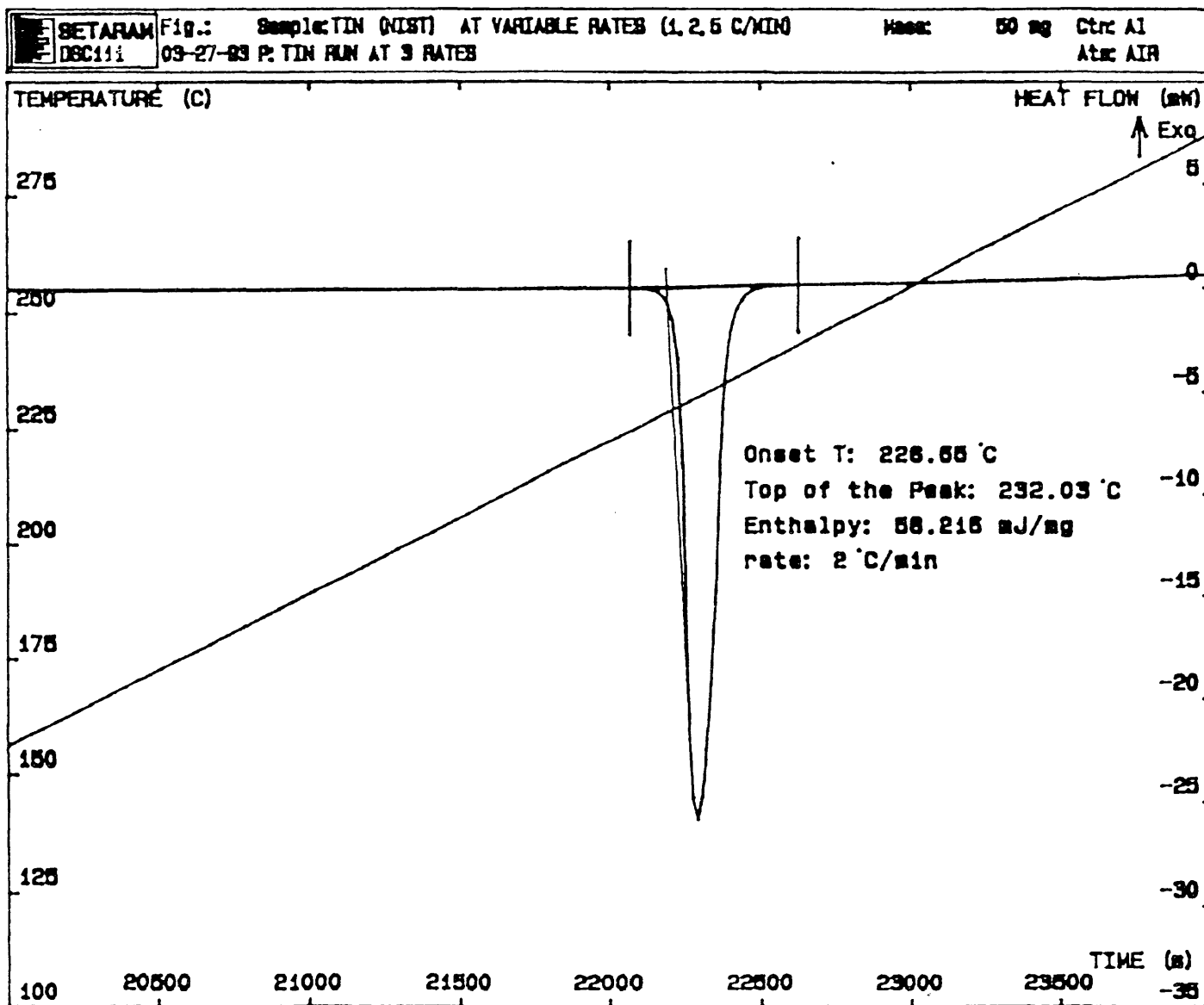
In order to produce a system with the greatest amount of flexibility and the broadest applicability, pressure cells were constructed to withstand hydrogen atmospheres at pressures up to 2000 psi and temperatures up to 500° C. Ongoing, and as yet unpublished, research by the Materials Testing Branch of NASA at the Kennedy Space Center indicated that Hastelloy C22 or C16 could handle these rigorous conditions and resist hydrogen embrittlement. Hastelloy C22 was readily available locally in the form of seamless 1/4 inch o.d. tubing. The C22 tubing also had a small enough coefficient of thermal expansion to prevent

expansion to crack the delicate DSC furnace. Before the cells were inserted into the furnace, the Hastelloy tubes were pressurized with 2000 psi of hydrogen and repeatedly heated up to 800 °C and the outer diameter was measured with a micrometer, while the tube was hot, to confirm that the tubes would not expand excessively at high temperatures. The only problems that have been encountered during the experiments has been warping in the center of the Hastelloy cells due to constant heating of the tubes over several hundred hours of use.

The accuracy and proper function of the DSC were confirmed by analyzing a sample of NIST certified tin. Tin was chosen because its melting point, 231.95 °C<sup>1</sup>, was very close to the transition temperatures anticipated for the hydrides to be investigated. The melting point of the tin was determined at three different ramp rates, 1, 2, and 5 °C/min. The thermogram of the tin sample run at 2 °C/min is shown in Figure 2. The onset temperatures observed at these three ramp rates were 230.3, 229.2, and 226.0 °C, respectively. Extrapolation of the onset temperature to a ramp rate of 0 °C/min, results in an onset temperature of 234.08, a 0.25% error.

The tin standard was then used to determine the effect of the pressure cells on the sensitivity and accuracy of the DSC. Again at rates of 1, 2, and 5 °C/min. the onset temperatures for the melting of the tin standard were determined. The values 234.01, 233.94, and 233.73 °C, respectively for the ramp rates 1, 2, and 5 °C/min. Figure 3 is the thermogram of the tin standard run at 2 °C/min with the high pressure cells in place. A plot of the data from the tin onset temperatures at three different rates gives an onset temperature of 231.34 °C when extrapolated back to a ramp rate of 0 °C/min. No further calibration of the DSC was required due to the very small error resulting from the presence of the pressure cells.

Figure 2. Thermogram of NIST tin standard run at 2 °C/min without pressure cells in place.





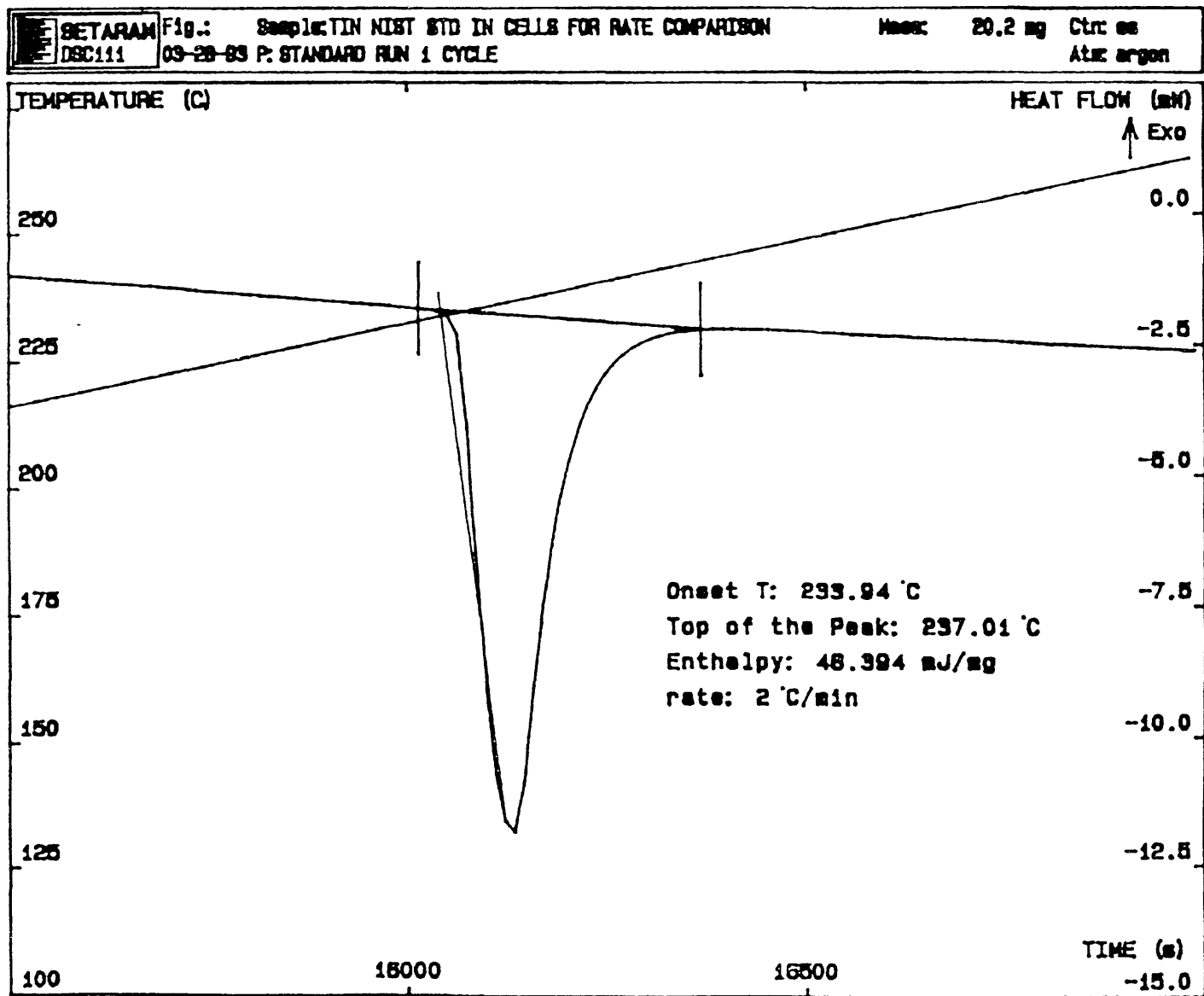
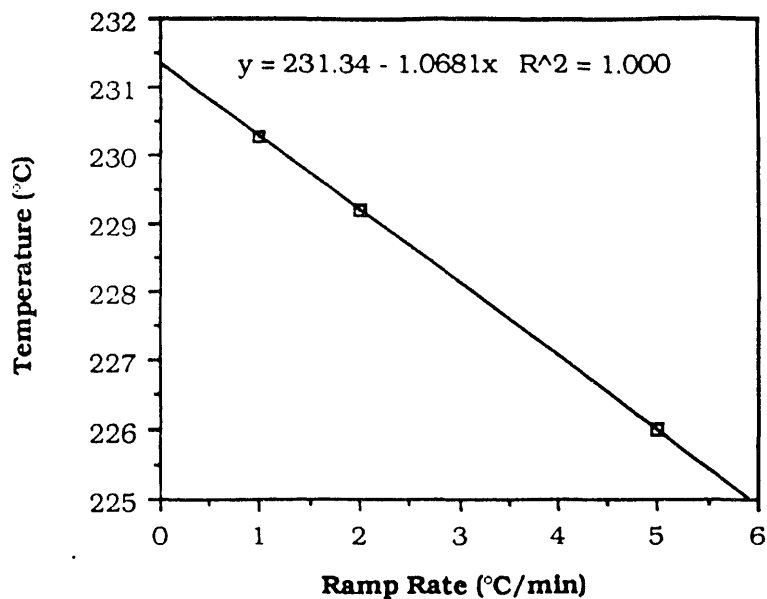
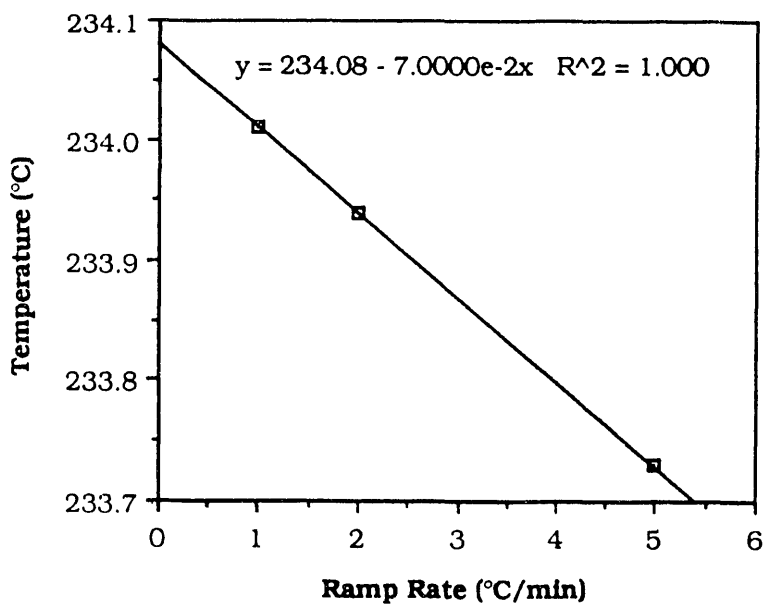


Figure 3. Thermogram of NIST tin standard run at 2 °C/min with pressure cells in place.



**Figure 4. Curve for determination of the melting onset temperature of a tin (NIST) standard at a ramp rate of 0 °C/min in DSC without pressure cells in place.**



**Figure 5. Curve for determination of the melting onset temperature of a tin (NIST) standard at a ramp rate of 0 °C/min in DSC with pressure cells in place.**

The pressure transducers were calibrated and found to respond linearly to pressure change as shown in Figure 6. The response of the transducers was found to change only slightly with temperature.

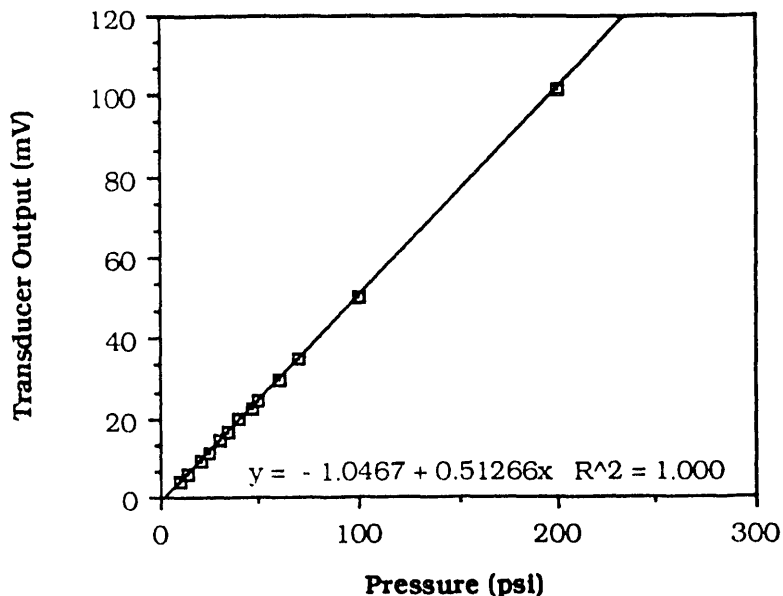
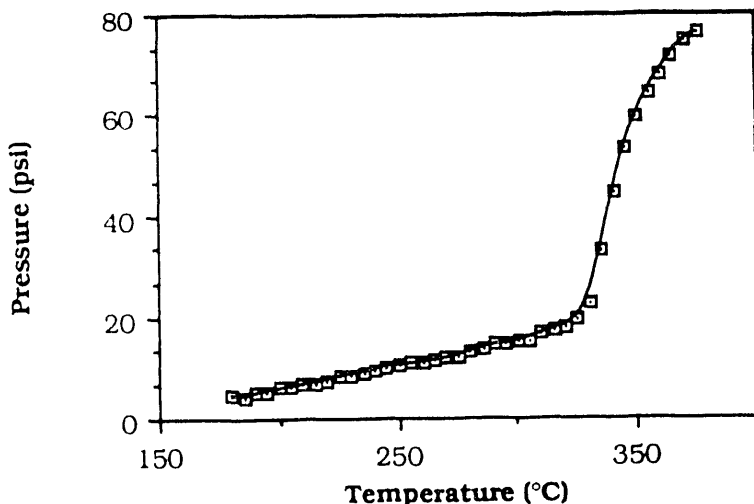


Figure 6. Calibration curve for pressure transducer.

### Magnesium Hydride Evaluation

Magnesium Hydride has been reported in the literature to decompose at 280 °C, releasing hydrogen at a pressure of 1 atm, and to be recyclable<sup>2</sup>. MgH<sup>2</sup> was chosen to test the newly developed system because of its reportedly reasonable decomposition temperature, ability to recycle, and ready availability. As a reference, a sample of the magnesium hydride was analyzed in the TVA at the Florida Solar Energy Center. A 2 gram sample was analyzed and the TVA data are presented in Figure 7. From Figure 8, a plot of  $\Delta P/\Delta T$  versus  $\ln(\bar{r}, T)$ , 337 °C was determined to be the temperature at which the rate of pressure increase was the greatest.

These data are the full extent of information that can be directly obtained from the TVA. During this experiment, the disadvantages of the TVA were very apparent. As stated, several grams of sample were required to perform the thermovolumetric analysis. The setup of the apparatus was time consuming and required two persons to manipulate, seal, and tighten the apparatus. The experiment required a total of 8 hours to accomplish.



**Figure 7. TVA data obtained from the analysis of  $MgH_2$  (FSEC).**

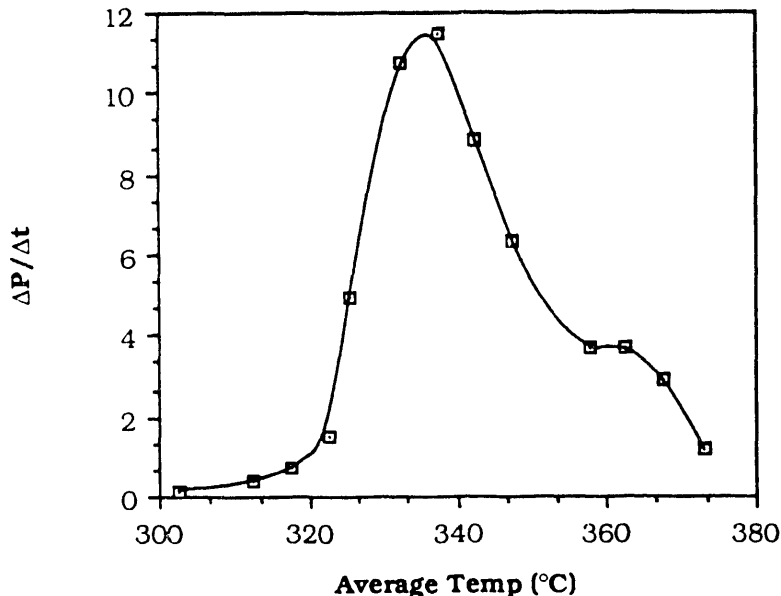


**Figure 8. First derivative plot of TVA data for  $MgH_2$  (FSEC).**

In our new system, small samples, around 50 mg can be analyzed rapidly and easily by a single person. The analysis requires only small amounts of gas and is therefore much safer than the larger volume TVA. The new system also allows direct measurement of onset temperatures and enthalpies of hydrogen uptake and release. Pressure changes occurring as a function of temperature can also be obtained. Further, the identities of any evolved gases can be determined allowing determination of the chemistry involved in the heat flow and pressure changes observed in the sample cell. The type of data that can be obtained from this new system are shown in Figure 9. This thermogram was generated by placing 55 mg of  $MgH_2$  in a stainless steel boat and placing the

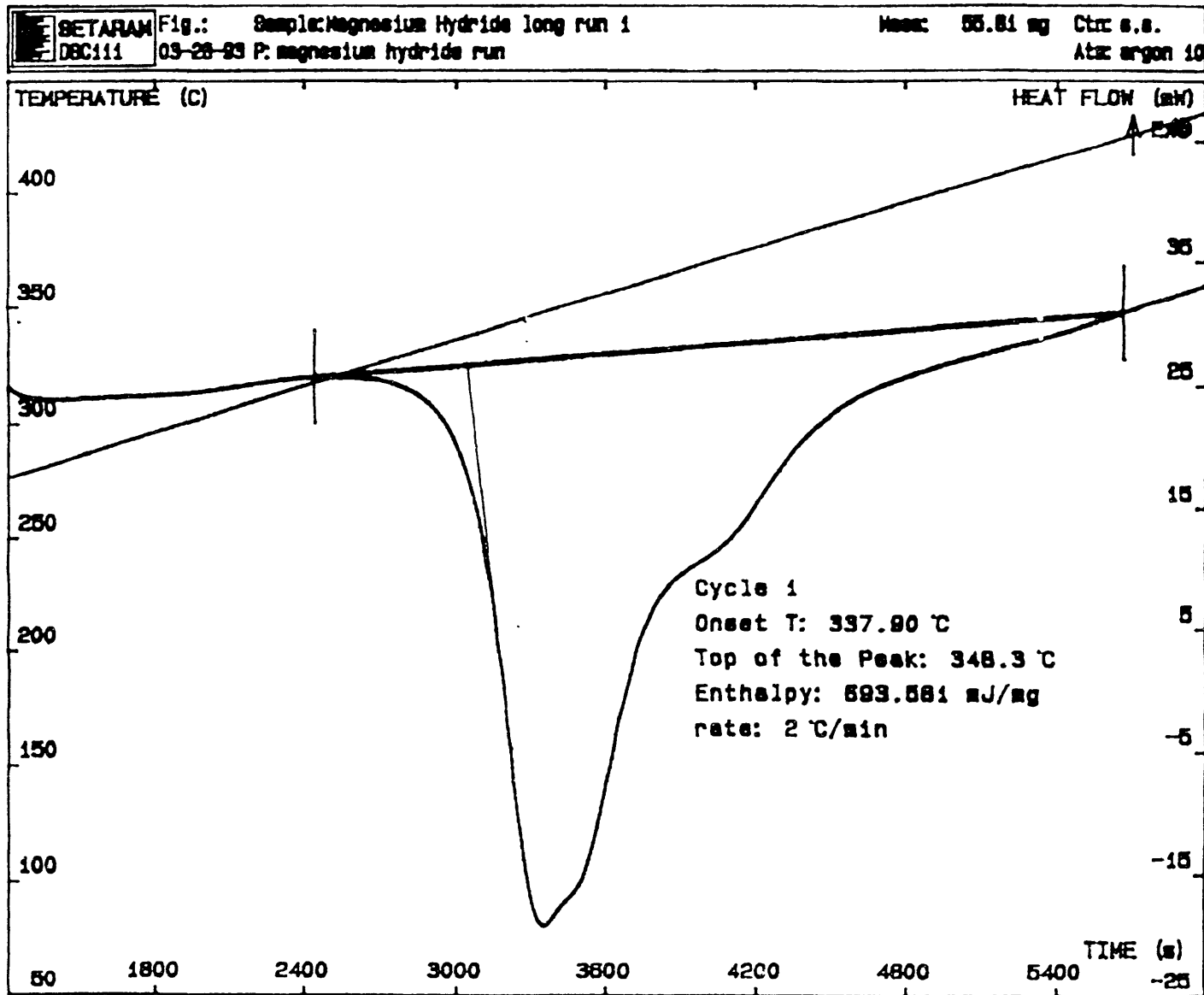
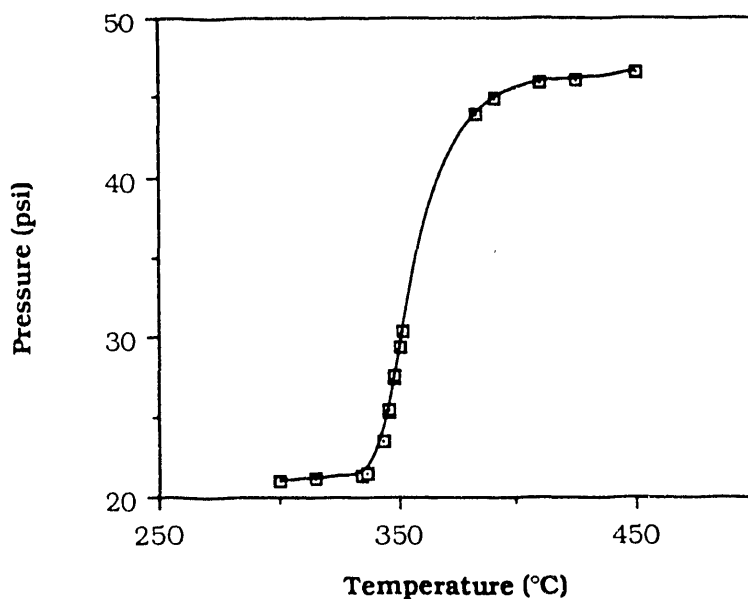


Figure 9. Thermogram of magnesium hydride in an argon atmosphere.

boat in the sample side of the high pressure cells in the DSC. An empty stainless steel boat was placed in the reference side. Both sides of the cells were purged with argon. The argon flow was then stopped and the cells sealed. The temperature of the DSC furnace was then increased from ambient temperature to 450 °C at 2 °C/min and both the heat flow in the sample and reference cells was monitored as a function of temperature. The downward peak in the thermogram indicates an endothermic event occurred at an onset temperature of 337.90 °C. The area under the peak indicates the enthalpy of the event. Notice also that the downward peak has two shoulders on it indicating the possible presence of more than one phase of the hydride or more than one mechanism for hydrogen release.

The pressure in the sample cell was also monitored as a function of temperature during this experiment. The data obtained are presented in Figure 10 and the first derivative plot of these data are shown in Figure 11. These two plots are virtually identical to those obtained for the same sample on the TVA , Figures 7 and 8, using a 3 g sample. The new system only required 55 mg of sample.



**Figure 10.** Pressure-Temperature data obtained during the first dehydriding of  $MgH_2$  in the DSC.

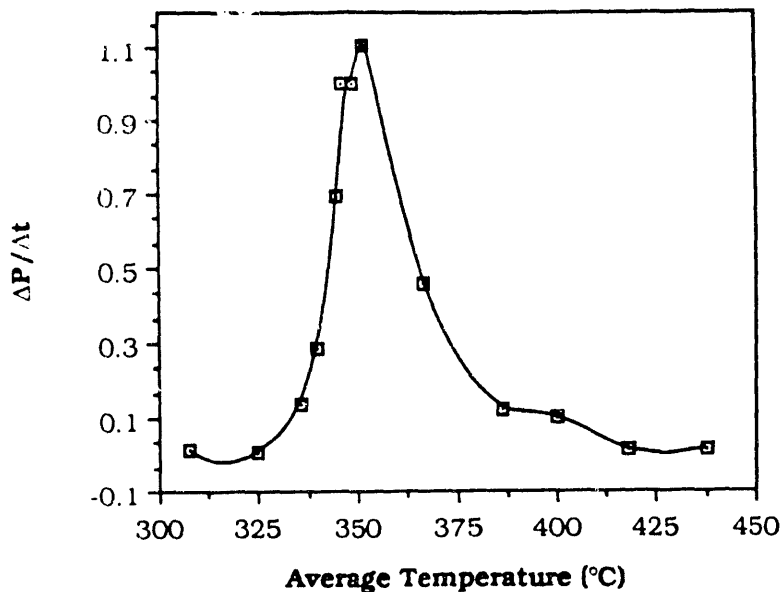
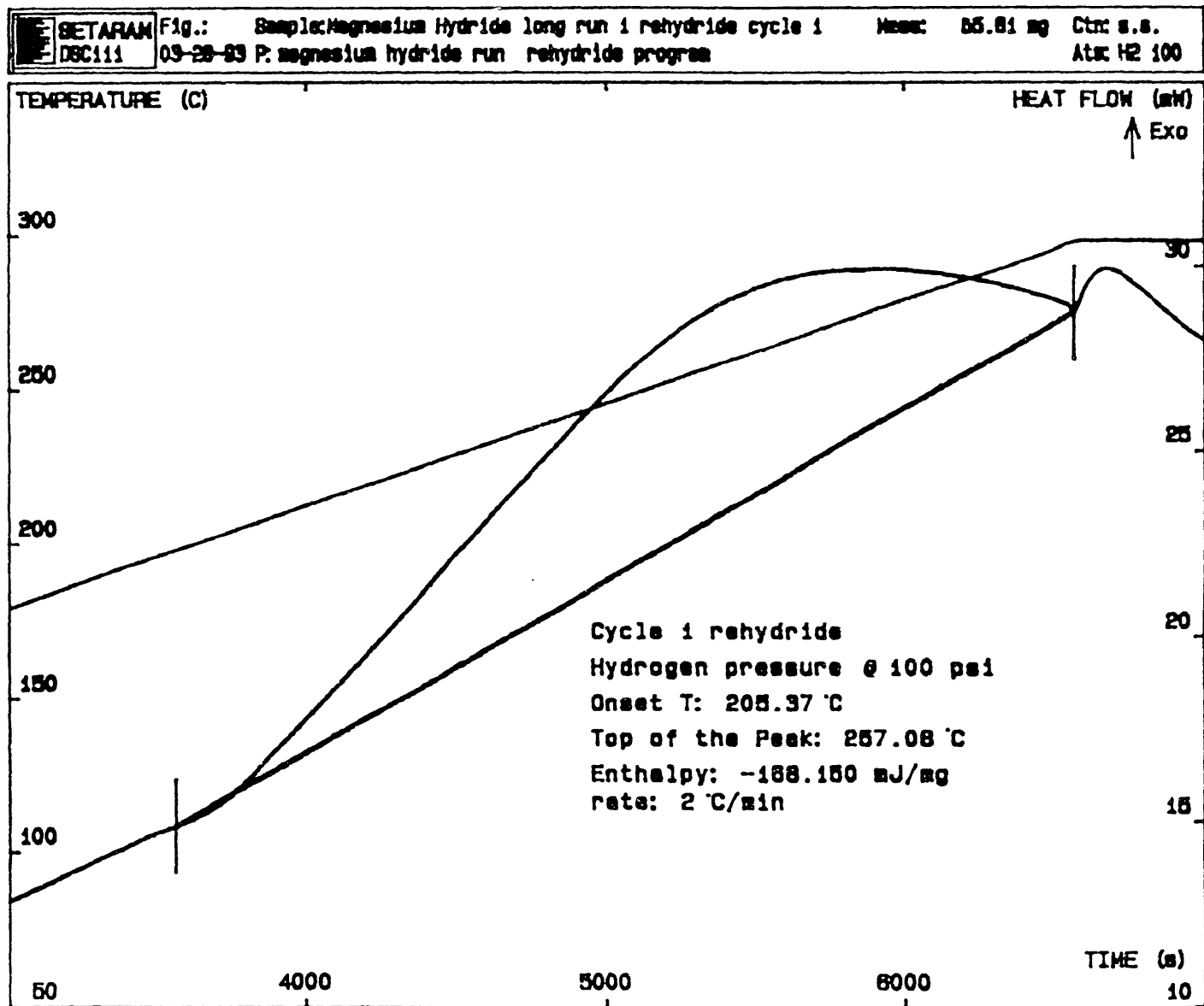


**Figure 11. First derivative plot of pressure data from first dehydriding of  $MgH_2$ .**

The ability of  $MgH_2$  to recycle was ascertained by pressurizing the cells to 100 psi hydrogen and increasing the temperature at a rate of 2 °C/min from 100 °C to 300 °C to determine if the metal would take up hydrogen. A definite thermal event occurred at 205 °C and continuing through the remaining temperature increase up to 300 °C, Figure 12. The pressure data show a decrease in pressure during the recorded thermal event, Figure 13. This plot shows a rapid pressure decrease beginning at about 205 °C.

From the results above, it is obvious that one of the most important aspects of this instrument is that it is possible to directly determine the onset temperature of the uptake and release of hydrogen through the DSC as well as from the pressure readings. Thermovolumetric instrumentation affords no such capability and can only indirectly show the hydrogen uptake and release transitions through the integration of the temperature-pressure data. Unlike the TVA, the pressure data and thermogram data from the DSC are not dependent upon one another.

Figure 12. Thermogram of magnesium hydride rehydrating.





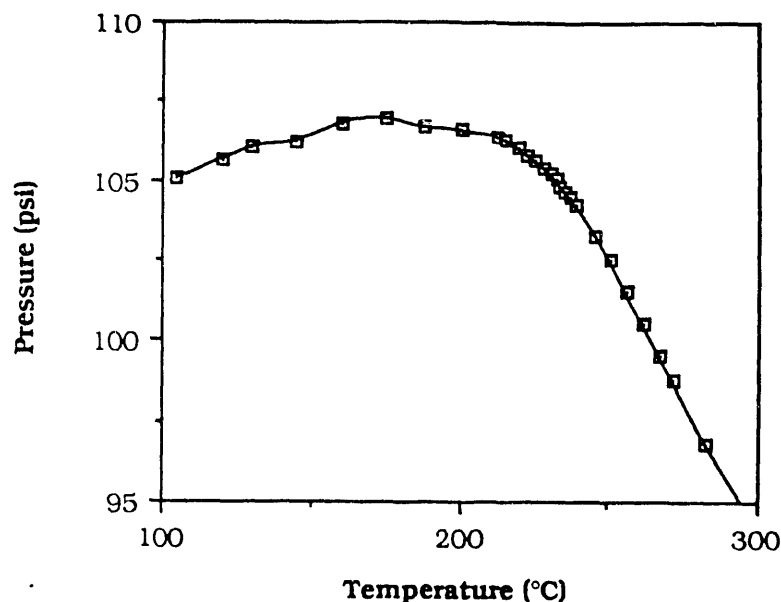


**Figure 13. Pressure-Temperature data obtained during the rehydrating of  $MgH_2$  in the DSC.**

The new system allows for rapid, multiple testing to be done on a single sample as well as for rapid sample changing. This makes it easy to determine the effect of varying hydrogen partial pressure on the onset temperatures of hydrogen release and uptake. The high sensitivity of the instrument also allows for the determination of the phase purity of the hydride and the relative stabilities of different phases. Since the DSC is computer controlled, it is possible to cycle a hydride between heating and cooling, and thus hydrogen release and absorption, over an extended period of time.

The thermogram shown in Figure 14 was generated by heating a sample of magnesium hydride in an argon atmosphere from ambient to 450 °C and then cooling at the same rate without changing the atmosphere in the cell. The large endotherm resulted from the dehydrating of the sample beginning at 304.83 °C. The small exotherm on the cooling side of the thermogram resulted from the uptake of hydrogen by the sample beginning at 273.44 °C. This is an interesting phenomenon because it shows that, after heating, magnesium hydride will take hydrogen back up even under an atmosphere containing a very low partial pressure of hydrogen.

The final phase involved the use of gas chromatography to determine the identity of the gas released during thermal events. Samples of pure hydrogen were used to determine the retention time of hydrogen in our GC. The value was measured to be 30 to 33 seconds. Then a real sample of  $MgH_2$  was analyzed. For this analysis, the pressure cells were purged with argon at 70 mL/min. The sample of  $MgH_2$  was weighed out into a stainless steel boat and inserted into the sample cell. The sample cell was then connected to the GC. The purge was continued at the same flow rate for the remainder of the analysis. A sample of the purge gas was analyzed to determine the baseline. The DSC furnace was heated from ambient to 450 °C at 2 °C/min and the purge gas was analyzed from 285 °C up to 400 °C at 5 °C intervals. The resulting gas chromatograms can be seen in Figure 15. A plot of the millivolt output from the GC versus the temperature for the injection is seen in Figure 16.

Due to the configuration of the DSC and the pressure cells, a gas chromatograph was able to be connected to the system. This is not possible with the TVA. TVA is based on a pressure-

Figure 14. Thermogram of a sample of  $MgH_2$ , both heated and cooled in the DSC high pressure cells with no argon purging at the maximum furnace temperature.

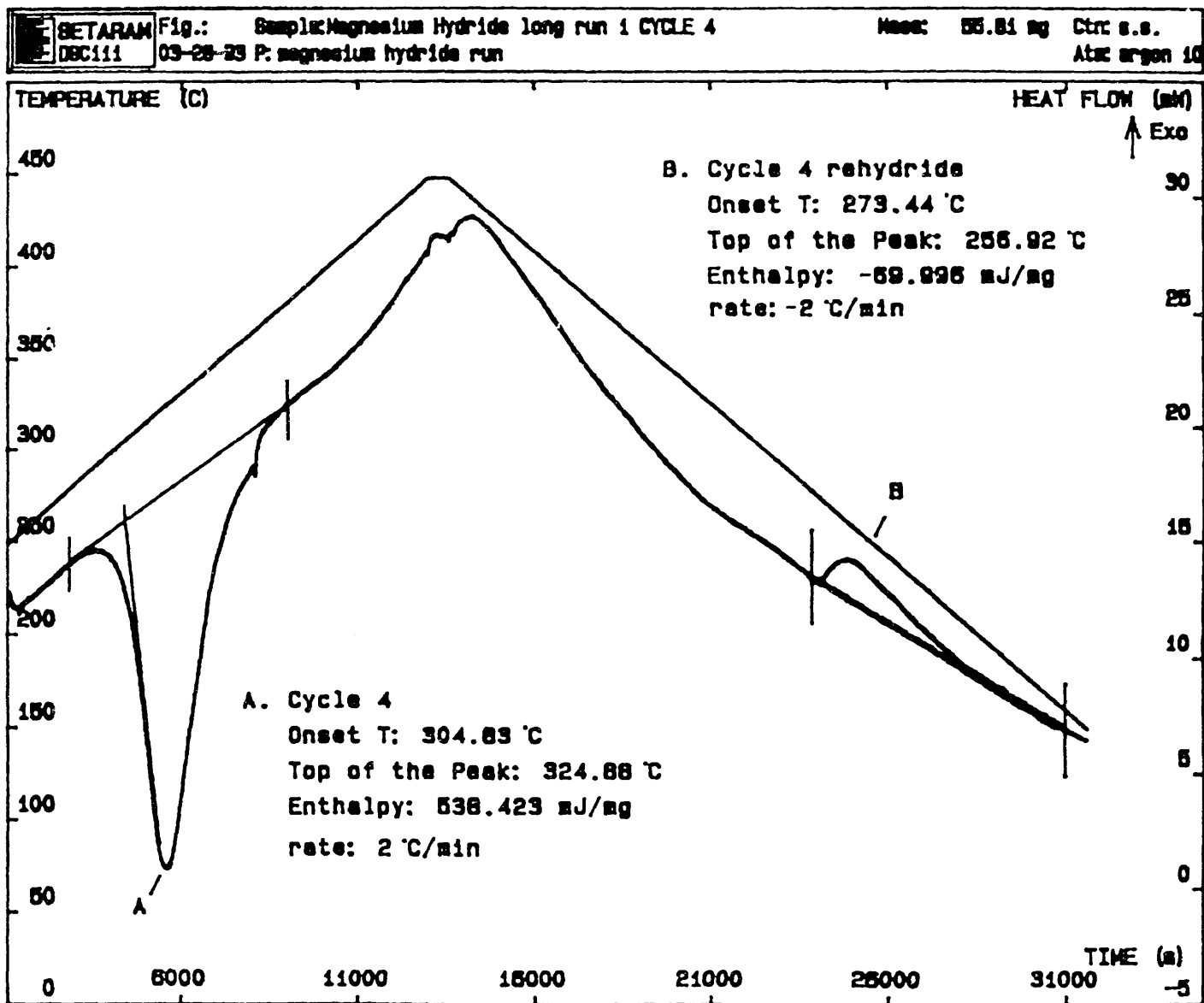
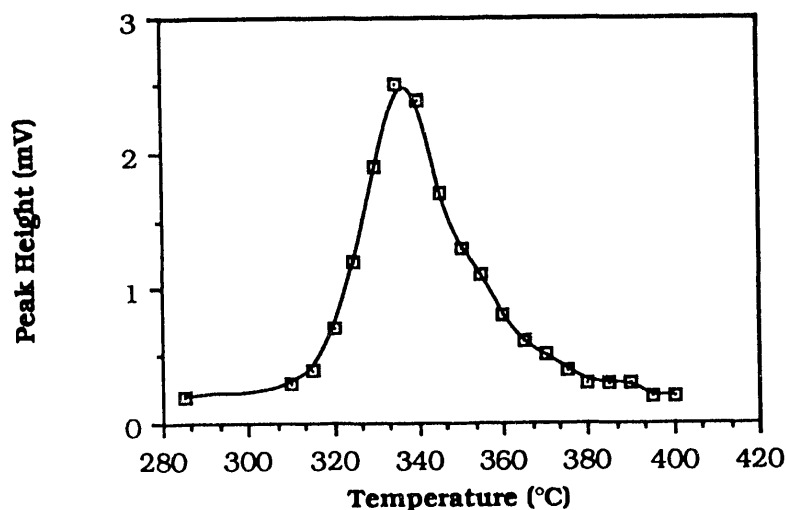




Figure 15. Peaks resulting from the gas chromatograms of evolved gas from magnesium hydride. Samples were taken every 5-10 °C.



**Figure 16. Relationship of peak height to temperature from the gas chromatograms for the dehydriding of  $MgH_2$ .**

### Proposed Future Work

This system will be improved by interfacing the GC and pressure transducers to a data acquisition system and another computer. Both the data acquisition system and computer have been obtained. Such interfacing will allow better data handling and display as well as differential pressure measurement. Differential pressure measurement between sample and reference cells in the DSC will allow much more sensitive pressure measurement.

Future work also involves study of new candidate hydrogen storage compounds as well as much more detailed study of currently investigated compounds. The new compounds to be studied will be light metal hydrides both alone and with small amounts of different transition metals deposited on their surfaces. We have already worked out the synthesis of these compounds and the literature indicates a decomposition temperature of around 180 °C. They have a large hydrogen capacity and are made of non-toxic components.

The more detailed study of current candidate compounds involves an investigation of the phase-temperature relationships and their influence on the properties of the compounds. The effect of recycle conditions will also be studied.

### References

1. NIST Standard Reference Materials Catalog, 1990 - 1991.
2. Bogdanovic, B.; *Int. J. Hydrogen Energy*, 1984, 937 - 941.

# **MAGNESIUM ALLOYS FOR HIGH HYDROGEN STORAGE CAPACITY AT LOW TEMPERATURES**

Supramaniam Srinivasan, M.P. Sridhar Kumar, Konstantin Petrov,  
Arnaldo Visintin and A. John Appleby  
Center for Electrochemical Systems and Hydrogen Research  
Texas Engineering Experiment Station  
Texas A & M University System  
College Station, TX 77843-3402

## **Abstract**

The objectives of this project are to investigate promising alloys for hydrogen storage, in order to find systems with (i) optimal plateau pressures and high capacities (considerably higher than for the state-of-the-art systems, which is about 1 to 1.5%) at low temperatures; (ii) fast hydrogen absorption/desorption kinetics, by use of catalytic additives; (iii) high stabilities for long term utilization; and (iv) tolerant to small quantities of impurities. A major aspect of this task will involve investigation of magnesium-based alloy systems which, according to some preliminary reports, show promise of high storage capacities under ambient conditions. Preliminary experiments reveal that materials, prepared by mechanical alloying, show promise for hydrogen storage. The potential of this technique will be fully explored. The thermodynamic and kinetic parameters of the hydriding/dehydriding reactions of selected alloys will be evaluated using the Sievert apparatus and microcalorimetry, which have both been appropriately modified in our laboratory for this purpose. The expected benefits of the proposed research are that finding reasonably low cost alloys with hydrogen storage capacities of greater than two to three percent will resolve the problem of fuel storage for low temperature fuel cells (proton exchange membrane, alkaline), vitally needed as power sources for zero emission vehicles and other mobile applications.

## Introduction

### Background - Rationale for Selection of Magnesium Based Alloys

Of the four methods of hydrogen storage (compressed gas, cryogenic liquid, metal hydrides and gas-solid adsorption), the metal hydride storage method is attractive from the points of view of high volumetric density and safety. Cost-effective hydrogen storage is also vital for hydrogen energy systems to be competitive with alternatives. A comparative analysis, of the capacities and energy densities of hydrogen storage for several hydride systems, compressed gas and liquid hydrogen, is presented in Table 1 (Lynch and Snape 1978). Also shown in the table are the energy densities for n-octane, diesel fuel and alternate fuels like natural gas, LPG and methanol. As evident from the table, currently available low temperature metal hydride systems (LaNi<sub>5</sub>, FeTi and V) have relatively low energy densities and these alloys have relatively high costs. Due to the impending legislation for zero emission vehicles, efficient and cost-effective hydrogen storage is vital for fuel cell powered vehicles. Thus, finding high energy density hydrogen storage alloys is essential for various applications which include integration with fuel cells-terrestrial and space.

Intermetallics of magnesium with some elements have relatively large hydriding/dehydriding capacities, when compared with AB<sub>2</sub> and AB<sub>3</sub> intermetallics (see Table 1) currently finding commercial

**Table 1. A Comparative Analysis of Hydrogen Storage Capacities and Energy Densities**  
(Also Shown are Energy Densities for the Conventional and Alternate Carbonaceous Fuels)

Medium	Hydrogen Storage Capacity		Energy Density	
	Wt%	g/ml	Heat of Combustion cal/g	cal/ml of vol.
MgH <sub>2</sub>	7.0	0.101	2373	3423
Mg <sub>2</sub> NiH <sub>4</sub>	3.16	0.081	1070	2754
VH <sub>2</sub>	2.07		701	4178
FeTiH <sub>1.95</sub>	1.75	0.096	593	3245
TiFe <sub>0.7</sub> Mn <sub>0.2</sub> H <sub>1.9</sub>	1.72	~0.09	583	~3050
LaNi <sub>5</sub> H <sub>7</sub>	1.37	0.089	464	3051
Liquid H <sub>2</sub>	12.5	0.070	4250	2373
Gaseous H <sub>2</sub>	1.25	0.017	510	240
Gas-solid	7.2	0.014	2448	460
N-Octane	15.8	0.110	11400	8020
Methanol	12.5	0.150	5420	4280
Ethanol	13.0	0.164	7095	5605

applications (for example nickel/metal hydride batteries). Magnesium alloys are also more cost-effective for hydrogen storage. The only factors impeding the successful use of Mg based systems in practical applications have been their relatively slow kinetics for hydrogen absorption and the rather high temperature needed for desorption. Several of the magnesium based systems, investigated to date, need high grade heat for decomposition. Efforts to overcome these disadvantages are well worthwhile and, if successful, are certain to have long ranging consequences.

## **Scope and Objective**

The main focus of this project is to develop metal-hydrogen systems with optimum plateau pressures, high capacities and with improved stabilities in both gas phase and in battery environments. The initial thrust is focussed on Mg-related intermetallic and composite systems. On a related project, the Center for Electrochemical Systems and Hydrogen Research(CESHR) is actively involved in the preparation, characterization and evaluation of hydride electrodes of modified  $AB_5$  and  $AB_2$  type alloys in collaboration with Brookhaven National Laboratory and Los Alamos National Laboratory. On this project, the most promising alloys will be evaluated for hydrogen storage in nickel/hydrogen batteries and for hydrogen electrodes in nickel/metal hydride batteries by Hughes Aircraft Company.

One of the major disadvantages to date with Mg related systems is the necessity for an initial activation treatment for hydrogen absorption. Also, the relatively low boiling point of Mg, when compared to those of the other alloying elements, necessitates special sample preparation procedures (such as encapsulation). These problems have prompted us to evaluate other preparation techniques (techniques other than the ones conventionally used like arc or induction-melting) for preparing Mg based alloys. Most of these disadvantages could be overcome by preparing the materials by mechanical alloying (highly energetic ball milling). This procedure leads to intensive mixing of the constituent elements. Preliminary reports suggest that mechanically alloyed Mg-based systems could be used as hydrogen storage materials(Stepanov et al 1987).

The main objectives of the first task will be to prepare and characterize selected magnesium alloys for hydrogen storage and elucidate the roles of the constituent elements and of the morphologies of the alloys during hydrogen absorption and desorption. The second task will involve a considerably lower effort and will consist of making a techno-economic assessment of hydrogen storage, for integration with proton exchange membrane fuel cells (PEMFC), the most promising power source for electric vehicles.

## **Technical Approach**

### **Survey of Literature for Selection of Candidate Alloys on a Fundamental Basis**

A recent publication suggests that the lanthanum-magnesium system ( $La_2Mg_{17}$ ) stores hydrogen to the extent of over 6% by weight, and it is claimed that a major part of it is stored reversibly under ambient conditions (Dutta and Srivastava 1990). According to a second publication from the same research group, another ambient hydriding/dehydriding system is the alloy Mg-x wt% FeTi(Mn), with storage capacities reaching nearly 3.5wt%(Mandal et al 1992), as compared to ~2% for the pure FeTi alloy, and this has been attributed to the presence of FeTi-Mg complexes. Additional reports (Wang et al 1984) on the Mg-Fe-Ni-Ti system also indicate the possibility of storing hydrogen in Mg based compounds under ambient or relatively mild conditions.

## Preparation of Alloys Using Mechanical Alloying and Other Techniques

Mechanical alloying has considerable advantages in that it is a fast process and results in highly activated powders of uniform size, which could be hydrided at an appreciable rate, even in the initial hydriding cycles. The mechanical alloying process generally results in amorphous or only partially crystalline material. Often this process is followed by an annealing treatment in order to obtain well defined crystalline material. In most cases, the alloys are active for hydrogen absorption, even without the annealing treatment. Studies on the mechanical alloyed Mg-50wt%Ni indicate that the nickel atoms, dispersed on the surface of Mg, exhibit increased catalytic activity, owing to electron transfer from Mg to Ni (Stepanov et al 1987). Also, an alloy of Mg containing only 0.1%Ni is hydrided at a higher rate and with a shorter induction period than that for pure Mg; further, electrodeposition of Ni on Mg has practically no effect on the hydriding rate. These and other studies clearly prove that mechanical alloying is not simply a mixture of two metals, but a metastable system with high reactivity due to the large interface between the metals, the presence of defects and the chemical interaction of the components. Previous studies show that mechanically alloyed Mg-55wt%Ni on exposure to hydrogen completely transforms into Mg<sub>2</sub>Ni in 3-4 cycles. In this case, MgNi<sub>2</sub>, which does not react with hydrogen and is almost always one of the products in the synthesis of Mg<sub>2</sub>Ni by the melting technique, is not formed.

## Thermodynamics and Kinetics of the Hydrogen Absorption/Desorption Reactions

### *Volumetric Measurements*

A modified Sievert apparatus has been set up to obtain thermodynamic and kinetic data on the metal-hydrogen systems. The schematic of the unit is shown in Fig 1. This system can operate from pressures as low as 10<sup>-4</sup>atm to pressures over 100atm, necessary for accurate determination of pressure-composition-temperature isotherms for hydriding/dehydriding processes. With proper sample temperature control, the kinetics of the reactions can also be followed and the parameters evaluated.

### *Microcalorimetry - Principles and Methods*

All phenomena of physico-chemical nature are accompanied by thermal effects; the precise magnitudes of these effects are of considerable practical and theoretical importance. Thermodynamic studies aim to measure the total quantity of heat, Q, produced by a given transformation over a period of time, or the heat flux independent of time. Highly sensitive microcalorimeters are capable of recording heat generation rates of the order of a microwatt and can be used to study processes with remarkable fidelity. The apparatus does not measure the quantity of heat produced directly from the process under investigation, but records the heat flux (the time derivative of Q, i.e., the rate of heat production = dQ/dt) as a function of time(t). The experimental observations are recorded as a continuous curve, which, after minor adjustments, is a correct representation of Q as a function of time:

$$Q=f(t) \quad (1)$$

This is the "thermokinetic" curve of the process under study. To obtain the quantity of heat, produced between times t<sub>1</sub> and t<sub>2</sub>, one simply measures the area under the curves for the time interval. The thermokinetic curve not only provides a measure of the heat evolution, Q, in a given time interval, but also gives an accurate representation of the kinetics of the process.



Thus, for more accurate determination of the thermodynamic and kinetic parameters of the hydriding and dehydriding reactions, than those obtained using the Sievert apparatus, a highly sophisticated microcalorimeter will be used. Fig 2 gives the schematic diagram of the microcalorimeter and Fig 3 that of the miniature Ni sample tube to be used in the measurements. This Ni tube, in turn, is connected to a modified Sievert apparatus, for use in various gas atmospheres.

### **Techno-Economic Assessments of Hydrogen Storage Sub-Systems**

One of the main applications for a hydrogen storage sub-system will be for proton exchange membrane fuel cell power sources particularly for zero-emission electric vehicles. CESHR is actively engaged in the development of PEMFCs and of electric vehicles and is focusing on hydrogen fuel, rather than methanol and a steam-reformer, being carried on board the vehicle. The ultimate power source for zero emission electric vehicles is the fuel cell and the PEMFC is the strongest candidate. For a zero-emission fuel cell powered vehicle, there is no alternative to hydrogen as the fuel. One of the major challenges is finding the ideal method for coupling the hydrogen storage system with the PEMFC. The objectives of this task will be to make a techno-economic comparison of the hydrogen storage options for PEMFCs.

### **Results to Date and Discussion**

A three pronged approach is followed in the first task. Firstly, a detailed literature survey is in progress on Mg based and other hydrogen storage alloys. This would greatly enhance our understanding of the Mg-hydrogen system and also help us to propose new formulations with superior and improved properties in respect to the reaction with hydrogen. The contract on this project was awarded in January 1993. Initial work focussed on the assembly of a modified Sievert Apparatus (as described in the previous section) and testing of a model system prepared by mechanical alloying and by arc-melting. Mechanical alloying produces samples in the amorphous state. Conversion to the polycrystalline state by annealing is essential to obtain desirable hydrogen absorption/desorption characteristics. Mechanically alloyed samples, which are annealed, have activities and sorption capacities comparable to those of the samples prepared by conventional melting techniques. This behavior has been demonstrated, on a few intermetallic compounds, by determining the pressure-composition-temperature isotherms. Fig 4 shows the hydrogen absorption isotherms for the mechanically alloyed AB5 type material as a function of temperature and Fig 5 compares the results on the same alloy prepared by arc-melting and mechanical alloying. The mechanically alloyed and arc-melted samples were prepared at Los Alamos National Laboratory and Brookhaven National Laboratory, respectively, for the nickel/metal hydride battery project at CESHR.

In order to determine the thermodynamic and kinetic parameters for the reactions, the highly sensitive microcalorimeter has been adapted to perform hydriding/dehydriding experiments over a wide range of pressures  $10^{-4}$  to 100atm. The microcalorimeter will be coupled with a vacuum unit for working under reduced pressures.

## **Proposed Future Work**

### **Preparation of Selected Alloys**

Our initial experiments will be on the La-Mg and the Mg-FeTi systems, using the mechanical alloying technique for sample preparation. Preliminary reports on these type of compounds (prepared by melt processes) indicate ambient temperature reversible hydriding (Dutta and Srivastava 1990, Mandal et al 1992). Mechanical alloying is most likely to improve this interaction with hydrogen. Experiments on alloys (with additives of other metals like Ce, Co, Si and Sn) to the above compositions will be performed to check if these additions will make the multi-component alloys more suitable for practical applications. These additions have proven to be beneficial for the AB<sub>3</sub> and AB<sub>2</sub> alloys, being investigated for hydride electrodes. During these studies, the potential of the mechanical alloying process will be fully explored and, at different stages, comparison will be made with the behavior of similar samples prepared by conventional melting techniques.

Future studies will also include systems other than the Mg based ones, which are also likely to show higher hydriding capacities (for example, compounds based on Zr-Mn and Ti-V systems). Finally, efforts will be made to formulate new multicomponent systems by coupling two or more of the above simple compounds and attempts will be made to optimize the compositions to result in more attractive hydrogen storage systems.

### **Physico-chemical Characterization of the Alloys**

The morphology and composition of the alloys will be determined using characterization techniques such as X-ray diffraction and SEM/EDAX. Pressure-composition-temperature isotherms of promising alloys will be measured using the modified Sievert apparatus to yield data on the plateau pressures, hydrogen absorption capacities and the enthalpies and entropies of the reactions. The microcalorimetric technique will be used to obtain quantitative data on the kinetics of hydriding and dehydriding.

### **Techno-economic Assessment of Hydrogen Storage Sub-systems**

This study will also consist of a techno-economic evaluation of the following methods of hydrogen storage for coupling with PEMFCs:

- compressed natural gas
- liquid hydrogen
- metal hydrides
- gas-solid adsorption

## **Acknowledgments**

The work was carried out under the auspices of the U.S. Department of Energy-National Renewable Energy Research Laboratory (Contract #XD-0-10088-1). The authors wish to thank the cooperation of Dr. Anaba Anani (a former coworker at CESH, presently at Motorola), Mr. James J. Reilly and Dr. J.R. Johnson of Brookhaven National Laboratory and Dr. Ricardo B. Schwarz and Mr. Paul B. Desch of Los Alamos National Laboratory for their contributions on the project "Hydrogen Storage Alloys for

Nickel/Hydrogen and Nickel/Metal Hydride Batteries," sponsored by Hughes Aircraft Company, the results of which are most valuable for this project.

## References

Dutta, K. and O.N. Srivastava. 1990. "Investigation on Synthesis, Characterization and Hydrogenation Behavior of the  $\text{La}_2\text{Mg}_{17}$  Intermetallic." *Int. J. Hydrogen Energy*, 15: 341-344.

Lynch, F.E. and E. Snape. 1978. "The Role of Metal Hydrides in Hydrogen Storage and Production." In *Proceedings of the 2nd World Hydrogen Energy Conference*, 1457-1524, Zurich, Switzerland: Eds. T.N. Veziroglu and W. Seifritz.

Mandal, P., K. Dutta, K. Ramakrishna, K. Sapru and O.N. Srivastava. 1992. "Synthesis, Characterization and Hydrogenation Behavior of  $\text{Mg-xwt}\%\text{FeTi}(\text{Mn})$  and  $\text{La}_2\text{Mg}_{17}\text{-xwt}\%\text{LaNi}_5$ -New Hydrogen Storage Composite Alloys." *J. Alloys and Compounds*, 184: 1-9.

Stepanov, A., E. Ivanov, I. Konstantchuk and V. Boldyrev. 1987. "Hydriding Properties of Mechanical Alloys Mg-Ni." *J. Less-Common metals*, 131: 89-97.

Wang Qi-dong, Wu Jing, Au Ming and Zhang Lian-Ying. 1984. "The Hydrogen Storage Properties and the Mechanism of the Hydriding Process of Some Multi-Component Magnesium Base Hydrogen Storage Alloys." In *Proceedings of the 5th World Hydrogen Energy Conference*, 1279-1290, Toronto, Canada: Eds. T.N. Veziroglu and J.B. Taylor.

## Figure Titles

Fig 1. Schematic of Hydrogen Storage Test Station - Modified Sievert Apparatus

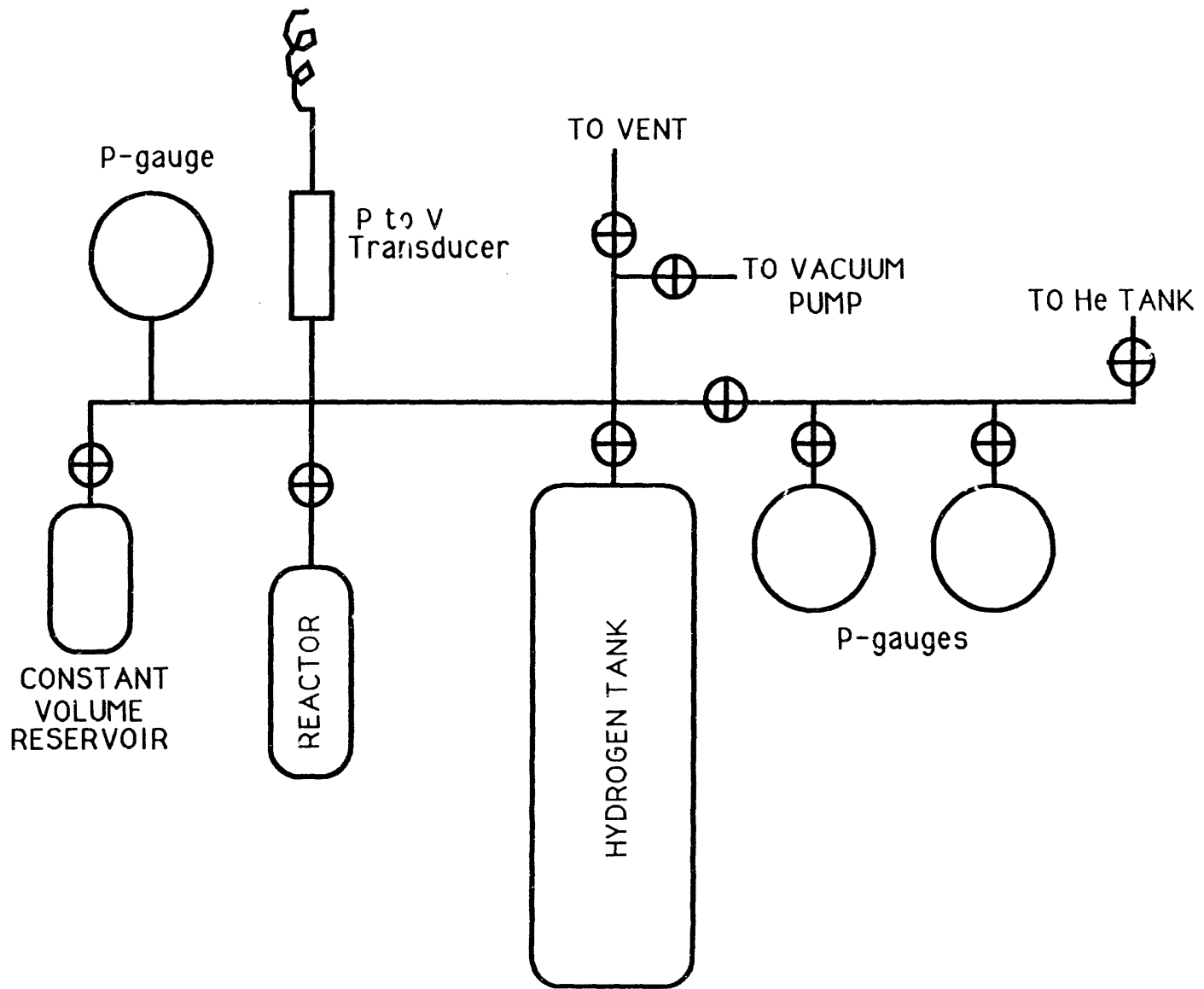
Fig 2. Schematic of Hart Scientific Microcalorimeter

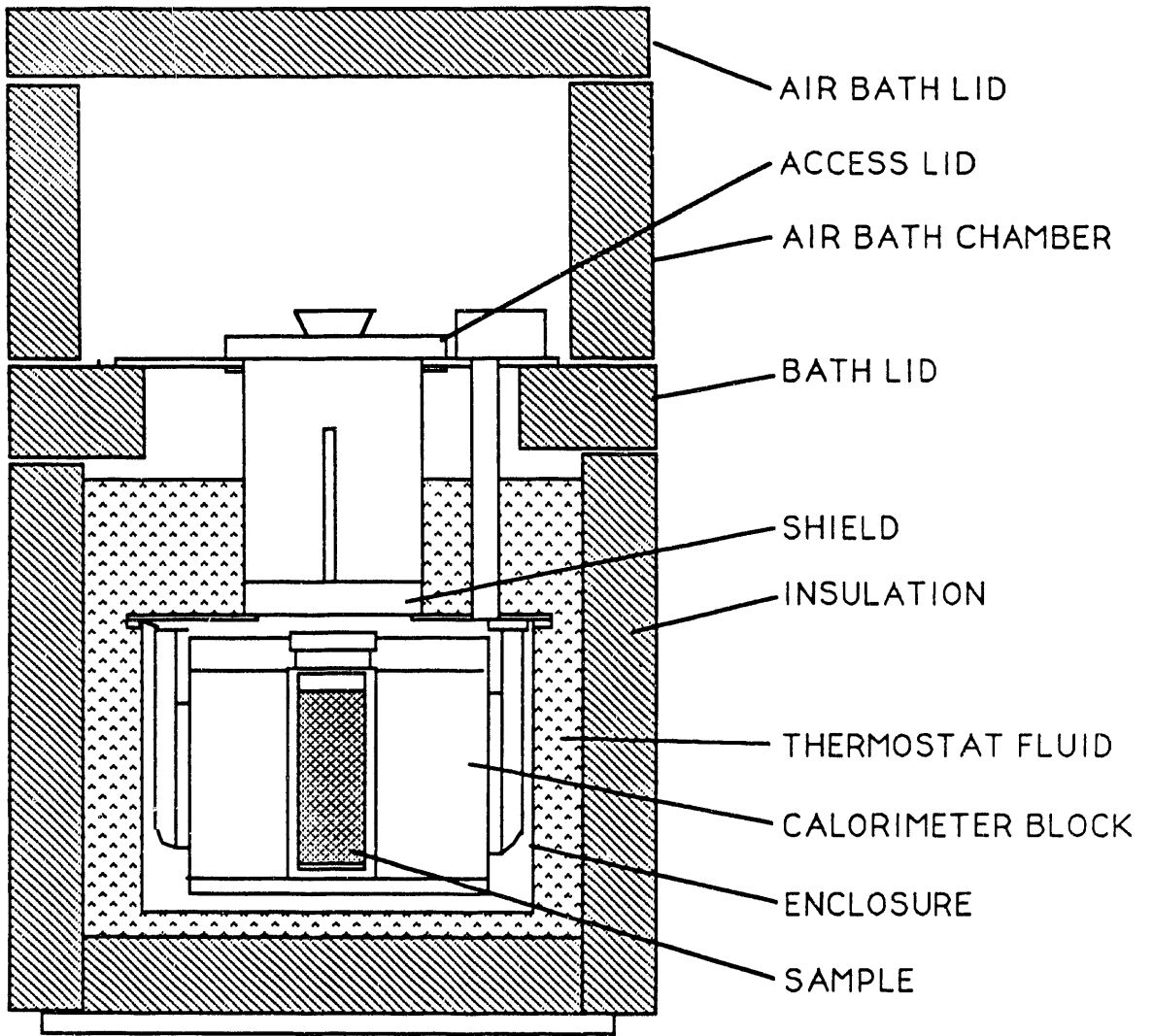
Fig 3. Schematic of Miniature Ni-sample Tube for Microcalorimetry Experiments

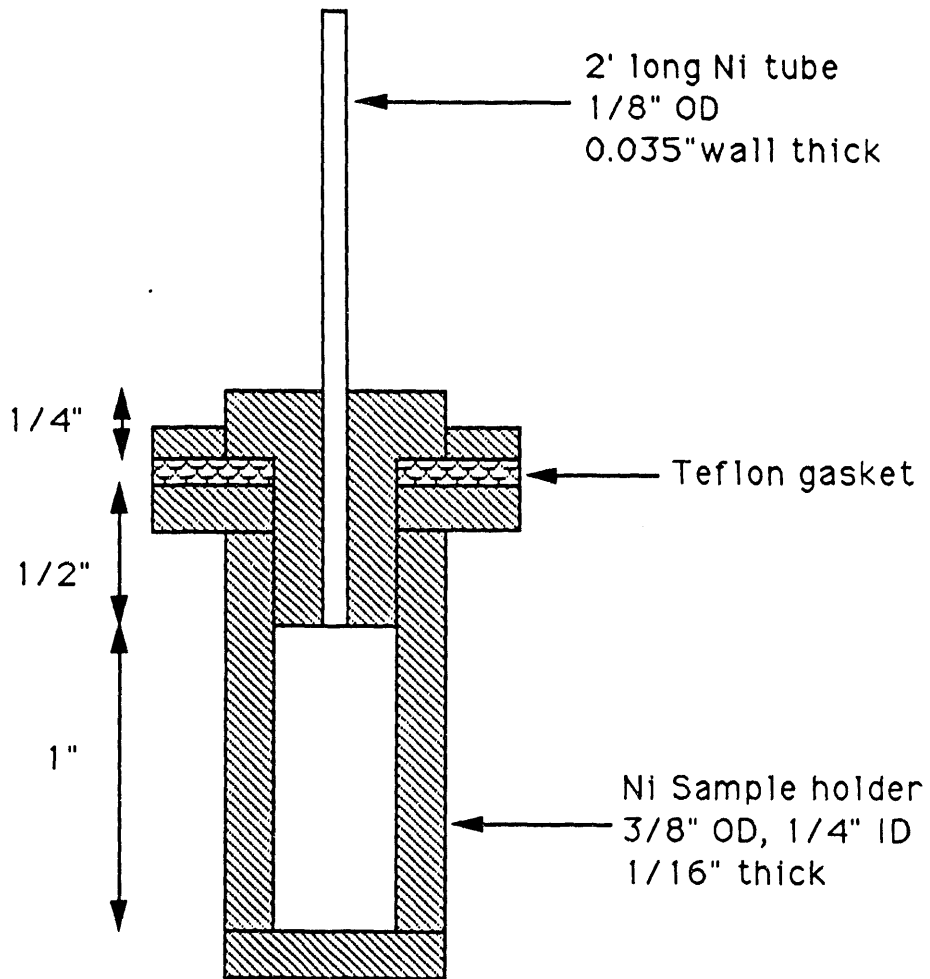
Fig 4. Hydrogen Absorption Isotherms for a Mechanical Alloyed AB<sub>5</sub> Type Material as a Function of Temperature

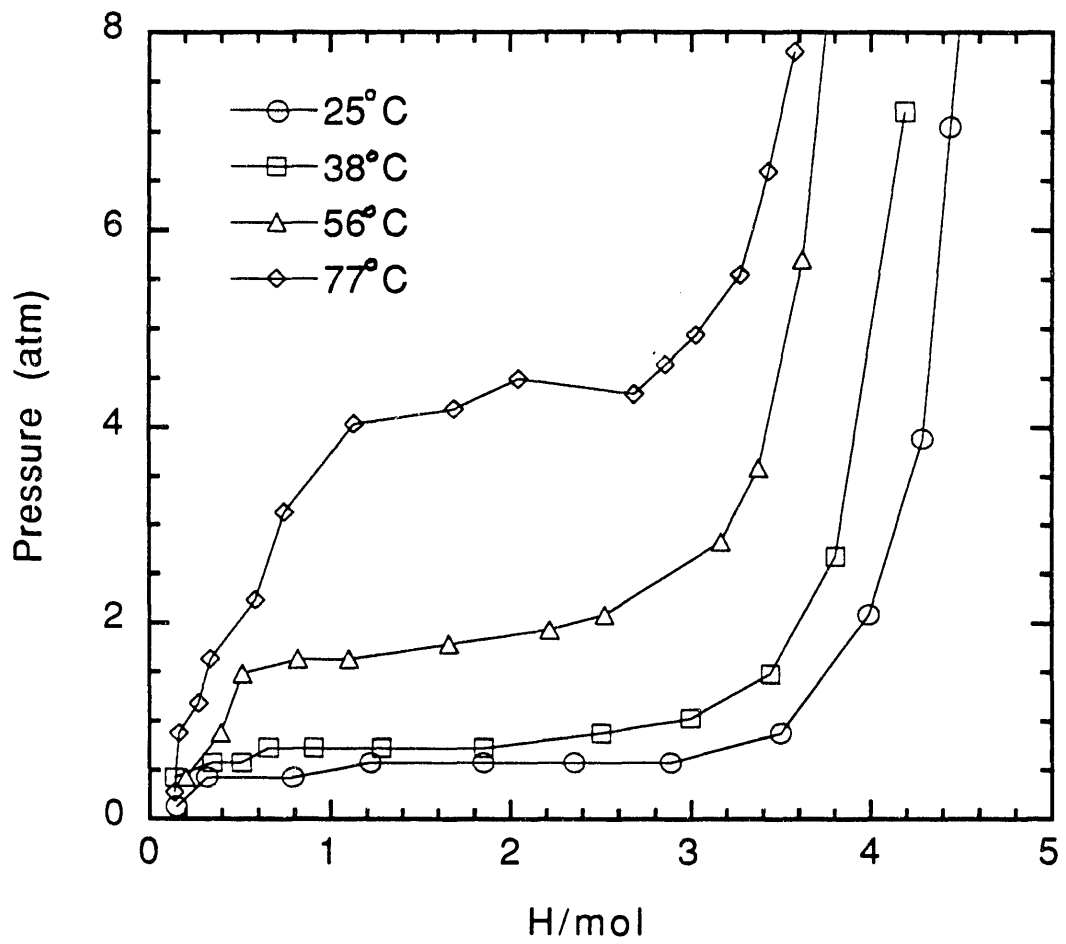
Fig 5. Comparison of Hydrogen Absorption Isotherms at 25°C for the AB<sub>5</sub> Type Material, Same Alloy as in Fig 4, Prepared by Arc-Melting and by Mechanical Alloying

SFT

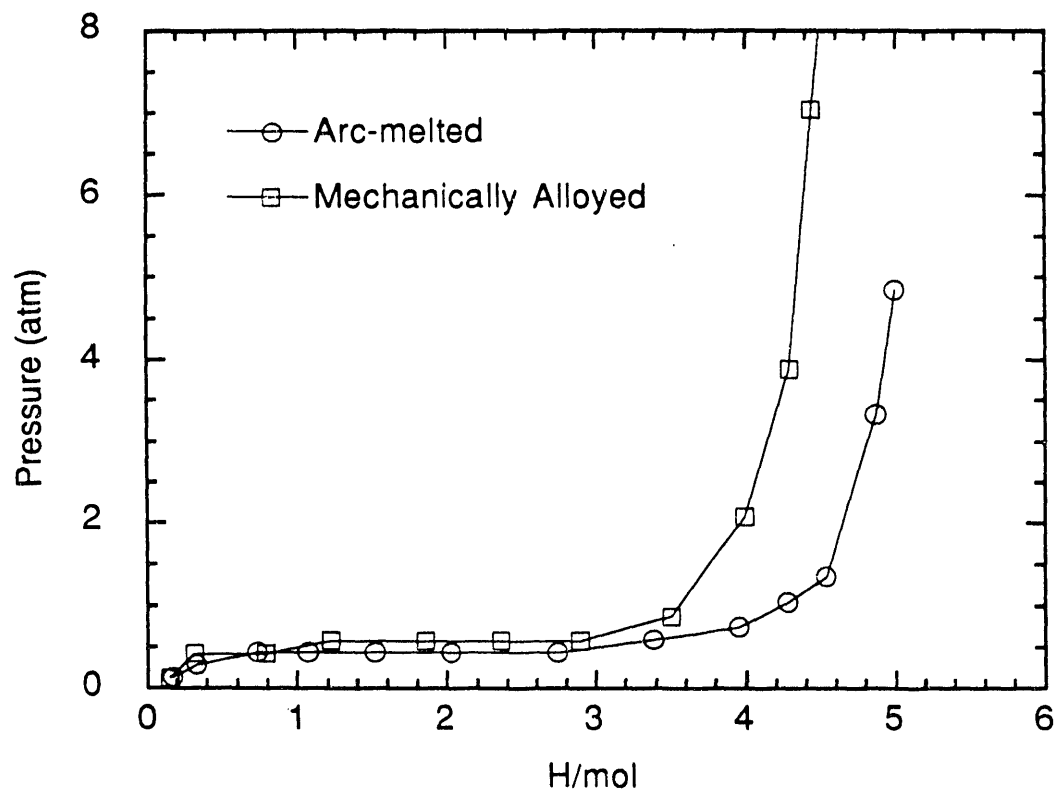














## **MODELING OF THE SOLAR HYDROGEN ENERGY SYSTEM**

Frano Barbir, Harold J. Plass, Jr., and T. Nejat Veziroglu  
Clean Energy Research Institute, University of Miami  
P.O. Box 248294, Coral Gables, FL 33124, U.S.A.

### **Abstract**

The energy language method has been used to develop a dynamic model which generated intersubstitution of energy sources and energy currencies in the energy market, and provided information on complex interactions between energy, environment and economics. Substitution of the fossil fuel system by the solar hydrogen energy system has been analyzed, with particular attention given to effects on economic growth and on the environment. The results have shown that an early transition to the solar hydrogen energy system would provide long term benefits to economy and to the environment.

### **Introduction**

The analyses of the solar hydrogen energy system and its interactions with the surroundings, performed during the past four years under the DOE/NREL sponsored project entitled Solar Hydrogen Energy System, Task A: Hydrogen Systems Application Analysis, investigated the requirements for establishing and operating such a system. Because the energy system is only a part of the economic system, which in turn is only a part of the environment, establishment of a new energy system, such as the solar hydrogen energy system, will inevitably have impacts on both the socio-economic system and the environment. These impacts can be analyzed only by taking into account the complex interactions between energy, environment and economy. A dynamic model has been developed, which included these complex interactions, although in a simplified way, and which enabled simulation and analysis of the long term

global trends resulting from the replacement of the global energy system.

## **Modeling Technique**

Odum (1983) has developed the energy circuit language for analysis and modeling of various systems. Although initially developed for ecological systems, this method has been successfully applied for modeling and simulation of human economic systems on regional, national and global levels (Odum, 1987; 1988; 1989). Society can be modeled as an energy system because the major socio-economic patterns are the ultimate result of energy usage. All primary energy forms have their origins in the environment, i.e., outside the socio-economic system. There is always an exchange of energy and materials between the socio-economic system and the environment. The dynamics of the economic process is therefore ultimately constrained by the availability of energy in the environment and its accessibility for economic consumption.

Energy circuit language is a simple but flexible way to visualize the structure and dynamics of the systems being analyzed. A special set of symbols has been developed in order to describe various components of the system and interactions between them (Odum, 1983). By combining the appropriate symbols, and following some specific but simple rules, it is possible to construct the energy diagram of the system. The symbols have rigorous kinetic and energetic definitions so that they not only provide graphic visualization of the model, but they also provide the equations for simulation.

This modeling technique provides a tool for the analysis of the behavior of the economic systems. Such models provide important physical information on the structure from which the behavior evolves. The models can be set to replicate patterns of real society, while at the same time they give an insight into the system structure which produces these patterns. In constructing a model of an energy-economic system, only long term changes in process dynamics are considered, such as consumption of resources from the environment and their use in building and maintaining a socio-economic infrastructure. It is not possible to account for the short term fluctuations.

Bodger and Baines (1988) have applied this technique to develop a model which simulates the penetrations of the new forms of primary energy sources, each having successively greater accessibility and availability. They managed to replicate some historical trends in energy consumption and performance of the socio-economic sector.

## **Model Description**

The world energy-economy-environment system has been modeled with energy circuit language method. The graphic diagram of the model is given in Fig. 1. The model relates total world assets and the global economy to the availability of renewable and nonrenewable resources in a very aggregate way. Boundaries of the system were selected at the global level. In that case the only energy flows crossing the boundary are global external energy sources coming into the system and degraded energy leaving the system.

The system draws energy from two kind of sources:

Renewable or flow limited sources. Incoming solar energy is a flow limited source because the system can extract only that much energy that is flowing in. The unused (untapped) portion leaves the system.

Non-renewable, i.e., fossil fuels. Fossil fuel reserves are drawn at the boundary because they could be considered either as a part of the system or as an outside energy source. They are represented as a tank, from which the system draws as much energy as needed, but only until there is enough reserves in the tank.

The second law of thermodynamics requires that any process disperses some of its available energy in degraded form, which leaves the system unable to do more work. This law also requires that any stored material, energy, goods, or information, depreciate, losing its concentrations, because its energy is dispersing. The flows of used energy leaving the system are shown in the diagram by pathways that go downward into the heat sink. These pathways represent only degraded heat energy. Any dispersing materials, commodities, services, or energy still concentrated enough to do work, form the network of pathways amongst the sources and storages.

The world energy-economy-environment system has been reduced to only three stored values:

Fossil fuel reserves are aggregated into a single tank, "F", i.e., coal, oil and natural gas are represented as a single source.

World economic assets, which in the model are represented as a physical storage "A", include all man-made physical structures, e.g., buildings, transport, communication networks, technological hardware, as well as the accumulation of skills, experience, knowledge and culture. It is the accumulation of hardware and software which is involved in the economic process and continuously being maintained, replaced and added to. In the dynamics of the process the assets have a twofold role: (i) they generates a demand for consumption of environmental resources, and (ii) provide the economic feedback necessary for generating goods and services.

Pollution tank, "P," stores pollutants being released by combustion of fossil fuels. Carbon dioxide has been selected as a measure of pollution, since the quantity of pollutants is proportional to the fossil fuels consumed, and CO<sub>2</sub> generation is also proportional to the fossil fuels consumed. Since carbon dioxide is a natural constituent of the atmosphere, only excess of CO<sub>2</sub> (above pre industrial level) is assumed to have negative effects on economy.

Interactions aggregate the entire economic process of creating goods and services. The flows coming into an interaction are environmental flows (in this case simply aggregated to only energy flows) and feedback of already stored goods and services. The result of this interaction is the economic product (goods and services).

The lines between the sources, storage tanks and interactions represent the flows of energy, materials, goods, services and information. The flow always has the same unit as the tank from which it has

originated or to which it is headed.

In the model, there are three pathways of resource use that generate economic assets, each slightly different. Each pathway actually represents a different stage of economic development:

(1) The lower pathway represents utilization of renewable resources in building and maintaining the world assets (e.g., agriculture, fishery, forestry, etc.). It actually represents undeveloped, non-industrialized economies.

(2) The next pathway represents developed economies that have tapped vast storages of mineral and fuel reserves to power their economies. Utilization of fossil fuel reserves has provided the growth of the economic activities and increased the world assets dramatically, particularly in the second half of this century. However, as already mentioned, there are at least two kinds of problems related to the utilization of the fossil fuels, i.e., (1) their reserves are finite and therefore sooner or later will be depleted, and (2) they create pollution on a local, regional and global scale.

(3) The solar hydrogen economy is considered as a new stage in the evolution and development of human civilization. A new source is actually added to the model, which represents solar energy available over vast desert areas of the world. This solar energy has not been used by human economic systems either directly or indirectly. Through hydrogen and electricity, it can be used in the economic process to provide essentially the same services as fossil fuels are providing today.

Once the graphic model has been completed, its relationships have been translated into mathematical equations by following the rules of the energy circuit language. Each flow, is represented by an equation, which are combined in differential equations, one for each storage tank. Table 1 provides the list of all the flows, sources and storages, as well as associated equations. In order to solve the resulting set of differential equations, the initial values and coefficients are required for each flow and storage. Year 1950 has been selected as the initial year. Most of the initial values (such as energy reserves, energy consumption, CO<sub>2</sub> content in the atmosphere, CO<sub>2</sub> emissions, etc.) were taken from the available statistical data (United Nations, 1991; Smil, 1991; White, 1987; German Bundestag, 1989). Selected initial values are shown in Table 1.

Because of their highly aggregated form, assets were taken as a normalized value (1 in 1990). Initial values for the resulting flows of assets (i.e., economic production, natural depreciation, and depreciation due to use of assets in production) were set by trial and error, so that model simulation replicates historical trends in energy consumption and economic production for the period 1950-1990 for which statistical data were available. World Gross Product, measured in constant 1990 U.S. dollars, is actually proportional to the economic production. Using statistical data for the World Product (World Bank, 1990), a conversion factor of \$268 trillion per normalized unit of assets is found to be applicable.

Utilization of solar energy through hydrogen as an energy carrier has been modeled to start in the year  $t_1$  ( $t_1$  2000). Penetration into the energy market has been assumed in logistic manner, according to Marchetti's (1973) observations. The time period required for the solar hydrogen to take 50 percent of the energy market ( $t_h$ ) is selected to be equal to the time required to go from 10% to 90% of the market, so called "takeover time" ( $t_o$ ). This time has been arbitrary selected to be 40 years, which is shorter than

"takeover times" for most of the fuels or energy technologies in the past. However, it is longer than the lifetime of energy equipment and infrastructure (which is usually considered as a minimum time required for painless transition). Penetration in a shorter time period is not likely, because of the economic stress which would occur since the new energy infrastructure would have to be built even before than the old one has been depreciated.

Initial values of storages and flows were used to determine the coefficients in the differential equations. The resulting set of the first order nonlinear differential equations has been solved by simple Euler's numerical integration, using one year as the time step.

## **Results and Discussion**

Computer simulation of the described model of energy-environment-economy interactions offers opportunity to examine a variety of different scenarios. The time period which has been selected for simulation is from 1950 to 2100. The period between 1950 and 1990 was used to verify the model and to determine missing coefficients. The real simulation starts in 1990. The time span of about one century is enough to find out long term trends. Short-term variations would be impossible to detect with such a simplified model.

Model simulation for the period between 1950 and 1990 has shown good agreement with the historical records for energy consumption, world gross product (as a measure of economic activity) and carbon dioxide in the atmosphere, as shown in Figs. 2, 3 and 4 respectively. If the world economy is based solely on utilization of fossil fuels (which means that the solar hydrogen sector is not activated at all) the consumption of fossil fuels will start to decline some time in the middle of the next century, after reaching a peak at about three times today's level. Decline in energy consumption will be accompanied by similar decline in economic activity. Carbon dioxide content in the atmosphere would continue to grow until the end of the century reaching 700 ppm - almost double what it is today.

In the case where utilization of solar energy and hydrogen is introduced in the energy market, energy consumption continues to increase, although at a lower rate than that between 1950 and 1990 (Fig. 2). Consequently, economic activity (Fig. 3) also continues to increase and would eventually reach a steady state some time in the future. Hydrogen introduction dramatically affects carbon dioxide in the atmosphere, which reaches the maximum before 2050 at 520 ppm (Fig. 4). From 2050, the carbon dioxide level in the atmosphere continues to decrease and eventually it would reach the pre-industrial revolution level.

Figures 5 and 6 show what would happen if transition to the solar hydrogen energy system is delayed 25 years. Energy consumption and economic activity would be higher than in "no hydrogen" scenario, but much lower than the case when hydrogen is introduced in the year 2000. Carbon dioxide would continue to increase until approximately 2070 reaching 620 ppm. If transition starts at 2050 there would be almost no positive effects. This suggests that an early transition to the solar hydrogen energy system would benefit the economy and the environment in the long run.

Historically, in the context of the longer time span, the fossil fuels era could be considered as a short interlude between the solar past and the solar future. In that short period (about three hundred years) fossil fuels made possible a tremendous development of the human civilization. However, if they are used to support the establishment of a permanent energy system such as the solar hydrogen energy system, they could be considered as a spark which provided a transition from the low level solar energy past to the higher level solar energy future. Solar energy is steadily available in a quantity which exceeds human needs by several orders of magnitude.

Any delay in action would make a transition more difficult, and the point of transition to hydrogen and solar energy could be another "lost moment in history" as feared by Winter (1990). If transition starts when economy begins to decline, it may be too late, because economy would not be able to afford investing in such a long term project as establishing of the new energy system.

As any system based on finite sources cannot grow forever, a system based on utilization of constant flow of incoming energy should reach a steady state. A steady state economy is defined as an economy with constant stocks of people and artifacts, maintained at some sufficient levels, by the lowest feasible flows of matter and energy. If economic development means getting more services per unit of throughput, and economic growth is defined as the increase of services by increasing the size of stocks, then it is clear that the steady state economy would force an end to pure growth but would not curtail, and in fact would stimulate, development (Daly, 1977). The steady-state level, which the human civilization can obtain, depends on the rate of utilization of available solar energy and the effort required to convert solar energy into more useful forms of energy.

Similar results were obtained by other researchers and modelers, using different mental and mathematical models. Hubbert (1973) concluded that exponential growth in fossil fuel consumption is not possible because fossil fuel resources are finite. After cessation of exponential growth, there is only one possible future steady state, but different levels are possible: (1) stabilization at maximum point, (2) overshoot and stabilization at some intermediate level capable of being sustained, (3) decline to zero or to some very low value. However, he has not discussed in detail the instruments for obtaining these steady states, although he did mention solar energy.

Odum (1983, 1987, 1988, 1989) argues that utilization of dispersed renewable energy sources, such as solar energy, yield a little if any net energy, and therefore could not provide a steady state at a level higher than it used to be before the industrial revolution started.

Similar prediction of world collapse, has been provided by Meadows, et al. (1972). Their results (using the model World3) have shown that population and industry output grow until combination of environmental and natural resource constraints eliminate the growth. Industrial capital begins to depreciate faster than the new investment can rebuild it, and the result is the collapse of the world economic system. They investigated other possible scenarios, and found that it would be possible to reach the steady state if sustainable policies (such as population control, technologies to reduce emissions, erosion and resource use) are implemented in the year 1995. If the same policies are implemented with a 20 years delay, there will be an overshoot and the steady state will be reached at some lower level. These results are qualitatively similar to those obtained in the present study.



## Conclusions and Recommendations for Future Work

Energy language method, originally developed for analysis and simulation of the ecological systems, is applicable for large-scale, long-term modeling of the socio-economic system. It is easy to understand and convenient to use. A model of global energy-environment-economy interactions has been developed and used for simulation of future trends, including the transition to the solar hydrogen energy system.

The results of the model simulation have shown that the present energy system will not be able to support economic growth in the next century. However, if the fossil fuel system is gradually replaced by the solar hydrogen energy system, the growth could continue (although at a slower rate) until a steady state is ultimately established.

The results has also indicated that the transition to the solar hydrogen energy system should start as soon as possible. Any delay could have a negative effect, i.e., increase in energy consumption, accelerated depletion of natural resources and a bigger burden on the already damaged environment.

This model is currently being enhanced by adding two additional categories also very important for interactions between energy, environment and economy - population and food.

The future work under this Task (Hydrogen Systems Application Analysis) should concentrate on the system study of the near term applications of hydrogen, and investigate the most promising possible pathways and illuminate the overall benefits of such applications. Promising (from the aspect of the near term commercialization) applications are fuel cells for transportation and for residential applications.

## References

- Bockris, J. O'M., and T.N. Veziroglu. 1985. A solar-hydrogen energy system for environmental compatibility, *Environmental Conservation*, Vol. 12, No. 2, pp. 105-118.
- Bodger, S., and J.T. Baines. 1988. Dynamics of an energy-economic system subject to an energy substitution sequence, *Energy Systems and Policy*, Vol. 12, pp. 167-178.
- Daly, H.E. 1977. *Steady State Economics*, W.H. Freeman and Co., San Francisco.
- German Bundestag, 1989, *Protecting the Earth's Atmosphere: An International Challenge*, German Bundestag, Bonn.
- Hubbert, M.K. 1973. Survey of world energy resources. *Can. Mining and Metallurgical Bull.* Vol. 66, pp. 37-53.
- Marchetti, C. 1977. Primary energy substitution models: On the interaction between energy and society, *Technol. Forecast. Soc. Change*, Vol. 10, pp. 345-356.
- Meadows, D.H., D.L. Meadows, J. Randers and W.W. Behrens, III. 1972. *The Limits to Growth*, Universe Books, A Potomac Associates Book, New York.
- Odum, H.T. 1983. *Systems Ecology*. John Wiley & Sons, New York.

- Odum, H.T. 1987. Models for national, international, and global systems policy, in L.C. Braat and W.F.J. van Liempot, eds., *Economic-Ecological Modeling*, Elsevier Science Publishers, Amsterdam, Holland.
- Odum, H.T. 1988. *Energy, Environment and Public Policy: A Guide to the Analysis of Systems*, UNEP Regional Seas Reports and Studies No. 95, United Nations Environment Programme, Nairobi, Kenya.
- Odum, H.T. 1989. Simulation Models of Ecological Economics Developed with Energy Language Methods. *Simulation*. August 1989: 69-75
- United Nations Organization. 1991. *Energy Statistic Yearbook 1989*, United Nations, New York.
- Smil, V. 1991. *General Energetics: Energy in the Biosphere and Civilization*. John Wiley & Sons, New York.
- White, D.A. 1987. Conventional oil and gas resources, in D.J. McLaren and B.J. Skinner, eds., *Resources and World Development*. Wiley, Chichester, pp. 113-128
- Winter, C.-J. 1990. Hydrogen and Solar Energy - Ultima Ratio Avoiding a "Lost Moment in the History of Energy," in T.N. Veziroglu and P.K. Takahashi, (eds.), *Hydrogen Energy Progress VIII*, Vol. 1, pp. 3-47, Pergamon Press, New York.
- World Bank, 1990, *World Development Report 1990*, Published for the World Bank by Oxford University Press, New York.

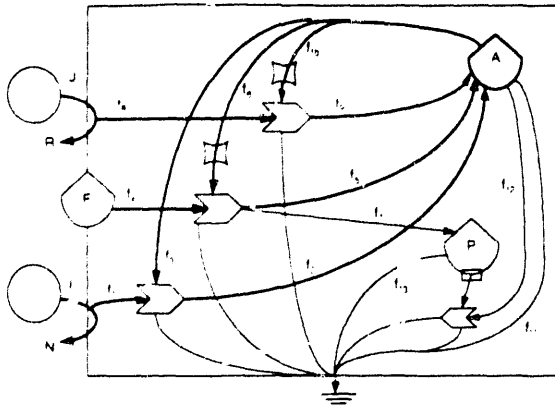


Figure 1 Global energy-economy-environment model diagram

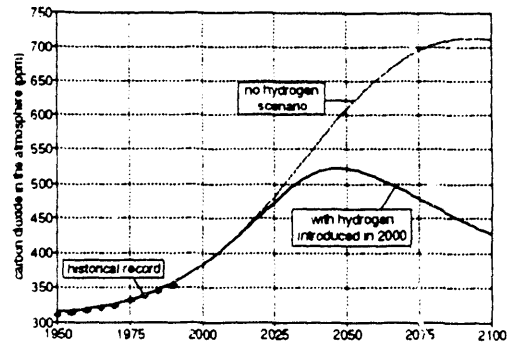


Figure 4. Carbon dioxide in the atmosphere (base case scenario)

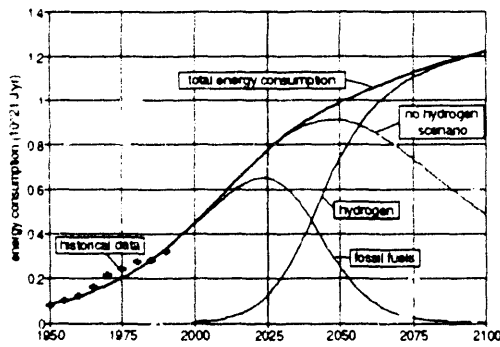


Figure 2. Energy consumption (base case scenario)

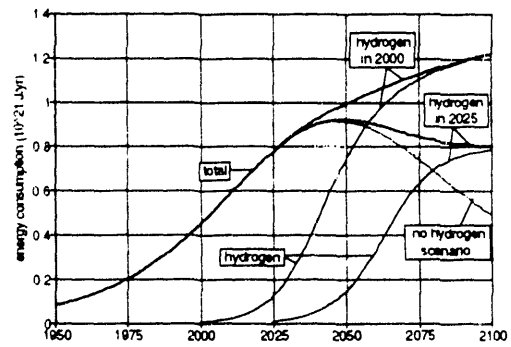


Figure 5. Energy consumption (initiation of hydrogen energy system is delayed 25 years)

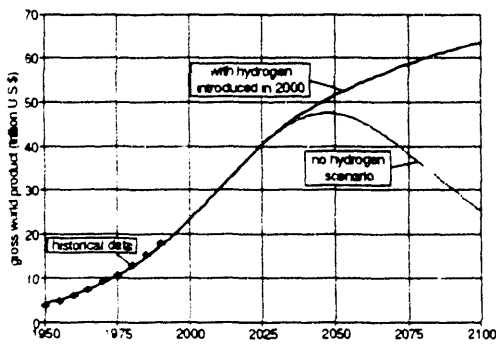


Figure 3. Gross world product (base case scenario)

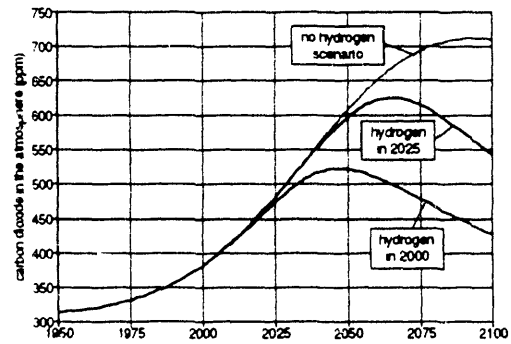


Figure 6. Atmospheric carbon dioxide (initiation of the solar hydrogen energy system is delayed 25 years)

**Table 1. Storages Sources and Flows, and Corresponding Equations for the Model**

	<b>Description</b>	<b>Equation (1)</b>	<b>Initial Value (2)</b>
F	Fossil fuels reserves	$dF/dt = -f_4$	$170 \times 10^{21}$ J (3)
A	Economic assets	$dA/dt = f_2 + f_5 + f_9 - f_3 - f_6 - f_{10} - f_{11} - f_{12}$	0.236 (normalized) (4)
P	Carbon dioxide in the atmosphere	$dP/dt = f_7 - f_{13}$	$0.310 \times 10^{21}$ kg (5)
I	Environmental resources	$I = \text{const.}$	0 (6)
N	Unused (untapped) environmental resources	$N = I / (1 + k_1 A)$	
J	Solar energy available for hydrogen production	$J = \text{const.}$	$25.1 \times 10^{21}$ J (7)
R	Untapped solar energy	$R = J / (1 + k_8 A)$	
f <sub>1</sub>	Utilization of environmental resources	$f_1 = k_1 AN$	0 (6)
f <sub>2</sub>	Production of assets resulting from f <sub>1</sub>	$f_2 = k_2 AN$	0 (6)
f <sub>3</sub>	Assets depreciation through use in production f <sub>2</sub>	$f_3 = k_3 AN$	0 (6)
f <sub>4</sub>	Fossil fuels consumption	$f_4 = k_4 AF$ or $D(1-\xi)$ (8)	$0.082 \times 10^{21}$ J/yr (9)
f <sub>5</sub>	Production of assets resulting from f <sub>1</sub>	$f_5 = (k_5/k_4)f_4$	0.0149 nau/yr (10)
m <sub>5</sub>	Gross World Product	$m_5 = p_5(f_5 + f_9)$	$4.0 \times 10^{12}$ \$/yr (11)
f <sub>6</sub>	Assets depreciation through use in production f <sub>5</sub>	$f_6 = (k_6/k_4)f_4$	0.0028 nau/yr (10)
f <sub>7</sub>	Carbon dioxide emissions resulting from f <sub>4</sub>	$f_7 = k_7 f_4$	$0.00615 \times 10^{15}$ kg/yr (12)
D	Energy demand	$D = f_4(1-\xi) + k_8 AR(\eta_{s-h}/\alpha_u)\xi$ (13)	$0.082 \times 10^{21}$ J/yr
ξ	Hydrogen's share in energy market	$\xi = \{1 + \exp[-\beta(t-t_i-t_h)]\}^{-1}$ (14)	0
h	Hydrogen consumption rate	$h = \xi D$	0
f <sub>8</sub>	Utilization of solar energy	$f_8 = (\alpha_u/\eta_{s-h})h$ (13)	0
f <sub>9</sub>	Production of assets resulting from h	$f_9 = (k_5/k_4)h$	0
f <sub>10</sub>	Assets depreciation through use in production f <sub>9</sub>	$f_{10} = (k_{10}/k_4)h$	0
f <sub>11</sub>	Assets depreciation	$f_{11} = k_{11}A$	0.00236 nau/yr (10)
f <sub>12</sub>	Assets degradation due to pollution	$f_{12} = k_{12}AP$	0.00059 nau/yr (10)
f <sub>13</sub>	Carbon dioxide absorption from the atmosphere	$f_{13} = k_{13}P$	$0.00372 \times 10^{15}$ kg/yr (15)

Footnotes for Table 1:

1. Coefficients,  $k_{1=1 \text{ to } 13}$  and  $p_5$ , are determined from the initial values.
2. All initial values are for the year 1950.
3. Fossil fuel resources, [United Nations, 1991; Smil, 1991, White, 1987):  
coal 150,000 EJ, oil and gas 20,000 EJ, total 170,000 EJ =  $170 \times 10^{21}$  J.
4. Assets were normalized so that  $A=1$  normalized asset units (nau) in 1990.
5. CO<sub>2</sub> content in the atmosphere before industrial revolution (German Bundestag, 1989):  
CO<sub>2</sub><sup>1850</sup> = 275 ppm =  $2.17 \times 10^{15}$  kg  
CO<sub>2</sub> content in the atmosphere in 1950 (ibid): CO<sub>2</sub><sup>1950</sup> = 315 ppm =  $2.48 \times 10^{15}$  kg  
Excess of CO<sub>2</sub> in the atmosphere:  $P = (2.48 - 2.17) \times 10^{15} = 0.31 \times 10^{15}$  kg
6. Environmental resources, other than those used to generate hydrogen and electricity, have been neglected, because their contribution in building and maintaining the assets is much smaller than the contribution from fossil fuel powered economic process.
7. Solar energy available for conversion into hydrogen is assumed to be 10% of solar radiation over the world's desert areas:  
World deserts: 3,140 million hectares =  $31.4 \times 10^{12}$  m<sup>2</sup>; solar radiation in deserts:  $8 \times 10^9$  J/m<sup>2</sup>/yr (Smil, 1991)  
Available radiation:  $0.1 \times (31.4 \times 10^{12} \text{ m}^2) \times (8 \times 10^9 \text{ J/m}^2/\text{yr}) = 25.1 \times 10^{21}$  J/yr
8. Share of fossil fuels in energy consumption starts to diminish after solar hydrogen has been introduced.
9. Fossil fuel consumption in 1950 (United Nations, 1991): 82 EJ/yr =  $0.082 \times 10^{21}$  J/yr
10. nau = normalized asset units; initial values are determined by model simulation between years 1950 and 1990.
11. Gross world product in 1950 (World Bank, 1990): \$4,000 billion/yr
12. CO<sub>2</sub> emissions in 1950 = (fossil fuel combustion) × (fossil fuel carbon content) =  
 $(0.082 \times 10^{21} \text{ J}) \times (75 \text{ kg}/10^9 \text{ J}) = 0.00615 \times 10^{15}$  kg/yr
13.  $\alpha_u$  = utilization efficiency advantage of hydrogen defined as  $\alpha_u = \eta_f/\eta_h$ , where  $\eta_f$  is the overall end-use conversion efficiency of fossil fuels, and  $\eta_h$  is the overall end-use conversion efficiency of hydrogen;  $\alpha_u = 0.73$  (Bockris and Veziroglu, 1985).  
 $\eta_{s-h}$  = overall conversion efficiency of solar energy to hydrogen (assumed to be 0.05).
14.  $\beta$  = penetration rate =  $4.4/t_0$ , where  $t_0 = 40$  yr = takeover time defined as the time required to go from  $\xi=0.1$  to  $\xi=0.9$ ).  
 $t$  = time;  $t_i$  = initiation time;  $t_h$  = half time (time required to reach half of the market) =  $t_0/2 = 40$  years;
15. It takes about 100 years until a quantity of CO<sub>2</sub> released into the atmosphere is reduced to about 30% of its original volume (German Bundestag, 1989). Therefore, the initial value for the flow  $f_{13}$  is:

$$f_{13} = [1 - 0.3^{(1/100)}]P = 0.00372 \times 10^{15} \text{ kg/yr.}$$



# ASSESSMENTS OF RENEWABLE HYDROGEN ENERGY SYSTEMS\*

Joan M. Ogden  
Center for Energy and Environmental Studies  
Princeton University  
Princeton, NJ 08544

## Abstract

Here we present technical and economic assessments of renewable hydrogen energy systems. The aim of this research is to identify promising paths towards use of renewable hydrogen as an energy carrier. We have considered several renewable hydrogen sources which could be developed over the next decade or so including electrolytic hydrogen from solar PV, solar thermal, wind, and hydropower, and hydrogen from biomass gasification; various options for storing and transmitting hydrogen; and several potentially important end-uses. The results of the study are summarized, and future research directions are suggested.

## Introduction and Background

Hydrogen is receiving increased attention as a low polluting alternative to fossil fuels, particularly in transportation. If hydrogen is derived from renewable resources, it would be possible in principle to produce and use energy on large scale with greatly reduced greenhouse gas emissions and very little local pollution.

For several years researchers at Princeton University's Center for Energy and Environmental Studies have been evaluating hydrogen energy systems. Initially we focussed on technical and economic assessments of solar photovoltaic hydrogen energy systems (Ogden and Williams 1989, Ogden 1990,

---

\* Prepared for the DOE/NREL Hydrogen Program Review Meeting, Cocoa Beach, Florida, May 4-6, 1993. This research was supported under NREL subcontract No. XR-2-11265-1.

Ogden 1991a,b). Over the past several years, we broadened our analysis to include other renewable hydrogen production technologies; biomass gasification (Larson and Katofsky 1992) and electrolysis powered by wind, solar thermal and hydropower (Ogden and Nitsch 1993). We have also carried out assessments of renewable hydrogen as a transportation fuel for use in zero emission fuel cell vehicles (Ogden and DeLuchi 1993, DeLuchi 1992, Ogden 1992).

Under our current NREL contract our research has focussed on assessing alternative strategies for developing renewable hydrogen energy systems (Ogden 1993). The aim of this work is to identify the most promising paths toward use of renewable hydrogen energy, highlighting key technologies for future research and development. We have considered a variety of sources of hydrogen including electrolytic hydrogen from solar PV, solar thermal, wind, and hydropower, and hydrogen from biomass gasification; various options for storing and transmitting hydrogen; and several important end- uses, transportation and residential heating.

Here we present the major findings of this study, and suggest areas for future research.

### **Assessment Methodology**

In our assessments, we consider the design of the entire energy system from production through end-use, as technological choices in one part of the system can have a strong impact on the other components. To evaluate pathways for producing and using hydrogen, we estimate the hydrogen production system performance and cost, the levelized cost of hydrogen production, the costs of hydrogen storage, transmission, distribution and delivery; and the life cycle cost of energy services to the end-user. Environmental effects (land, water and resource requirements; emissions of pollutants and greenhouse gases) are estimated and infrastructure and consumer issues are discussed. The economic assumptions used in our assessment are shown in Table 0.

### **Results of Renewable Hydrogen System Assessments**

Our results can be summarized as follows [details are given in (Ogden 1993, Ogden 1992)]:

**\* In the early part of the next century, renewable hydrogen could become competitive with other sources of hydrogen** (Figure 1, Table 1). Based on post-2000 projections for PV, wind and electrolysis technologies, we find that it would be possible to produce electrolytic hydrogen at a cost of \$12-27/GJ. Because of the modular nature of PV, wind and electrolysis technologies, these costs could be achieved at relatively small scale. For hydrogen production capacity of 14,150 Nm<sup>3</sup>/day (0.5 million scf H<sub>2</sub>/day or enough to refuel about 300 fuel cell vehicles/day each with a 400 km range), PV or wind electrolysis would be roughly competitive with small scale steam reforming of natural gas. At large scale (1.4-2.8 million Nm<sup>3</sup>/day or 50-100 million scf/day), hydrogen from biomass gasification would be the least costly renewable option. Biomass hydrogen would cost about \$6-9/GJ to produce, which would be competitive with hydrogen from steam reforming of natural gas (at DOE projected post-2000 natural gas prices of \$4-6/GJ), and probably less expensive than hydrogen from coal.

**\* There are good to excellent resources for renewable hydrogen production globally and in most areas of the United States. Land and water requirements would be modest.** With PV electrolysis alone, it would be possible to supply enough hydrogen for all light duty vehicles in the US (assuming 2010 driving levels and that hydrogen fuel cells were used), using only 0.1% of the US land area. With



wind power alone, 2% of the US land area (15% of the environmentally developable wind resource) would be needed, and with biomass alone 3% of the US land area (70% of the currently idled cropland) would be needed (Figure 2). It would be possible to produce significant quantities of renewable hydrogen almost anywhere in the United States. Very long distance transport of fuel would probably not be necessary, as many populated areas of the US are fairly close to good solar, wind or biomass resources (Figure 3, Table 2). Globally, renewable hydrogen resources could meet foreseeable energy demands (Figure 4).

**\* For gaseous hydrogen delivery systems, compression and storage (for intermittent sources like wind or PV), pipeline transmission, local distribution and delivery as a transportation fuel would add a total of about \$6-8/GJ to the cost of hydrogen.** (Figure 5). At small levels of demand, production of hydrogen from on site steam reforming of natural gas or electrolysis appear to be the least expensive options. As demand increases, large centralized hydrogen production could be phased in. At this scale, biomass hydrogen is the least costly renewable option, with delivered costs about half those of electrolytic hydrogen. The total delivered cost of electrolytic hydrogen transportation fuel would be \$18- 26/GJ (a cost of energy equivalent to \$2.5-3.6/gallon gasoline), and biomass hydrogen \$12-15/GJ (\$1.6-1.9/gallon gasoline).

**\* In the early part of the next century, renewable hydrogen could become attractive as a transportation fuel for hydrogen fuel cell vehicles.** Even though renewable hydrogen would be several times as expensive as gasoline, and hydrogen fuel cell vehicles would probably cost considerably more than gasoline vehicles, our analysis suggests hydrogen fuel cell vehicles might compete on a life cycle cost basis (Figure 6). Assuming that goals for fuel cells and advanced batteries are achieved, this would occur because fuel cell vehicles would be 2-3 times as energy efficient as gasoline vehicles, would have a longer lifetime and lower maintenance costs (Ogden and DeLuchi 1993).

**\* Delivered fuel cost alone is not a good indicator of the economic competitiveness of hydrogen as a transportation fuel.** This is particularly true for high quality fuels like hydrogen which can be used very efficiently and cleanly. Better economic indices are: 1) the life cycle cost of energy services (cents/km); 2) the fuel cost per km; and 3) the "break even gasoline price" (e.g. the price of gasoline that would make the life cycle cost of transportation for a gasoline powered internal combustion engine vehicle equal to that of a hydrogen vehicle).

**\* For transportation applications, consumer issues such as refueling time and vehicle range could be as important as life cycle cost.** Hydrogen fuel cell vehicles could potentially be general purpose zero emissions vehicles with a much shorter refueling time than battery powered electric vehicles (several minutes for compressed has storage vs. several hours to recharge electric batteries).

**\* Fuel cycle emissions (including fuel production, transmission and use) of pollutants [NO<sub>x</sub>, CO, particulates, SO<sub>x</sub>, and VOCs (volatile organic compounds)] and greenhouse gases would be greatly reduced with renewable hydrogen transportation fuels used in fuel cell vehicles (Table 3).**

**\* In the near term, hydrogen for fuel cell vehicles would probably come from natural gas. In the longer term, renewable sources such as biomass gasification and PV or wind electrolysis could be introduced.**

## Proposed Future Research

### ***Role of Natural gas In a Transition to Hydrogen***

Much of our work to date has involved assessments of the long term prospects for renewable hydrogen. In the next phase of our research, we would like to examine near-term strategies for introduction of hydrogen, as well. Here our assessments and those of other analysts suggest that natural gas could play an important near term role as a transition fuel leading toward a hydrogen energy system, based on renewable sources (Birk 1992, Blazek 1992, Lynch 1992). There are a number of reasons why the expanded use of hydrogen from natural gas is likely to be the first step toward a renewable hydrogen energy system:

1) Most industrial hydrogen today is derived from natural gas. At present, steam reforming of natural gas is the least expensive way of producing hydrogen over a wide range of plant sizes (Figure 1).

2) The natural gas infrastructure is vast and widespread. In the US over 650,000 miles of distribution mains serve 45 million customers (Blazek 1992), distributing 19 EJ per year of energy. In contrast, the present hydrogen distribution infrastructure consists of a few hundred miles of industrial pipelines, plus fleets of trucks delivering compressed hydrogen or liquid hydrogen. Although about 1 EJ per year of hydrogen is consumed in the US, most of this is produced and used on site for chemical processes. Merchant hydrogen (hydrogen which is distributed) amounts to about 0.5% of the total. However, there are several ways the natural gas infrastructure could be used to bring hydrogen to consumers. First, it is possible to produce hydrogen on site from natural gas using steam reforming, even at relatively small scale. Since most large users of hydrogen currently produce it on site from natural gas, this is in essence how most hydrogen is distributed today. Alternatively, hydrogen could be blended into natural gas at concentrations of 15-20% by volume without major changes in the gas distribution system or in consumer appliances (Blazek 1992). Blending could be done at the gas utility plant, with hydrogen produced from natural gas, biomass or other sources. Under certain combustion conditions, hydrogen/natural gas blends would produce lower emissions of CO or NO<sub>x</sub> than pure natural gas, when used directly as "hythane" in modified compressed natural gas vehicles (Lynch 1992, Foute 1992). If pure hydrogen were needed for fuel cell vehicles, it might be possible to separate out the hydrogen at the point of use (Mezzina 1992).

3) Use of natural gas in vehicles is growing rapidly, and the technologies for natural gas "filling stations" are being demonstrated and improved. This experience could be valuable for hydrogen vehicles as well, since vehicles using compressed hydrogen gas would require similar equipment.

4) Hydrogen might find a near term niche market as a pollution reducing additive to natural gas. Compressed natural gas vehicles run on "hythane," (a blend of 15% hydrogen by volume with 85% natural gas) have lower emissions of CO than comparable vehicles run on natural gas (Lynch 1992, Foute 1992). Although current hythane vehicles have NO<sub>x</sub> emissions that are slightly higher than those with natural gas, it may also be possible to tune the engine to produce lower NO<sub>x</sub> emissions with hythane (Lynch 1993). A CNG filling station in Denver is already dispensing hythane for airport service vehicles. As fuel cell vehicles are introduced, experience with hydrogen as a component of transportation fuel will be important.

In previous work, we estimated the cost of producing hydrogen for fuel cell vehicles via steam reforming of natural gas. In the near term, this appears to be the least expensive way of producing hydrogen for vehicle applications at both large and small scale. In future work, we propose look in detail at a range of issues involving a transition from natural gas to hydrogen, focussing on the introduction of hydrogen

as a transportation fuel for zero emission vehicles.

A variety of options exist for producing hydrogen transportation fuel from natural gas. (Some of these possibilities are sketched in Figure 7, where the production method, distribution system, filling station and end-use are shown.) These include:

Hydrogen produced in a large steam reforming plant and distributed via truck as a compressed gas or liquid to a filling station.

Hydrogen produced in a large steam reforming plant and distributed via gas pipelines to a network of filling stations.

Hydrogen produced on site via small scale steam reforming of natural gas.

Methanol produced from natural gas, and reformed on board a fuel cell vehicle to produce hydrogen

To examine alternative strategies for producing hydrogen from natural gas as a first step toward use of renewable hydrogen, a number of questions would be addressed:

- 1) What is the delivered cost of hydrogen transportation fuel derived from natural gas for various supply options and levels of demand (ranging from small demonstration fleet to city supply)?
- 2) What would a hydrogen filling station look like for various options? Under what conditions does it make sense to produce hydrogen at the filling station?
- 3) How does the type of on board hydrogen storage system used on the vehicle impact the design of the hydrogen supply system?
- 4) How does hydrogen from natural gas compare to renewable hydrogen sources in terms of resource size and environmental impacts?
- 5) In the longer term, a range of renewable hydrogen supply options (Figure 8) might be phased in. What are the synergisms between renewable systems and natural gas hydrogen systems?

### ***Development of an Assessment Methodology For Evaluating Hydrogen Energy Systems (Extending Pathway Analysis)***

For many important applications, hydrogen can be used much more efficiently and cleanly than other liquid and gaseous fuels. Because hydrogen (like electricity) is a high quality form of energy, which can be used with high efficiency, the delivered fuel cost alone is not a good indicator of the economics of using hydrogen. (This is clearly apparent in the transportation case study presented above.) Moreover, the technologies for using hydrogen (for example, fuel cells in vehicles) are radically different than those for gasoline or natural gas (internal combustion engines). Because a hydrogen energy system would involve significant changes in the way energy is produced and used, assessing the merits of using hydrogen (vs. other fuels or electricity) for particular application requires that a number of perspectives be considered: that of the fuel producer (fuel production costs), the fuel distributor (distribution costs, infrastructure), the consumer (cost of energy services, quality of the service, convenience) and of society

(emissions, policy, external costs).

The National Hydrogen Program recently released its Five Year Plan for Hydrogen (USDOE 1992). In order to identify promising hydrogen technologies and set priorities for future research, an assessment method called pathway analysis was employed. An energy pathway is defined as a "conversion chain linking primary resources to ultimate end-use consumption," and "Hydrogen pathways involve the production and delivery of hydrogen from primary energy sources to the consumption point."

Although pathway analysis in its present form considers a number of important factors (energy conversion efficiency at each stage of the energy system, hydrogen plant capital cost, transmission and distribution system capital cost, primary energy resource requirements, and emissions of pollutants and greenhouse gases), several key elements have not yet been included such as operation and maintenance costs for producing and delivering hydrogen, and consumer life cycle costs of using hydrogen for various applications. It is stated in the plan that a full comparison should include these factors. As set forth in the plan, an initial milestone of the Hydrogen Program Plan (to be completed in 1994) is to "Refine pathway economic evaluation to incorporate operating or life cycle costs or both..."

In future work, we propose to formulate an assessment methodology which would include those factors not currently addressed by pathway analysis. This method would be similar to that used in our assessments of hydrogen energy systems (Ogden and Williams 1989, Ogden 1993, Ogden and Nitsch 1993, Ogden and DeLuchi 1993):

Several economic figures of merit would be used:

- 1) The total levelized cost of hydrogen production would be calculated, including hydrogen plant capital costs, feedstock costs, and other operation and maintenance costs.
- 2) The delivered cost of hydrogen for particular applications would be calculated including levelized costs for storage, transmission, local distribution and delivery to the consumer in the desired form.
- 3) The life cycle cost of energy services (such as transportation) to the consumer would be calculated for hydrogen and for competing energy carriers. Here, the efficiency and cost of the end-use system would be considered.

Environmental effects would also be considered:

- 4) The resource, land and water requirements for alternative energy systems would be estimated.
- 5) Emissions of pollutants (NO<sub>x</sub>, SO<sub>x</sub>, particulates, hydrocarbons, etc.) and greenhouse gases would be estimated.

Finally, consumer and infrastructure questions would be addressed:

- 6) For example, for applications such as automotive transportation, refueling time and vehicle range could be as important to the consumer as life cycle cost.

We would apply this method to a variety of cases, similar to the "energy pathways" Appendix of the Hydrogen Plan. The aim of this work would be to produce a paper, which would be circulated to

researchers at NREL and other university, government and industry groups for comment. We would hope that this paper would be useful to program planners and policymakers as they evaluate different hydrogen pathways to set priorities for hydrogen energy research.

### **Acknowledgments**

This work was supported under NREL subcontract No. XR-2-11265-1. The author would like to thank Eric Larson, Ryan Katofsky and Robert Williams (Princeton University) and Mark DeLuchi (University of California, Davis) for useful discussions and input during the course of this research.

## References

- Birk, J.R., Mehta, B., Fickett, A., Mauro, R., Serfass, J. June 22-25 1992. A bridge to the future hydrogen-electric economy, Additive to the Proceedings of the 9th World Hydrogen Energy Conference, Paris, France.
- Blazek, C.F., Biederman, R.T., Foh, S.E. and Jasionowski, W. March 18-20, 1992. Underground storage and transmission of hydrogen, Proceedings of the Third Annual Meeting of the National Hydrogen Association, Washington, DC.
- DeLuchi, M.A., Larson, E.D., and Williams, R.H. October 1991. Biomass methanol and hydrogen for transportation, Princeton University Center for Energy and Environmental Studies Report No. 250, Princeton, NJ.
- DeLuchi, M. A. 1989. Hydrogen vehicles: An evaluation of fuel storage, performance, safety, environmental impacts and cost, International Journal of Hydrogen Energy, 14:81-130.
- DeLuchi, M.A. 1992. Hydrogen fuel-cell vehicles, Institute of Transportation Studies Research Report No. UCD-ITS-RR-92-14, University of California, Davis.
- Electric Power Research Institute, September 1987. Technical Assessment Guide, Volume 2: Electricity End Use; Part 1: Residential Electricity Use-- 1987.
- Elliott, D.L., Wendell, L.L., and Glower, G.L. September 28, 1990. U.S. areal wind resource estimates considering environmental and land-use exclusions," AWEA Windpower Conference, Washington DC.
- Foute, S. et. al. March 18-20, 1992. The Denver hythane project, Proceedings of the Third Annual Meeting of the National Hydrogen Association, Washington, DC.
- Gregory, D. P., Tsaros, C. L., Arora, J. L. and Nevrekar, P. 1980. The economics of hydrogen production, American Chemical Society Report, 0-8412- 0522-1/80/47-116-003.
- Energy Information Administration December 1990. Energy consumption and conservation potential: supporting analysis for the National Energy Strategy, SR/NES/90-02, Washington, D. C.
- Larson, E.D., Katofsky, R.E. July 1992. Production of methanol and hydrogen from biomass, Princeton University Center for Energy and Environmental Studies Report No. 271, Princeton, NJ.
- Larson, E.D., Katofsky, R. May 11-15, 1992. Production of hydrogen and methanol from biomass, in Advances in Thermochemical Biomass Conversion, Interlaken, Switzerland.
- Lynch, F. March 18-20, 1992. Near term pathways toward hydrogen energy, Proceedings of the Third Annual Meeting of the National Hydrogen Association, Washington, DC.
- Mezzina, A., 1992. Private communication.
- Ogden, J. M., Williams, R. H. 1989. Solar Hydrogen: Moving Beyond Fossil Fuels, Washington DC:World Resources Institute. 123 pp.
- Ogden, J.M., Williams, R.H. 1990. Electrolytic hydrogen from thin-film solar cells," International Journal

of Hydrogen Energy, 15:155-163.

Ogden, J.M. March 13-15, 1991. Hydrogen from solar electricity, Proceedings of the Second Annual National Hydrogen Association Meeting, Arlington, VA.

Ogden, J.M. 1991. Cost and performance sensitivity studies for solar photovoltaic electrolytic hydrogen systems, Solar Cells, 30: No. 1-4: 515.

Ogden, J.M., DeLuchi, M.A. 1993. Solar hydrogen transportation fuels, to appear in Proceedings of the Conference on Transportation and Global Climate Change, American Council for an Energy Efficient Economy, Washington, DC.

Ogden, J.M. May 6-7, 1992. Renewable hydrogen energy systems studies, Proceedings of the NREL Hydrogen Program Review Meeting, Honolulu, Hawaii.

Ogden, J.M. and Nitsch, J. 1993. Solar hydrogen, in T. Johansson, H. Kelly, A.K.N. Reddy and R.H. Williams, eds. Renewable Energy: Fuels and Electricity from Renewable Resources, Island Press, Washington DC.

Ogden, J.M. January 20, 1993. Renewable hydrogen energy systems studies, draft final report for NREL subcontract No. XR-2-11265-1.

Solar Energy Research Institute March 1990. The potential of renewable energy, an interlaboratory white paper, Appendix F. Report No. SERI/TP-260- 3674.

Sperling, D.A., DeLuchi, M.A. March 1991. Alternative transportation fuels and air pollution, report to the OECD Environment Directorate, Organization for Economic Cooperation and Development, Paris.

U.S. Department of Energy. June 1992. Office of Conservation and Renewable Energy, Hydrogen program plan 1993-1997, DOE/CH10093-147.

**Table 0. Conversion factors**

=====

1 EJ = Exajoule ( $10^{18}$  Joules) = 0.95 Quadrillion BTUs

1 GJ = Gigajoule ( $10^9$  Joules) = 0.95 Million BTUs

1 million standard cubic feet H<sub>2</sub>/day = 28,300 Nm<sup>3</sup> H<sub>2</sub>/day = 362 GJ/day (HHV)

100 hectares = 1 km<sup>2</sup> =  $10^6$  m<sup>2</sup> = 0.39 square miles = 247 acres

1 gallon gasoline = 0.1304 GJ (higher heating value)

\$1/gallon gasoline = \$7.67/GJ = \$8.09/MBTU

Hydrogen used by fuel cell passenger automobile = 18 GJ/year or 0.05 GJ/day  
(for a car with fuel economy equivalent to 74 mpg, driven 10,000 miles/yr)

---

**Economic assumptions**

=====

All costs are given in average 1989 US dollars.

For hydrogen production plants, compression, storage and transmission systems levelized costs were calculated in constant dollars assuming (EPRI 1987):

Real discount rate = 6.1%

Annual insurance = 0.5% of installed capital cost

Annual property taxes = 1.5% of installed capital cost

All hydrogen costs are based on the higher heating value of hydrogen



**Table 1. Current and projected production costs of hydrogen<sup>a</sup> (\$/GJ)<sup>a</sup>**

	<u>1991</u>	<u>Near Term</u>	<u>Post 2000</u>
<u>Renewable sources</u>			
Electrolytic hydrogen (for plants producing 0.5 million scf/day (180 GJ) <sup>b</sup> from:			
Solar PV (SW US)	54-121	29-57	12-19
Wind (630 W/m <sub>2</sub> )			16
(500 W/M <sup>2</sup> )	48	26	21
(350 W/M <sup>2</sup> )	72	32	27
Solar Thermal (SW US)	45-60	37-63	22-30
Off peak hydroelectricity <sub>c</sub>	10-20	10-20	10-20
Hydrogen from biomass gasification <sup>d</sup>			
Large plant 50 milion scf/day)			6.2-8.8
<u>Fossil souces</u>			
Hydrogen from steam reforming of natural gas <sup>e</sup>			
Large plant (100 million scf/day)	6.1-8.1	6.1-8.1	8.1-10.1
Small plant (0.5 million scf/day)	11-14	11-14	14-17
Hydrogen from coal gasification <sup>f</sup>			
Large plant (100 million scf/day)	8	8	8
Medium plant (25 million scf/day)	13	13	13

<sup>a</sup> Levelized hydrogen production costs are given.

<sup>b</sup> A hydrogen plant producing 180 GJ/day could provide enough energy to fuel about 1000 fuel cell fleet vehicles, each travelling 48,000 km/yr.

<sup>c</sup> Assuming that off-peak hydroelectricity at existing sites costs 1 to 4 cents per kWh.

<sup>d</sup> Assuming that the biomass feedstock costs \$2 to 4 per GJ.

<sup>e</sup> Assuming that natural gas costs \$2 to 4 per GJ in the 1990s and \$4 to 6 per GJ beyond the year 2000, which is the range projected for the year 2000 for industrial and commercial customers.

<sup>f</sup> Costs for hydrogen from coal gasification are based the steam-iron process (Gregory et. al. 1980), assuming coal costs \$1.78/GJ, which is the projected cost for the year 2000.

**Table 2. Renewable Hydrogen Potential In the United States<sup>a</sup>**

State	Hydrogen (EJ/yr) from					Ratio of total to state energy use for trans- port with FCVs <sup>f</sup>
	Hydroelectric <sup>b</sup> Off-peak	Undevel.	Biomass <sup>c</sup>	Wind <sup>d</sup>	Solar PV <sup>e</sup>	
Alabama	0.018	0.005	0.042	0	<b>0.810</b>	6.4
Arizona	0.015	0.021	0	0.029	<b>2.414</b>	21.4
Arkansas	0.007	0.012	0.018	0.064	<b>0.831</b>	10.9
California	0.056	0.096	0.015	0.171	<b>2.770</b>	3.5
Colorado	0.003	0.021	<b>0.159</b>	<b>1.396</b>	<b>2.020</b>	35
Connecticut	0.001	0.002	0	0.015	0.000	0.8
Delaware	0	0.002	0.0001	0.006	0.024	1.3
Florida	0.0003	0.0004	0.010	0	<b>0.816</b>	2.0
Georgia	0.013	0.010	0.054	0.003	<b>0.823</b>	3.7
Idaho	0.014	0.066	0.064	<b>0.212</b>	<b>1.315</b>	51
Illinois	0.0002	0.003	0.054	<b>0.177</b>	<b>0.79</b>	3.1
Indiana	0.0006	0.0007	0	0	<b>0.478</b>	2.7
Iowa	0.0008	0.004	<b>0.161</b>	<b>1.600</b>	<b>0.794</b>	28
Kansas	0.00001	0.001	<b>0.233</b>	<b>3.106</b>	<b>1.450</b>	55
Kentucky	0.005	0.011	0.035	0	<b>0.562</b>	4.8
Louisiana	0	0.004	0.012	0	<b>0.671</b>	4.9
Maine	0.004	0.025	0.004	<b>0.163</b>	<b>0.385</b>	12.8
Maryland	0.003	0.002	0.001	0.009	<b>0.131</b>	1.0
Massachusetts	0.002	0.003	0	0.073	0.097	1.0
Michigan	0.003	0.005	0.016	<b>0.189</b>	<b>0.757</b>	3.3
Minnesota	0.001	0.003	<b>0.150</b>	<b>1.907</b>	<b>1.057</b>	22
Mississippi	0	0.001	0.060	0	0.712	9.2
Missouri	0.003	0.008	<b>0.122</b>	<b>0.151</b>	<b>1.039</b>	7.2
Montana	0.014	0.032	<b>0.222</b>	<b>2.961</b>	<b>2.190</b>	182
Nebraska	0.002	0.003	<b>0.111</b>	<b>2.520</b>	<b>1.223</b>	73
Nevada	0.005	0.0004	0.0003	<b>0.145</b>	<b>2.240</b>	50
New Hampshire	0.003	0.005	0	0.012	<b>0.104</b>	0.3
New Jersey	0.0001	0.0006	0.00007	0.029	0.093	0.5
New Mexico	0.0004	0.0006	0.039	<b>1.263</b>	<b>2.473</b>	69
New York	0.026	0.016	0.005	<b>0.180</b>	<b>0.546</b>	2.1
North Carolina	0.012	0.013	0.012	0.020	<b>0.693</b>	3.3
North Dakota	0.003	0.004	0.256	3.512	<b>1.002</b>	195
Ohio	0.0008	0.002	0.020	0.012	<b>0.509</b>	1.6
Oklahoma	0.005	0.007	0.093	<b>2.105</b>	<b>1.217</b>	31
Oregon	0.036	0.036	0.042	<b>0.125</b>	<b>1.441</b>	19
Pennsylvania	0.005	0.020	0.008	<b>0.131</b>	<b>0.557</b>	2.2
Rhode Island	0.00005	0.0001	0	0.003	0.013	0.6
South Carolina	0.008	0.010	0.021	0.003	<b>0.455</b>	4.0

State	Hydrogen (EJ/yr) from					Ratio of total to state energy use for transport with FCVs <sup>f</sup>
	Hydroelectric <sup>b</sup> Off-peak	Undeveloped	Biomass <sup>c</sup>	Wind <sup>d</sup>	Solar PV <sup>e</sup>	
South Dakota	0.010	0.005	<b>0.169</b>	<b>2.99</b>	<b>1.212</b>	168
Tennessee	0.014	0.004	0.025	0.006	<b>0.584</b>	3.9
Texas	0.004	0.020	<b>0.319</b>	<b>3.454</b>	<b>4.412</b>	13.8
Utah	0.001	0.015	0.019	0.070	<b>1.600</b>	33
Vermont	0.002	0.004	0.00001	0.014	<b>0.107</b>	6.4
Virginia	0.005	0.011	0.007	0.035	<b>0.563</b>	3.0
Washington	<b>0.142</b>	0.070	0.080	0.096	<b>0.825</b>	8.9
West Virginia	0.001	0.017	0.00006	0.015	<b>0.299</b>	5.6
Wisconsin	0.003	0.004	0.049	<b>0.163</b>	<b>0.675</b>	6.3
Wyoming	0.002	0.015	0.021	<b>2.168</b>	<b>1.719</b>	184
Total	0.455	0.660	2.76	31.30	47.56	10.4

<sup>a</sup> Locally significant resources (defined here as 0.1 EJ per year or more) are highlighted in boldface type.

<sup>b</sup> The off-peak hydroelectric potential for hydrogen production is estimated assuming that power equal to the installed capacity in each state could be available 25% of the time for off-peak hydrogen production. It is assumed that all the undeveloped hydropower is devoted to hydrogen production. An AC electrolyzer efficiency of 79% is assumed. Hydropower capacity (existing and undeveloped) are from the Federal Energy Regulatory Commission.

<sup>c</sup> The biomass potential is based on lands held in the Conservation Reserve Program, which could be reforested with biomass plantations. It is assumed that biomass productivity of 15 dry tonnes per hectare per year is achieved, and that the biomass has a higher heating value of 19.38 GJ per dry tonne. The higher heating value efficiency of converting biomass to hydrogen via gasification is assumed to be 70%. An additional amount of idled cropland would be available for biomass plantation development. Other sources of biomass such as residues and urban waste are not taken into account. They might add about 6-8 EJ nationally, if they were available (SERI 1990).

<sup>d</sup> The wind energy available in each state is estimated for Class 3 and higher wind resources, assuming that 100% of urban and environmentally sensitive land, 50% of forest land and 30% of agricultural land are excluded (Elliot 1990). An AC electrolyzer efficiency of 79% is assumed. The hydrogen produced is:

Wind Class	Hydrogen (EJ/yr)	Land Use (km <sup>2</sup> )	% Contiguous US Land Area
Class 3	15.2	579449	7.5%
Class 4	14.0	415117	5.4%
Class 5	0.9	27944	0.4%
Class 6	0.9	17203	0.2%
Class 7	0.2	273	0.003%
Total Wind Class 3-7	31.2	1041842	13.6%

° The PV hydrogen produced on 1% of the state area is estimated based on the annual average solar resource in each state. A DC electrolysis efficiency of 84% is assumed, with 93% coupling efficiency for the PV array and electrolyzer.

† Here the total renewable hydrogen potential in each state is compared to the energy which would be used for light duty vehicles in that state, based on projections for 2010 driving levels, if gasoline light duty vehicles were replaced by fuel cell vehicles with three times greater efficiency.

**Table 3. Percentage change in gm/km emissions from alternative-fuel light-duty vehicles, relative to gasoline vehicles, year-2000<sup>a</sup>**

Feed/Fuel/Vehicle	-----Criteria pollutants <sup>b</sup> -----		Greenhouse			
	NMOC	CO	NO <sub>x</sub>	SO <sub>x</sub>	PM	Gases <sup>c</sup>
NG/methanol/ICEV	-50	0	0	-100	lower	-2
U.S. power mix/BPEV	-95	-99	-56	+321	+153	-11
NG/hydrogen/FCEV	-100	-100	-100	-100	-100	-43
Biomass/hydrogen/FCEV	-100	-100	-100	-100	-100	-67 <sup>e</sup>
Biomass/methanol/FCEV	-90	-99	-99	-100	-100	-86 <sup>e</sup>
Solar/hydrogen/FCEV	-100	-100	-100	-100	-100	-87 <sup>e</sup>
Solar/hydride/ICEV	-95	-99	? <sup>d</sup>	-100	lower	-88 <sup>e</sup>
Solar power/BPEV	-100	-100	-100	-100	-100	-100
All-solar/H <sub>2</sub> /FCEV	-100	-100	-100	-100	-100	-100 <sup>f</sup>
<b>Baseline emissions</b>						
on gasoline, g/km	0.48	3.81	0.28	0.03	0.01	305.3

<sup>a</sup> The percentage changes shown are with respect to the baseline g/km emissions shown at the bottom of this table. ICEV = internal-combustion-engine vehicle; BPEV = battery-powered electric vehicle; FCEV = fuel-cell vehicle. Adapted from (DeLuchi 1992).

<sup>b</sup> The estimates of relative emissions are based on data reported in (Sperling and DeLuchi 1992) and (Ogden and DeLuchi 1992).

<sup>c</sup> The percentage changes refer to the sum of emissions of CO<sub>2</sub>, CH<sub>4</sub>, N<sub>2</sub>O, CO, NO<sub>x</sub>, and NMOCs (Non-methane organic compounds) from the entire fuel production and use cycle (excluding the manufacture of vehicles and equipment). Emissions of gases other than CO<sub>2</sub> have been converted to an equivalent amount of CO<sub>2</sub>, where equivalent is defined in terms of global warming caused over a certain time period. Results are based on (DeLuchi 1991).

<sup>d</sup> Hydrogen internal combustion engine vehicles tested to date have shown a very wide range of NO<sub>x</sub> emissions. A hydrogen engine can be designed to operate very lean and will have very low NO<sub>x</sub> emissions due to the reduced temperature. However, if such an engine is operated at full power, which requires an air- fuel mixture of 1:1, the NO<sub>x</sub> emissions will increase substantially.

<sup>e</sup> With renewable hydrogen or methanol, greenhouse gas emissions are reduced, but are not necessarily zero. With biofuels, some emissions result from fossil fuel use while cultivating, fertilizing and harvesting biomass. For these cases, it is assumed that hydrogen is compressed at the service station using the projected mix of power sources in the US in the year 2000 (EIA 1991).

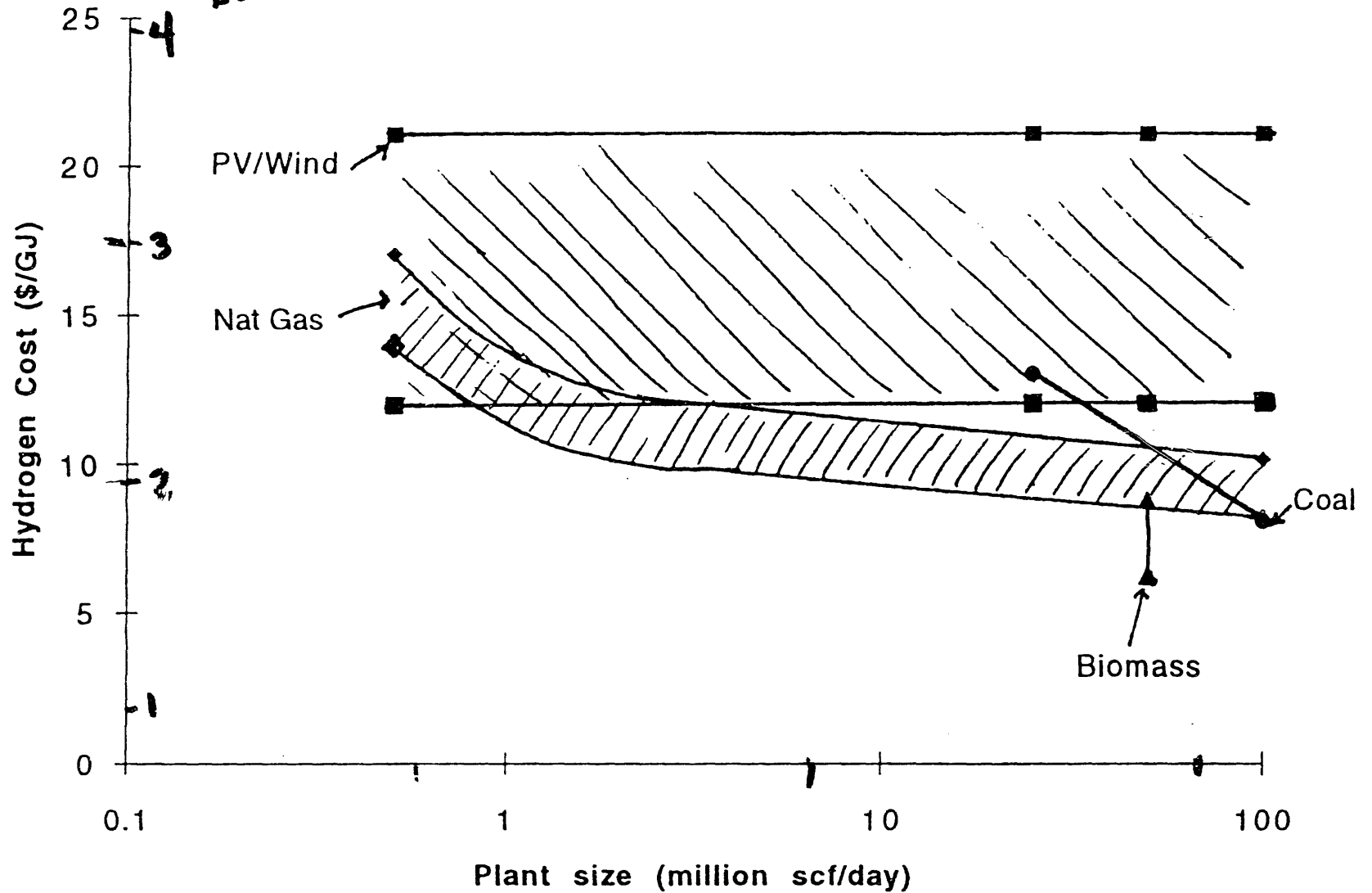
<sup>f</sup> If solar power were used for compression, greenhouse gas emissions for solar hydrogen would be zero.

## Figure Captions

1. Production cost of hydrogen from renewable and fossil sources, based on post-2000 projections for PV, wind, electrolysis technologies.
2. Land areas required for renewable hydrogen production to meet energy demands for all US light duty vehicles at projected 2010 driving levels, assuming that fuel cell vehicles are used.
3. Potential statewide resources for renewable hydrogen production. (Renewable hydrogen resources are estimated in Table 2). The ratio of the potentially available renewable hydrogen resource in each state to the demand in that state for transportation fuel is shown. In all but a few states, more than enough transport fuel could be produced within the state to meet demands.
4. Global resources for renewable hydrogen production.
5. Delivered cost of hydrogen transportation fuel for various production levels.
6. The life cycle cost of transportation for alternative fueled vehicles. EV = electric vehicle, FCEV = fuel cell electric vehicle, ICEV = internal combustion engine vehicle.
7. Options for supplying Hydrogen Transportation Fuel from Natural Gas
8. Renewable options for Hydrogen Transport Fuel

Deliv.  
H<sub>2</sub>  
cost  
(\$/gal. g.  
eq.)

### Hydrogen Production Cost vs. Plant Size



179

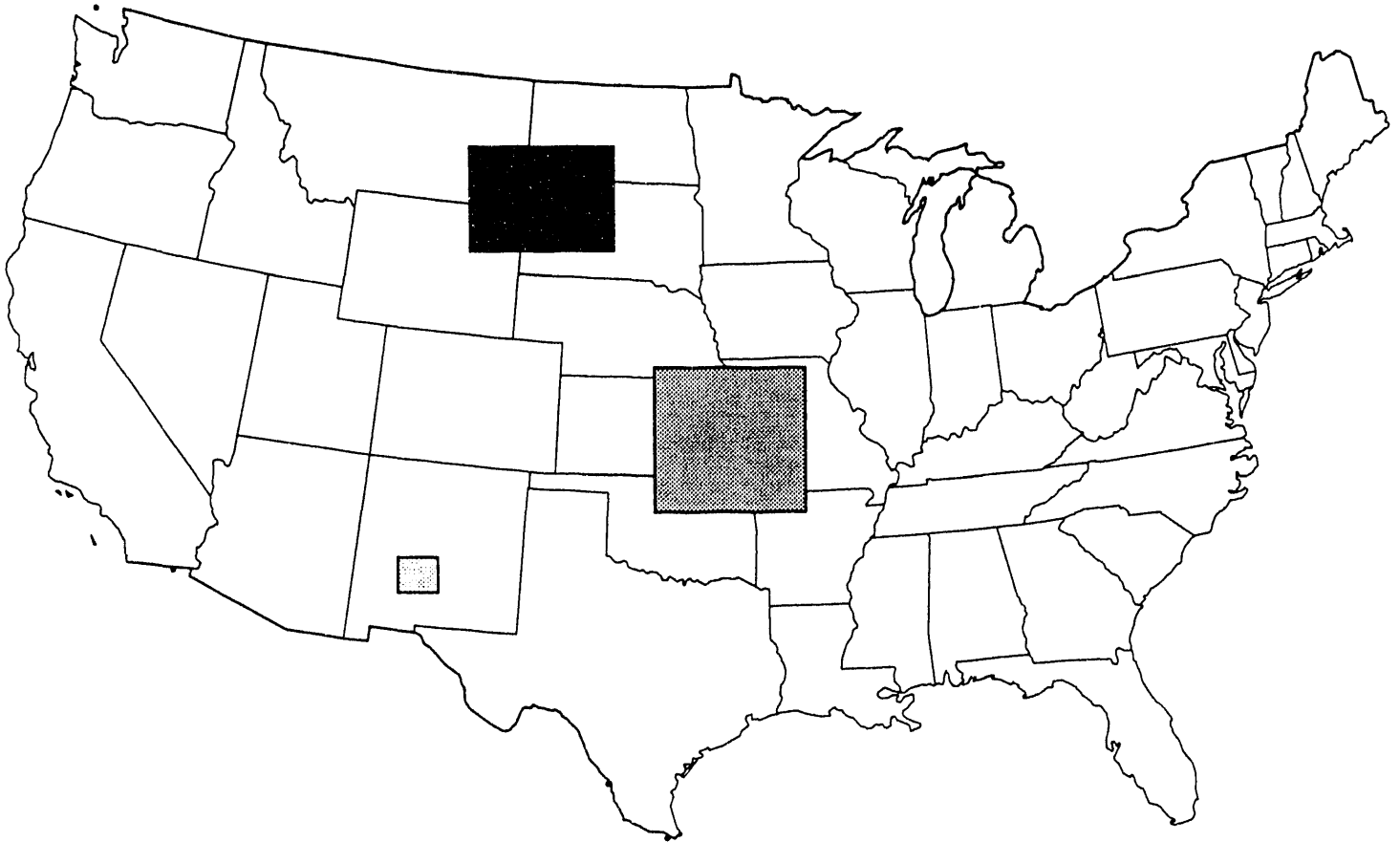
3000  
1000




30,000  
10,000

300,000  
100,000

PCS  
FCV

# LAND AREA TO SUPPLY U.S. CARS AND LIGHT TRUCKS (4.8 EJ/YR)

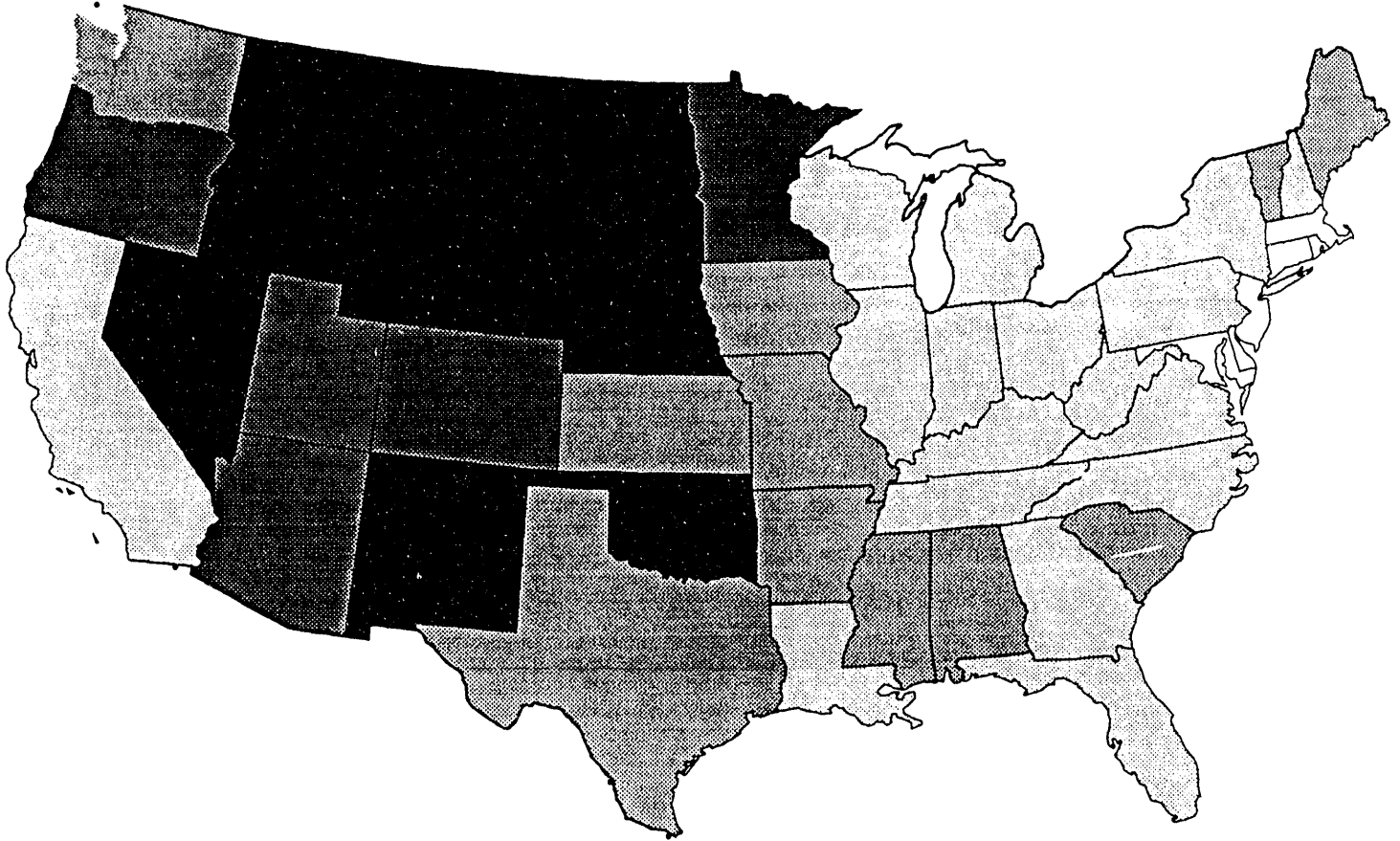


% U.S. LAND AREA		
	PV	0.1%
	WIND	2.0%
	BIOMASS	3.0%

1% U.S. DESERT AREA  
15% ENVIRON. DEVEL. U.S. WIND  
70% IDLED CROPLAND



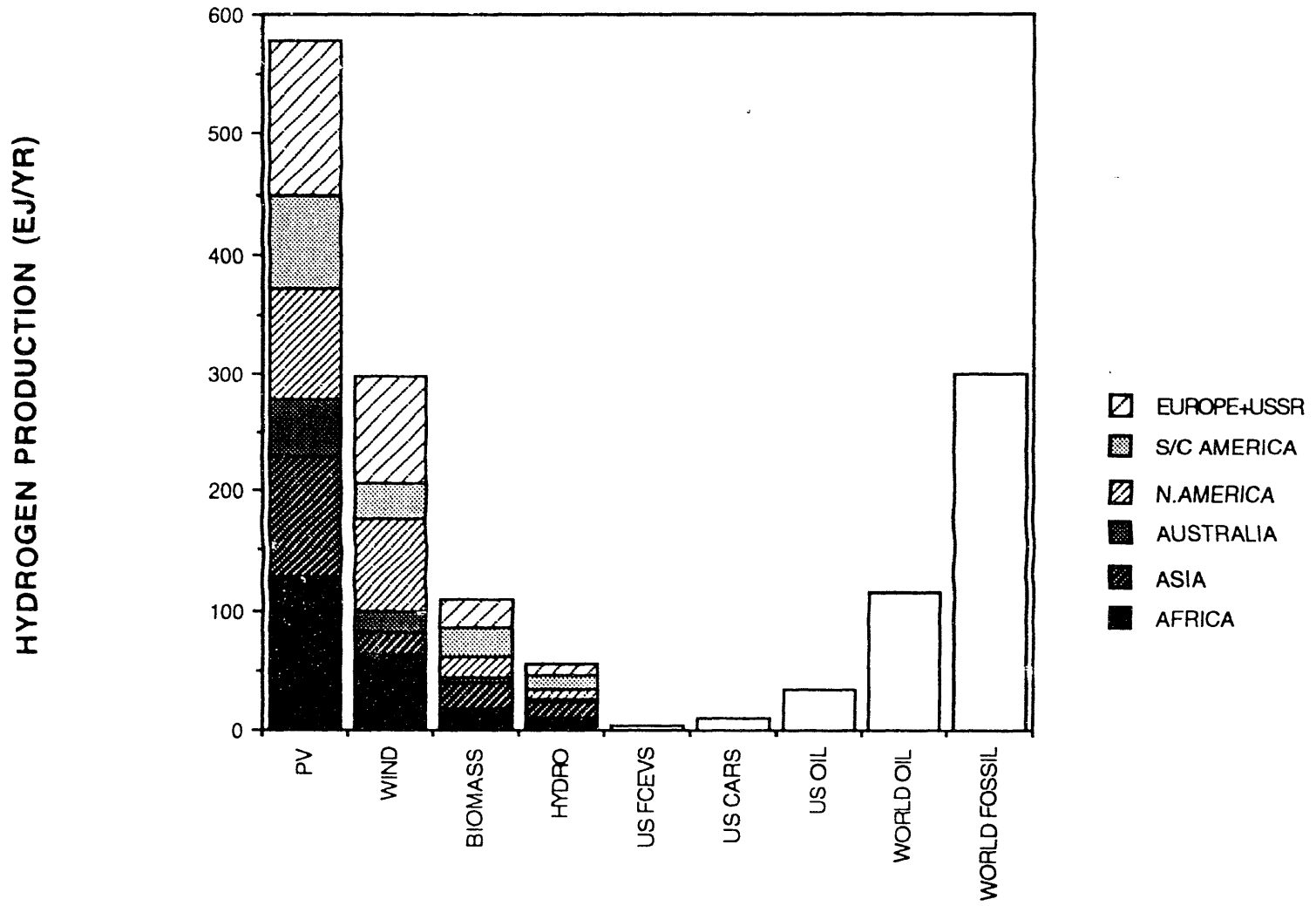
# RENEWABLE H<sub>2</sub> RESOURCES FOR TRANSPORTATION



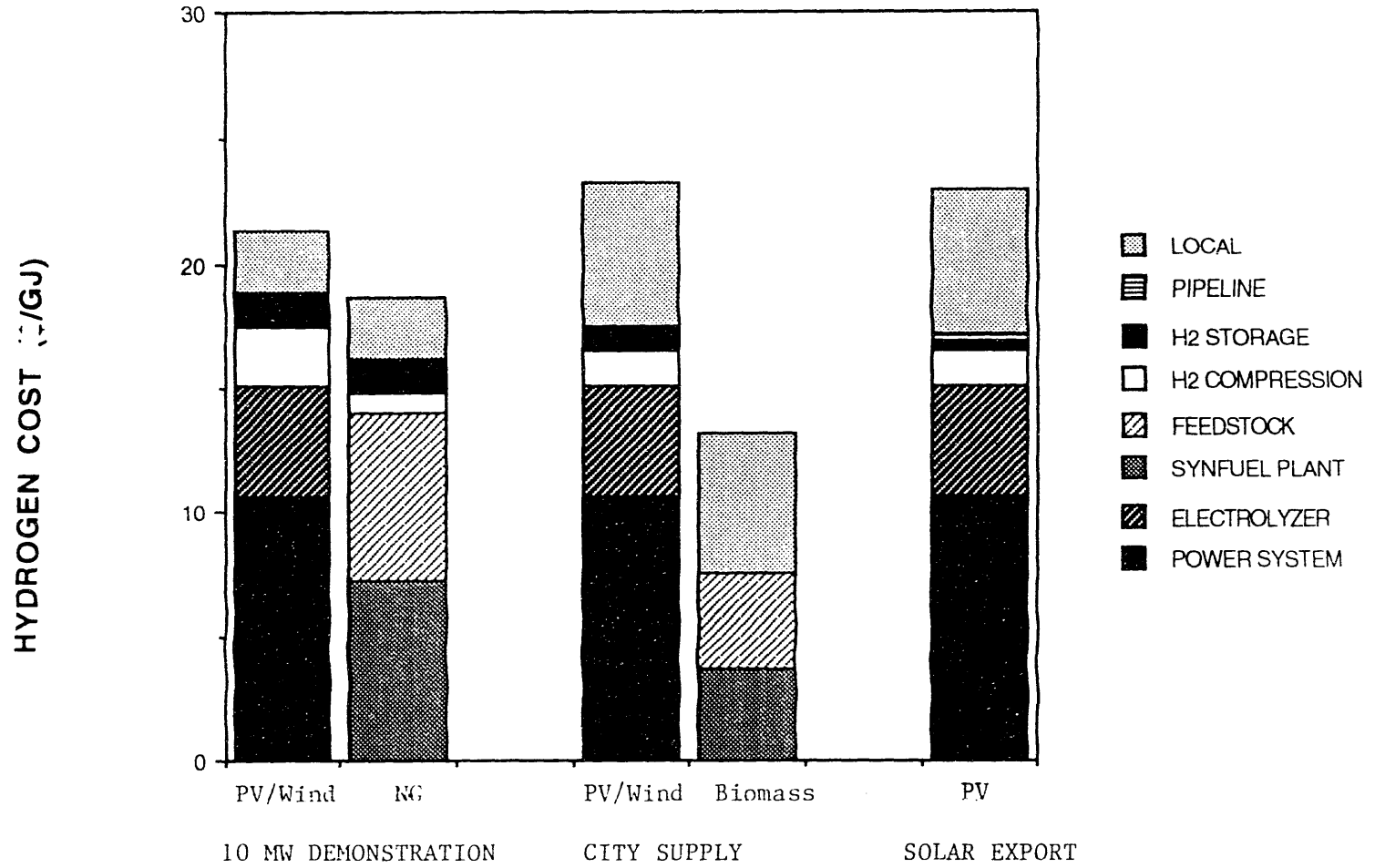
	H <sub>2</sub> (EJ/YR)
HYDRO	1.0
BIOMASS	6.0
WIND	31.0
PV	48.0
TOTAL	86.0

H <sub>2</sub> SUPPLY	
FCV DEMAND	
<1	
1-3	
3-10	
10-30	
>30	

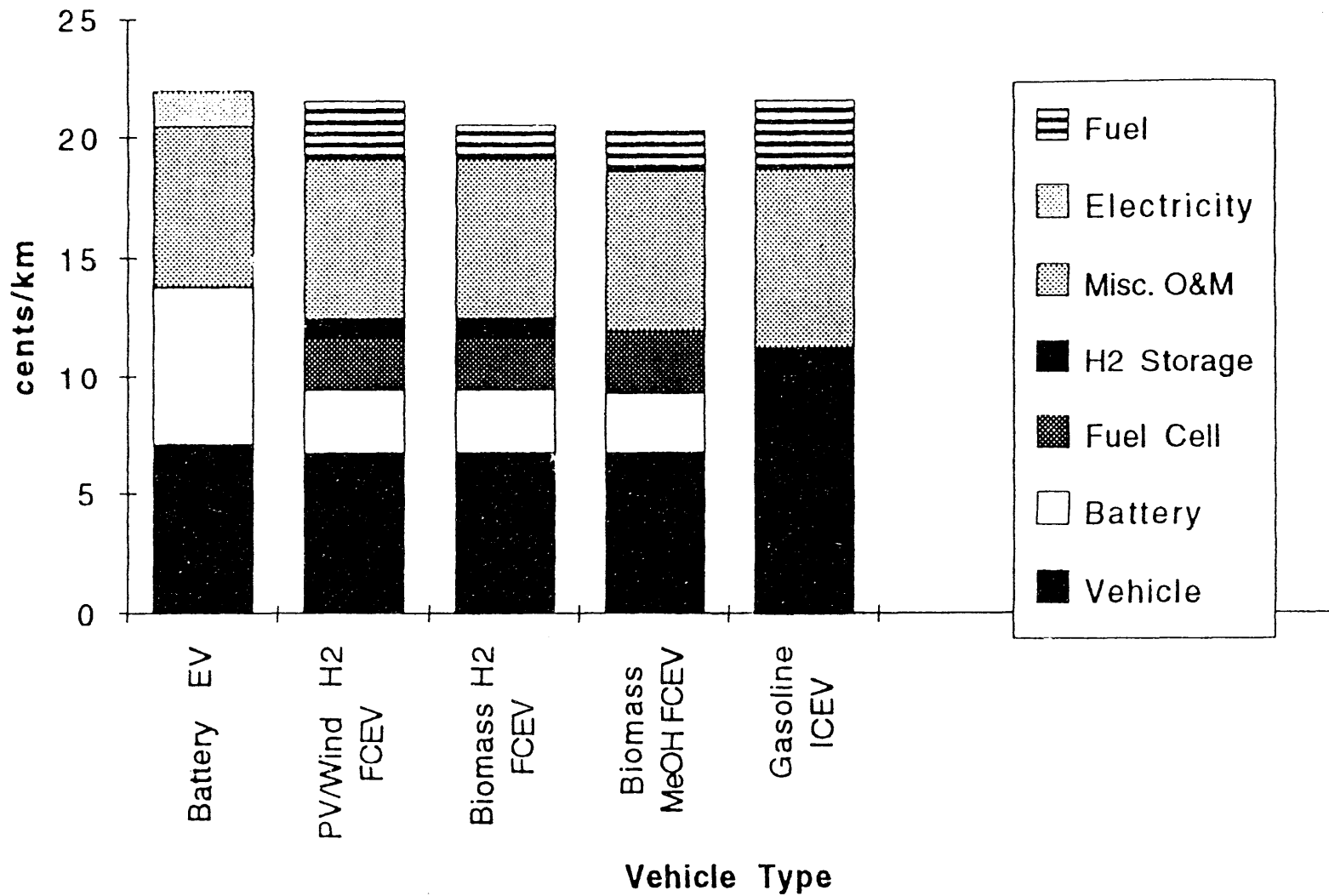
# POTENTIAL RESOURCES FOR RENEWABLE HYDROGEN PRODUCTION (EJ/YR)



# DELIVERED HYDROGEN COST (\$/GJ) FOR THREE PLANT SIZES



# Lifecycle Cost of Transportation (cents/km)



# OPTIONS FOR SUPPLYING H2 FROM NATURAL GAS

**PRODUCTION                      DISTRIBUTION                      FILLING STA.                      END-USE**

**LARGE STEAM  
REFORMING PLANT  
NG -> H2**

**H2 VEH.**

**H2 GAS PIPELINE**

**COMP. H2 GAS**

185

**H2 COMP. GAS TRUCK**

**COMP. H2 GAS**

**LH2 TRUCK DELIVERY**

**LH2**

**NG WELL**

**NG DISTRIB. SYSTEM**

**SMALL STEAM  
REFORMING PLANT  
NG -> GH2**

**H2 VEH.**

**LARGE PLANT  
NG -> MeOH**

**MeOH TRUCK**

**MeOH STATION**

**MeOH FCEVS  
(ONBOARD  
REFORMING  
MeOH -> H2)**

## RENEWABLE OPTIONS FOR H2 TRANSPORT FUEL

<b>PRODUCTION</b>	<b>DISTRIBUTION</b>	<b>FILLING STA.</b>	<b>END-USE</b>
LARGE BIOMASS GASIFIER PLANT BIOMASS -> H2			H2 VEH.
	H2 GAS PIPELINE	COMP. H2 GAS	
	H2 COMP. GAS TRUCK	COMP. H2 GAS	
	LH2 TRUCK DELIVERY	LH2	
LARGE PLANT BIOMASS -> MeOH	MeOH TRUCK	MeOH STATION	MeOH FCEVS (ONBOARD REFORMING MeOH -> H2)
OFF-PEAK, PV OR WIND POWER	ELEC. DISTRIB. SYSTEM	ELECTROLYSIS AT FILLING STATION	H2 VEH.
OFF-PEAK, PV OR WIND ELECTROLYSIS	H2 DISTRIBUTION	COMP. H2 GAS	H2 VEH.
		STAND-ALONE PV ELECTROLYSIS	H2 VEH.

# **GASEOUS FUEL TRANSPORT LINE LEAKAGE - NATURAL GAS COMPARED TO HYDROGEN**

M.N. Swain, G.J. Schade, and M.R. Swain  
University of Miami  
Miami, FL 33124

## **Abstract**

An experimental study of gaseous fuel leakage from pipelines was conducted by leaking two gases (in the first case methane and in the second case hydrogen) out the end of a 4.5" (11.4 cm) diameter pipe. Methane was used to represent natural gas. The boundaries of the combustible cloud formed were determined by discharging an electric arc at various locations in and around the cloud. By testing for combustibility in this manner the locations of the boundaries of the combustible cloud were measured. The experimentally determined boundaries of the combustible cloud were then compared to the calculated boundaries predicted by the computational fluid dynamics program FLUENT version 3.03.

Since the comparison required an accurate estimate of the lean limit of combustion at the conditions found during the experiment, it was necessary to run a second set of experiments to determine the lean limit of combustion at those conditions.

Additionally, a computer model of the size and shape of gas clouds formed by hydrogen leaking inside a building is being carried out. It seems possible to construct a building which greatly reduces the possibility of accidental combustion of leaking hydrogen gas.

## Introduction

An experimental study was conducted to determine the shape and size of the combustible gas cloud formed if hydrogen or natural gas leaks from a pipeline. The local combustibility of the gas cloud formed was determined by discharging an electric arc at various locations in and around the cloud. The combustible gas cloud shapes and sizes so determined were compared with predictions from a computer model of the gas clouds. The computer model was found to be in good agreement when lean limits for combustion of 10% for hydrogen and 5.9% for methane, by volume, were used. These are the commonly accepted values for downward propagating flames.

Additionally, findings from a computer model study of gas cloud shape and size inside buildings is presented. This study investigated the influence of building geometry and passive venting on the formation of combustible gas clouds. The intent was to determine under what conditions a "hydrogen safe building" could be constructed. That is to say what leakage rates of hydrogen can be vented from properly designed buildings without producing sizable quantities of combustible fuel-air mixtures.

### **Description of Experimental Apparatus (Combustible Cloud Boundaries)**

The experimental part of this work effort included the construction of a full scale leak test apparatus. The apparatus produced leaks comparable to minor damage, poorly mated fittings, cracks or other foreseeable failures in outdoor pipelines. The leaks were tested by using an ignition source to locate the periphery of the combustible gas cloud produced by the leak. The testing was done at flow rates of 50 SCFM (23.6 liter/sec) for hydrogen and 15 SCFM (7.1 liter/sec) for methane. These flow rates were consistent with the leaks that could occur in hydrogen pipelines operating at an elevated pressure to produce the same energy transmission rate in the hydrogen pipeline as in a comparable methane pipeline.

The apparatus used to collect the experimental data for outdoor leakage was a 20 foot (6.1 m) long pipe of 4.5 inch (11.4 cm) outside diameter. The test gas (hydrogen or methane) was held compressed in a bank of four tanks. A square edge orifice meter was used to measure the flow rate of the test gas. The square edge orifice plate was installed between two flanges connecting sections of the 20 foot (6.1 m) pipe. The design of the orifice plate and the inlet and outlet lengths of the meter were chosen for high accuracy (Stearns R.F. et. al., 1951). An incline water manometer was used to measure the pressure drop across the square edge orifice. Temperature measurements were made with chromel-alumel thermocouples. The pipe extended 6 feet (1.8 m) after passing through the wall to the exterior of the building. The ignitor was suspended by 3 wires to allow position control in 3 dimensions. The ignitor was a spark gap driven by a automobile type spark coil and capacitive discharge ignition system.

### **Experimental Results (Combustible Cloud Boundaries)**

The results of the tests to determine combustible cloud boundaries are shown in figures 1 and 2. The clouds formed were less than 1 foot (0.3 m) wide, up to 6 feet (2 m) tall and extended as much as 3 feet



(1 m) beyond the end of the horizontal pipe. In each case 21 attempts were made to ignite the cloud. The positions of those ignition attempts are shown in figures 1 and 2. 20 of the attempts were in a vertical plane that passed through the central axis of the pipe. That is the plane shown in figure 1 and 2. Comparison of points near the edge of the predicted cloud boundary showed poor repeatability in the ignition results. Ignition did not occur for points more than 4 inches (0.1 m) outside the predicted boundary and did occur for those points well inside the predicted boundary. The agreement between the computer model and the experimental results was good when the lean limit of hydrogen was assumed to be approximately 10% hydrogen. The same can be said for the comparisons the computer model results to experimental results when the lean limit of combustion of methane was assumed to be 5.9%.

## Description of Computer Model

FLUENT<sup>1</sup> a computational fluid dynamics software package which models fluid and heat transfer problems with a finite difference scheme; was used to solve the continuity, momentum and concentration equations with the appropriate boundary conditions for this work. The model assumes that:

- i) Flow may be partially turbulent.
- ii) The fluid is Newtonian and incompressible.
- iii) Temperature in the domain is constant.

## Discussion of Results

The purpose of this work was to determine the size of the combustible cloud of gases and detonable cloud of gases produced by methane (natural gas) or hydrogen leaking into an outdoor environment. This is useful in assessing the comparative risk posed by leaks of methane (natural gas) or of hydrogen. Assessment of risk in this case involves two components: likelihood and severity. Likelihood is assessed from the size of the ignitable cloud. The larger the cloud the more likely it is to be ignited. The severity is assessed from the quantity of chemical energy contained in the gas mixture within the boundaries of the combustible cloud and the detonable cloud. This yields a first order estimate of the safety risk (Table 1).

In all, the computer model predictions were not in absolute agreement with the measured data in seven of the 42 data points taken.

There are seven points that are not in agreement with the computer model. The lack of agreement could be dismissed as part of the inability to reproduce exactly the same gas cloud for each test. An

---

<sup>1</sup> FLUENT is a trade name for Computational Fluid Dynamics Software Creare, X Inc., Hanover, New Hampshire.

investigation of flame kernel growth rate at the fuel gas concentrations that existed in these tests is a weak indication that the actual fuel-air cloud may have been slightly smaller than predicted by the computer model. The term "weak indication" is used because considerably more experimental data would have to be taken to make the assertion statistically significant.

		<u>Methane</u>	<u>Hydrogen</u>	<u>Ratio CH<sub>4</sub>/H<sub>2</sub></u>
Combustible	Gas Cloud Volume (liter)	130	111	1.17
Combustible	Gas Cloud Energy (kJoule)	434	200	2.17

### **Computer Model of Indoor Leakage**

The ongoing study of hydrogen leakage inside buildings has finished a parametric analysis of vent location and size. The parameters studied were lower vent (floor vent) position and size, upper vent (ceiling vent) position and size, and leakage flow rate. A brief description of the findings are displayed in figure 3. Figure 3 shows the hydrogen gas concentration versus time at the boundary of the gas cloud shown in the small room pictorials surrounding the graph. The average concentration of hydrogen in the room is lower than the concentration depicted in the graph because, as can be seen, the gas cloud is small relative to the size of the room. The hydrogen concentration inside the cloud is larger than the concentration depicted in the graph and the hydrogen concentration outside the cloud (the rest of the room) is lower than the concentration depicted in the graph. The vent configurations producing curves in the upper portion of the graph are less desirable. The findings were as follows:

A room with a single vent, whether in the floor or ceiling, accumulates a combustible mixture relatively rapidly. A single vent does not allow for circulation but only exit of gas mixture from the room at the same rate the pure gas is entering the room from the leak. The fact that the accumulation rate of hydrogen is only slightly higher when the single vent is in the floor can be attributed to diffusion of the hydrogen because the residence times of the gas mixture are so long.

The room pictorial in the lower right hand corner of the figure has a standard vent both above and below the hydrogen leak. This configuration produces a significantly lower hydrogen accumulation rate.

Dividing the area of the lower vent into two vents, one on each side of the room (the first pictorial above the bottom right hand side of the figure), has little effect on the accumulation rate of hydrogen in the room.

Moving the lower vent to the other side of the room (the second pictorial above the bottom right) causes the hydrogen to accumulate slightly more rapidly.

Moving the upper vent to the other side of the room (the pictorial in the upper right hand corner of the figure) has a dramatic effect, increasing the accumulation rate to a value slightly higher than that of the single vent configurations.

Doubling the upper vent size (the first pictorial to the left of the bottom right hand corner of the figure) slightly reduces the accumulation rate of hydrogen in the room.

Moving the lower vent to the opposite side of the room (the second pictorial to the left of the bottom right hand corner of the figure) has no discernible effect on the accumulation rate.

Decreasing the upper vent size (the lower left pictorial) significantly increases the hydrogen accumulation rate.

In summary: lower vent size had a weak effect on combustible gas cloud size unless the lower vent becomes very small. Lower vent position had the least effect on cloud size. Upper vent size had a stronger effect on cloud size than did lower vent size. The benefit from increasing upper vent size diminishes with large vent sizes. Upper vent position had the strongest effect on cloud size. Leak flow rate had a strong effect on combustible gas cloud size and position.

The modelling of rooms with varying roof geometry is now ongoing.

## **Future Work**

The experimental determination of the size and shape combustible gas clouds formed by ruptured high pressure (3000 psi) hydrogen and natural gas containers is proposed as future work.

The present certification standards for compressed fuels deal with the problems associated with gaseous fuel containment. These standards do not, however, deal with the problems created when the gases do escape from containers.

There are two standards for certification of compressed gas fuel tanks, DOT FRP-1 Standard and NGV2 which is an ANSI standard. DOT standards deal with pressure cycling, burst pressures, severe environmental exposure, thermal shock, exposure to bonfires and gunfire. NGV2 standards do not include thermal shock tests but do include tests for damage resistance, permeation in plastic liners, flaw tolerance and high temperature composite creep.

By their nature these tests assume failure once the compressed gas begins to escape and therefore assess risk of escape not risk of combustion and severity of combustion should escape occur.

The testing suggested for future work would be to experimentally simulate the instantaneous removal (breakage) of the valve from a high pressure container by using a remotely controlled solenoid valve. The size and shape of the combustible gas cloud produced would then be determined by discharge of electric arcs, in much the same way it has been done in the previous work. Budget permitting, measurements of radiated heat and pressure rise at various distances would also be made.

This testing would allow assessment of both the risk and severity of an accident should gases escape rapidly from a high pressure container due to severe damage.

## Conclusions

1. Clouds formed by leaking methane are slightly more likely to undergo ignition than are clouds formed by hydrogen leaking at the same energy flow rate. This determination is made because the combustible methane cloud, on the average, is slightly larger than the comparative combustible hydrogen cloud (Table 1).
2. Methane clouds produce a higher risk, in terms of severity, than do hydrogen clouds when severity is assessed by determining the energy contained within the ignitable cloud (Table 1).
3. It appears possible to design a hydrogen safe building.

## References

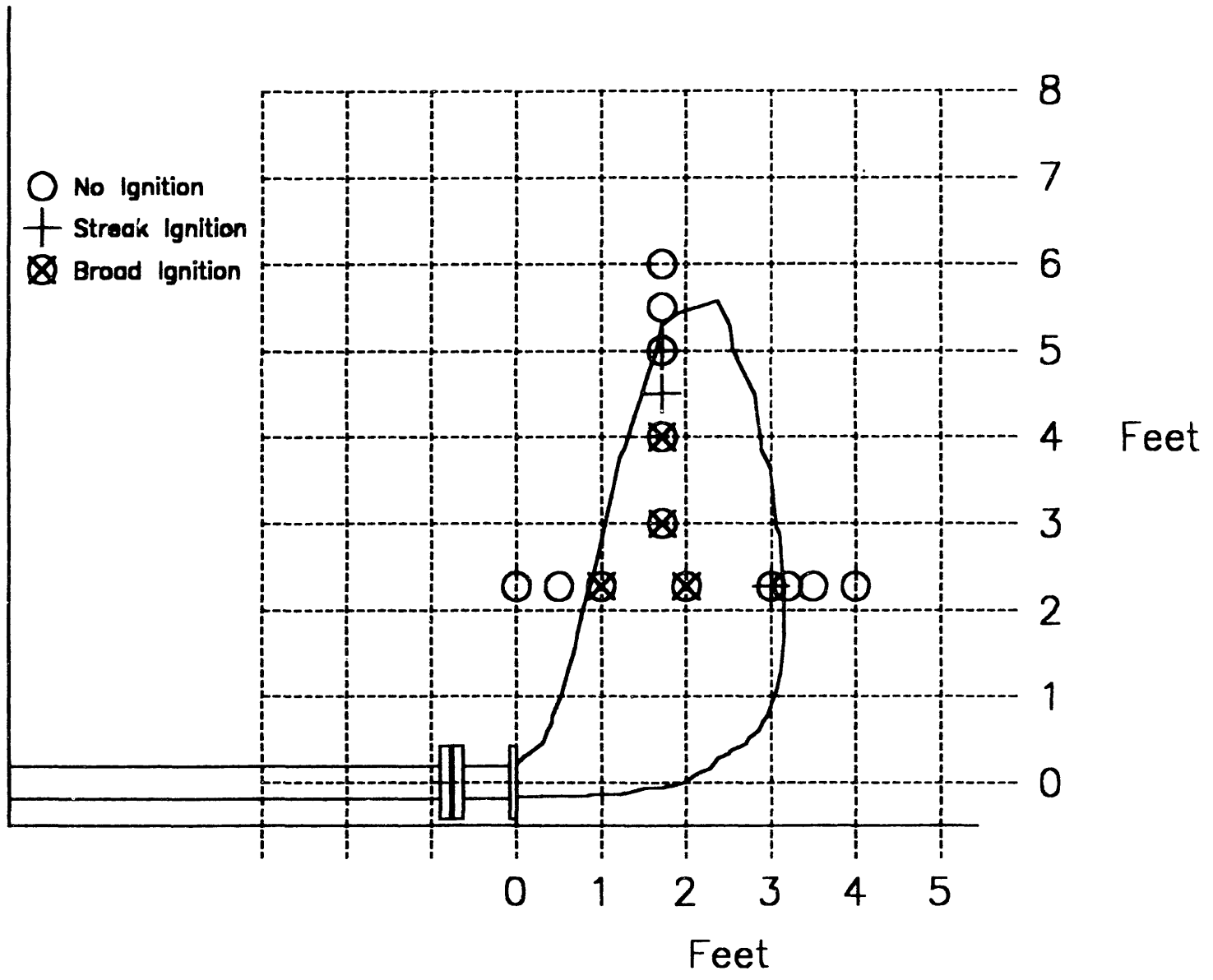
Stearns, R.F., 1951, Flow Measurement with Orifice Meters, Van Nostrand, New York, New York

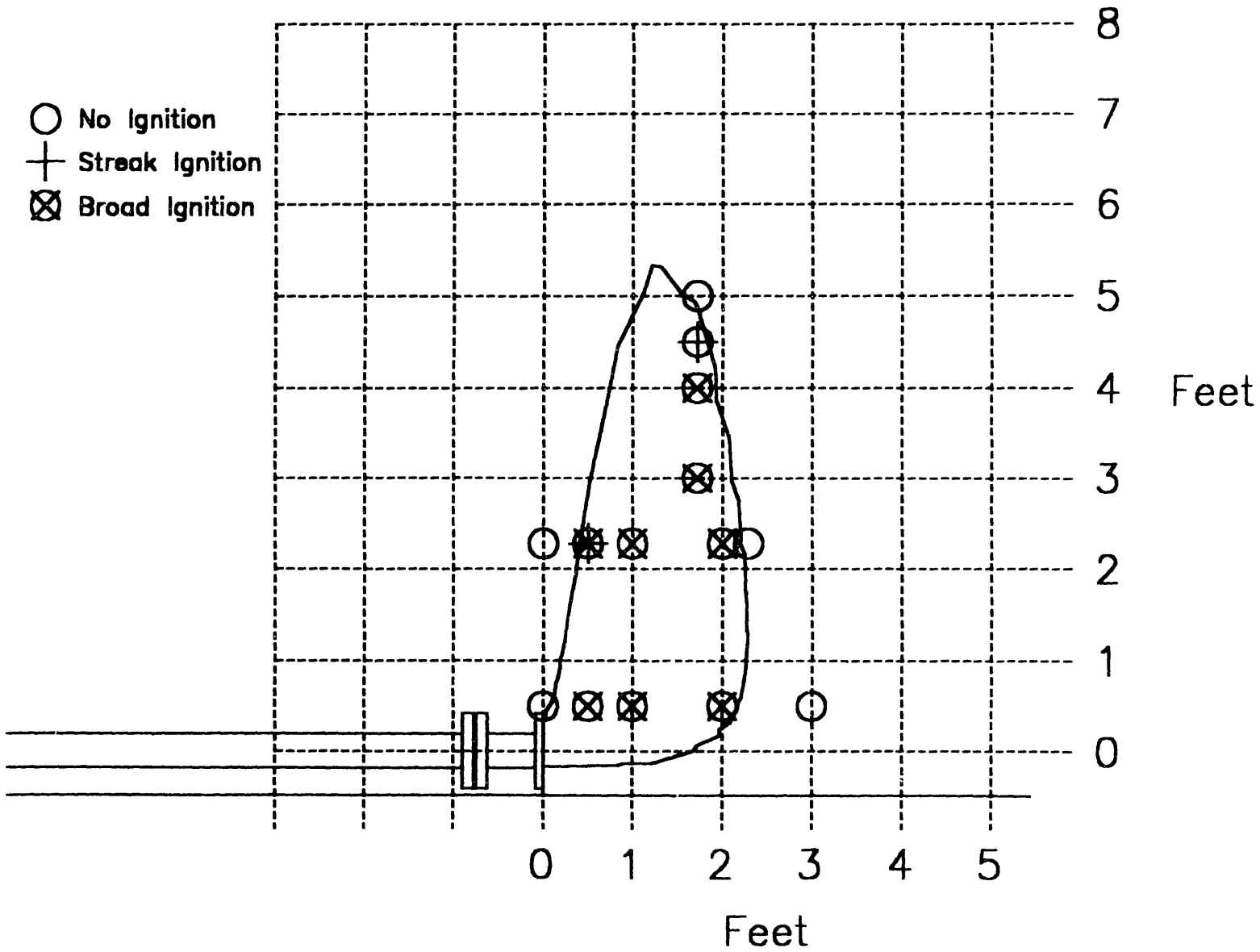
## Figures

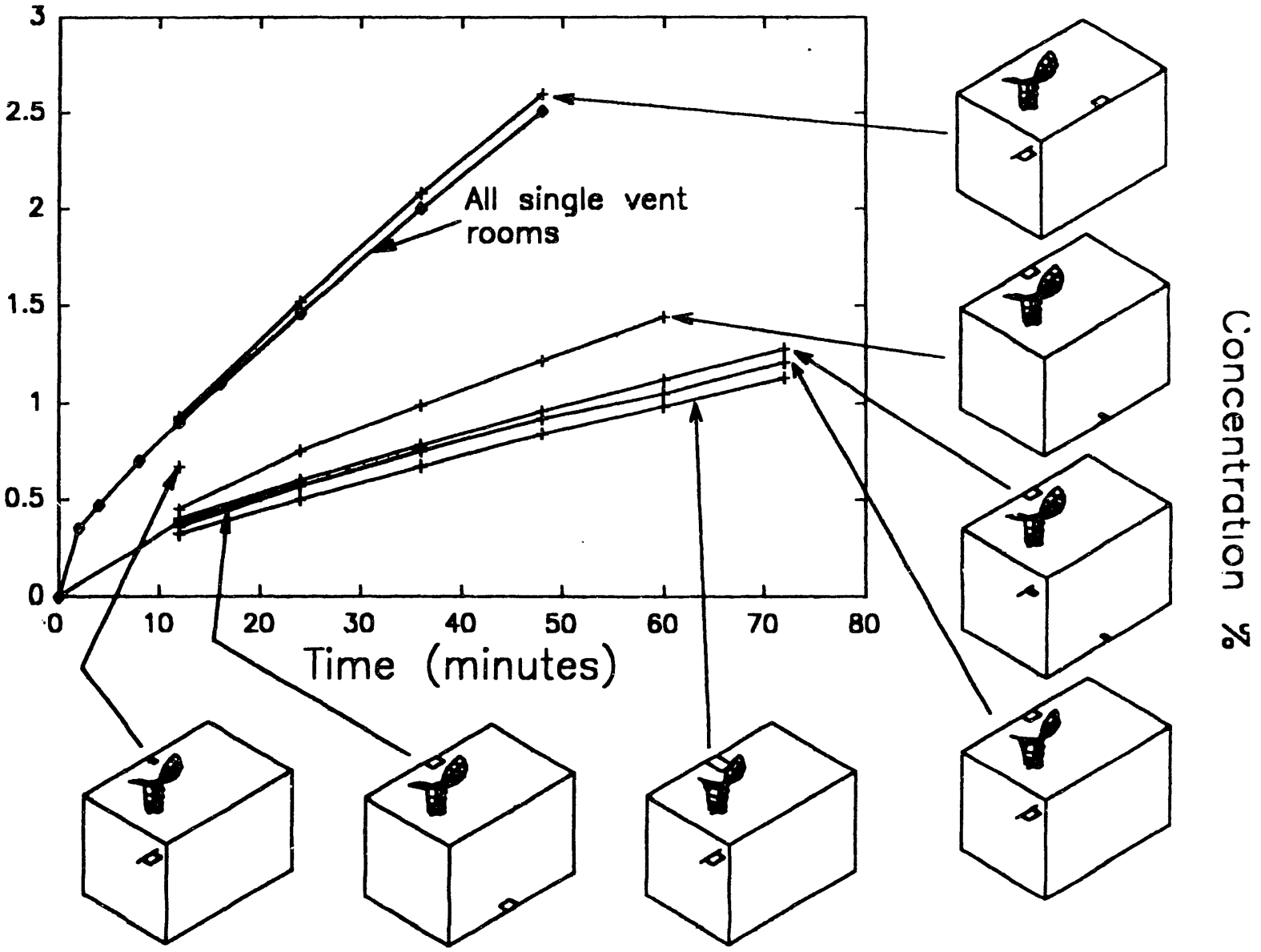
Figure 1 - Combustible methane cloud with ignition locations used in experiments

Figure 2 - Combustible hydrogen cloud with ignition locations used in experiments

Figure 3 - Hydrogen concentration versus time









# **A SURVEY OF INDUSTRIAL INTEREST IN HYDROGEN-RELATED TECHNOLOGIES**

Robert L. Mauro,  
Debbi L. Smith,  
Jeffrey A. Serfass  
National Hydrogen Association

## **Abstract**

The paper presents the findings of a survey of non-National Hydrogen Association members by the National Hydrogen Association on the non-members interest in hydrogen and hydrogen-related technologies. The survey approached over thirty firms that ranged from suppliers to potential users of hydrogen. In the twenty-three corporate responses received, the study found some companies performing hydrogen research with interest focused on hydrogen-related technologies that could use other fuels. The survey also identified industry concerns, barriers to industrial hydrogen-research, and some potential hydrogen research projects.

## **Introduction**

Hydrogen is a clean fuel just beginning to emerge from its role as a rocket fuel and chemical additive, to a role of energy carrier and a fuel capable of serving environmentally attractive end-uses. Hydrogen applications that take advantage of hydrogen's unique properties are now being developed by government organizations with a number of sponsored research programs. Over the next five years, many of the newer hydrogen-fuel-related technologies will be entering the demonstration phase of their life cycle. Eventually, however, programs intended to achieve commercial applications in market settings must tap industrial research and commercial interests. To ensure commercial success, industry must be a partner in the research programs and the early demonstration activities. In response to this requirement, the National Renewable Energy Laboratory, acting on behalf of DOE, asked the National Hydrogen Association (NHA) to undertake this survey and determine the range of industry knowledge, interest, and involvement with hydrogen and related technologies.

## Purpose of the Study

The purpose of this study is to:

- Determine industry knowledge and interest in hydrogen;
- Identifying current industry activities that are related to hydrogen;
- Determine barriers to increased industry involvement in hydrogen and hydrogen-related technologies; and
- Discover the extent of industry interest in joint research programs with the federal government and others.

The study is also intended to identify what areas might be the most fertile for joint government/private industry research projects.

### Procedure

This project began with the identification of the scope of industrial organizations that are likely to be important to broader applications of hydrogen as a fuel, with a diversity of company sizes and industrial segments. The list of targeted industries are listed in Figure 1 and includes hydrogen producers, utilities, corporations involved with storage, and a range of end-users from various industries such as automobile manufacturing. At NREL's request, the study avoided current NHA members since it was assumed that the NHA already understood the interests and capabilities of NHA members and this understanding would be reflected in the study conclusions.

In all, thirty individuals at 23 companies were interviewed.

The NHA staff, with the guidance of the NHA's Technology Review Committee, developed an interview guide to be used initially in personal meetings, and later used to develop a telephone interview guide.

- Aerospace
- Automobile, bus and locomotive
- Chemical
- Electrolysis
- Fuel cells
- Gaseous hydrogen storage tanks, vessels compressors and piping
- Hydrides and carbon storage
- Hydrogen production
- Liquid hydrogen cryogenic equipment
- Petroleum
- Photovoltaic, wind and solar thermal
- Reformers, gasification, oxidation and pyrolysis
- Turbines and engines

**Figure 1:** Types of Companies likely to have research interest in advanced technologies related to hydrogen fuel

A breakdown of the 33 firms contacted is as follows:

- Five are companies involved in equipment or systems related to hydrogen
- Four are manufacturers of hydrogen storage equipment

- Eighteen companies are involved in businesses that could use hydrogen in processing, aerospace, vehicle, electricity production or other applications
- Two companies are utilities that might use hydrogen for energy conversion and also distribute hydrogen
- Four companies are A&E or consulting firms with a background or interest in hydrogen.

Twenty-two of the companies that we attempted to contact were large. The remaining eleven companies were considered small.

The mix of the 23 firms actually interviewed is:

- Five hydrogen production equipment companies
- Two hydrogen storage equipment companies
- Twelve companies of interest for their potential hydrogen applications
- Two utility companies
- Two A&E or consulting firms.

The results of the interviews were analyzed for each of these four purposes:

1. To determine hydrogen knowledge and interest;
2. To determine research and development activities and views on the federal R&D program
3. To determine views on the barriers to greater interest in hydrogen; and
4. To determine interest in joint research with the government and specific project interests.

## Results To Date

The results of this study are presented by company type, with the results pertaining to each of the study objectives presented. The study objectives were:

- To determine industry interest in hydrogen and related technologies
- To find out what industry is doing in hydrogen R&D and/or applications
- To find out what it would take to increase industry involvement in hydrogen-related R&D
- To find out whether there is interest in joint government/industry hydrogen-related projects.

### Firms Engaged In Technologies Related to Hydrogen

The firms interviewed that are considered to be engaged in technologies related to hydrogen production are the following:

1. Haldor Topsoe
2. Koch Process Systems
3. SEA Corporation
4. Teledyne
5. Texaco

**Industry Interest In Hydrogen and Related Technologies** – Not surprisingly each of the interviewed firms and NHA members engaged in technologies related to hydrogen production or hydrogen liquefaction see the potential for growth in their business as the hydrogen market grows. However, only Texaco identified the market segment that they saw providing this growth -- transportation. Texaco's hydrogen production focus is on gasification technology. Teledyne Corporation's and SEA Corporation's interests are in electrolysis, SEA's being particularly interested in the application of electrolysis with PV.

**Industry Activities In Hydrogen-Related R&D and Applications** – With the exception of Koch Process Systems and Haldor-Topsoe, each of the hydrogen production technology companies interviewed were doing research related to hydrogen production. Teledyne is involved in improved electrolysis equipment. SEA's has a program, *Powergrid 1000*, which aims to produce DC power from PV for hydrogen production at \$.034/kWh. SEA is also promoting the addition of hydrogen to Los Angeles gas lines, which already has a small amount of hydrogen mixed in with its natural gas. Texaco is developing its gasification technology to produce hydrogen from a variety of fossil fuels at its Montebello research facility.

**Incentives or Barriers to Increased Industry Involvement** – The hydrogen production technology companies responded to the questions about increased involvement with their concerns for the barriers they see.

The barrier issues that surfaced are that:

- The price of hydrogen limits its market growth
- The lack of applications limit interest in markets
- The federal government needs to increase funding of hydrogen-related research with the focus of the funding on basic research, electrochemistry, and biomass
- More demonstrations are required to link development efforts to commercial markets.

There were no incentives mentioned for hydrogen development by producers.

*Industry Interest in Joint Industry Government Projects* -- All the companies engaged in hydrogen production technologies are interested in joint industry government projects. Four of the five companies interviewed either stated or implied that they would have to see some commercial advantage to a joint venture -- new or expanded market opportunities. All of the responding producers express some level of concern with respect to ownership of "intellectual property" arising from the research. There was much less concern expressed about the difficulty of contracting with the Government. Two of the four firms have had Government contracts.

## **Hydrogen Storage**

The two firms considered to be engaged in equipment related to hydrogen storage are the following:

1. Geoscience
2. Pressed Steel Tank

***Industry Interest In Hydrogen and Related Technologies*** – The two companies' businesses are already oriented to hydrogen. Both are engaged in storage-related equipment and produce tanks for hydrogen storage.

***Industry Activities In Hydrogen-Related R&D and Applications*** – Geoscience is promoting research on hydride storage and safety. They view the use of hydride storage as one way of minimizing the safety risk with hydrogen storage.

***Incentives or Barriers to Increased Industry Involvement*** – Both companies emphasized the need for demonstrations. Geoscience also emphasized the need for basic research in hydrogen storage. They view hydrogen as a long term technology. Geoscience is concerned about the safety issues associated with hydrogen use and feels that it must be addressed.

***Industry Interest In Joint Industry Government Projects*** – Pressed Steel Tank indicated no near-term interest in being involved in cost-shared hydrogen research programs. Geoscience indicated that it would depend on how the program was conducted. They felt that SERI had done a poor job in running the solar program in which they wanted to participate. They have thought about doing some calorimetry

research on controlling the amount of energy released from storage. They have some patents in this field and are concerned about ownership of "intellectual property".

## **Utilities**

The following utilities were interviewed in this study:

1. Pacific Gas & Electric
2. Southern California Edison

**Industry Interest In Hydrogen and Related Technologies** – Both of the utilities interviewed have significant interest in a variety of hydrogen-related technologies but neither has near-term interest in hydrogen-related programs per se. Hydrogen is too long-term for Pacific Gas & Electric and hydrogen is unlikely to be cost-effective for Southern California Edison.

**Industry Activities In Hydrogen Related R&D and Applications** – Both utilities are involved with fuel cells and renewable methods of power generation. They are also both involved in various energy storage technologies. Both utilities are increasingly using natural gas for their fossil power plants and both have large R&D programs.

**Incentives or Barriers to Increased Industry Involvement** – Neither company sees itself using hydrogen until it is economic, except for hydrogen cooling of generators.

**Industry Interest In Joint Industry Government Projects** – Interest in joint projects with Government was not asked.

## **Consulting & A&E Firms**

The following consulting and architect/engineering firms were interviewed:

1. Aerospace Corporation
2. Arthur D. Little

**Industry Interest In Hydrogen and Related Technologies** – Both Arthur D. Little and Aerospace Corporation do contract research for the Federal Government. Arthur D. Little also does much of its business with private clients. Aerospace Corporation's is a government dedicated firm that does no business for private clients and can not compete with private business. Their largest contractor is the Air Force.

Aerospace Corporation's principal hydrogen interest is in aerospace applications but they do some environmental business. In the 1980's they did do vehicle studies involving hydrogen for DOE. Arthur D. Little's principle interest in hydrogen is as a transportation fuel.

**Industry Activities In Hydrogen Related R&D and Applications** – Arthur D. Little stated that the key need for hydrogen use in transportation was infrastructure. There is a need to demonstrate a hydrogen service station with reforming of natural gas. Arthur D. Little is not keen on PV produced hydrogen, but they did see a future for hydro and wind produced hydrogen. They would like to see a demonstration of wind electrolysis in the Aleutian Islands. Arthur D. Little is involved in fuel cell and storage

development. They have a relationship with Daimler-Benz and are working on hydrogen-fueled internal combustion engines.

***Incentives or Barriers to Increased Industry Involvement*** -- Arthur D. Little indicated that the principle transportation issue is infrastructure.

***Industry Interest In Joint Industry Government Projects*** -- Both firms do contract research. Aerospace Corporation is a "Federal Contract Research Center" and can not bid competitively. Neither firm funds significant research with its own funds.

Aerospace Corporation may be interested in participating in DOE's hydrogen program and provide program evaluation support, including evaluation of proprietary technology since they cannot compete with private industry.

Arthur D. Little suggested the following projects:

- Verify hydrogen storage mechanism and push them to the limit.
- Verify gasoline station-sized reforming of natural gas into hydrogen.
- Safety

### **Businesses Engaged In Potential Hydrogen Applications**

The following businesses are considered to be involved in potential hydrogen applications:

1. Chevron Research & Technology
2. Dow Chemical
3. Electric Boat
4. General Atomics
5. General Motors
6. Lectrodryer
7. Martin Marietta
8. McDonnell Douglas
9. Monsanto
10. Pentastar Electronics (Chrysler)
11. Rocketdyne (Rockwell International)
12. United Technologies

***Industry Interest In Hydrogen and Related Technologies*** -- The companies considered in this study can be broken down into aerospace companies, automobile companies and others. Two of the aerospace companies have no interest in hydrogen except as a user. The companies with an involvement in NASP or the SST are interested in hydrogen for high speed aircraft applications. Two of the defense-related companies are interested because they are in, or are thinking of getting back into, energy businesses in the areas of ocean thermal energy use and PV.

The auto companies are interested in automobile applications. The other two companies, Chevron and Lectrodryer, are interested in hydrogen for use in process enhancement. Lectrodryer views hydrogen as the one fuel not contaminated by water. It is considered the cleanest fuel for drying. Chevron has no interest in hydrogen as an automobile fuel.

**Industry Activities In Hydrogen Related R&D and Applications** – Of the twelve applications-related companies five indicated that they had hydrogen programs. All five were aerospace companies doing research on hydrogen fuel. McDonnell Douglas is also doing research on light weight hydrogen storage tanks for high speed aircraft applications. Martin Marietta is handling much of the ground support for refueling these craft with liquid hydrogen.

The auto companies are scanning the hydrogen literature but have not made a commitment to hydrogen as a vehicle fuel.

Dow Chemical's research effort is focused on the solid polymer electrolyte fuel cell. They expressed little interest in hydrogen per se even though they are a hydrogen producer and a user of dc power in some of their plants. Monsanto is doing research in hydrogenation.

United Technologies Corporation has an active fuel cell development and commercialization program in a subsidiary/joint venture with Toshiba. They are also doing hydrogen research in home heating applications. Lectrodryer has no ongoing research effort.

**Incentives or Barriers to Increased Industry Involvement** – Chevron would become interested in hydrogen if the automakers took hydrogen seriously as a vehicle fuel. General Motors, Dow Chemical, and Chrysler are interested in fuel cells much more than hydrogen. They do not care what fuel is used to operate the fuel cell. Environmental concerns might drive the automakers to hydrogen. Of the aerospace companies only Martin Marietta expressed interest in considering reentering the terrestrial hydrogen energy field.

**Industry Interest In Joint Industry Government Projects** -- Only United Technologies Research Center, of the twelve companies interviewed, indicated that they would be willing to fund a joint research program on hydrogen. Many of the other companies would not participate at any cost-sharing formula until they see a relatively near-term business opportunity as its outgrowth.

General Motors indicated that their Allison Division, which is performing solid polymer fuel cell research might be receptive to joint industry government projects, but not G.M. Research Laboratories, which was contacted in the survey.

Hydrogen is not taken very seriously as a fuel. Its costs are considered too high for conventional applications, the infrastructure doesn't exist for anything but industrial applications, and the environmental legislation that might provide greater incentives for hydrogen applications is not envisioned, as being adequate to make hydrogen applications economic.

Where serious hydrogen interest exists, it is due to specific application interests associated with focused development programs, not because of broad interest in hydrogen systems. Hydrogen interest in industry exists where there are near-term business opportunities or longer-term technology developments have hydrogen as a component.

Long-term research and demonstrations are supported by most interviewees, but with one principal caveat shared by many of the companies. Management will have to perceive a credible long-term strategy that has sufficient near-term opportunity to warrant management's attention. Near-term payoff, in this case, may be 10 years or longer, but not so long that its value is severely discounted.



In addition to a credible strategy, demonstrations are necessary to build interest in hydrogen. However, NHA staff's experience in building commercialization programs suggests that isolated demonstrations, unconnected to following commercialization steps as part of a credible, self-incentivized plan will not lead anywhere.

The hydrogen research effort is grossly under-funded, and should be substantially increased. The payoff in energy flexibility and environmental benefits are large enough and the promise of costs and energy efficiency improvements are great enough to warrant a serious research, development and demonstration program.

Industry participation in joint government projects depends on a credible market for the product or hydrogen and satisfactory resolution of "intellectual rights" issues. Contract problems and government paper work requirements are less important issues than intellectual property rights, particularly for firms that have previously had federal contracts.

The following projects were either suggested or implied by respondents:

- Ocean thermal energy conversion system producing hydrogen;
- Solid polymer fuel cell demonstration for an automobile;
- Demonstration of integrated photovoltaic/electrolysis systems;
- Demonstration of wind produced hydrogen in the Aleutian Islands, with shipment to the lower 48 states;
- Verify hydrogen storage mechanisms for transportation and push them to the limit.
- Verify gasoline station-sized reforming of natural gas into hydrogen. Develop and demonstrate a hydrogen service station utilizing a small efficient reformer fueled by a natural gas distribution pipeline.
- Performance evaluation of competitive emerging technologies by third party.

Two other projects alluded to during the interview were the addition of hydrogen to natural gas pipelines in the L.A. area using renewable produced hydrogen, and the testing of various fuels in pilot scale gasifiers to maximize hydrogen production and obtain a more accurate estimate of hydrogen production costs from gasification processes.

### **Follow-on Activities**

The continuation of this activity will consist of following up on the hydrogen-related projects mentioned in the survey by:

- Preparing summaries and identifying interested parties to each of the projects
- Recommending approaches to implementing joint industry government projects

- Prepare a workshop with interested parties to discuss structures that allow industry and government to work together more easily on hydrogen related projects.

### **Acknowledgments**

The authors express their gratitude to William Hoagland, Hydrogen Program Manager at the National Renewable Energy Laboratory. His office is responsible for managing the Hydrogen Program of the U.S. Department of Energy. Thanks is also extended to Dr. Russell Eaton of the Department of Energy for his continued support of the National Hydrogen Association and whose office is responsible for implementation of the Matsunaga Hydrogen Research and Development Act, the legislation that called for this study.

The authors also wish to express their appreciation to National Hydrogen Association's Montego Parker who very capably performed the telephonic interviews and helped interpret the results of this study.

**DATE  
FILMED**

*11 / 5 / 93*

**END**

